MAY 1960 VOLUME 7 (1960) No. 2

GREGG M. SINCLAIR LIBRARY
UNIVERSITY OF HAWAII
8-7-63

NUCLEAR INSTRUMENTS & METHODS

A JOURNAL ON ACCELERATORS, INSTRUMENTATION AND TECHNIQUES IN NUCLEAR PHYSICS

EDITOR: K. SIEGBAHN - UPPSALA

CONTENTS

ROBERT L. BURMAN and AVIVI I. YAVIN, Multi-purpose magnetic particle analyzer 101
ERIK KARLSSON and KAI SIEGBAHN, A new design for a beta-ray spectrograph for relative measurements 113
ARPAD BARNA, J. HOWARD MARSHALL and MATTHEW SANDS, A nanosecond coincidence circuit using transistors 124
D. N. EDWARDS and B. ROSE, An extension of the transfer matrix method to a beam transport system containing a solenoid 135
A. DERUYTTER, A 4π-fission detector 145
A. F. FISCHMANN-ARBEL and ISRAEL BAR-DAVID, A method of linear pulse amplifier design . 153
M. DE CROËS, W. PARKER and K. SEVIER JR., Thin film thickness distribution by alpha absorption 160
G. W. HUTCHINSON, R. RUBINSTEIN and W. H. WELLS, A transistorized ring scaler of resolving time 0.3 μs 167
J. R. WATERS, A "time expander" for precision neutron time-of-flight experimentation 174
K. S. KUCHELA and L. H. PESHORI, Application of bidirectional Dekatron tubes in low level beta activity measurements by cancellation technique 179

(continued on p. 3 of cover)

NORTH-HOLLAND PUBLISHING COMPANY - AMSTERDAM

NUCLEAR INSTRUMENTS AND METHODS

A journal on accelerators, instrumentation and techniques in nuclear physics

EDITOR: K. SIEGBAHN, UPPSALA

EDITORIAL BOARD:

J. B. ADAMS (CERN)
F. A. ALSINA (Buenos Aires)
E. AMALDI (Rome)
H. L. ANDERSON (Chicago)
K. T. BAINBRIDGE (Cambridge, Mass.)
P. R. BELL (Oak Ridge)
R. E. BELL (Montreal)
A. BERTHELOT (Saclay)
H. BRINKMAN (Groningen)
E. H. COOKE-YARBOROUGH (Harwell)
S. DE BENEDETTI (Pittsburgh)
M. DE HEMPTINNE (Louvain)
A. DE-SHALIT (Rehovoth)
M. DEUTSCH (Cambridge, Mass.)
S. DU TOIT (Pretoria)
B. S. DŽELEPOV (Leningrad)
W. GENTNER (Heidelberg)
P. C. GUGELOT (Amsterdam)
H. HALBAN (Paris)
O. HAXEL (Heidelberg)
P. HUBER (Basel)
S. KIKUCHI (Tokyo)
J. KOCH (Copenhagen)
M. S. KOZODAEV (Moscow)
S. LIVINGSTON (Cambridge, Mass.)
E. M. MCMILLAN (Berkeley)
M. G. MEŠČERJAKOV (Moscow)
P. B. MOON (Birmingham)
M. L. OLIPHANT (Canberra)
W. PAUL (Bonn)
A. S. RAO (Bombay)
G. SALVANI (Rome)
P. SAVIĆ (Belgrade)
P. SCHERRER (Zürich)
CH. SCHMELZER (CERN)
H. W. B. SKINNER (Liverpool)
R. TANGEN (Oslo)
D. TAYLOR (Northampton)
V. I. VEKSLER (Moscow)
G. VON DARDEL (CERN)
O. WERNHOLM (Stockholm)
R. R. WILSON (Cornell)
S. D. WINTER (Saclay)

INSTRUCTIONS FOR CONTRIBUTORS

Contributions may be sent to the Editor, Professor K. Siegbahn, Institute of Physics, University of Uppsala, Sweden, either directly or through the intermediation of one of the members of the Editorial Board. Contributions may be written in English, French or German but should always, except for very short papers, be supplied with a brief abstract in English. Figures should be in inked original drawings or glossy prints and they should be sufficiently large. Contributors should make sure that important details in drawings and photographs will show up clearly in the diminished copy used by the publisher.

Books for review should be sent to Professor Siegbahn.

Objective and descriptive material on endeavours and product developments from the industry for the section "Spotlight on Industry" should be sent directly to the publishers, North-Holland Publishing Company, P.O. Box 103, Amsterdam.

Nuclear Instruments and Methods is published monthly. The subscription price of a volume of 360 pages is $ 17.00 (130 s), postage free.

Subscriptions should be sent to the publishers, North-Holland Publishing Company, P.O. Box 103, Amsterdam or to any subscription-agent.

No part of this issue may be reproduced in any form, by print, photoprint, microfilm or any other means without written permission from the publisher.

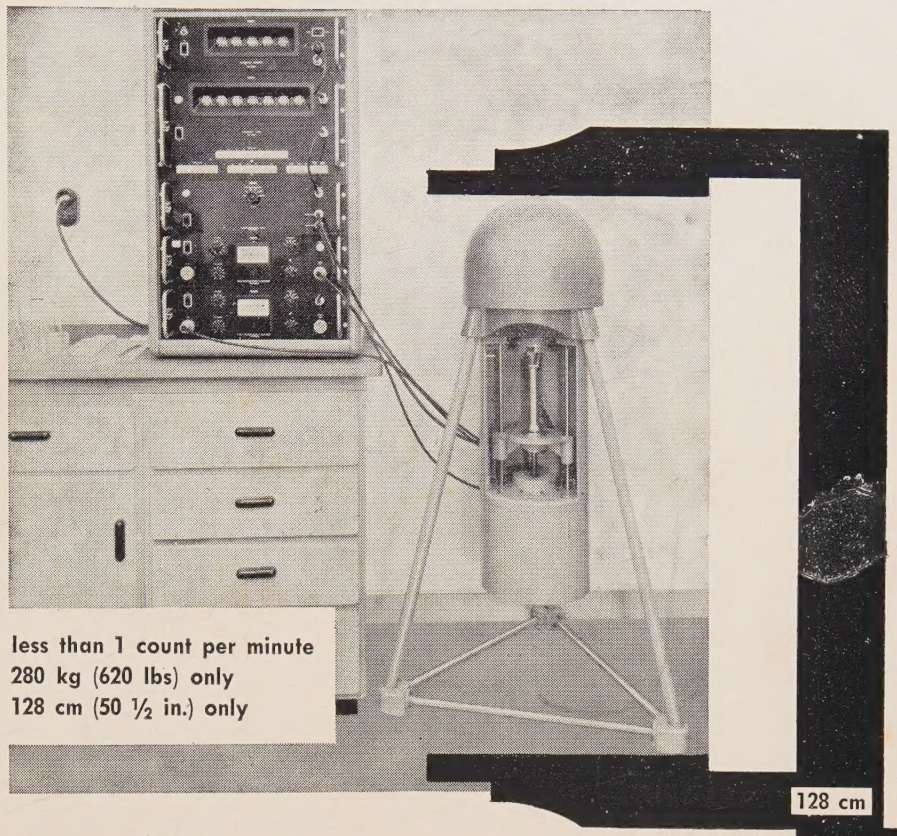

Background : less than 1 count per minute
Weight : 280 kg (620 lbs) only
Height : 128 cm (50 ½ in.) only

low-level beta counting

Low-level beta counting is brought to an elegant and simple solution by the novel Philips anti-coincidence assembly, type PW 4127, together with its associated electronic equipment.
The assembly comprises two radiation-sensitive elements only, viz. a low-level beta counting tube*), and a single guard tube which replaces the conventional array of dozens of guard tubes hitherto required for low-level work.
By virtue of this unique design tons of shielding material are eliminated; the electronic circuitry is considerably simplified, and hence overall reliability is greatly improved. Reproducibility is guaranteed by the fixed geometry of the sample with respect to the counting tube.
With a background of less than 1 count per minute, it is now possible to measure in a 300 mg sample a beta activity (e.g. Sr^{90} or Tl^{204}) of $(5 \pm 0.5) \times 10^{-12}$ Curie in only one hour.

***) Two types available:**

type 18515 for measuring low-energy beta radiation, with a 1.5 mg/cm² mica window;

type 18516 for general low-level beta work, with a 10 mg/cm² Cr-Fe window.

PHILIPS
nuclear equipment

N.V. PHILIPS' GLOEILAMPENFABRIEKEN - EINDHOVEN - HOLLAND

NEW!

E-H MILLIMICROSECOND PULSE GENERATOR

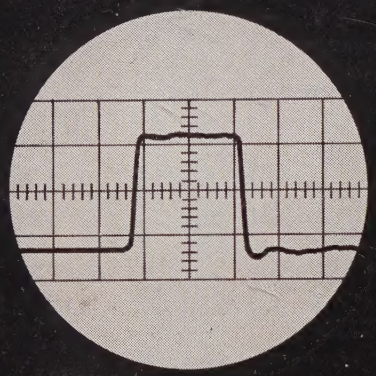

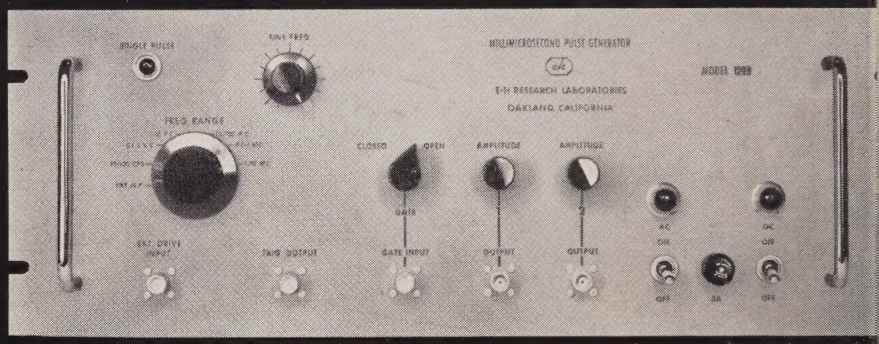

Model 120B f.o.b. Oakland, Calif. $1275

RISE TIME OF LESS THAN 2.5 MILLIMICROSECONDS

REPETITION RATE OF 10 cps to 10 Mc

plus these other features

- **PRECISION PULSE WIDTHS** 2.5 to 25 millimicroseconds
- **INDEPENDENT OUTPUTS** Two fully controlled 0-8 volt outputs
- **FLEXIBLE** Internal or external drive, provision for external gating and single pulse operation

Here is a new all-electronic instrument with the performance features—and quality engineering—you need for advanced applications.

The 120B's fast rise time and high repetition rate make it unexcelled for general laboratory use in development, production and testing of diodes, fast transistors, cables, pulse transformers, delay lines and video amplifiers . . . for development and check-out work in the computer field, for rf applications, and in nuclear test work. *For more information on the 120B or other E-H pulse generators, write or wire E-H.*

SPECIFICATIONS

RISE TIME (10% to 90%)
Less than 2.5 millimicroseconds

PULSE WIDTH
2.5 to 25 millimicroseconds

REPETITION RATE (External or Inter
10 cps to 10 Mc

OUTPUTS
(Two Independent Output Channels)
Amplitude, 0 to minus 8 volts (use E
model ZT pulse transformer for polarity inversion and impedance matching)
Impedance, 93 ohms

TRIGGER OUTPUT
Positive 15 volt pulse

CONNECTORS
All BNC type

TRIGGER ADVANCE
120 millimicroseconds

EXTERNAL DRIVE
Delay, 50 millimicroseconds
Amplitude required, 3 volts rms

ELECTRONIC GATE
Gating time, less than 100 millimicroseconds
Amplitude required, positive 20 vol

E-H RESEARCH LABORATORIES, INC.
1922 PARK BLVD. • GLENCOURT 2-1314 • OAKLAND 6, CALIFORNIA

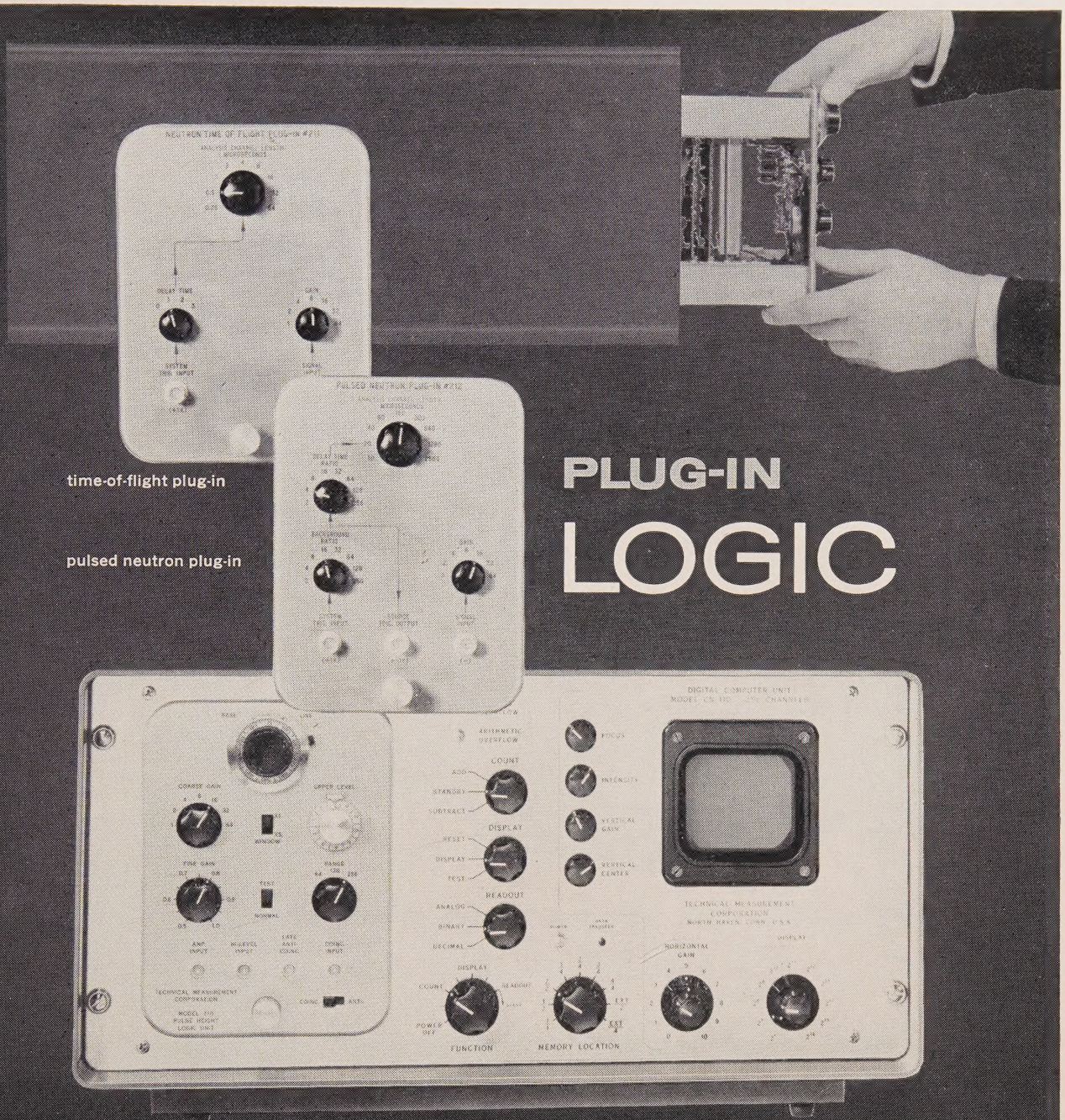

time-of-flight plug-in

pulsed neutron plug-in

PLUG-IN LOGIC

Logic is interchangeable in the TMC Model CN-110 Pulse Analyzer. Into the all-transistor, 30-pound, 256-channel digital computer you can plug Pulse Height Analysis, Pulsed Neutron, Time-of-Flight or special program units. Out of it you can get Analog, Digital or Binary data. You can carry the system and set it up almost anywhere. It is guaranteed for two years.

These instruments and all accessory units are now being delivered. Complete details of design, construction and operation are contained in a new 6-page folder available on request.

220 data handling unit

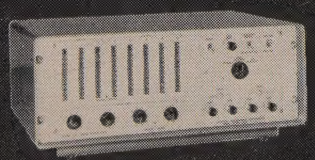

• We have excellent openings for Transistor Circuit Designers •

TMC

TECHNICAL MEASUREMENT CORPORATION

441 WASHINGTON AVENUE, NORTH HAVEN, CONN.

Pulse Height Analysis

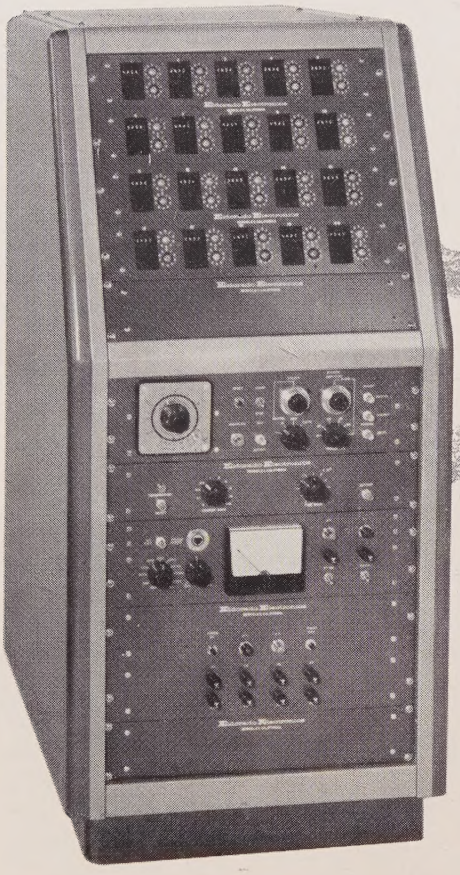

Hours faster with the

Eldorado 4100

The Eldorado 4100 is the fastest multi-channel pulse height analyzer commercially available to the nuclear physicist. Its high resolution and exceptional stability dramatically shorten many experiments. For example, an experiment requiring from 7 to 42 hours with a time conversion type analyzer can be done in 8 to 25 minutes with the 4100. Such performance considerably reduces research costs.

APPLICATIONS *The 4100 is particularly well-suited for experiments requiring accurate analysis of (1) isomeric states, (2) isotopes with extremely short half-lives, (3) isotope mixtures having complex photo-peak structures.*

SPECIAL ADVANTAGES

Stability. The 4100's double pulse resolution—better than 1.0 microsecond—is achieved without sacrifice of stability. The system's stability figures (see specifications) compare favorably to the best for slower computer-type analyzers. Since lower ordered channels are free from non-linearity, each data point in the spectrum is equally useful and valid.

Low Dead Time. Users of the 4100 can often neglect count-loss correction factors because dead time is less than 0.2 microsecond. At an input counting rate of 300,000 counts per minute, dead time is less than 2% of the total experiment time.

KEY SPECIFICATIONS **Number of Channels,** 20. **Channel Width,** 1 volt, nominal. **Channel Width Stability,** Typically, better than 1% of a channel per week. **Zero Level Stability,** Better than 0.1% per week. **Window Width,** 20 volts, nominal. **Window Position Range,** 5 to 105 volts in 5 preset steps or continuous. **Channel Count Capacity,** 1,000,000. **Double Pulse Resolution Complete Analyzer,** 1.0 microsecond at window amplifier input. **Channel Scalers,** 10.0 microseconds.

For more details, write for Eldorado Bulletin D-4100.
Please address Dept. 79

Eldorado Electronics
2821 TENTH STREET • BERKELEY 10, CALIFORNIA

NEW.....

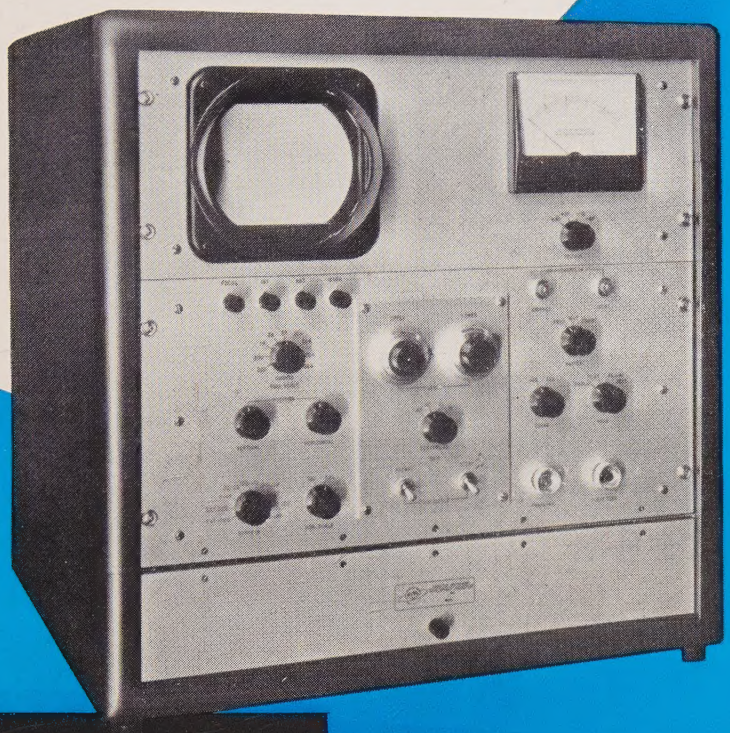

Model 34-12 Transistorized 400 CHANNEL ANALYZER

- Ferrite Core Memory
- External Programming
- Memory Subgrouping
- Time Analyzer Mode
- Live Display on 5" CRT
- Crystal Controlled Live Timer
- 10^5 Count Capacity
- Address Identification
- 0.5 % Linearity
- Prompt and Delayed Coincidence and Anti-Coincidence
- Spectrum Transfer Circuit
- Auto-Print
- Auto-Record
- Print and Record Simultaneously (OPT.)
- Dead Time Meter
- Auto Transfer Circuit
- Free Course of Instruction
- Installed by Factory Engineer

RIDL announces a new 400 Channel-Analyzer

To the RIDL family of transistorized analyzers is added a new 400-channel analyzer—the Model 34-12—now in production and being delivered. The Model 34-12 may be operated as a Multichannel Pulse Height Analyzer or as a Multichannel Scaler (Time Analyzer).

The Model 34-12 is designed to save valuable man-hours in the laboratory by providing full automation through such features as Auto-Print, Auto-Record and an automatic transfer circuit. A built-in crystal controlled live timer allows automatic dead time correction. The addition of automatic background correction allows final data readout without laborious manual corrections and/or replotting of data. The Model 34-12 may also be used as four simultaneous 100-channel analyzers without loss of resolution.

To this maximum development of automatic data gathering and analysis, RIDL now adds a new focus, AUTOMATIC DATA PROCESSING. This brings the ultimate in automation to the Model 34-12. To normal printing and plotting is added readout on magnetic tape, punched tape, or serial entry printers. This allows either system or instrument control or programming, multiple detector data processing, or sorting and routing of selected data. Whatever your data readout and processing needs may be, our staff is ready at all times to discuss them with you.

The Model 34-12 is another of the NEW line of instruments designed and developed by RIDL. Whatever your instrumentation problems, RIDL has the solution. Our staff is always available to answer your inquiries. For complete information on the Model 34-12 400-Channel Analyzer, write Department WB today.

RIDL INC.

Radiation Instrument Development Laboratory, Inc.

5737 SOUTH HALSTED STREET • CHICAGO 21, ILLINOIS
PHONE: TRiangle 3-2345 • Cable Address: RADILAB

Pye Limited — Atomics Division are supplying Reactor Cameras to LATINA POWER STATION which is being completed by the Nuclear Power Plant Company Ltd., and A.G.I.P. Nucleare for S.I.M.E.A. (Societa Italiana Meridionale per l'Energiee Atomica)

Television is a vital technique in the observation of gas-cooled reactors. The type of camera shown is in regular use at Calder Hall Nuclear Power Station – England, and is to be used at Latina. It carries its own lighting and in addition to visual inspection of the reactor interior, permits the removal of objects from the reactor using the special grab-attachment. All the camera facilities are controlled remotely. Direct experience over a number of years has enabled Pye to design cameras that will withstand high levels of nuclear radiation, temperature and pressure. Models can be supplied for use in water cooled reactors. If you have any specialised closed-circuit television or remote handling requirements, contact Pye Limited and avail yourself of their experience.

PYE OF CAMBRIDGE
CENTRE OF SCIENTIFIC RESEARCH

PYE LIMITED ATOMICS DIVISION - CAMBRIDGE ENGLAND

TNPG

A partnership has been established between The Nuclear Power Plant Company Limited and AEI—John Thompson Nuclear Energy Company Limited to design and construct better and cheaper nuclear power stations

This new enterprise is called

The Nuclear Power Group

and combines the research development manufacturing and construction resources of these industrial concerns of world-wide renown.

ASSOCIATED ELECTRICAL INDUSTRIES LIMITED

CLARKE, CHAPMAN AND COMPANY LIMITED

ALEX. FINDLAY AND COMPANY LIMITED

HEAD, WRIGHTSON AND COMPANY LIMITED

SIR ROBERT McALPINE AND SONS LIMITED

C. A. PARSONS AND COMPANY LIMITED

A. REYROLLE AND COMPANY LIMITED

STRACHAN AND HENSHAW LIMITED

JOHN THOMPSON LIMITED

WHESSOE LIMITED

RADBROKE HALL · KNUTSFORD · CHESHIRE

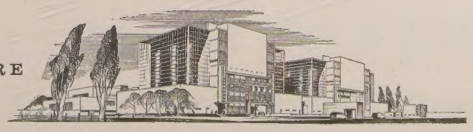

TGA NP 15 C

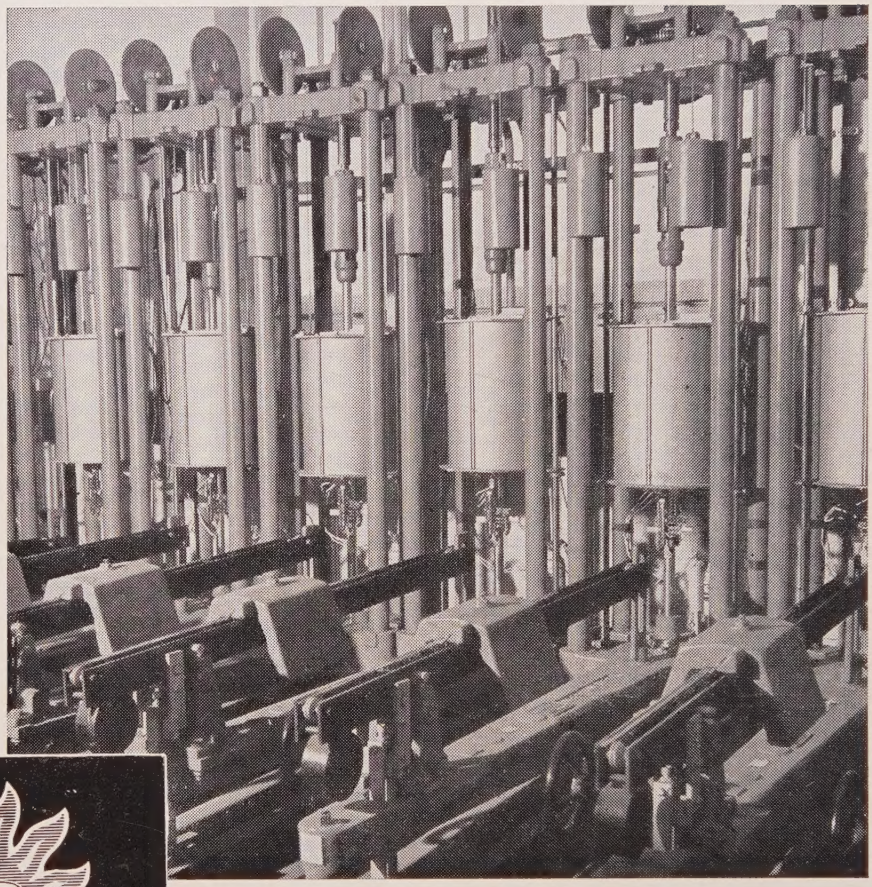

Some of the Creep Testing Machines used in our Research Department

BEARCOMO

CONSETT SPECIAL STEELS FOR LATINA PROJECT

The making of high-grade steel for a diversity of uses – mechanical, structural and scientifiic – has placed Consett Iron Company Limited in the front rank of steel producers.

The new demands of Industry have brought about the birth of special steels – such as "CONLO I" giving the highest degree of resistance to brittle fracture of any easily weldable non-alloy steel at present available. This was the steel chosen for the construction of reactor vessels at Nuclear Power Stations in Great Britain.

For use in the new and larger power stations such as LATINA, we developed the special steel "BEARCOMO" – in which the widely incompatible requirements of resistance to creep and notch toughness were met and reconciled. This steel was supplied to the order of Messrs. Whessoe Ltd., Darlington, England.

"BEARCOMO" is one of our patented steels – but, like "CONLO I", it is only one of our wide range of special steels for special jobs. Our booklet "Steels for the Job" published at Consett, describes them in some detail. Perhaps you would like to write for a copy.

Our technical and research departments will also welcome enquiries from anyone whose problem is . . . STEEL.

CONSETT IRON COMPANY LIMITED

CONSETT, COUNTY DURHAM, ENGLAND

Pyrotenax THERMOCOUPLES AND COMPENSATING CABLES WILL SAFEGUARD THE HEART OF LATINA

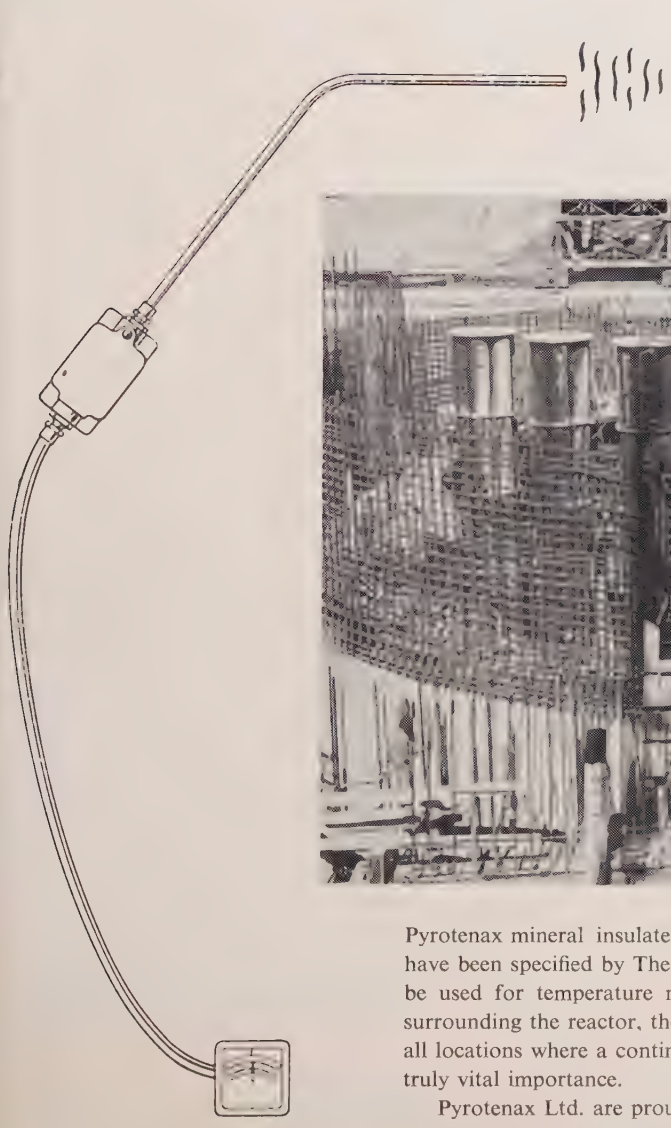

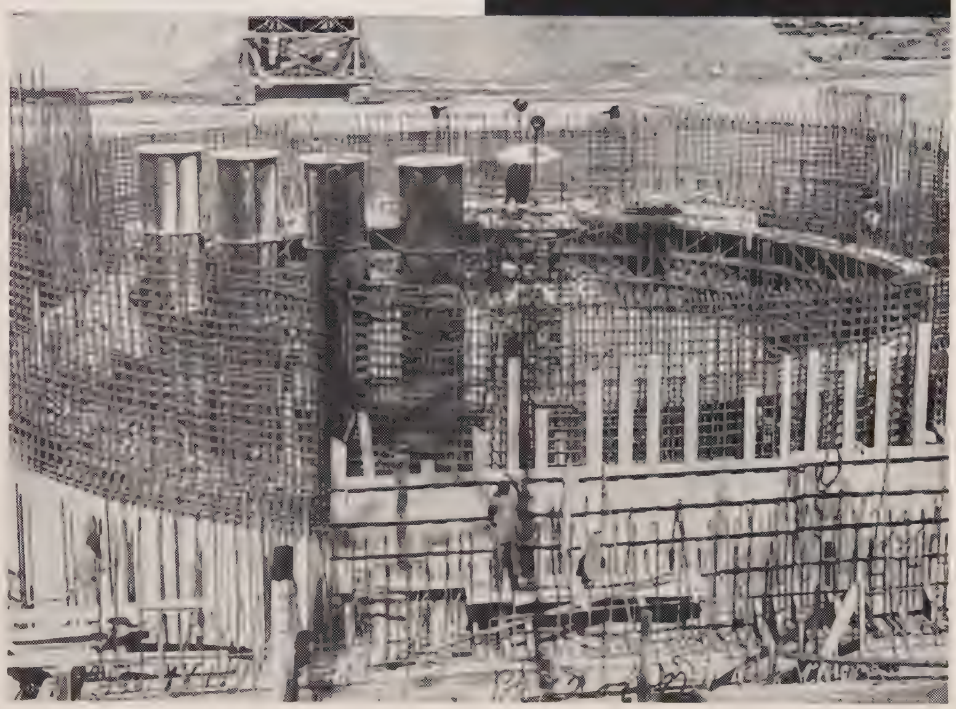

Pyrotenax mineral insulated metal sheathed Thermocouples and Compensating Cables have been specified by The Nuclear Power Plant Co. Ltd. for Latina in Italy. They will be used for temperature measurement of the fuel element cans, the biological shield surrounding the reactor, the graphite moderator blocks and the reactor vessel itself – all locations where a continuous and utterly dependable indication of temperature is of truly vital importance.

Pyrotenax Ltd. are proud to be making such an important contribution to the safe working and realiability of this nuclear power station – a project that is bound to set a standard not only in Italy but in many other countries.

Pyrotenax thermocouples are made in a variety of metals and alloys and in overall diameters from .266″ down to .040″.

Full technical details in Publication 31/AA/121.

PERFECTED BY EXPERIENCE
Pyrotenax
m.i. THERMOCOUPLES

THE MOST PRACTICAL THERMOCOUPLES FOR NUCLEAR AND INDUSTRIAL APPLICATIONS

Use of the trade name "Pyrotenax" is exclusive to the products of Pyrotenax Limited and its associates

PYROTENAX LIMITED · HEBBURN-ON-TYNE · ENGLAND

INTERNATIONAL

advertise
YOUR NUCLEAR PRODUCTS IN

sell
YOUR NUCLEAR PRODUCTS

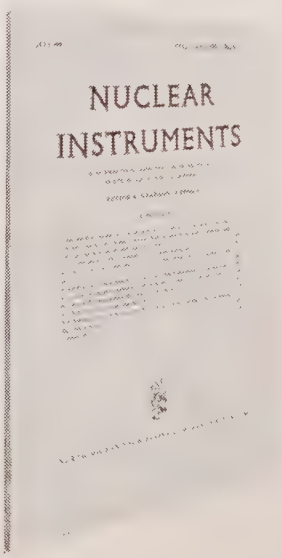

reap
YOUR NUCLEAR SALES
REWARDS

world wide
KEY NUCLEAR MANAGEMENT
NUCLEAR SCIENTISTS
NUCLEAR ENGINEERS
NUCLEAR PRODUCTION
PERSONNEL

SUBSCRIBE TO

you reach
THE WHOLE
NUCLEAR SALES WORLD IN

Entirely international in scope Nuclear Instruments and Methods is the one nuclear scientific journal that has an established subscription clientele throughout the whole world-where-ever nuclear men are at work—they want your nuclear products—they need your nuclear products—advertise in Nuclear Instruments and tell them WHAT – HOW – WHERE they can get your nuclear products

GO INTERNATIONAL WITH YOUR SALES PROGRAM TODAY WRITE

WILLIAM F. BAARS - ADVERTISING MANAGER NORTH-HOLLAND PUBLISHING COMPANY

P.O. BOX 103 – AMSTERDAM, HOLLAND

INTERNATIONAL

planning european power

AND NOW ITALY – LATINA

General Radiological Limited have supplied instrumentation for all the British Nuclear Power Stations. In addition they have supplied nucleonic instruments for the Argonaut Research Reactors at Slough England, Milan Italy, and Delft Holland.

Now, for the reactor in Europe's latest atomic power station, Latina near Rome, the Nuclear Power Plant Company Limited have specified complete instrumentation by General Radiological Limited

ONE OF THE *murphy* GROUP OF COMPANIES

general radiological LIMITED

NUCLEAR ENGINEERING DIVISION

15/18 Clipstone Street, Gt. Portland Street, London, W1. Tel. Museum 5080

NEW FROM TEXAS NUCLEAR CORP.

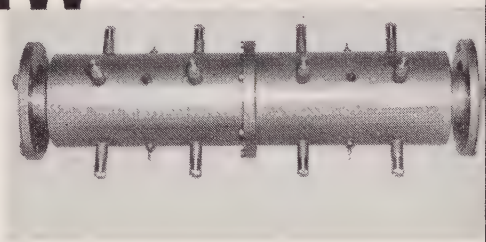

- For focusing an ion beam at large distances from the accelerator
- Cancels astigmatism produced by analyzing magnet
- Increases useful ion beam intensity

TEXAS NUCLEAR CORPORATION

WRITE DEPT. E

P. O. Box 9267 Austin 17, Texas

FOR SCINTILLATION & PROPORTIONAL COUNTING

Non-overloading Linear Amplifiers

MODELS 108 and 108 p

* GAIN–40,000, continuously variable
* RISE TIME–0.2 microsecond
* ACCEPTS + AND — PULSES

Tremendous Dynamic Range

EXCEEDS 1,000,000 (0.1 mV to 100 V)

Excellent linearity for small pulses in the presence of tremendous overloads that paralyze other amplifiers.
Model 108 P includes precision trigger type Pulse-Height Selector.

Model 413 Mercury relay precision sliding Pulser

The **one** pulser that fills **every need** of the Nuclear Physics Laboratory
0 to 100 Volts

10 full scale ranges from 1 mV to 100 volts
Fast rise and exponential decay of 1, 3, 10. 30, and 100 microsec simulate pulses from scintillation, proportional and Geiger counters.
Incorporates both manual control and precision motor drive.
The ideal instrument for precise calibration and test of pulse-height analyzers and other nuclear instrumentation.

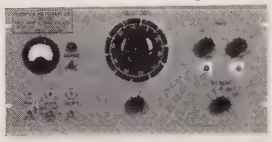

Window widths are determined AUTOMATICALLY, 10 × more ACCURATELY, 40 × FASTER than with conventional pulsers.

Model 108 Amplifier . . . . . $ 545.00
Model 108 P Amplifier (includes pulse-height selector) $ 595.00
Model 413 Precision Sliding Pulser . . . . . $ 630.00
Prices f.o.b. Silver Spring. Md.

RADIATION INSTRUMENT CO.

P.O. BOX 733 SILVERSPRING, MARYLAND, U.S.A.

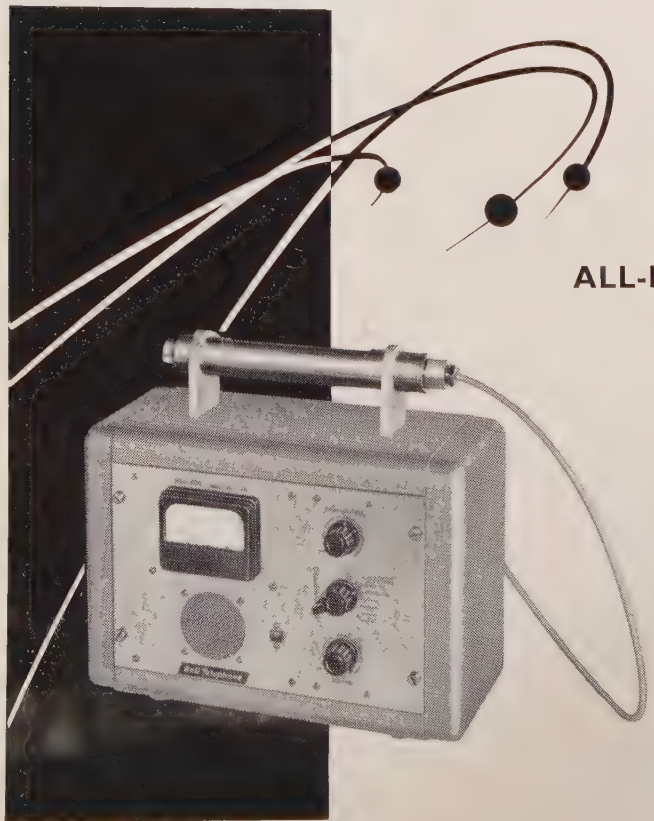

ALL-ROUND, LOW PRICED MONITOR

Typically developed as a laboratory equipment the monitor 111-A1 combines quality and high performance with low cost.

- Completely transistorized
- Designed as portable type
- Very low count rate: 0 to 5 c.p.s. full scale
- Highest count rate: 0 to 5000 c.p.s. full scale
- Equalizing accumulators
- Automatically recharged from A.C. mains
- Priced $ 410 F.O.B. Antwerp

For further information on this and other applications in the field of "Electronics for Nucleonics" ask :

AN ITT ASSOCIATE

Bell Telephone Mfg Co

"NUCLEAR ENERGY DIVISION"
33, Berkenrodelei
HOBOKEN-Antwerp
Belgium

NOW... DATA PRINT-OUT IN MANY FLEXIBLE MODES OF OPERATION!

High-Speed Scaler and Electronic Timer

OPERATING MODES

- **Preset Count:** 15 settings from 10 to 500,000 counts.
- **Preset Time:** 18 settings from 0.1 to 50,000 seconds.
- **Combined Preset Time & Count:** any of the time or count settings may be used simultaneously with the system stopping when the first preset event occurs.
- **Data Print-Out:** both scaler and timer provide "staircase" outputs. Time, counts, or both may be printed out or code punched on cards or tape.
- **Automatic Recycling:** The system will recycle automatically, if desired, following occurrence of a preset event and data print-out. In this case, print-out can be cumulative or destructive. Both print-out and automatic recycling can be used in any mode of operation.

These units are not only highly flexible but are also of the fine research quality typical of all Hamner Instruments. Scaler and Timer may be used together to provide the operational modes listed above. They may also be used independently.

N-803 TIMER

Stability:	100 CPS, crystal controlled.
Preset Time:	18 ranges from 0.1 sec. to 50,000 secs.
Elapsed Time:	to 10,000 secs.
Panel Dimension:	3½" height for standard Rack Mounting.

N-276 SCALER

Pulse Pair Resolution:	better than 1 us
Continuous Repetition Rate:	1 megacycle.
Indication:	6 electronic decades. (7 in model N-277)
Preset Time: **Combined Preset Time and Count:** **Preset Count:**	As previously described
Internal Calibration:	60 cycle
Input Sensitivity:	4V minimum, + or — by front panel switch
Panel Dimension:	3½" height, for standard Rack Mounting.

WORLD-WIDE DISTRIBUTION AND ENGINEERING SERVICES

EXPORT DEPARTMENT: 202 East 44th Street N.Y.C.
CABLE: Henleysale, RCA Teletype 210 N.C.Y.

Hamner

Hamner Electronics Co., Inc.

Department 4, P.O. Box 531, Princeton, New Jersey, PEnnington 7-1320

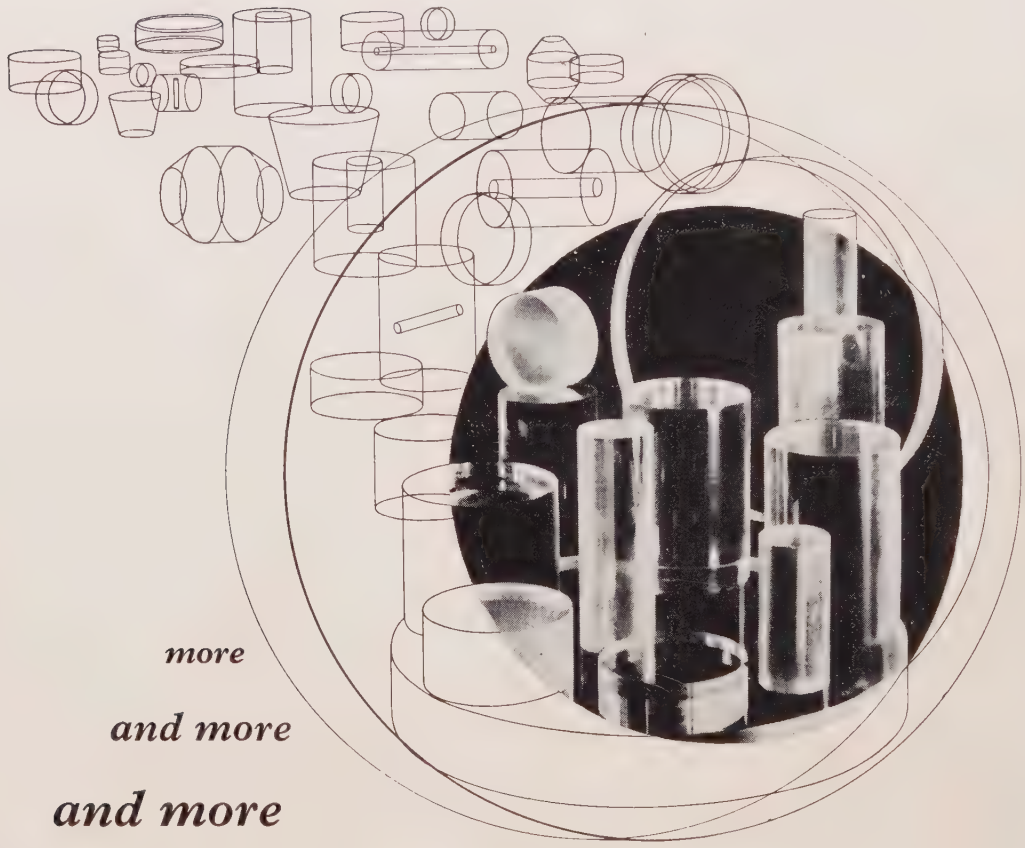

more

and more

and more

Scintillators

Nash & Thompson have now added Sodium Iodide, Caesium Iodide and Neutron Detectors to their extensive range of scintillators.

ORGANIC CRYSTALS. Anthracene, Stilbene, Terphenyl, in discs and cylinders.

PLASTICS. NATON-11 and NATON-136, high sensitivity, high transmission, based on either polyvinyl toluene or polystyrene. Available in discs, cylinders, ingots, foils, and filaments.

LIQUIDS. Ready made, sealed in glass containers to your specification, or in scintipaks

SCINTIPAKS. Accurately mixed dry constituents sealed in polythene envelopes, ready for dissolving in a suitable solvent as required.

CHEMICALS. Scintillation purity for making your own phosphors.

SODIUM IODIDE. Highest resolution, ready canned, in sizes up to 4″ dia × 3″ high, or 5″ dia × 2″ high.

CAESIUM IODIDE. In blocks up to 3″ dia × 3″ high.

Write or telephone for full information

Nash & Thompson LTD

Hook Rise, Tolworth, Surbiton, Surrey. Elmbridge 5252.

JSP 5689

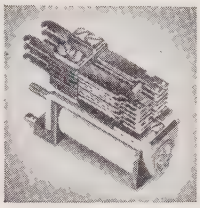

customer evidence...

8

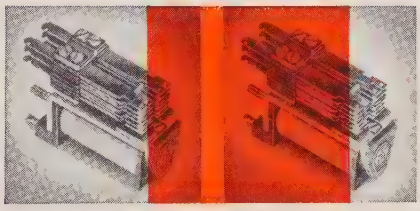

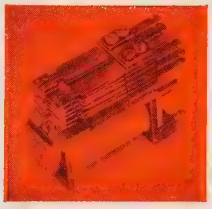

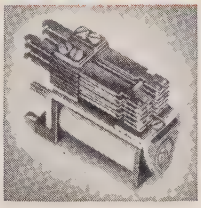

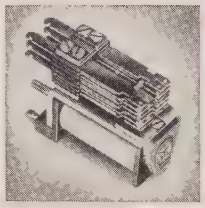

operations

Modestly we claim that under suitable conditions this new miniature will give service in excess of 10 million operations but 100 millions leaves us breathless and not a little proud. Capable of handling springset arrangements of up to 12 springs normal duty loading and switching at speeds of better than 10 m.s. when required, the G.P.S.T. is a natural for computers and similar applications.

See us on Stand D.153 at the I.E.A. Exhibition, Grand Hall, Olympia, London, from May 23rd — May 28th.

ETELCO

For more details please write to the
TECHNICAL SERVICES DEPT.
ELECTROMECHANICAL DIVISION
BEESTON · NOTTINGHAM

ETELCO LIMITED · HEAD OFFICE · 22 LINCOLN'S INN FIELDS LONDON W.C.2
ER8a

Elcor inc.
1225 W. BROAD ST.
FALLS CHURCH, VA.

MODEL A 309
CURRENT INDICATOR AND INTEGRATOR

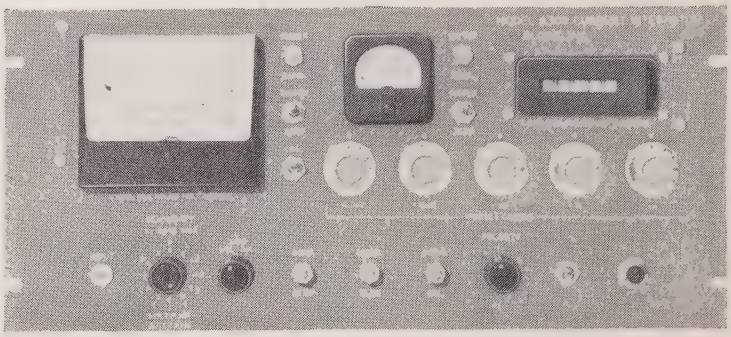

MODEL A 309 A

FEATURES

- Wide current range: 1 x 10^{-3} to 3 x 10^{-9} amp. in 12 switch settings.
- High accuracy: 1% of full scale.
- Internal calibrating current source to check proper operation.
- Front panel switch allows instrument to be used with current of either polarity.
- Pre-setting feature provides means of safeguarding against overexposure.
- Developed especially for use with Van de Graaff and other high-voltage accelerators.
- Permits many experiments with particle accelerators that would otherwise be difficult or impossible.
- Register readout gives digital accuracy on charge measurement.

The versatility and accuracy of two instruments in one!

1. Measures currents from 1 milliampere to 3 milli-microamperes.
2. Integrates input current and registers accumulated charge.

GENERAL DESCRIPTION The Model A309 Current Indicator and Integrator is a sensitive current indicator that also measures the total charge collected in a given length of time. Developed especially for use with high-voltage particle accelerators such as the Van de Graaff generator, the instrument is also ideally suited for other applications requiring the measurement of accumulated charge or the integration of a variable current.

The full-scale sensitivity of the instrument can be varied from 1 milliampere to 3 milli-microamperes in twelve ranges. For convenience in checking the performance and accuracy of the instrument, an internal calibrating current source is provided for each range. The accumulated charge is indicated on a 5-decimal digit register. Any number up to 99,999 can be preset into the instrument, and upon reaching the corresponding charge a relay closes to actuate a warning device or control auxiliary equipment. In applications where X-rays are being generated, this feature affords protection against accidental over-exposure.

Input current of either polarity can be measured and integrated, and a front panel switch enables the instrument to be immediately changed from one polarity to the other. Advanced circuit techniques have been employed to achieve low input impedance, negligible drift, and a high overall accuracy and reliability.

Two models are available with the same specifications except for the method of presetting. In the Model A309A the presetting means consists of five front-panel switches. Presetting in the Model A309B is accomplished by manual adjustment of five presetting wheels that are accessible through the hinged cover of the register used in this model.

SPECIFICATIONS

1. Input current for full-scale meter deflection — 1 x 10^{-3} to 3 x 10^{-9} ampere in twelve switch settings.
2. Polarity of input current — positive or negative, controlled by front-panel switch.
3. Current indicating means — 4½″ meter.
4. Charge indicating means — 5-decimal-digit register and 2½″ meter
5. Maximum charge indicating capacity — 99,999 units.
   Note: Each unit is equal to one coulomb multiplied by the numerical value of the full-scale current.
6. Maximum integrating time — 28 hours.
7. Integrating rate for full-scale current — 1 unit per second.
8. Method of presetting:
   Model A309A — five front-panel switches.
   Model A309B — five presetting wheels in register.
9. Accuracy (Indicating and integrating accuracy, based on full-scale current) — 1%.
10. Maximum drift — .01% per hour.
11. Maximum input voltage for full-scale current — 2 millivolts.
12. Minimum signal-source impedance for 1% accuracy — 1 ohm divided by numerical value of full-scale current.
13. Calibration — Internal reference current provided for each current range.
14. Power Input — 110–125 volts, 50-60 cps.
15. Dimensions — 19″ wide x 8¾″ high x 13¼″ deep.
16. Mounting — standard 19″ relay rack.
17. Weight — approximately 25 lbs.
18. Price: Model A309A — $1674.00.
    Model A309B — $1524.00.

ELCOR, — INC. • 1225 W. BROAD STREET • FALLS CHURCH, VA.
Telephone JEfferson 2-7718
A subsidiary of Fairfax Manufacturing Co., Inc.
Bulletin No. 24-1258

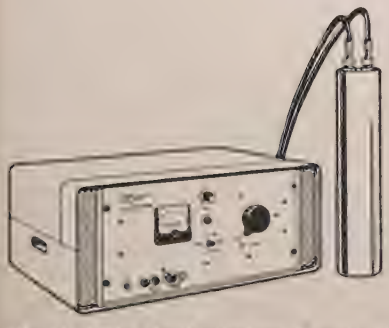

* the Kaman neutron source
small - lightweight - portable

10^7 neutron/pulse - nominal.
5 microseconds — pulse length.
Adjustable - 1-10 pulses/sec.
H^3 (d, n) He^4 reaction.
Accelerator Unit — 4" OD x 18" long.
Control Unit — 21¾" x 15¼" x 10½".

The NT-60-8 Pulsed Neutron Generator Assembly . . . an Exclusive Development by

KAMAN NUCLEAR
COLORADO SPRINGS, COLORADO
A Division of the Kaman Aircraft Corporation

Research and Development in Nuclear Weaponry and Instrumentation.

The place of the Particle Accelerator in Basic Research...

Neutron Activation Analysis-XI

The irradiation of most atomic nuclei by very slow (thermal-velocity) neutrons causes these nuclei to become radioactive. The subsequent emission of beta or gamma radiations from these nuclei is characteristic of the particular isotope. If the *energy* and *rate of emission* of the radiations are known, the isotope can be identified.

The *magnitude* of the radioactivity is directly related to the amount of the isotope present in the neutron-bombarded sample. Since the detection of radioactivity is an extremely sensitive technique, to the point that individual particles or quanta of radiation can be counted, neutron activation analysis permits the accurate appraisal of very small amounts of an element — often smaller than can be readily detected by normal analytical techniques.

Advantages in Activation Analysis

Neutrons are able to pass through a considerable thickness of most substances. It is possible, therefore, to analyze materials in solid, liquid, or gaseous phases, usually with a minimum of sample preparation. A relatively short time is expended in a single analysis — an advantage where large numbers of samples are involved. The radioactivity created in the process is, for the most part, of short duration and low intensity, necessitating only reasonable care in the handling of the bombarded samples.

Neutron activation analysis is a relatively new technique whose scope is limited only by the ingenuity of the analyst. For example, isotopes which appear to be insensitive to the thermal-neutron activation method can often be detected by fast-neutron reactions or through charged-particle bombardment.

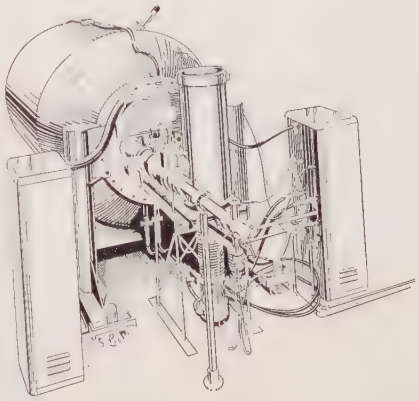

Horizontal 3-Mev Type K Van de Graaff giving neutron output up to 6 × 10^{11} neutrons per second.

The Van de Graaff® as a Neutron Source

Prolific neutron outputs are obtainable from Van de Graaff positive-ion accelerators, from the Be^9 (d, n) B^{10} reaction. The neutrons from this reaction emerge from the beryllium target in all directions with an angular distribution which is not quite isotropic, but has an assymetry in the forward direction of the deutron beam of about 2:1.

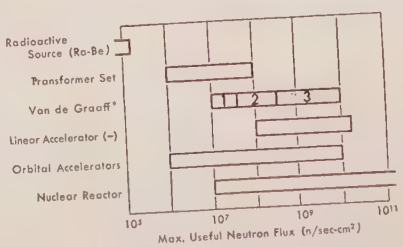

Chart showing comparative neutron fluxes obtainable with various sources. (The numbers in the Van de Graaff bar designate the maximum voltage ratings of the accelerators).

The neutrons emerge with energy groups in the 0.7- to 7-Mev range. To slow these energetic neutrons down to "thermal" velocities (in the region of 2200 meters/second, corresponding to about 0.02 ev), a moderating mass of paraffin, water, or similar hydrogenous material surrounds the neutron-producing target. Inside the moderator, thermal neutrons travel in all directions, producing a neutron flux measured in terms of neutrons per second passing through an area of one square centimeter (n/sec-cm²).

Samples can be placed inside the moderator for neutron bombardment, by inserting them into a hole about 2 cm from the target, to take advantage of the maximum flux. Reasonably large samples can often be accommodated in the volume within a 6-cm radius from the target, with a flux variation less than a factor of two, especially if they are aqueous solutions or organic materials.

Activation analysis offers solutions to many serious problems in research or in process control. Detailed information about activation analysis, including tabulation of thermal-neutron activation characteristics of the isotopes, is available on request.

High Voltage Servicing Company, Ltd.
London, England

High Voltage Engineering (Europa) N.V.
Amersfoort, The Netherlands

HIGH VOLTAGE ENGINEERING CORPORATION

BURLINGTON MASSACHUSETTS

It is with the deepest regret that we have to announce the sudden deaths of two members of our editorial board,

CORNELIS JAN BAKKER *of CERN*

and

DONALD J. HUGHES *of Brookhaven National Laboratory.*

The rôles of Bakker and Hughes in contemporary physics are well known to the readers of this journal. By dedicating this issue of our journal to them we express our deep gratitude to our two passed friends and collaborators.

THE EDITOR

NUCLEAR INSTRUMENTS AND METHODS 7 (1960) 101–112; NORTH-HOLLAND PUBLISHING CO.

MULTI-PURPOSE MAGNETIC PARTICLE ANALYZER †

ROBERT L. BURMAN and AVIVI I. YAVIN

Physics Department, University of Illinois, Urbana, Illinois

Received 7 January 1960

A flexible magnetic particle analyzer is proposed. It will be used as (1) a broad range spectrograph; (2) a high intensity spectrometer; and (3) a high resolution spectrometer free of kinematic broadening effects.

1. Introduction

A double focussing magnet as a spectrometer was described in 1946 by Svartholm and Siegbahn[1]). They showed that if $B(r) \propto 1/r^{\frac{1}{2}}$ in the neighborhood of $r = R$ (where R is the radius of the 360° magnet), a point source of monoenergetic charged particles will come to a focus at an angle $\theta = 2^{\frac{1}{2}}\pi = 254.56°$ in both the radial and axial directions.

Judd[2]) discussed the question of two directional focussing for different field indices n (where $n = -(r/B)\,(\mathrm{d}B/\mathrm{d}r)$), and different magnet angles θ††. He treated the case in which both object and image are located outside the magnetic field. The equations which he derived are very useful for any magnet, although only the first order effects were considered in this paper. The equations are:

$$\tan^{-1}n^{1/2}d_0 + \tan^{-1}n^{1/2}d_z + n^{1/2}\theta = \pi \qquad (1)$$

and

$$\tan^{-1}(1-n)^{1/2}d_0 + \tan^{-1}(1-n)^{1/2}d_r + (1-n)^{1/2}\theta = \pi\,, \qquad (2)$$

where d_0 is the object distance (as measured from the entrance face of the magnet) and d_z and d_r are the axial and radial image distances respectively (as measured from the exit face of the magnet). All distances in Judd's paper are in units of R.

† This work was supported in part by the joint program of the U. S. Atomic Energy Commission and the U. S. Office of Naval Research.

†† Note that in the Svartholm-Siegbahn case $n = \frac{1}{2}$ and $\theta = 360°$.

$$M_r = [(1-n)^{1/2}d_0 \sin(1-n)^{1/2}\theta - \cos(1-n)^{1/2}\theta]^{-1}\,, \qquad (3)$$

where M_r is the radial magnification. The dispersion D_p is given by

$$D_\mathrm{p} = \frac{\delta x}{\delta P/P} = \frac{1+M_r}{1-n} \qquad (4)$$

where δx is the normal displacement from the optical axis of an image point of particles with momentum $P + \delta P$. The resolution Q can be expressed as

$$Q = \frac{P}{\delta P} = \frac{D_P}{S'} = \frac{D_P}{\alpha M_r S} = \frac{1+M_r}{\alpha M_r S\,(1-n)}\,, \qquad (5)$$

where S' is the collector slit width, α is a number somewhat greater than unity (the aberration factor), and S is the source width. These five equations are sufficient for calculations of object and image distances, dispersion and resolution, slit sizes for a required resolution, etc. A 180° double focussing spectrometer utilizing the $n = \frac{1}{2}$ principle was constructed at the California Institute of Technology[3]).

Judd and Bludman[4]) extended Judd's previous calculations to include aberration and fringing effects by expanding the field in the power series given by

$$B_z(r)_{z=0} = B_0\,[1 - \tfrac{1}{2}\rho + (\beta_0 + \beta_1 a + \beta_2 a^2 + \ldots)\rho^2 + (\gamma_0 + \gamma_1 a + \ldots)\rho^3 + \ldots]\,, \qquad (6)$$

[1]) N. Svartholm and K. Siegbahn, Arkiv för Math., Astr, och Fysik **33**, No. 21 (1946).

[2]) D. L. Judd, Rev. Sci. Instr. **21** (1950) 213.

[3]) C. W. Snyder, S. Rubin, W. A. Fowler and C. C. Lauritson, Rev. Sci. Instr. **21** (1950) 852.

[4]) D. L. Judd and S. A. Bludman, Nucl. Instr. **1** (1957) 46.

where $\rho = (r - R)/R$, $B_0 = p/eR$, and a is the distance along the optical axis over which the fringing field decreases by an order of magnitude (about one magnet gap length). The machining of a magnet to take care of these second and third order effects is difficult due to the complex field configuration required. A magnet of this type which has been constructed by Asaro and Perlman at the University of California has an energy resolution of 0.1% for a solid angle of 0.009 steradians.

Double focussing can be achieved by a uniform-field magnet by either utilizing fringing field effects or by using a quadrupole magnet. The first method was discussed by Cross[5]) who showed that axial focussing is achieved in the regions of the fringing field provided the particles enter and leave the magnet at an angle ε (between the path of the particle and the face of the magnet) different from 90°. The magnet angle θ should be small so that the particles will spend an appreciable amount of time in the fringing field (relative to the time they spend in the main field). This requirement causes the object and image distances to be large and therefore impractical for small experimental rooms. An additional disadvantage is that the solid angle becomes smaller as the magnet angle θ is decreased.

Browne and Buechner[6]) suggested a broad range magnetic spectrograph. Their spectrograph has a uniform magnetic field with a circular boundary of radius R. The source is placed at a distance R from the edge of the field. Particles with energy E_0 will be deflected 90° and will focus radially at a distance R from the exit face of the magnet. Other particles with $0.5\,E_0 \leq E \leq 1.2\,E_0$ will focus on a hyperbolic surface with the origin being at the center of the circle defined by the boundary of the field.

Enge[7]) suggested a combined magnetic spectrograph and spectrometer. He added a quadrupole magnet to the Browne-Buechner spectrograph, resulting in axial focussing with an axial image distance which could be adjusted to the now slightly changed radial image distance. When the quadrupole magnet is turned off, the main magnet can be used as a broad range spectrograph. With the quadrupole magnet on, the range of energies is narrowed but the intensity of each energy component increases so that the combination of the two magnets (hereafter referred to as a spectrometer) becomes more suitable for electronic counting techniques. Enge suggested that the main magnet be placed with its medium plane perpendicular to the scattering plane when it is used as a spectrograph, and with its medium plane parallel to the scattering plane when it is used as a spectrometer. We shall refer to the former position as the "perpendicular position" and the latter one as the "parallel position".

Mileikowsky[8]) suggested an astigmatic magnet with $n \neq 0.5$ and therefore $d_z \neq d_r$, in order to avoid kinematic broadening of the image point. This kinematic broadening is caused by the motion of the recoil nucleus in combination with the finite size of the angular aperture of the entrance to the magnet. It can be shown that when light elements are used as targets, the kinematic energy spread for a scattering-angle aperture of 1° can be one order of magnitude greater than the resolution. Enge[7]) showed that the kinetic broadening could be eliminated to a first order by rotating the Browne-Buechner spectrograph to the parallel position and turning the quadrupole magnet on.

A suggestion is made in this paper to apply Mileikowsky's idea of an astigmatic magnet to Enge's spectrometer. The magnet used in Enge's spectrometer should be kept in the perpendicular position when used both as a spectrograph and as a spectrometer. The current in the quadrupole magnet can now be adjusted to yield any value of $d_z - d_r$. It will be possible to cover the continuous region from complete astigmatism ($d_z = \infty$) and therefore small effective solid angle to no astigmatism ($d_z = d_r$) and therefore large effective solid angle. The relative ease of the continuous adjustment of

[5]) W. G. Cross, Rev. Sci. Instr. **22** (1951) 717.

[6]) C. P. Browne and W. W. Buechner, Rev. Sci. Instr. **27** (1956) 899.

[7]) H. A. Enge, Rev. Sci. Instr. **29** (1958) 885.

[8]) C. Mileikowsky, Arkiv för Fys. **7** (1954) 57.

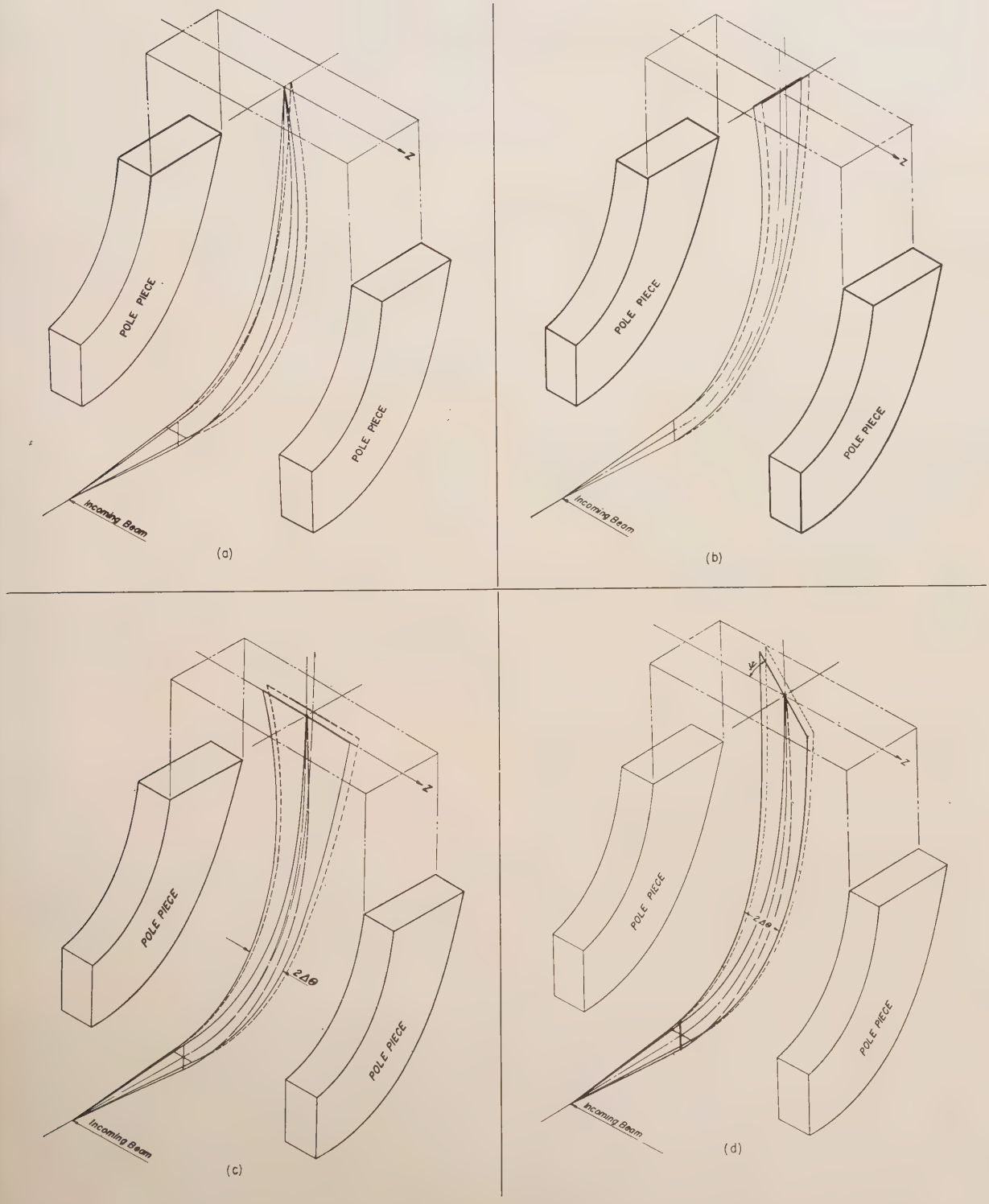

Fig. 1. Astigmatic correction for the kinematic broadening in a 90° deflection magnet. Spectral images for two energetically-neighboring reaction channels for (a) a stigmatic magnet and a recoil nucleus of infinite mass; (b) a stigmatic magnet and a recoil nucleus of finite mass; (c) an astigmatic magnet and a recoil nucleus of infinite mass; and (d) an astigmatic magnet and a recoil nucleus of finite mass.

$d_z - d_r$ is very advantageous and should be compared with the difficulty of adjusting n, which in effect means adjusting $d_z - d_r$, in the Mileikowsky case.

2. Kinematic Broadening

The Q-value equation for the reaction in which particle 1 is impinging on a target nucleus 2 and particle 3 is scattered leaving a residual nucleus 4 is[9])

$$Q = E_3\left(1 + \frac{m_3}{m_4}\right) - E_1\left(1 - \frac{m_1}{m_4}\right) - \\ - \frac{2}{m_4}(E_1 E_3 m_1 m_3)^{1/2}\cos\theta\,, \quad (7)$$

where θ is the laboratory scattering angle. When eq. (7) is differentiated with respect to θ, and the terms are rearranged, the result expressed in per cent energy change per degree is

$$\frac{\partial E_3}{E_3 \partial\theta} = -\frac{2\,(m_1 m_3 E_1/E_3)^{1/2}\sin\theta}{m_3 + m_4 - (m_1 m_3 E_1/E_3)^{1/2}\cos\theta}\,\frac{100\pi}{180}\,. \quad (8)$$

For the elastic scattering of alpha particles from C^{12} at scattering angle 90° eq. (8) yields

$$\frac{\Delta E_3/E_3}{\Delta\theta} \approx 1.2\%\ \mathrm{deg}^{-1}\,.$$

This kinematic broadening puts a severe limitation on the solid angle (see figs. 1a, b).

If now a reaction-particle spectrometer (with $B \propto 1/r^n$) is placed in the perpendicular position, n is made different from 0.5 and the detector plate is placed in the radial image point, the image will be a line in the axial direction. This line will be parallel to the axial (z) direction when the recoiled nucleus has an infinite mass so that no kinematic broadening exists (see fig. 1c) whereas for a recoiled nucleus with a finite mass the line will be tilted with respect to the axial direction by an angle ψ (see fig. 1d). Groups of identical particles which leave the residual nucleus at closely spaced energy levels will still be distinguishable, since the kinematic effect is now displayed at the ends of the lines (causing similar tilts to all spectral lines), and the resolving power and solid angle are preserved. In fact, if the n is changed from 0.5 to 0.6, the resolution improves slightly[2]). If $2l$ is the length of the astigmatic image line, then $2l\sin\psi$ is the line width due to the kinematic broadening. Mileikowsky suggested that

$$2l \simeq \tfrac{1}{2}G \quad (9)$$

where G is the gap width. Judd[2]) showed that for n near $\frac{1}{2}$, the astigmatism for $\theta = \pi$ and $d_0 \approx d_z \approx d_r$ is

$$d_z - d_r = 5\,(1 - 2n)\,R^{\dagger}\,. \quad (10)$$

These two relations (9, 10) yield

$$n \approx \frac{1}{2}\left(1 - \frac{G}{20R\tan\Delta\theta}\right) \quad (11)$$

where $2\Delta\theta$ is the acceptance scattering angle. Mileikowsky suggested that the best way of adapting an $n = 0.5$ magnet to an astigmatic magnet is to insert thin plane sheets of iron between each pole piece and the yoke.

Assuming a unit magnification in both radial and axial directions, and using equation (10) the tilting angle can be expressed as

$$\psi = \tan^{-1}\left[-\frac{2}{5}\frac{1}{(1-n)(2n-1)} \times \right. \\ \left. \times \frac{(m_1 m_3 E_1/E_3)^{1/2}\sin\theta}{m_3 + m_4 - (m_1 m_3 E_1/E_3)^{1/2}\cos\theta}\right]. \quad (12)$$

It is clear from eq. (12) that ψ depends on the mass m_3 of the scattered particles. This property makes it possible to distinguish between two scattered particles of the same magnetic rigidity, but different masses.

EXAMPLE 1

Consider 40 MeV alpha particles impinging on a C^{12} target. Let the magnet accept particles at a scattering angle of 90°. The elastically scattered alpha particles will have an energy of 20 MeV. On the other hand, protons from the reaction $C^{12}(\alpha, p)N^{15}$ will have the same magnetic rigidity if the N^{15} is left at a level of excitation ≈ 8 MeV. If we choose $n = 0.6$, the

[9]) David Halliday, Introductory Nuclear Physics, (John Wiley & Sons, Inc., New York, 1950) p. 378.

† Note that Judd expressed his equations in units of R, so he wrote equation (10) as $d_z - d_r = 5\,(1 - 2n)$.

tilting angle for the elastically scattered alpha particles will be

$$\psi_\alpha = \tan^{-1}\left[-\frac{2}{5}\frac{1}{0.4\cdot 0.2}\frac{(4\cdot 4\cdot 2)^{1/2}}{4+12}\right] = -60.5^\circ .$$

The tilting angle for the protons will be

$$\psi_p = \tan^{-1}\left[-\frac{2}{5}\frac{1}{0.4\cdot 0.2}\frac{(4\cdot 1\cdot 2)^{1/2}}{1+15}\right] = -41.5^\circ .$$

Since there is a difference of 19° between the two angles it should be easy to distinguish between the two lines except for the central region where they overlap.

It is clear also from eq. (12) that ψ depends on the mass m_2 of the target nuclei. This property makes it possible to distinguish between idéntical particles scattered from different isotopes of the same element, or from target contaminations.

EXAMPLE 2

Consider alpha particles impinging on a natural carbon target. This target consists of nuclides C^{12} and C^{13} as well as contaminations such as O^{16}, etc.

With $n = 0.6$, the tilting angles for the elastically scattered alpha particles at 90° are

$$\psi = -60.5^\circ \text{ for } C^{12}(\alpha,\alpha)C^{12} ,$$

$$\psi = -58.3^\circ \text{ for } C^{13}(\alpha,\alpha)C^{13} ,$$

and,

$$\psi = -52.2^\circ \text{ for } O^{16}(\alpha,\alpha)O^{16} .$$

It is evident that in addition to the difference in energy between the groups of alpha particles, there is also a slight but still noticeable difference in the tilting angles.

3. The Browne-Buechner Broad Range Spectrograph

The Browne-Buechner spectrograph has a uniform magnetic field with a circular boundary of radius R and center at C (see fig. 2). If a source of monoenergetic particles is placed at a radius R from the edge of the field†, an image will be formed at a distance R† from the exit edge of the field if the radius of curvature (of the central ray) is R. The angle of deflection in this case is 90°. A minimum aberration is possible in such an arrangement for a given angular

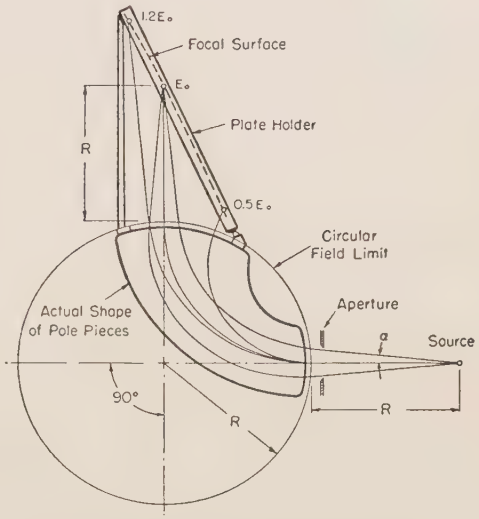

Fig. 2. Schematic drawing of spectrograph.

spread at the source[10]). Moreover, the circular boundary provides for a normal entrance and exit for the central ray of any other monoenergetic group of particles differing in energy by 50 (or even 100) per cent from the energy of the first group. The various groups will have different radii of curvature for the central rays, but each group can simultaneously come to a focal point. These focal points lie on a well defined (hyperbolic) focal surface. This magnet is called a broad range spectrograph since it provides for a simultaneous recording of a broad range of energies.

3.1. RADIAL FOCUSSING

By using the first-order focussing theory of Barber we can easily derive the radial focussing properties of the Browne-Buechner type of magnet. The geometry of the problem is illustrated in fig. 3. The object and image distances (as measured from the faces of the magnet) are d_0 and d_r respectively, and the radius of

† The distance from the face of the pole piece should be $R + 2G$, since the effective radius (including the effect of the fringing field) is $R + G$.

[10]) E. Segrè, Experimental Nuclear Physics (John Wiley & Sons, Inc., New York, 1953) p. 589; (the paper is by K. T. Bainbridge).

curvature of the particle in the magnetic field is r. Our derivation follows that in the article[6]) by Browne and Buechner.

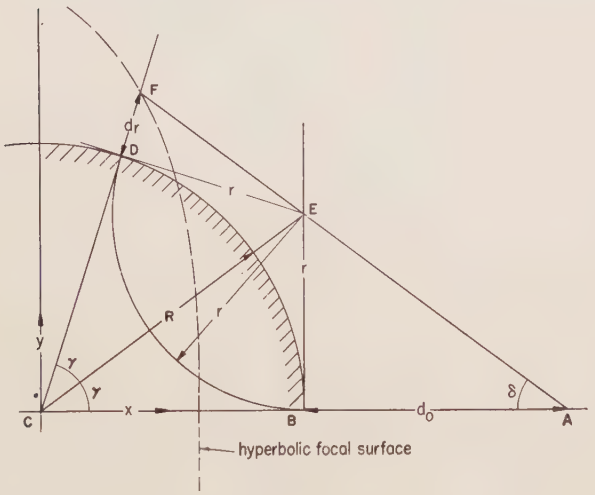

Fig. 3. Drawing for focus theory calculations.

Since the triangles EBC and EDC are congruent, the angle ∠ EDC is a right angle. Hence the beam enters and leaves normal to the boundary of the magnetic field, and we can use the first order theory of Barber's rule to locate the image point F. As shown in fig. 3, we construct the line through $\overline{AE}$ to intersect the line through $\overline{CD}$ at the point F. Using the x-y axes shown, we find the position of the focal point as a function of r as follows:

$$x = \overline{CF} \cos 2\gamma$$

$$y = \overline{CF} \sin 2\gamma ,$$

and

$$\frac{\overline{CF}}{\sin \delta} = \frac{R + d_0}{\sin (\pi - 2\gamma - \delta)} = \frac{R + d_0}{\sin 2\gamma \cos \delta + \cos 2\gamma \sin \delta};$$

thus

$$\overline{CF} = \frac{R + d_0}{\sin 2\gamma \cot \delta + \cos 2\gamma} .$$

As a function of the radius of curvature, we have

$$\sin\gamma = \frac{r}{\sqrt{r^2 + R^2}}, \cos\gamma = \frac{R}{\sqrt{r^2 + R^2}}, \text{ and } \cot\delta = \frac{d_0}{r} ,$$

so that

$$\overline{CF} = \frac{(R + d_0)(R^2 + r^2)}{2d_0R + R^2 - r^2} . \qquad (13)$$

Thus we get

$$\begin{cases} x = \dfrac{(R + d_0)(R^2 - r^2)}{2d_0R + R^2 - r^2} \\ \\ y = \dfrac{(R + d_0)(2rR)}{2d_0R + R^2 - r^2} . \end{cases}$$

3.2. FOCAL SURFACE

If we write the solution for the focal point as

$$\begin{cases} x = \dfrac{H(R^2 - r^2)}{G - r^2} \\ \\ y = \dfrac{H2rR}{G - r^2} , \end{cases} \qquad (14)$$

where $H = R + d_0$ and $G = 2d_0R + R^2$, we can eliminate r to get

$$\left[x - \frac{H(G + R^2)}{2G}\right]^2 - \frac{y^2(H - R)^2}{G} = \frac{H^2(G + R^2)^2}{4G^2} - \frac{H^2R^2}{G} , \qquad (15)$$

which gives the focal surface as a hyperbola. For the special case $d_0 = R$ (the condition under which the Browne-Buechner magnet is usually operated) we have the focal line

$$(x - \tfrac{4}{3}R)^2 - \tfrac{1}{3}y^2 = \tfrac{4}{9}R^2 . \qquad (16)$$

This hyperbola has its center at $(\frac{4}{3}R, 0)$ and the focal point at the origin C. The asymptotic slopes are $\pm\sqrt{3}$, so that, if we define the useful range of r by the requirement that the focal point be a finite distance outside the magnet, we want $x^2 + y^2 > R$ and $2\gamma < \tan^{-1}(-\sqrt{3})$, or $R/\sqrt{3} < r < \sqrt{3}\,R$.

If we define E_0 to be the energy corresponding to $r = R$, the magnet will simultaneously focus particles with energies from $\frac{1}{3}E_0$ to $3E_0$ along the hyperbolic focal surface (eq. (16)). The effect of the fringing field will, in general, further restrict the usable energy range. A practical range is $0.5E_0 \leq E \leq 1.2E_0$.

3.3. DISPERSION

We define the dispersion as $(E/R)\,(\mathrm{d}s/\mathrm{d}E)$, where s is the arc length along the hyperbolic focal line. Since $E \propto r^2$ we use $E\,(\mathrm{d}/\mathrm{d}E) = \frac{1}{2}r\,(\mathrm{d}/\mathrm{d}r)$ and find

$$\frac{E}{R}\frac{\mathrm{d}s}{\mathrm{d}E} = \frac{r}{2R}\frac{\mathrm{d}s}{\mathrm{d}r} = \frac{r}{2R}\sqrt{\left(\frac{\mathrm{d}x}{\mathrm{d}r}\right)^2 + \left(\frac{\mathrm{d}y}{\mathrm{d}r}\right)^2}\,, \quad (17)$$

where

$$\frac{\mathrm{d}x}{\mathrm{d}r} = -\frac{4\,(R + d_0)\,r d_0 R}{(2d_0R + R^2 - r^2)^2}$$

$$\frac{\mathrm{d}y}{\mathrm{d}r} = \frac{2\,(R + d_0)\,(2d_0R^2 + r^2R + R^3)}{(2d_0R + R^2 - r^2)^2}\,,$$

so that we have the dispersion D as

$$D = \frac{E}{R}\frac{\mathrm{d}s}{\mathrm{d}E} = \frac{r(R + d_0)}{(2d_0R + R^2 - r^2)^2} \times$$

$$\times \sqrt{4d_0\,(d_0r^2 + d_0R^2 + r^2R + R^3) + (R^2 + r^2)^2}\,. \quad (18)$$

Again, specializing to the case $d_0 = R$

$$D' = \frac{E}{R}\frac{\mathrm{d}s}{\mathrm{d}E} = \frac{2rR}{(3R^2 - r^2)^2}\sqrt{9R^4 + 10R^2r^2 + r^4}\,. \quad (19)$$

3.4. MAGNIFICATION

Using fig. 4 we shall calculate the magnification M_s defined as $\Delta s/\Delta h$, where Δs is the shift along the focal line caused by a lateral displacement Δh of the source. We then have

$$\Delta h = (R + d_0)\,\Delta\gamma \quad \text{and} \quad \Delta s = \frac{(R + d_r)\,\Delta\gamma}{\sin\beta}\,,$$

so that

$$M_s = \frac{R + d_r}{(R + d_0)\sin\beta}\,. \quad (20)$$

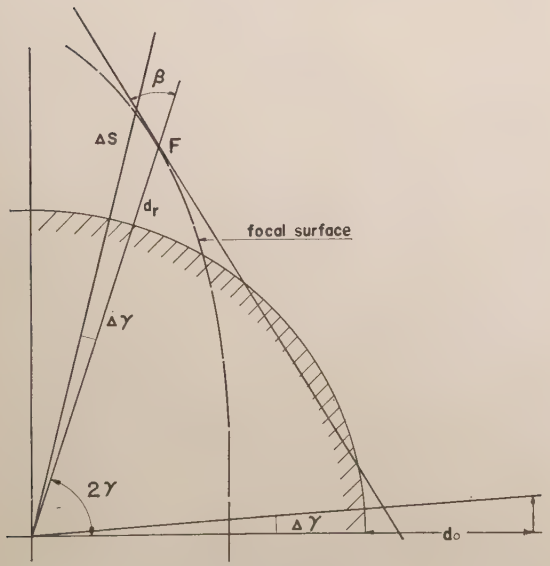

Fig. 4. Drawing for magnification calculations.

Here,

$$\beta + 2\gamma = \tan^{-1}\left(\frac{\mathrm{d}y}{\mathrm{d}x}\right),$$

so that

$$\sin\beta = \frac{\sin 2\gamma}{\sqrt{1 + \left(\frac{\mathrm{d}y}{\mathrm{d}x}\right)^2}} - \frac{\mathrm{d}y}{\mathrm{d}x}\frac{\cos 2\gamma}{\sqrt{1 + \left(\frac{\mathrm{d}y}{\mathrm{d}x}\right)^2}}\,. \quad (21)$$

Then, using eqs. (17) and (13), we find

$$M_s = \frac{\left(\frac{R + d_r}{R + d_0}\right)\frac{2R}{r}\left(\frac{E}{R}\frac{\mathrm{d}s}{\mathrm{d}E}\right)}{\frac{\mathrm{d}y}{\mathrm{d}r}\cos 2\gamma - \frac{\mathrm{d}x}{\mathrm{d}r}\sin 2\gamma}$$

or,

$$M_s = \frac{R^2 + r^2}{r\,(R + d_0)}\left(\frac{E}{R}\frac{\mathrm{d}s}{\mathrm{d}E}\right) = \frac{R^2 + r^2}{r\,(R + d_0)}\,D\,. \quad (22)$$

3.5. ABERRATION

For $d_0 = r = R$ (90° deflection) the particle paths are symmetrical about the central ray. The focussing condition is then good to second order, and the aberration will depend on α^3, where α is the half-angle of acceptance shown in fig. 2. At deflection angles other than 90° the aberration will be proportional to α^2. Measurements of the aberration given by Browne and Buechner[6]) agree with these predictions. They further indicate that it is not the aberration which limits the resolution, but rather source size, target thickness, initial beam energy resolution, etc.

3.6. LINE TILTING

We would expect a point source to form a line image, since the $n = 0$ magnet has no axial focussing. As shown in section 2, the line image will be tilted at an angle ψ; the situation for the Browne-Buechner magnet is shown in fig. 5. Particle number 1, which emerges at an angle larger than θ, has a lower energy in the laboratory than the normal particle, number 2, which emerges at the angle θ, while particle number 3 has a larger energy than number 2. The tilting angle is then given by

$$\tan\psi = \frac{\Delta s}{\Delta z}$$

where Δs can be found from the dispersion

formula, eq. (19), with the energy shift ΔE given by eq. (8). Since there is no axial focussing, we have

$$\Delta z = (2 + \tfrac{1}{2}\pi)\, R\Delta\theta\,.$$

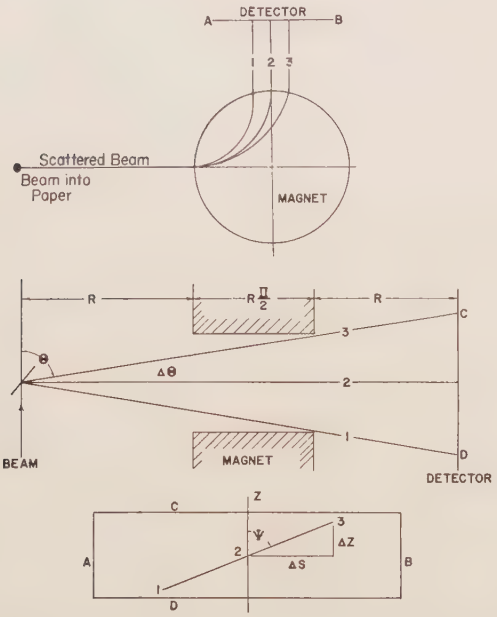

Fig. 5. Line tilting for the Browne-Buecher magnet.

Then

$$\tan\psi = \frac{\Delta s}{\Delta z} = \frac{DR\,\dfrac{\Delta E_3}{E_3}}{(2 + \tfrac{1}{2}\pi)\, R\Delta\theta} = \frac{DR\,\dfrac{1}{E_3}\dfrac{\partial E_3}{\partial\theta}\Delta\theta}{(2 + \tfrac{1}{2}\pi) R\Delta\theta} = \frac{2D\,\dfrac{1}{E_3}\dfrac{\partial E_3}{\partial\theta}}{4 + \pi}$$

or

$$\psi = \tan^{-1}\left[-\frac{4D}{4+\pi}\,\frac{\sqrt{m_1 m_3 E_1/E_3}\,\sin\theta}{m_3 + m_4 - \sqrt{m_1 m_3 E_1/E_3}\,\cos\theta}\right]. \tag{23}$$

3.7. SOLID ANGLE

Using $\Delta\theta$ as the half angle of acceptance (in degrees) of the scattered beam in the scattering plane, and α as the half-angle (in degrees) in the perpendicular plane, the solid angle subtended by the magnet is

$$\Omega \simeq 4\,\alpha\Delta\theta\left(\frac{\pi}{180}\right)^2 \quad \text{steradians.} \tag{24}$$

The angle $\Delta\theta$ is limited by the gap width of the magnet. For G equal to the gap width,

$$\Omega_G = 2\alpha\,\frac{\pi}{180}\,\frac{G}{(1 + \tfrac{3}{2}\pi) R} \simeq$$

$$\simeq 1.36 \times 10^{-2}\alpha\,\frac{G}{R} \quad \text{steradians}\,. \tag{25}$$

The angle α is essentially limited by effects of the fringing field to be less than 2.5°. The solid angle subtended at the detector will be further reduced by the width W (in the axial direction) of the sensitive surface.

$$\Omega_W = 2\alpha\,\frac{\pi}{180}\,\frac{W}{(1 + \tfrac{1}{2}\pi) R} \simeq$$

$$\simeq 9.75 \times 10^{-3}\alpha\,\frac{W}{R} \quad \text{steradians}\,. \tag{26}$$

4. The Combined Magnetic Spectrograph and Spectrometer

The combined magnetic spectrograph and spectrometer which was suggested by Enge[7]) is a combination of a Browne-Buechner spectrograph and a quadrupole magnet. The quadrupole magnet, which precedes the spectrograph, provides the axial focussing which is missing in the regular Browne-Buechner magnet, and so converts the spectrograph into a double focussing spectrometer (see fig. 6). Most of the features (such as resolution, small aberration, etc.) are preserved to a great extent especially at an angle of deflection 90°, whereas the solid angle is increased. Enge indicates that when the spectrometer is turned into the parallel position, the kinematic broadening can be mostly eliminated.

We would like to suggest that it is more advantageous to keep the magnet in the perpendicular position when the magnet is used both as a spectrograph and a spectrometer. The reasons are two: (1) the acceptance angle 2α in the medium plane of the magnet is geometrically larger than the acceptance angle 2β in the other plane (the plane parallel to the direction of the field). In angular distribution work, the acceptance scattering angle $2\Delta\theta$ should be as small as possible in order to preserve the structure of the distribution. For this reason it is advantageous to have $2\Delta\theta = 2\beta$, and the spectrometer in the perpendicular position.

(2) The cost of rotating the magnet from the perpendicular position when used as a spectrograph†, to the parallel position, when used as a spectrometer, is great. The kinematic broadening, on the other hand, can be eliminated by the use of Mileikowsky's idea.

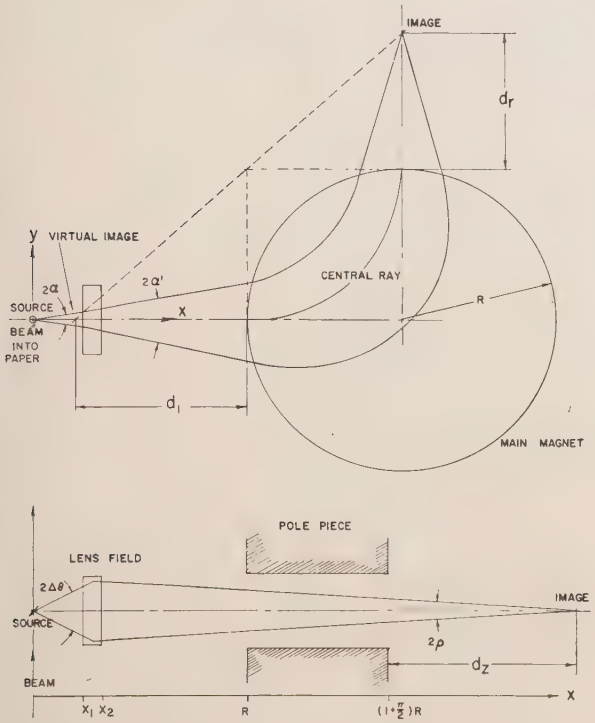

Fig. 6. Quadrupole lens and broad-range spectrograph magnet combined to form double focussing spectrometer.

4.1. QUADRUPOLE LENS

The radial focussing properties of the Browne-Buechner magnet are modified by the quadrupole lens only in that a virtual object, at a distance d_1 from the cylindrical field boundary, serves as the source for the main magnet. The quadrupole lens is assumed to provide the entire axial focussing for the system.

Assuming coordinate axes as shown in fig. 6, with the z-axis parallel to the magnetic field of the main magnet, the y-axis perpendicular to it, and the x-axis along the "normal" path of the scattered beam, we can calculate the focal properties of the quadrupole lens following Enge's treatment[7]). The magnetic field in the quadrupole lens is

$$B_z = -\frac{B_1}{a} y\,, \qquad B_y = -\frac{B_1}{a} z\,,$$

where B_1 is the field at the pole tips and "a" is the distance from the center line to the pole tips. The equations of motion of a charged particle in the lens are

$$\frac{\mathrm{d}^2 z}{\mathrm{d}x^2} + K^2 z = 0 \qquad \text{and} \qquad \frac{\mathrm{d}^2 y}{\mathrm{d}x^2} - K^2 y = 0\,, \quad (27)$$

where we have anticipated the correct convergence. Here

$$K^2 = \frac{B_1}{a} \cdot \frac{1}{Br}\,,$$

where Br is the magnetic rigidity (momentum per unit charge) of the particle. For the 90° deflection in the main magnet, we need $Br = B_0 R$ where B_0 is the field in the main magnet, and R is the radius of curvature of the boundaries. By applying the boundary condition that the logarithmic derivatives be continuous at the physical limits (x_1 and x_2) of the quadrupole lens, Enge obtains the following relationships:

$$d_z = x_2 - \frac{1}{K} \tan K(x_2 - \lambda_1) - R(1 + \tfrac{1}{2}\pi) \quad (28)$$

$$d_1 = R - x_2 + \frac{1}{K} \coth K(x_2 - \lambda_2) \quad (29)$$

$$\begin{cases} \lambda_1 = x_1 - \dfrac{1}{K} \tan^{-1}(Kx_1) \\ \lambda_2 = x_1 - \dfrac{1}{K} \coth^{-1}(Kx_1)\,, \end{cases} \quad (30)$$

where d_z is the distance to the axial image (the image formed by the quadrupole lens) and d_1 is the distance from the virtual image of the quadrupole magnet to the Browne-Buechner magnet. Eq. (28) holds exactly for $r = R$ (90° deflection); for the general case, the term $R(1 + \frac{1}{2}\pi)$ should be replaced by

$$R\left(1 + \pi - 2 \sin^{-1}\left(r/\sqrt{R^2 + r^2}\right)\right).$$

These relationships may be kept constant for different energy particles by making $K^2 = B_1/aRB_0$ a constant. This is most easily done by

† It has to be in this position because of the kinematic broadening. It is possible to correct slightly for this broadening by changing the position of the detector plates.

running the two magnets in series. Enge points out that the requirements that the hysteresis loops of the magnets track together limits the ratio of B_1 to B_0 to about $B_1/B_0 \leqslant 0.6$ to 0.7.

4.2. RADIAL FOCUSSING

Using the distance d_1 from eq. (21) in place of d_0, the radial focal surface is again a hyperbola as given by eq. (15). In particular, for a 90° deflection we have the focal point given by eq. (14) as

$$x = 0\,, \qquad y = R + \frac{R^2}{d_1}\,, \tag{31}$$

so that the radial image distance from the magnet is

$$d_r = \frac{R^2}{d_1}\,. \tag{32}$$

4.3. DISPERSION

The dispersion is given by eq. (18) with d_0 replaced by d_1. For 90° deflection,

$$D_s = \frac{E}{R}\frac{\mathrm{d}s}{\mathrm{d}E} = \frac{R + d_1}{2{d_1}^2}\sqrt{R^2 + 2Rd_1 + 2{d_1}^2}\,, \tag{33}$$

where D_s is the dispersion along the focal surface. If we want the dispersion along a direction normal to the particle trajectory, we need

$$D_n = D_s\,|\sin\beta\,|$$

where β is shown in fig. 4. From eq. (21) of the previous chapter

$$\sin\beta = \frac{(\mathrm{d}y/\mathrm{d}x)\cos 2\gamma}{\sqrt{1 + (\mathrm{d}y/\mathrm{d}x)^2}} - \frac{\sin 2\gamma}{\sqrt{1 + (\mathrm{d}y/\mathrm{d}x)^2}}$$

or, at 90° deflection ($r = R$), using eqs. (13) and (17)

$$|\sin\beta\,| = \frac{1}{D_s}\frac{R + d_1}{2d_1}\,. \tag{34}$$

The dispersion normal to the beam trajectory is then simply

$$D_n = \frac{R + d_1}{2d_1}\,. \tag{35}$$

4.4. MAGNIFICATION

The inverse focal length of the quadrupole lens in the x-y plane is

$$\frac{1}{f_y} = K\sinh K\,(x_2 - x_1) \tag{36}$$

and the distance from the first principal plane to the entrance face of the lens is

$$P_y = \frac{\cosh K\,(x_2 - x_1) - 1}{K\sinh K\,(x_2 - x_1)}\,. \tag{37}$$

Hence, since the object distance to the first focal plane is

$$x_y = x_1 + P_y - f_y\,, \tag{38}$$

we have the quadrupole magnification in the y-direction as

$$M_{Q_y} = \frac{f_y}{x_y}\,\frac{1}{x_1 K\sinh K\,(x_2 - x_1) + \cosh K\,(x_2 - x_1)}\,. \tag{39}$$

The magnification along the focal surface of the Browne-Buechner magnet (which follows the quadrupole magnet) is given by eq. (22) with d_0 replaced by d_1 and $r = R$; the product of this and M_{Q_y} yields

$$M_s = \frac{2RD_s/(R + d_1)}{x_1 K\sinh K\,(x_2 - x_1) + \cosh K\,(x_2 - x_1)}\,, \tag{40}$$

where D_s is the dispersion, $(E/R)\,(\mathrm{d}s/\mathrm{d}E)$. The magnification M_n along a line normal to the particle trajectory at the focal point is

$$M_n = M_s\,|\sin\beta\,|\,,$$

where $|\sin\beta\,|$ is given by eq. (34), so that

$$M_n = \frac{R/d_1}{x_1 K\sinh K\,(x_2 - x_1) + \cosh K\,(x_2 - x_1)}\,. \tag{41}$$

In the x-z plane the second focal length f_z and the principal plane distance P_z are

$$\frac{1}{f_z} = K\sin K\,(x_2 - x_1)$$

$$P_z = \frac{1 - \cos K\,(x_2 - x_1)}{K\sin K\,(x_2 - x_1)}\,. \tag{42}$$

Using the image distance

$$x'_z = (1 + \tfrac{1}{2}\pi)\,R + d_z - (x_2 - P_z + f_z)$$

we get

$$M_z = \frac{x'_z}{f_z} =$$

$$= [d_z + (1 + \tfrac{1}{2}\pi)\,R - x_2] \times$$

$$\times\, K\sin K\,(x_2 - x_1) - \cos K\,(x_2 - x_1)\,. \tag{43}$$

4.5. ASTIGMATISM AND LINE TILTING

The astigmatism, $d_z - d_r$, is found from eqs. (28) and (32)

$$d_z - d_r = x_2 - \frac{1}{K}\tan K(x_2 - \lambda_1) - R(1 + \tfrac{1}{2}\pi) - \frac{R^2}{d_1}. \tag{44}$$

From eqs. (27) and (28) we can find the emergent half angle ρ (see fig. 6) for a given half angle $\Delta\theta$:

$$\rho = -Kx_1 \frac{\cos K(x_2 - \lambda_1)}{\sin K(x_1 - \lambda_1)} \Delta\theta\,, \tag{45}$$

where $\tan\rho$ and $\tan\Delta\theta$ were replaced by ρ and $\Delta\theta$ respectively. The tilting angle ψ, is found from

$$\tan\psi = \frac{\Delta s}{\Delta z} = \frac{\Delta\theta R \dfrac{1}{E_3}\dfrac{\partial E_3}{\partial\theta} D}{(d_z - d_r)\rho},$$

where D is either D_s (eq. (33)) or D_n (eq. (35)). This leads to

$$\psi_{s,n} = \tan^{-1}\left[\frac{2RD_{s,n}}{d_z - d_r}\frac{\sin K(x_1 - \lambda_1)}{Kx_1\cos K(x_2 - \lambda_1)} \times \right.$$
$$\left. \times \frac{\sqrt{m_1 m_3 E_1/E_3}\sin\theta}{m_3 + m_4 - \sqrt{m_1 m_3 E_1/E_3}\cos\theta}\right]. \tag{46}$$

4.6. SOLID ANGLE

The quadrupole lens opening should be approximately equal to the gap width, G, of the main magnet. Since the maximum particle displacement in the y- or z- direction inside the lens is $a/\sqrt{2}$, we want $a \simeq G/\sqrt{2}$. Assuming that the quadrupole acceptance angles define the solid angles, we solve eqs. (27) with the boundary conditions

$$\begin{cases} y = \dfrac{a}{\sqrt{2}} & \text{at} \quad x = x_2 \\ \dfrac{dz}{dx} = 0 & \text{at} \quad z = \dfrac{a}{\sqrt{2}} \end{cases}$$

to get the maximum solid angle

$$\Omega \simeq 4\tan(\Delta\theta)\tan\alpha$$
$$= 4\left[\frac{a}{\sqrt{2}}K\cos K(x_1 - \lambda_1)\right]\left[\frac{a}{\sqrt{2}}K\frac{\sinh K(x_1 - \lambda_2)}{\cosh K(x_2 - \lambda_2)}\right]$$

or

$$\Omega = 2a^2K^2\cos K(x_1 - \lambda_1)\frac{\sinh K(x_1 - \lambda_2)}{\cosh K(x_2 - \lambda_2)}. \tag{47}$$

In practice, however, the solid angle will probably be limited by an aperture, with limits of $\Delta\theta \leqslant 1°$ and $\alpha' \leqslant 2.5°$. The ratio of α' (see fig. 6) to α is

$$\frac{\alpha'}{\alpha} = \frac{\sinh K(x_2 - \lambda_2)}{\sinh K(x_1 - \lambda_2)}. \tag{48}$$

4.7. OPERATION

The parameters of the quadrupole lens are a, x_1, x_2 and $K^2 = B_1/aRB_0$. The magnet gap fixes a minimum value for a, while space limitations define x_1. An appropriate x_2 is then selected. Variations of K through the ratio B_1/B_0 can then be used to vary the tilting angle $\psi_{s,n}$ and the axial image size $(d_z - d_r)\rho$.

5. Examples

5.1. SPECTROGRAPH

Results of sample calculations based on the formulae of section 3 assuming $R = 66$ cm, and $d_0 = r = R$ are listed:

$$D = \frac{E}{R}\frac{ds}{dE} = \sqrt{5}\,, \qquad M_s = \sqrt{5}\,.$$

An energy resolution of 1/1000 corresponds, then, to a displacement at the detector of $\Delta s = 1.47$ mm and a maximum object width of 0.66 mm. Using the data of Example 1 from section 2, the calculated tilting angle for $C^{12}(\alpha,\alpha)C^{12}$ is $\psi = -23.9°$, while for the reaction $C^{12}(\alpha, p)N^{15}$ we find $\psi = -12.0°$. The solid angle of the system with a detector slit of 2 cm and an acceptance angle $\alpha = 2.5°$, is 7.4×10^{-4} steradians.

5.2. SPECTROMETER

Sample calculations from the formulae of section 4, using $R = 66$ cm, $a = 1.1$ cm, $x_1 = 18$ cm, $B_1/B_0 = 0.6$, $\Delta\theta = 1°$ yield values of $K = 1/11$, $x_2 = 24.2$ cm, $x_2 - x_1 = 6.2$ cm, $d_1 = 54.6$ cm, $d_r = 79.8$ cm, and $d_z = 305.2$ cm. From this we find

$$D_n = 1.1\,, \quad M_n = 0.57\,, \quad M_z = 21.1\,.$$

An energy resolution of 1/1000 corresponds to $\Delta s = 0.72$ mm and a maximum object width of 1.27 mm. Using the same data from section 2

as above, we get $\psi_n = -78°$ for C^{12} (α, α) C^{12}, and $\psi_n = -67°$ for C^{12} $(\alpha, p)N^{15}$. Using eq. (24) with $\Delta\theta = 1°$, $\alpha' = 2.5°$, and $\alpha'/\alpha = 2.1$ we find a solid angle of 1.5×10^{-3} steradians.

6. Discussion

The spectrometer (whether parallel or perpendicular) has a 2 — 4 times larger effective solid angle than the spectrograph (for the 90° deflection particles). Other properties, such as dispersion, resolution, etc., do not change much.

The comparison of the perpendicular spectrometer with the parallel spectrometer yields the following features:

(1) The parallel spectrometer has a slightly larger effective solid angle due to the fact that in the parallel position the quadrupole magnet focusses in the direction perpendicular to the scattering plane. When the spectrometer is in the perpendicular position, this axial focussing occurs in the scattering plane, so that any resulting increase in the axial acceptance angle tends to average the angular distribution out. It should be noted on the other hand that initially (before turning the quadrupole magnet on) the perpendicular position is more advantageous since in this position the axial acceptance angle (which is the smaller of the two acceptance angles) is in the scattering plane.

(2) The perpendicular combined spectrograph-spectrometer is simpler to construct since it does not require a special arrangement for the conversion from a spectrograph to a spectrometer. This simplicity makes it also much cheaper.

(3) Both spectrometers can be adjusted to take care of the kinematic broadening†.

† *Note added in proof*: Professor H. A. Enge has pointed out to us that the separation between the tilted lines produced by the astigmatic spectrometer might be obscured by the large axial magnification. In order to avoid this effect, the object height must be limited.

NUCLEAR INSTRUMENTS AND METHODS 7 (1960) 113–123; NORTH-HOLLAND PUBLISHING CO.

A NEW DESIGN FOR A BETA-RAY SPECTROGRAPH FOR RELATIVE MEASUREMENTS

ERIK KARLSSON and KAI SIEGBAHN

Institute of Physics, University of Uppsala, Uppsala

Received 5 February 1960

A new semicircular beta-spectrograph is described. The focusing field is obtained from a well-stabilized electromagnet. The instrument is provided with special arrangements for careful relative measurements. The energy calibration can be made very reproducible by means of a special source exchange arrangement and the recording film can be exposed by sections along its length. Resolution and transmission characteristics are discussed and a method for using mass-separated sources is presented.

1. Introduction

In an institute for nuclear spectroscopy it is generally important to have as many different types of spectrometers and spectrographs as possible so as to approach a problem from several points of view. It has been found that a semicircular beta-spectrograph with photographic recording is a valuable complement to double-focusing and lens spectrometers with individual particle counting. Most semicircular focusing spectrographs are equipped with a permanent magnet, to secure good field stability. This, however, has the disadvantage that the entire energy region of interest cannot be studied without changing the magnetization, which is rather inconvenient. Therefore, in some institutes a set of three different instruments is employed to cover all possible energies[9]). In the present instrument we have chosen an electromagnet with the current stabilization problem solved by a new type of circuit and the result is a versatile instrument, which can be applied to relative measurements of both energies and intensities with good precision.

2. The Magnet

The electromagnet has been described earlier[1]). It was first used in beta-spectroscopy[1]) and later for spin resonance work[2]). In the latter case the homogenuity of the magnetic field was greatly improved by making the pole-pieces optically flat and parallel to within 1 μ over their whole surface. As can be seen from ref. [2]) fig. 6 the field gradient is now very small and the magnet is thus suitable for high resolution beta-spectroscopy.

The total weight of the magnet is about 1 ton. It is placed with its symmetry axis horizontal in order to make the air gap easily accessible. It is excited by two coils with a total resistance of 2.8 Ω. The low resistance of the coils is shown to be an advantage in connection with the current stabilization problem (cf. page 114). The coils can also be water-cooled. This is, however, not necessary with the currents and fields ordinarily used in beta-spectroscopy, but may be useful for temperature control of the whole magnet with a thermostat system in cases where extreme stability of the field is required.

The magnet is normally excited with batteries which give 14 volts and have a capacity of 415 Ah and at normal field strengths this is sufficient for 2–3 weeks continuous operation. When necessary the charging of the batteries can—due to the current stabilizer described in the next section—take place parallel to the magnet and the exposure times may then be increased practically indefinitely. To use a d.c. mains supply is also possible, but as this is sometimes disturbed by outside effects, a separate battery supply is to be prefered.

The dimensions of the magnet are given in

[1]) K. Siegbahn, Ark. Mat. Astr. Fys. **30**A, No. 20 (1944) 1.
[2]) K. Siegbahn and G. Lindström, Ark. Fys. **1** (1949) 193.

ref.[1]). The pole gap is 42 mm, and the diameter of the pole shoes is 30 cm. Because of the reconstruction for spin resonance work mentioned above[2]) the magnet was rather locked-in and as a result of this, the vacuum chamber to be placed between the pole shoes had to be largely "tailor-made" in order to suit the magnet.

The position of source and film in the vacuum chamber was carefully selected so as to make the electron paths go through the most homogeneous parts of the field. The largest electron radius permitted is 10.8 cm. Outside this region the field drops sharply.

3. Current Stabilization

Stabilization of the magnetic field can be considered the most important problem in this type of instrument. As the energy resolutions reached are in the range 10^{-3}—10^{-4} the requirements of field stability must be set a factor of two better, that is at about 5×10^{-5}. Further, the field must remain stable for a long time as the exposures sometimes last for several days.

To keep the magnetic field constant is mainly a current stabilization problem. Considering Ohm's law for the magnetic circuit, we have approximately

$$B_{\mathrm{air}} A (l)_{\mathrm{air}} = NI \frac{1}{\Lambda_{\mathrm{iron}}(l,\mu_j) + \Lambda_{\mathrm{air}}(l)}$$

where B is field strength, A area of the magnet poles, NI ampere-turns, Λ the reluctances, μ_j the relative permeability of the iron and l is the linear dimension of the magnet. It is realized that temperature changes also influence the field.

1. By heat expansion of the iron core which also effects the width of the air gap.

2. By changes of the permeability of the iron.

The second effect which is the largest can be roughly estimated if the fraction of the m.m.f. spent on driving the flux through the iron is known. A value of 0.05 for this fraction is representative for the magnetization region used. The relative change in field strength is then approximately 5% of the relative change in permeability. Using the curves of Terry[3]) it is found that the latter is about $2 \times 10^{-3}/^{\circ}$ C for room temperature which gives about $10^{-4}/^{\circ}$ C for the field variation. This is on the limit of what might be permitted but temperature control can, as pointed out above, easily be made by regulating the cooling water when the highest resolution is necessary. The power used to excite the magnet is only 2–5 W so there is no big problem in keeping the temperature of the cooling water constant. Another error may occur by heat expansion of the brass that supports film and source holder. The relative changes expected are of the order of $2 \times 10^{-5}/^{\circ}$ C, the expansion coefficient of brass.

An efficient current stabilization can only be achieved by using a feed-back-system. The current is fed through a series resistance and the voltage appearing between the ends of the resistance is compared to a standard voltage. Any difference between the two voltages is fed back in such a way as to counteract the main current variations. The reference voltage is mostly obtained from a standard dry cell. Another way is to use the signal from a nuclear induction probe for the feed-back system[4]). This method is very accurate because it refers directly to the magnetic field, but comparatively high field strengths are needed since the intensity of the signal is approximately proportional to the square of the field. As this means very small dimensions of the spectrograph, which leads to trouble with scattering and background in a photographically recording instrument, the method was not suitable for our purposes. In the feed-back loop some kind of electronic valve must be used for the control of the main current, e.g. an electron tube or a transistor. With electron tubes a voltage of 100–200 volts is needed and the current let through rarely exceeds a few hundred mA per tube. Consequently, when constructing coils for magnets to be used with an election tube stabilizer one has to make them with a high resistance and the voltages needed will often become inconviniently high.

[3]) E. M. Terry, Phys. Rev. **30** (1910) 133.
[4]) G. Lindström, Ark. Fys. **4** (1951) 1.

For a low-voltage battery-excited magnet like ours no means have been at hand for using the more conventional type of circuit. In the last few years, however, the appearance of high power transistors has greatly changed the situation. At present 50 W transistors are commercially available. One single transistor can pass with the shunts, which are made from constantine wire. The temperature of the bath is kept constant within $\pm$ 0.2° C.

The over-all stability of the magnet current is thus estimated to be a few parts in 100 000 which is sufficient for the intended measurements.

It is worth noticing that this good stability is

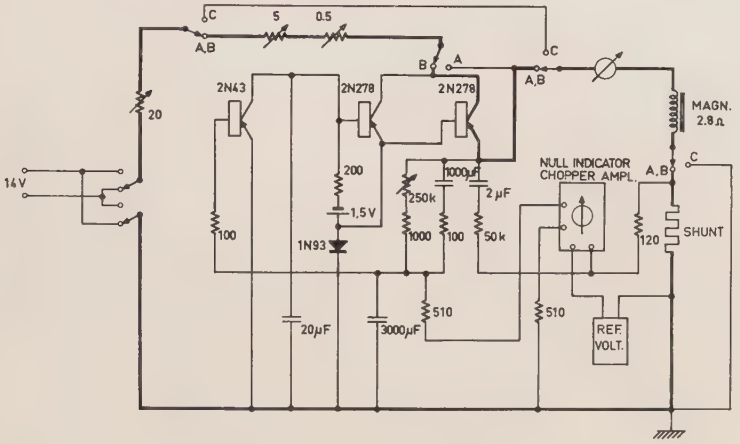

Fig. 1. Current stabilizing system.

up to 5 amps at the voltages present in our circuit. This is just sufficient for our purpose (cf. fig. 7). The feed-back circuit used is mainly the same as the one described by Garwin[5]). The shunt voltage is compared with the reference voltage from a Mallory mercury cell by means of a Honeywell-Brown Null Indicator. The null-indicator converts and amplifies the error signal and after passing through a phase-sensitive rectifier it is fed back via a drive stage to the transistor 2N278 where the main current regulation takes place (fig. 1). The sensitivity of the null-indicator is very high and the feed-back oscillations have been observed to take place between the limits $\pm$ 1 $\times$ 10^{-6} volts. The drift of the zero point is quoted by the manufacturer to be less than $\pm$ 1 $\times$ 10^{-6} volts per hour at the amplification used. As the reference voltage is of the order of 1 volt, the figures mentioned can be taken as a measure of the relative accuracy, with which the stabilizer follows the reference voltage.

The reference voltage cell is immersed in a thermostattically controlled oil bath together maintained even if large variations occur in the voltage supply. As a test the resistance in the circuit was abruptly changed by 50%. No noticable difference could be seen on the null-instrument meter.

4. The Vacuum Chamber

The construction of the vacuum chamber can be seen from fig. 2. It consists of a ring of rolled brass with soldered brass bottom and an aluminium lid which is removable for access to the interior. Pointing upwards in the spectrograph is the opening for the film- and source-holder. The vacuum chamber had to fit the 42 mm air gap in the magnet, and the walls of the chamber were made as thin as possible with regard to the pressure in order to get as much space as possible inside. The inside height is thus 30 mm. The scattering of electrons from the valls has been found to be negligible.

The vacuum system is very simple. It consists of an Edwards air ballast rotary pump 1S50 and an Edwards oil diffusion pump 203.

[5]) R. L. Garwin, Rev. Sci. Instr. 28 (1958) 223.

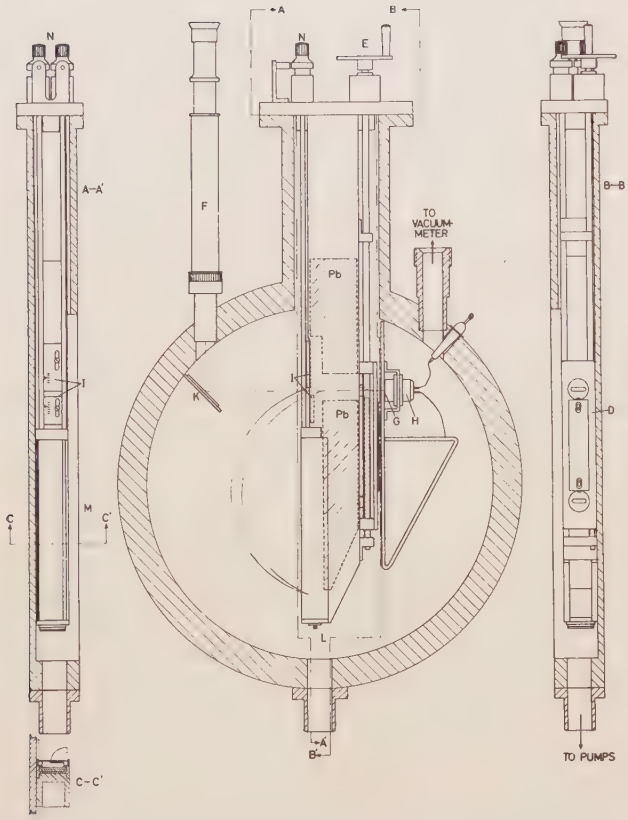

Fig. 2. Vacuum chamber with source and film holder. For interpretation of letters D-L see text.

Owing to the small volume to be evacuated (about 2 litres) no roughing circuit is employed; the only valve used is one between diffusion pump and vacuum chamber. When the chamber has been opened to change film or source, the air is just pumped through the hot diffusion pump and high vacuum is reached in less than one minute. During half a years's daily operation this has not been found to affect the performance of the oil (Dow Corning No. 703). The vacuum chamber and the rotating pump are provided with separate air-inlet valves.

The vacuum is measured with a Leybold Combitrone instrument, which is a combination of a pirani-type and a penning vacuumeter. This instrument covers the range 10^{-1}–10^{-5} mm Hg and has the advantage of easy handling and resistance to damage by careless operation.

The vacuum maintained during the measurements has been found better than 10^{-4} mm Hg.

5. The Source and Film Holder

The energies of conversion electron lines are measured by relative methods only. The number of exactly determined lines in different energy regions and in various isotopes is now so great that it is always easy to find suitable calibration lines. An absolute determination comprises the measurement of the magnetic field and one or two distances (depending on the geometry used). A careful field measurement is always difficult and will cause much trouble in a case like ours where the field is changed rather frequently.

No magnetic field measuring device has therefore been provided. Instead much care has been taken in making the energy calibration as exact as possible. The construction is inspired by similar arrangements in optical spectroscopes. It is preferrable always to have calibration lines on the same film as the spectrum to be measured. The calibration can no doubt, be done once for each field, but that would need a very careful adjustment of source and film positions, to get reproducible results. Also, since the field is often changed or shut off between measurements it does not take much more trouble to calibrate each run separately, and the errors can then be greatly reduced. The calibration can be done in a relatively short time, say one hour, and strong calibration sources are generally available. It would be an advantage if the calibration could be performed without breaking the vacuum and taking out the source and film holder, as this would mean an unavoidable change of conditions during measurements. The evident solution of this problem is having both sources in the spectrograph during the whole run with suitable means provided for changing the positions of the two sources from outside.

The construction of the film and source holder is seen from fig. 2. The active substances are usually deposited on thin wires mounted onto an aluminium ring. The source rings are placed in two holes in a slide (D), which is operated from outside by means of a precision screw (E). The active wires must be put in exactly the same position during the exposures. For this purpose an optical system has been built in. The wire

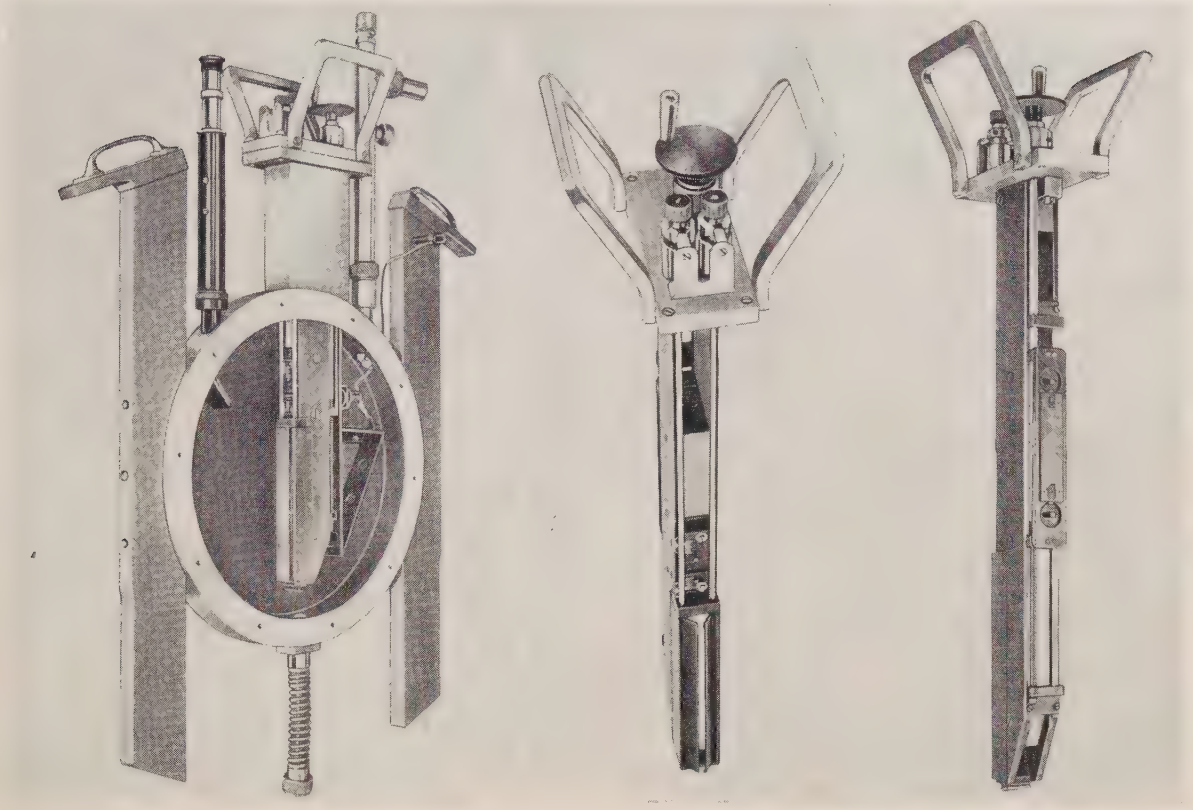

Fig. 3 (a) Fig. 3 (b) Fig 3 (c)

Fig. 3. (a) Spectrograph chamber with lid opened and source and film holder inserted. (b) Source and film holder (showing slit arrangement and shutter system). (c) Source and film holder (showing source arrangements).

is seen in the microscope (F) against a hair-cross (G) which is fixed in the vacuum chamber. The light from the lamp (H) passes the source position and the slit (I) and is then deflected by the mirror (K) into the microscope. The wire source is moved into position by the precision screw very accurately; for thin wires with an accuracy of 1 μ. Simultaneously it is checked that the source is in proper position relative to the slit, i.e. perpendicular to the slit-film line. One also has an opportunity to check that everything is correct inside the spectrograph before the exposure is started. Once and for all the position of the hair-cross is set by a mirror method on a line normal to the centre of the slit for fixed position of the source holder. The adjustment of the wire parallel to the slit is done before inserting the source holder by aiming at the edges of the slit. The two sources are situated 10 cm apart. The calibration source which is usually the stronger one is placed in the farthest position as seen from the film in order to reduce the γ-background during the main exposure. A thick lead shield is also provided making the γ-radiation from this source small in comparison with that of the one being measured. Between the source position and the film is a second lead shield which is about 6 cm at the nearest distance to the film. This has been found to be sufficient in all recordings so far performed.

The film is placed in a casset which is put in from the end (L). In front of the casset is a shutter system (M) (consisting of two "doors") also operated from outside by control knobs (N) Each of these can be put open, half-open or closed. The present shutters are made of brass thick enough to stop 1 MeV electrons. This makes it possible to expose the film by sections along its length. The shutter system is valuable in several respects.

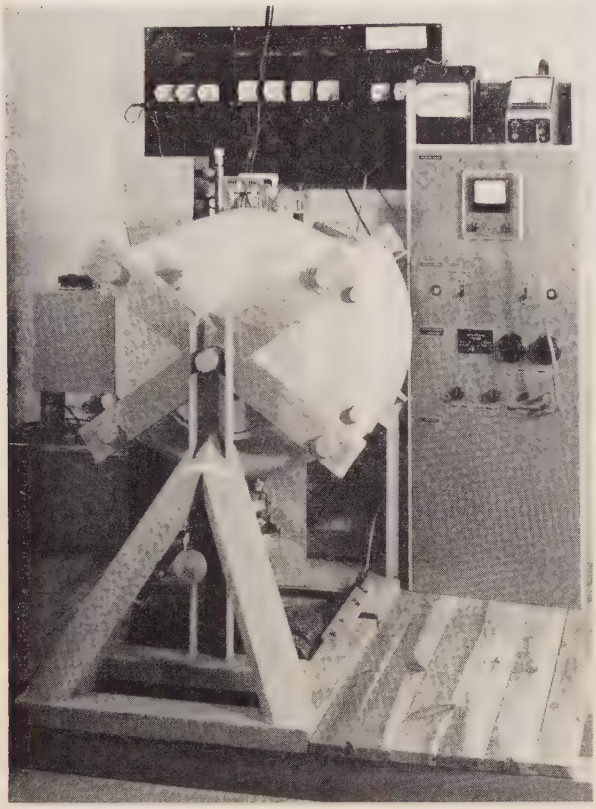

Fig. 3 (d)

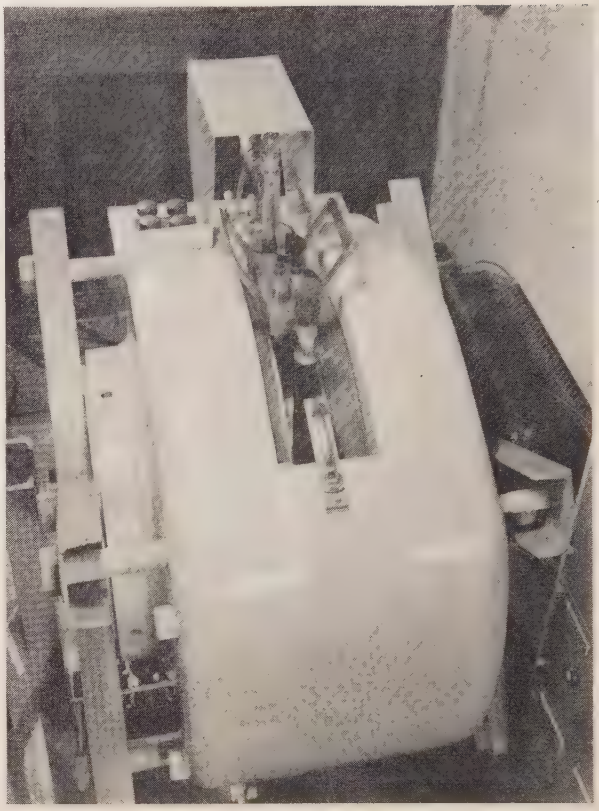

Fig. 3 (e)

Fig. 3 (d) Complete view of the spectrograph with current regulation units and vacuum arrangements.
(e) Assembled view of spectrograph seen from above.

(a) When calibrating the calibration lines are usually exposed over the middle section of the recording film while the unknown lines reach over the whole film strip. (See fig. 9a.)

(b) When following a complex decay chain, different sections of the film are exposed at different stages of the decay. This makes it easy to separate lines belonging to different isotopes in the chain. It is to be noted that the use of the same film and the same developing procedure makes the spectra more comparable in intensity than had otherwise been possible. An example is given in fig. 10.

(c) It is often found that the lines in different parts of a photographic spectrum have widely different shapes. This is caused by geometrical differences for the electron paths and is very difficult to avoid. If, however, a comparison of two such lines is desired, it can be done by changing the field between the recording of two different sections of the film in such a way that the two electron paths are the same in both cases. The same advantages as in (b) are valid also in this case.

(d) Both shutters are closed when the film and source holder is put into the vacuum chamber. They are not opened until sufficiently low pressure is reached in the tank. This also makes possible the use of light for the optical system inside the spectrograph. The spectrograph room need not be darkened when changes are made because the film holder is carried away to the dark-room before the shutters are opened.

The recording films used have been Gevaert-X-ray film and Ilford G-film (Industrial). The electron sensitivity has been found to be about the same for both types. The Ilford film, however, gives the smaller background and has therefore been used most extensively. Provision has also been made for the use of photographic plates.

The slit is of the type described by Slätis[6]). The angle that determines the width of the electron beam permitted through the slit is then equal for all electron radii.

The distance between slit and source is 5 cm. Other pertinent dimensions are:

Film length: 16.8 cm.
Film breadth: 1.9 cm.
Largest electron radius accepted: 10.8 cm.
Smallest electron radius accepted: 4.0 cm.
Free height of source wire: 1.3 cm.
Width of vacuum chamber: 3 cm.

6. Some Properties of the Spectrograph

6.1. RESOLUTION AND TRANSMISSION

It is well known that the semicircular method is very inferior to the space-focusing spectrometers as far as transmission is concerned. When looking at the resolution the situation is, however, somewhat better, especially as a great part of the spectrum can be surveyed simultaneously with a high resolution which would take a long time with particle counting spectrometers. To clarify the properties of the present spectrograph, resolution and transmission curves were calculated from equations (23) and (25) in ref. [7]).

$$R_0 = \frac{1}{2\rho}\{s + \omega + \rho(\varphi^2 + \psi^2)\}$$

$$T = \frac{\varphi\psi}{\pi}$$

where s is the source width; ω is resolution of the recording film, φ is half the aperture of the slit and ψ the mean angle subtended by the film as seen by the electrons. The relative half-width R is approximately half the base line width R_0. In the theoretical resolution diagrams plotted (figs. 4 and 5) R has been put equal to $\frac{1}{2}R_0$. From fig. 4 which is drawn for the mean radius 7.0 cm the resolution can be seen to be influenced rather strongly by the factor including ψ. Therefore, it is realized that not much is to be gained by decreasing the source width to below 50 μ. If higher resolutions are wanted it is possible to decrease ψ by activating only the middle part of the source wire and using only the central section of the film.

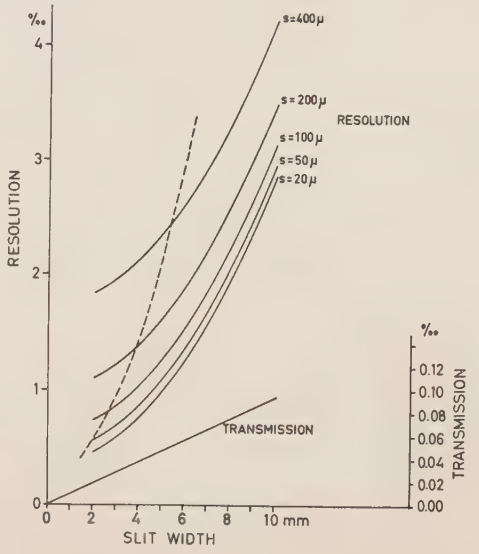

Fig. 4. Transmission and resolution characteristics of the spectrograph. Dashed line shows best choices of source and slit widths for maximizing L/R.

Fig. 4 is used as a guide for chosing the appropriate source width and setting the slit. If all the available activity can be concentrated to as small a source as wanted without causing self-absorption it is, naturally, most favourable to use the smallest wire size, i.e. it gives the largest T/R ratio. Often, however, only a certain specific activity can be obtained. In this case it is of interest instead to reach the maximum ratio of L/R, where L is the luminosity

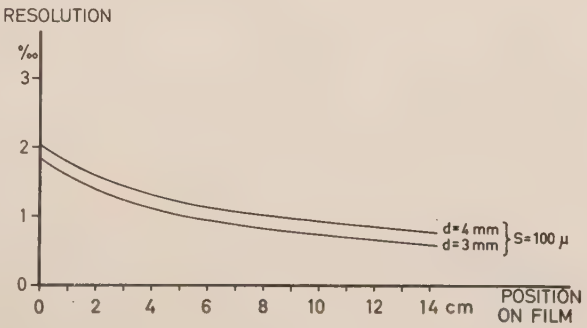

Fig. 5
Theoretical resolution for different positions along the film.

[6]) H. Slätis, Ark. Fys. 8 (1954) 441.
[7]) K. Siegbahn, Beta- and Gamma-ray Spectroscopy (North-Holland Publishing Company, 1955) 62.

$$L = sh\frac{\varphi\psi}{\pi} \quad (h \text{ is source height}).$$

Consider the problem of chosing the correct s and d for a desired resolution. From

$$R = \frac{s}{4\rho} + \frac{\omega}{4\rho} + \frac{d^2}{16b^2} + \frac{\psi^2}{4}$$

one obtains

$$s = 4\rho R - \omega - \frac{\rho d^2}{4b^2} - \rho\psi^2 ,$$

where b is source-slit distance.

We want to maximize the quantity sd which is proportional to the luminosity.

$$sd = (4\rho R - \omega - \rho\psi^2)\, d - \frac{\rho}{4b^2} d^3$$

$$\frac{\partial(sd)}{\partial d} = 4\rho R - \omega - \rho\psi^2 - \frac{3}{4}\frac{\rho}{b^2} d^2 .$$

For each wanted value of R we get a value of d from the relation

$$d = \sqrt{\frac{4}{3}\frac{b^2\,(4\rho R - \omega - \rho\psi^2)}{\rho}} .$$

The "best" values of s and d thus obtained for $\rho = 7.0$ cm are connected in fig. 4 with a dashed line.

The resolution and transmission is not expected to be the same for all parts of the film in this instrument. The finite size of the source and the lack of space focussing contributes to this variation as does the correction introduced by our geometrical arrangement for which the expression quoted for R is not exactly valid. The latter correction which is not included in the calculation of diagram 4, comes from the fact that the source and film are not in the same plane. It increases the expected half-widths by a factor 1.22 for the smallest radius and 1.03 for the largest radius accepted. Taking all corrections into account diagram 5 has been computed in order to get an idea of the situation in a typical case.

Throughout the calculations the magnetic field has been considered perfectly homogenous. As mentioned before (p. 113) the homogenuity of the field is indeed very good. As small variations in the field do not make much worse the spread of nearby electron rays, possible inhomogenuities do not affect the resolution characteristics as much as they do the ρ-values. The diagrams 4 and 5 are thus fairly reliable which has also been proved experimentally. In this calculation ω, has been put equal to 20 μ which is somewhat arbitrary and could perhaps be lowered by a factor 2.

6.2. GEOMETRY

As seen from fig. 2 the geometry used is that with the entrance slit in the same plane as the photographic film and the source on a perpendicular to the plane going through the middle of the slit. This should not distort the shape of the lines in any part of the spectrum (8); on the other hand it is an intricate problem to measure the ρ-values exactly. This problem has, however partly been removed by the method used for relative measurements (section 6.3).

6.3. CALIBRATION

For an absolute determination of the energies the two parameters B and ρ must be measured. As pointed out above it is difficult to measure ρ directly with great accuracy. In the method of Slätis this has been overcome by measuring the distances in two steps[8]). This means an introduction of fixed calibration edges in front of the film or plate, and a certain amount of continous blackening caused by background γ-radiation, scattered electrons or continous β-spectra is needed if the edges are to be made visible as sharp shadows on the film. We have found that the background blackening in our instrument is

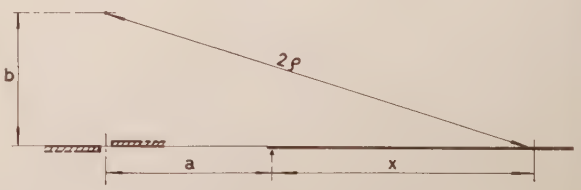

Fig. 6. For explanation of the quantities a, b, x and ϱ used in calibration calculations.

[8]) H. Slätis, Ark. Fys. **6** (1953) 415.
[9]) H. Slätis, Nucl. Instr. **2** (1958) 332.

too small to be used for this purpose—as a matter of fact all means have been tried to reduce it. One possibility is to expose one third of the film to light from the internal lamp, but this has not yet been tried†.

If the distances are measured along the film we shall have to determine instead of ρ the two quantities x and b (fig. 6). It is then sufficient with one mark on the film from where the comparator measurements are started, and the known calibration lines are used to evaluate the constant B if the distances a and b can be measured accurately. As the exact measurement of a and b is no easy matter it may be preferrable to evaluate them by measuring one more calibration line for each if so many exactly known calibration lines are available.

Summing up:

(1) If only B is unknown one calibration line is needed;

(2) If both a and B are unknown two calibration lines are needed;

(3) If both a, B and b are unknown three calibration lines are needed.

In some cases method (3) has been tried. It has several obvious advantages. It involves three measurements of distances along the same line from one common point which may be chosen arbitrarily. Thus only one comparator run provides all the necessary data. The sources of error are greatly reduced; the position of source and slit need not even be known roughly. The calculation in (3) is based on the solution of the system of equations (cf. fig. 6)

$$(x_1 + a)^2 + b^2 = \frac{4(B\rho_1)^2}{B^2}$$

$$(x_2 + a)^2 + b^2 = \frac{4(B\rho_2)^2}{B^2}$$

$$(x_3 + a)^2 + b^2 = \frac{4(B\rho_3)^2}{B^2}.$$

† Light exposure has also been used in the work of Slätis.

The procedure might seem somewhat tedious, but is done with a computing machine in 3–4 hours if the number of un-known lines is about 25.

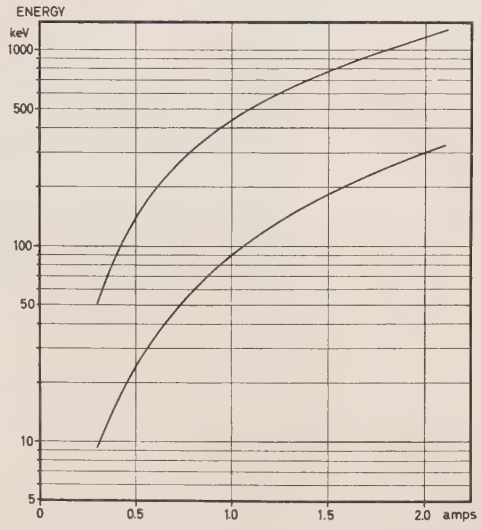

Fig. 7
Energy intervals recorded plotted against magnet current.

In order to test the reliability of this calibration method a number of lines in the ThB spectrum were measured in the comparator starting out from the well determined F, I and J-lines (Ellis' notation). The energies obtained were

F-line	148.11 ± 0.01 keV	(calibration line)
G-line	189.24 ± 0.04 keV	
H-line	209.57 ± 0.05 keV	
I-line	222.21 ± 0.03 keV	(calibration line)
I_a-line	222.87 ± 0.05 keV	
J-line	234.61 ± 0.03 keV	(calibration line)
J_a-line	237.68 ± 0.05 keV	
J_c-line	283.58 ± 0.07 keV.	

The errors in the energy measurements generally fall below twice the errors of the calibration lines. Assuming that the F, I_a, J and J_a-lines arise from the same nuclear transition converted in the K, L_{II}, M_I and N_I-shell respectively, we make the following comparisons

	I_a — F	J (cal-line) — F	J_a — F
Electron energy difference	74.76 keV	86.50 keV	89.57 keV
Binding energy difference	74.83 keV	86.54 keV	89.60 keV

The agreements are thus found to be satisfactory. In the calculations the magnetic field has been considered perfectly uniform. An error due to a monotonous change in the mean field cause it involves the measurement of the distance from the slit which is not very well defined.

In a few cases a calibration curve was drawn for energy regions where closely spaced calibration lines were available. As these curves are far from linear they are, however, not applicable in general for precision measurements.

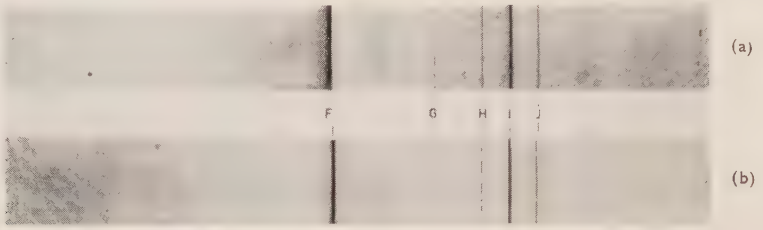

Fig. 8. (a) Example of ThB-spectrum (source on W wire). (b) Example of ThB-spectrum (source on Al foil).

along the different electron paths is, however, to a great extent eliminated if the fixed points are appropriately spread out over the considered energy region. Similarly, errors arising from a bad adjustment of the slit position leading to deviations from the right angle geometry do not enter, because ρ can still be described as an equation of second order in x.

The gross energy intervals taken in by the spectrograph are seen from fig. 7 which is used as a guide when adjusting the magnet current to its appropriate value for each special problem.

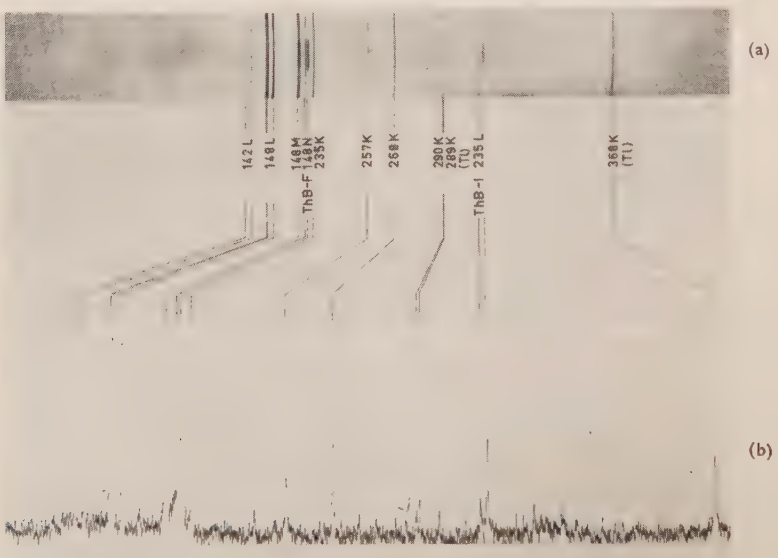

Fig. 9. (a) Spectrum of mass separated $Pb^{200} + Tl^{200}$, with ThB calibration in central section. (b) Microphotogram of the same spectrum recorded along the central section. Notice the large low energy tail of ThB F-line (wire source) as compared to the lines of the main spectrum (Pb source on Al foil).

When the constant b has been well determined by a number of such measurements it may be used for later calibrations according to method (2). The further reduction to (1) is difficult, be-

7. Source Preparation

The sources have mostly been prepared on thin wires of tungsten or monel, mounted onto aluminium rings. For activation in the Th-B

chamber lucite rings were used to ensure that no activity deposits on the ring. Electroplating methods have been used most extensively. In all cases, where wire sources were used it was, however, established that the lines were heavily broadened by backscattering. We have, in an investigation of Pb- and Tl-isotopes, made use of mass separated samples. The activity was collected on a thin Al-foil in the mass separator. To get a small source width a mask, also made of Al-foil, with an opening of 0.15 × 10 mm was placed in front of the collecting strip. Through the opening in the mask were pierced two small pinholes to make it possible to adjust the source into its correct position. The activity obtained amounted to about 10% of the total yield for the isotope when the half-width of the isotope in the separator was 2 mm. It is to be noted that the mask which contains the major part of the activity can still be used as a source in other spectrometers. The sources prepared in this way for the spectrograph are of course relatively free from admixtures of adjacent isotopes. Fig. 8 gives an example of a Pb^{200} + Tl^{200} activity exposed for 20 hours. The strength was less than 100 μc. The absence of backscattering makes it possible to resolve weak lines even in the vicinity of very strong ones. ThB sources on masked Al-foils have also been prepared in an emanation chamber (fig. 8b). Experiments are under way to apply similar techniques to electroposition.

Fig. 10. Spectrum of Pb isotopes (with daughters) produced in the reaction Tl (75 MeV p,$\varkappa$n) Pb. The different parts of the spectrum are recorded at the following intervals after the end of the irradiation. Upper section: 1.30–3.30 hours. Middle section: 10.30–13.30 hours. Lower section: 22.30–26.30 hours.

NUCLEAR INSTRUMENTS AND METHODS 7 (1960) 124–134; NORTH-HOLLAND PUBLISHING CO.

A NANOSECOND COINCIDENCE CIRCUIT USING TRANSISTORS†

ARPAD BARNA, J. HOWARD MARSHALL and MATTHEW SANDS

California Institute of Technology, Pasadena, California

Received 30 December 1959

A transistor coincidence circuit is described which is intended to be used for scintillation counting of high energy particles. Details of the performance of the basic components are given both with test pulses and with photomultiplier pulses in a counting arrangement. Resolving times as low as 2 nanoseconds were measured††.

1. Introduction

Most of the experiments in progress at the CalTech 1 GeV electron synchrotron which use scintillation and Čerenkov counters require coincidence circuits with a resolving time of a few nanoseconds. These resolving times are required either for time-of-flight selection, or for the reduction of accidental coincidences from counters with high singles rates. Usually two-fold fast coincidences are required. More complicated coincidence combinations are obtained by the use of slower circuits operated from the outputs of several primary two-fold coincidence circuits. Until recently the fast coincidence circuits used in this laboratory have been patterned after the circuit of Wentzel[1]) or that of Garwin[2]).

With the advent of the Philco 2N501 transistor, which has a characteristic response time comparable to that of the usual vacuuum tubes, it became possible to consider constructing transistor coincidence circuits with resolving times limited by the response of the scintillation counters. The lower power consumption, smaller size, and presumed greater reliability, of the transistor circuits would make it possible to employ larger numbers of these circuits as is required for the growing complexity of experiments in high-energy physics. The two-fold coincidence circuit to be described was designed with these factors in view.

† This work was supported in part by the U.S. Atomic Energy Commission.

†† One nanosecond (nsec) = 10^{-9} sec.

2. The Circuit

The configuration of the coincidence circuit is shown by the basic schematic diagram of fig. 1.

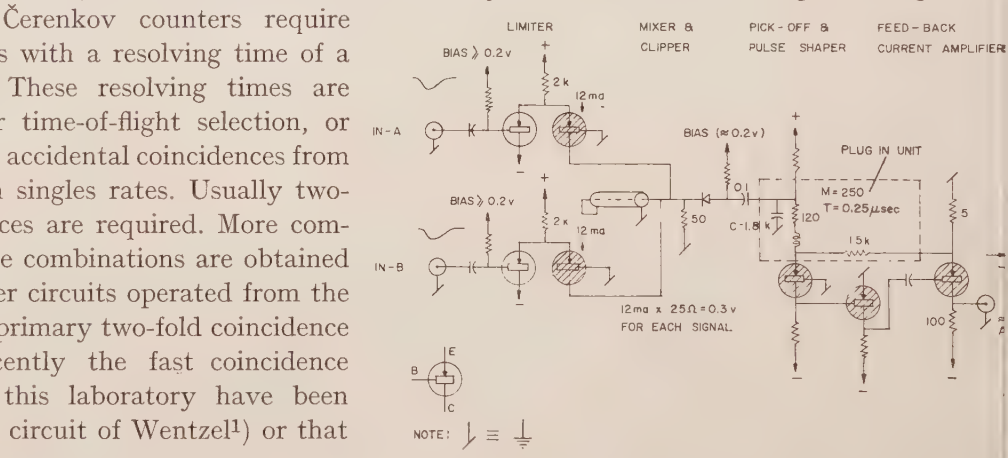

Fig. 1. Basic schematic of the coincidence circuit. Transistors: 2N501 (Philco).

The configuration is one of common usage[3]) and has been referred to by Wentzel[1]) as a "plate addition circuit". The input circuits, consisting of two transistors in a "long-tail-pair" serve as limiters. Negative input signals turn off fixed currents flowing in the clipping line, whose length determines the coincidence resolving time. A pick-off diode is biased to remain non-conducting for single input signals, but to conduct on the coincidence signals. The diode

[1]) W. A. Wentzel, Millimicrosecond Coincidence Circuit for High Speed counting, Univ. of California Radiation Laboratory Report UCRL-8000 (October 2, 1957).

[2]) Richard Garwin, Rev. Sci. Inst. **24** (1953) 618.

[3]) Fast coincidence circuits based on the addition of two limited currents on a clipping line were first described to one of us (M. S.) by Martin Deutsch in 1949.

current is integrated on the capacitor C, which discharges through a pulse-shaping network into the low-impedence input of a feedback current amplifier. The output drives a terminated cable (normally 50 or 100 ohms) and is intended to operate counters or other—usually slower—coincidence circuits. The duration of the output pulse and the gain of the output amplifier can be adjusted to satisfy the needs of a particular experiment by the choice of a suitable plug-in unit which contains the elements shown within the broken line rectangle.

2.1. THE INPUT LIMITER

A detailed diagram of the input circuit is shown in fig. 2. The base of the input transistor is biased 0.17 volts or more positive with respect to the base of the second transistor. A current of 12 mA, determined by the emitter supply resistor flows through the second transistor. Negative input signals greater than 0.2 volts will begin to transfer the current to the input transistor and to reduce the current flowing into the clipping line. Because of the high transconductance of the transistors, an input signal of 0.25 V, maintained for a long time, is sufficient ot effect this current transfer. To obtain a rapid cut-off of the current in the second transistor, however, the input current must be comparable with the standing current in the circuit. For the 2N501 the basic time limitation is given by the α time-constant $(= 1/2\pi f_\alpha)$ of 0.4 nsec. The response time for small signals is expected to be (see Appendix I) $\tau_\beta \approx \beta\tau_\alpha$, where β is the current gain of the transistor and is typically about 50 for these transistors. For the circuit shown, input signals of about 1 volt will give input currents about equal to the standing current and can be expected to cut-off the standing current in about 1 nsec.

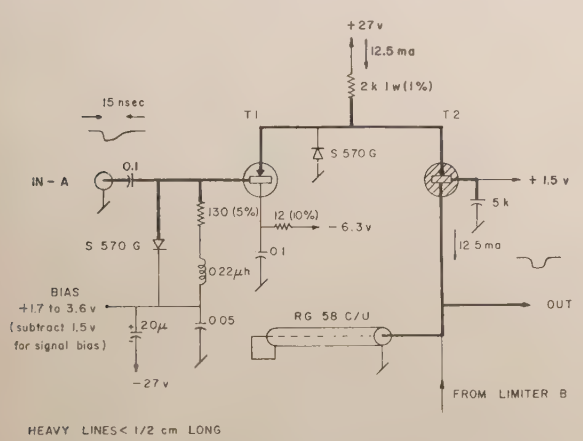

Fig. 2. The input limiter. T_1: 2N501-2; T_2: 2N501.

Measurements of the response of the input limiter are shown in fig. 3. The rise-time (10 percent to 90 percent) of the signal which appears on the clipping line is plotted as a function of the input signal amplitude for three input bias settings. The input signals were obtained from a fast pulser, $T_R < 1$ nsec, and the output was observed with an oscilloscope†. The "input amplitude" is defined as that which would appear from a terminated input cable. The error in the measurement of the rise-times is about 0.5 nsec. The curves show the expected behavior. Signals only slightly above the signal biases (1.5 volts less than the bias of the input transistor) give large output rise-times. An input amplitude one volt or more above the signal bias is required to obtain rise times less than 2 nsec. The minimum rise-time expected for this circuit can be estimated as $2.5\,[\tau_\alpha{}^2 + \tau_c{}^2]^{\frac{1}{2}}$ where τ_c is the time constant of the collector and stray capacitances in combination with the terminated line resistance $\tau_c \approx 15\ \text{pF} \times 25\ \Omega = 0.4$ nsec. The expected rise-time is then 1.4 nsec in good agreement with the observations.

The principle advantage of this limiter is that the circuit is normally biased in an insensitive condition. Signals much smaller than the desired ones do not disturb the quiescent current. Also, small positive overshoots from the mismatching of cables will not have the undesirable effects observed when the usual pentode limiter is driven positive. It is this property of the limiter circuit which permits the use of the simple mixing arrangement adopted for this circuit. (See the discussion—particularly that associated with fig. 2—in Wentzel's report[1].)

Further advantages of the two transistor limiter are that it provides an adjustable input

† Edgerton, Germeshausen, and Grier, Model 2236A.

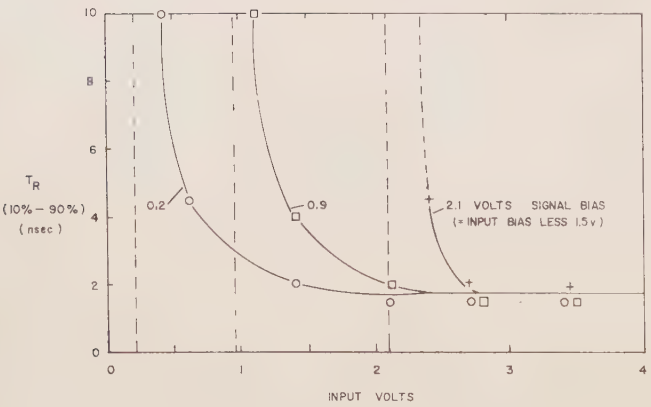

Fig. 3. The limiter rise time as a function of the input pulse amplitude.

threshold; that it minimizes direct capacitative coupling from the input to the clipping line; and that it presents to the input terminal an impedance which approximately terminates a 125 ohms cable.

The resistor-inductor combination in the base bias circuit of the input transistor presents a high impedance path for the leading edge of the signal so that the whole signal current passes to the transistor. The input diode limits positive transients at the input so as to prevent breakdown of the input transistor. The diode at the common emitter junction protects the transistors against abnormally large negative input signals.

2.2. MIXER AND CLIPPER

The limited current signals from the input circuits are added linearly on a 50 ohm short-circuited clipping line. The "clipping" width is defined as twice the one-way transit time of the clipping line. Clipping widths of 3 to 10 nsec are expected to be most commonly used. The 50 ohm impedence of the line was chosen to give the best match of the capacitative time constant at the collector, to the transistor response time.

2.3. PICK-OFF AND PULSE SHAPER

A diagram of the pick-off and pulse shaping circuit is shown in fig. 4. A bias current of normally about 6 mA (adjustable from 0 to 13 mA) is drawn from the "Coinc. Bias" terminal. This sets a forward current of 6 mA through diode D_1 and applies, via R_3 and R_2 a back voltage bias of about 0.18 volts across diode D_2. Both of these are "fast" diodes with a storage time of less than 1 nsec. The combination of R_1 and D_1 has a signal resistance of 50 ohms for negative currents of 6 mA or less. Thus the 12 mA limited current from a single input operates into a terminated clipping-stub and produces clipped pulses of $(0.012)\ (50/2) = 0.3$ volt amplitude. These pulses are too small to overcome the bias-plus-offset of diode D_2. (The "offset" of these diodes is about 0.2 volts, at which forward voltage the diode current is only 0.3 mA.)

With coincidence signals the total limited current of 24 mA produces 0.6 volt across the clipping line. During these "doubles" pulses the current in diode D_1 cuts off and 6 mA flows through diode D_2 and resistor R_4 to the capacitor C. This combination also presents an impedance of approximately 50 ohms to the clipping cable. A detailed analysis of the circuit shows that the combination D_1, R_1, D_2, R_4 presents a nearly constant resistance of 50 ohms to the clipping cable for signal currents from zero to 12 mA.

The current through D_2 on coincidences deposits a charge of approximately 6 mA times the clipping width, onto the capacitor C. For a 6 nsec clipping width the capacitor voltage rises to only about 0.02 volt. The discharge of this capacitor through R_4, R_6 and L (after the coincidence) provides a shaped current pulse into the low impedance input of the output current amplifier. The shaped pulse has a duration (to half of its peak value) of 0.85

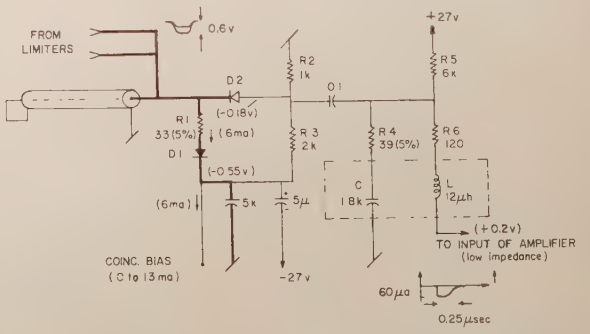

Fig. 4. Coincidence pick-off and output pulse shaper. Diodes: Q3-100 (Qutronic).

$(R_4 + R_6)\,C$. The inductor L provides the shape of a "shunt compensated" pulse with critical damping. The configuration of C, R_4, R_6 and L provides a sharp leading edge to the current pulse which attains its maximum value at the end of clipped coincidence signals and decays with zero initial slope. The resistor R_5 provides an operating bias current for the following amplifier. The pulse shaping elements C and L are part of a passive plug-in-sub-assembly and can be selected to give any desired output pulse duration. The values shown in fig. 4 give a pulse duration of 0.25 μsec, which was desired for operating the pulse spectrometer used for testing the coincidence circuit.

A detailed analysis of the pick-off circuit has been made assuming that the signals at the clipping stub have an exponential rise and that the diodes D_1 and D_2 are ideal rectifiers. With these assumptions the peak current of the shaped pulse is given by

$$I_{\max} = k\,\{t_0 - 1.4\tau - \tau \ln [1 - \exp(-t_0/\tau)]\}\,, \quad (1)$$

where t_0 is the clipping width, τ is the rise time-constant of the limited current pulse; and

$$k = \frac{I_0}{2}\,\frac{R_0}{R_0 + R_4}\,\frac{0.85}{T}\,M \quad (2)$$

where I_0 is the coincidence current (24 mA), R_0 is the characteristic resistance of the clipping line; T is the output pulse width (to half of peak); and M is the amplification of the current amplifier. Measurements of the output current amplitude as a function of the clipping length are given in Section 4, and agree with eq. (1).

2.4. OUTPUT AMPLIFIER

The output amplifier is designed to provide a signal amplitude suitable for operating subsequent discriminating and coincidence circuits. The amplifier diagram is given in fig. 5. The current signal from the pulse shaping circuit of fig. 4 is fed to the emitter of the input transistor T-5. For a step input current the emitter impedance is 50 ohms, resistive, for times $\approx \tau_\alpha$ but is about 4 ohms for times longer than about 12 nsec (see Appendix 1). (The effective input impedance of the amplifier is reduced below the above value for signals of long duration by the negative feed-back.) The characteristics of the pulse shaper depend only on the input impedance of the amplifier for times comparable with the duration of the output pulse. The

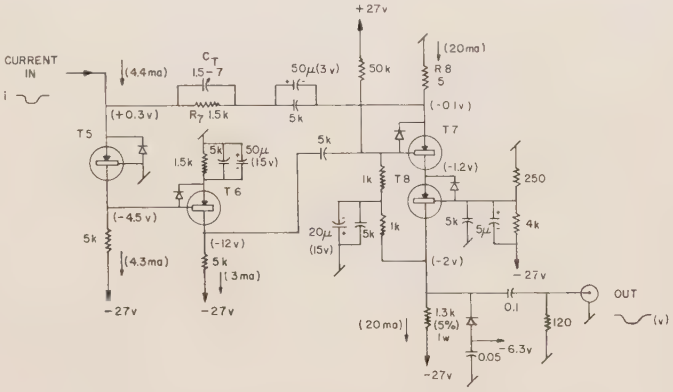

Fig. 5. The output amplifier. T_5: 2N501; T_6, T_7, T_8: 2N501-2. Diodes: 1N99 (All protective).

long-time input resistance of the amplifier (< 4 ohms) will thus have a negligible effect on the pulse shaper.

The transistor T-5 has a current gain to its collector of about 0.98. Its output current is coupled to the base of T-6 with an efficiency of 0.98. Transistors T-6 and T-7 together provide a current gain of $(50)^2$. The overall current gain to the collector of T-8 is about 2000 when the coupling factors for the base circuits are included. A fraction of the output current, which flows through T-7 and T-8, is fed back via R_7 to the input with a return factor of nearly $R_8/R_7 = 1/300$. The net current gain of the amplifier is then $300\,[1 + 300/2000]^{-1} = 260$ (nominally 250). There is thus a feedback factor of 7 which will stabilize the long-time amplification, but is used mainly to shorten the response-time of the amplifier. The resistors R_7 and R_8 are also contained in the plug-in unit of the pulse-shaper, as the gain and rise-time required of the amplifier depend on the pulse width selected. The gain of the amplifier is stabilized primarily by providing stabilized currents to all of the transistors. The currents are stabilized for T-5 and T-6 by the large resistances in the emitter circuits and for T-7 and T-8 by D.C.

feedback to the base of T-7. The latter feedback also stabilizes the collector voltage of T-7 and T-8, as is required to ensure that the dissipation of these high-current output stages does not exceed the maximum rating of 25 milliwatts.

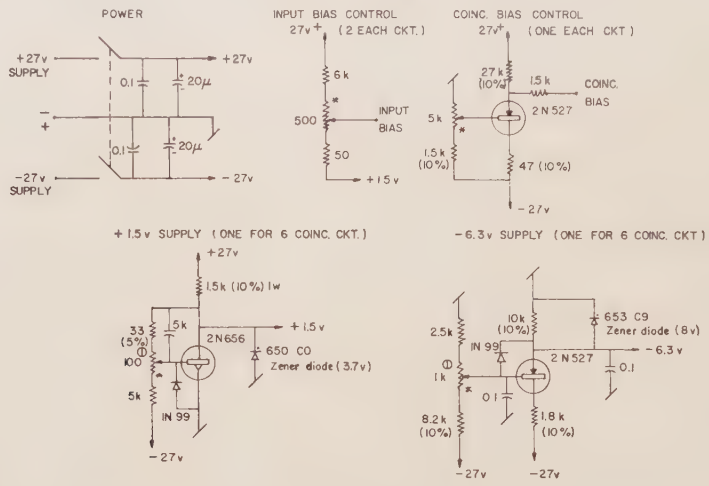

Fig. 6. Power and bias circuits.

The transistor T-8 serves to isolate the feedback circuit from the output, and particularly to reduce the capacitative feedback to the base of T-7 which would have a deleterious effect on the transient response of the amplifier.

The overall transient response of the amplifier is adjusted by setting C_T so as to obtain the minimum rise-time without overshoot for the output pulse. The rise-time obtained with the values shown is about 40 nsec.

All the diodes shown are normally non-conducting and serve to protect the transistors against excessive voltages in the presence of abnormal transients, or at the failure of other components.

2.5. POWER AND BIASES

The power for the coincidence circuit is obtained from two 27 volt supplies†, one negative grounded, one positive. The auxiliary fixed voltages (+ 1.5 V and — 6.3 V), the input bias voltages, and the coincidence bias current are derived from the primary sources by the auxiliary transistor stages shown in fig. 6.

† Lambda Model LT-2095M.

3. Construction

The coincidence circuit components shown in figs. 2, 4, and 5 are mounted on a 20-cm by 12-cm copper plate, 1.5 mm thick in the manner of a typical computer plug-board. External signal connections are made via BNC (Type 31-222) connectors mounted near the "front" end of the board, as is the connection to the clipping line. All components are mounted on ceramic terminal strips. Power and bias leads are brought to the unit via a plug-board type connector at the rear end of the board. The coincidence circuit board is shielded from external fields by copper cover plate (held by banana jacks). Photographs of the coincidence circuit board are shown in fig. 7.

In an alternate design the copper plates have a 3.5 cm front panel to provide space for the bias adjustment potentiometers. (See Appendix 2.)

The performance of the circuit depends critically on the layout and wiring of the components, particularly those of the input, limiting, and pick-off circuits. The inductance and capacitance of all leads shown by heavy lines in figs. 2 and 4 must be kept to a minimum. In particular the base and emitter leads in the limiter circuit are cut to $\frac{1}{2}$ cm and wired as directly as possible.

The expected failure rate of the transistors is an exponential function of the power dissipation;

accurate stabilization of the operating voltages and currents is, therefore, desirable. For this reason, the resistors in the diagrams are 1 percent tolerance resistors (Welwyn Type C, 1 watt

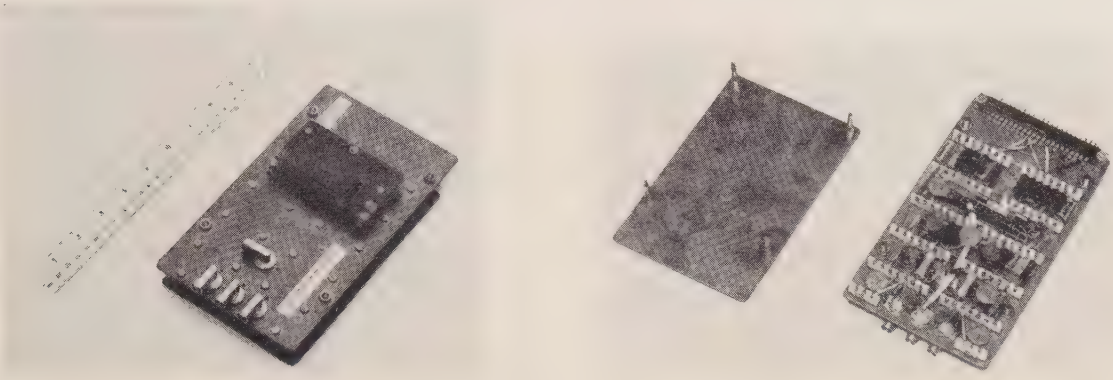

Fig. 7. Two views of a coincidence board.

where so indicated, $\frac{1}{2}$ watt otherwise) unless marked otherwise. All capacitors are 50 volt ceramic or electrolytic unless indicated differently.

The coincidence boards are mounted in a plug-board rack, usually 4 to 6 together. The power and bias control wires are connected via the plugs to a separate control chassis which serves up to 6 coincidence boards. The control chassis has also a meter and switch which permits monitoring all of the supply voltages, the input bias potentials, and the bias currents of the coincidence circuits. A rack containing 4 coincidence circuits and a control panel are shown in photographs of fig. 8. (In one of the photographs two auxiliary boards are also shown in the plug rack.)†

4. Performance

The performance of the coincidence circuit has been measured with input signals from a pulser and with signals from scintillation counters in a particle flux.

4.1. PULSER TESTS

Two input signals were obtained by a "tee"

† *Note added in proof*: It has been discovered that with some power supplies the turn-on transient is coupled directly to the bases of transistors T-1 and T-8 via the bypass electrolytic capacitors shown connected to the —27V supply, resulting in some transistor failures. These capacitors should be connected to ground (with suitable polarity).

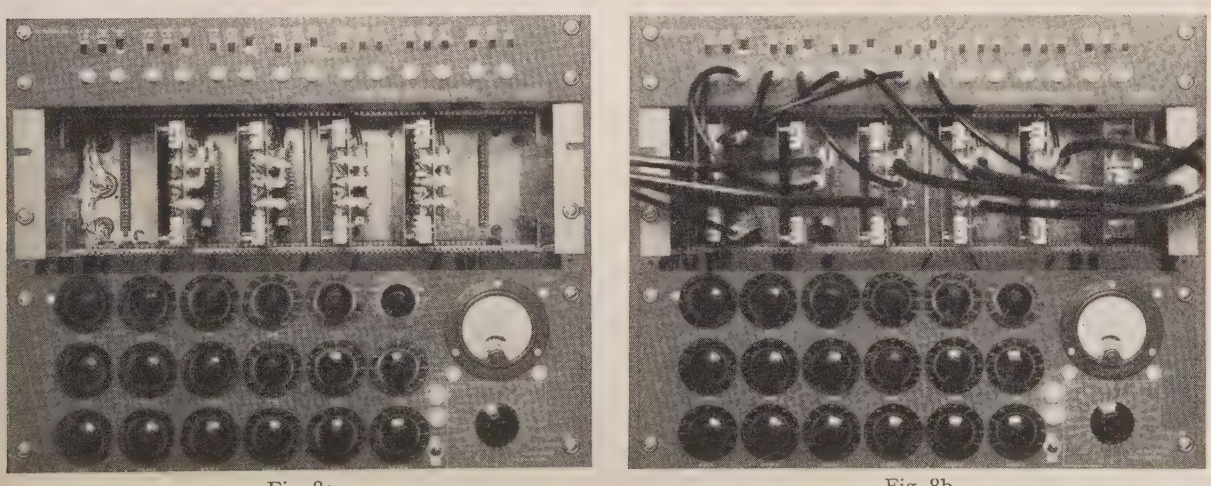

Fig. 8a Fig. 8b

Fig. 8. Photographs of a rack with four coincidence boards and a control panel. Photograph (a) shows the circuits before the input cables are connected. Photograph (b) shows the circuits cabled for an experiment.

from a mercury relay pulser and fed via matched 125 ohm cables and separate attenuators to the two input terminals. The signal rise-times were less than 1 nsec. Measurements were made of

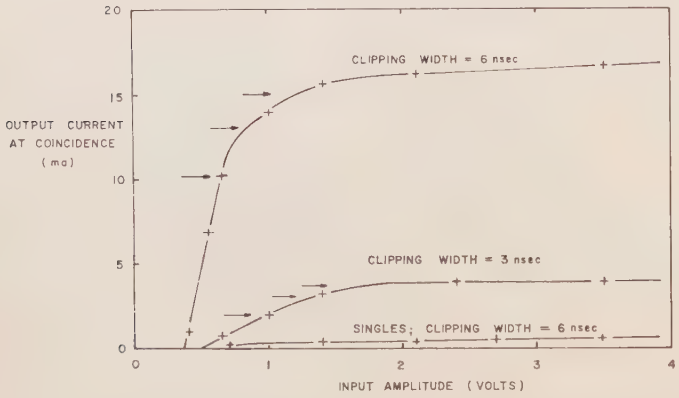
CLIPPING WIDTH = 6 nsec
CLIPPING WIDTH = 3 nsec
SINGLES; CLIPPING WIDTH = 6 nsec
OUTPUT CURRENT AT COINCIDENCE (ma)
INPUT AMPLITUDE (VOLTS)

Fig. 9. Amplitude of output current pulse as a function of input pulse amplitude for clipping widths of 3 nsec and 6 nsec. The horizontal arrows indicate the bias levels used for the subsequent measurements.

the amplitude of the output signal current (observed on an oscilloscope) as a function of the input signal amplitudes and delays. For these measurements the input amplitude is defined as that signal amplitude which would appear if the input cable were terminated in its characteristic impedence (125 ohms). The input pulse was rectangular with a width of 10 nsec. The measurements were made with a 6 nsec and with a 3 nsec clipping width in the coincidence circuit. The latter is considered the smallest width which will give reliable operation. For all of the measurements reported here the circuit was operated with the minimum input bias, with the coincidence bias set at 6.5 mA, and with the amplifier pulse-width and gain at 0.25 μsec and 250, respectively (as obtained with the parameters of figs. 4, 5).

The output amplitude as a function of the input amplitude, for equal input signals, is shown in fig. 9. In figs 10, 11 are plotted the results of measurements of the output amplitude at coincidence as a function of the amplitudes of the two input signals. It is evident that the circuit will operate satisfactorily on input signals of short rise time if their amplitudes are about 0.5 to 1.5 volts; the larger amplitude being required for the shorter clipping widths. The horizontal arrows indicate the bias settings used in the measurements described below.

In fig. 12 the output amplitude is shown as function of the clipping width for equal, coincident inputs (both inputs = 3.6 volts). The curve in the figure has been computed from eq. (1) (section 2) with the parameters k and τ adjusted to fit the curve to the observations. The values of τ and k obtained by this fit agree within 25 percent with values computed from the known circuit parameters.

The output amplitude as a function of the

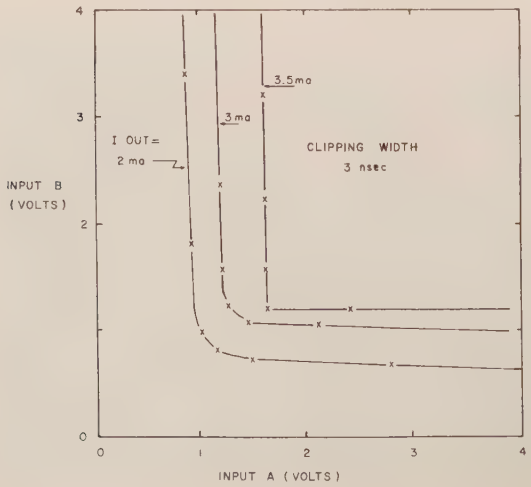

Fig. 10. Input signal amplitudes required to give output currents (peak), at coincidence, of 2.0, 3.0, and 3.5 mA, with a 3 nsec clipping width.

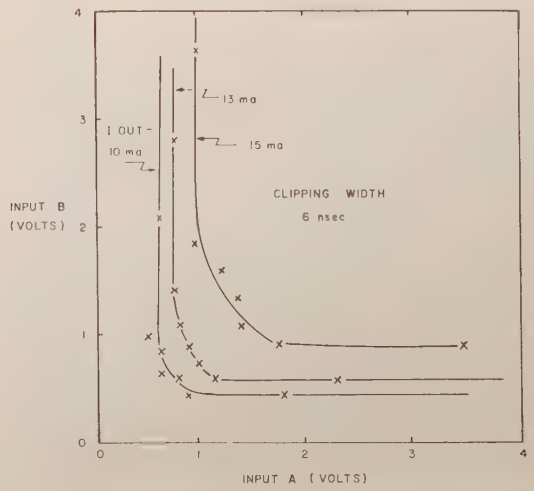

Fig. 11. Input signal amplitudes required to give output currents (peak), at coincidence, of 10, 13, and 15 mA, with a 6 nsec clipping width.

relative delay of the input signals is given in fig. 13. The width of these curves is approximately equal to clipping width as is expected.

4.2. COUNTER TESTS

Measurements have been made of the performance of the coincidence circuit when operated by the signals from two scintillation counters. Three scintillation counters approximately 16 cm × 20 cm × 1 cm, coupled by 10 cm light pipes to 6810-A photomultipliers, were arranged to count the particles from a target in the bremsstrahlung beam of the CalTech synchrotron. The first two counters of the array operated the fast coincidence circuit. The first counter was not shielded, and had a singles counting rate, during the beam pulse of about 10^6 pulses per second, (mostly electrons). The second counter was separated from the first by 5 cm of lead and had a singles rate of about 10^5 pulses per seconds (during the beam pulse). The third counter of the array was placed behind the second counter and was completely surrounded by an additonal 10 cm of lead. The output of the coincidence circuit was fed (with further amplification) to a 20 channel pulse spectrometer (kick-sorter). The third counter

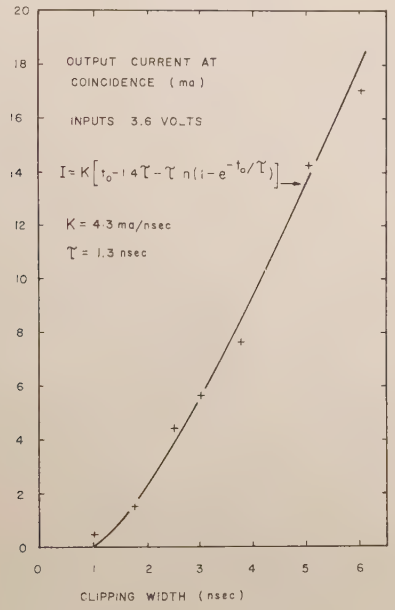

Fig. 12. Output current at coincidence as a function of the clipping width, for coincident inputs.

operated conventional 0.1 μsec circuits and its output was used to gate the spectrometer so that the events which were recorded corresponded to

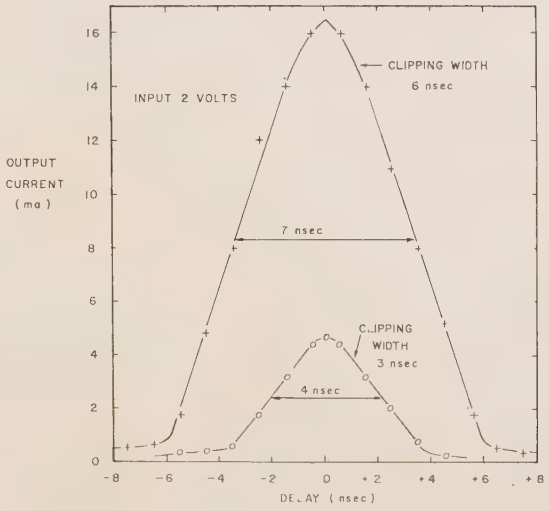

Fig. 13. Output current as a function of the relative delay of the input signals.

minimum ionizing particles traversing the first two counters (mostly relativistic pions).

The photomultiplier tubes were operated with a total voltage of about 2.5 kilovolts. With these voltages the pulse height from minimum ionizing particles was about 3 volts and had a rise-time of about 4 nsec when the cable was terminated at both ends with 125 ohms.

Pulse spectra obtained from the coincidence circuit, with the input cable lengths adjusted to give the maximum counting rates, are shown in figs. 14, 15. The spectrum is quite sharp for the 6 nsec clipping width, but is rather broad for the 3 nsec clipping width. The cause of this pulse spread has not been certainly identified, but is presumed to be related to the rather long rise-time of the input signals.

The coincidence rate as a function of the relative delay of the two input signals was measured by taking pulse spectra such as those in figs. 14, 15 with the length of cable to the two inputs adjusted to give several relative delay times between the two input signals. With each delay setting the pulse spectrum was obtained for the same integrated flux in the synchrotron beam. The results of these measure-

ments is given by plotting the total number of output pulses larger than some particular amplitude. These amplitudes called "Output Bias" are expressed in terms of the current out

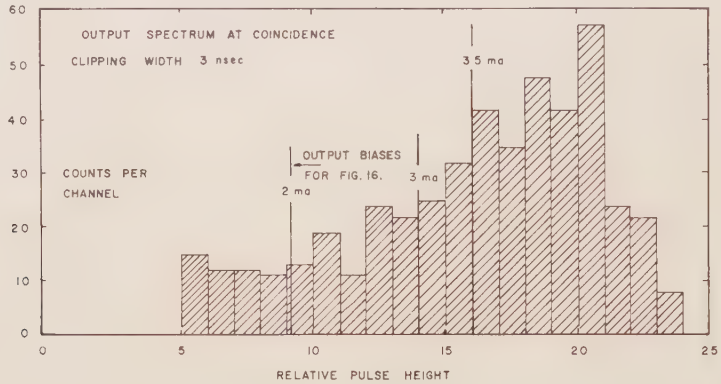

Fig. 14. Spectrum of output pulses, for 3 nsec cliping width, with the circuit operated by scintillation counters.

of the coincidence circuit, and are indicated by the heavy lines in figs. 14, 15.

The counting-rate vs. delay curves obtained are given in figs. 16, 17. The curve of fig. 17 for an output bias of 10 mA appears to give a high efficiency at coincidence—as is also confirmed by comparison with fig. 15. The "resolving time" for this configuration is about 5 nsec. Higher biases decrease the resolving time with some loss of efficiency. The curve of fig. 16 for an output bias of 2 mA gives the same counting rate at coincidence as is obtained with the 6 nsec clipping width and shows that the efficiency is again high, and the resolving time is 2.5 nsec. A resolving time of 1.5 nsec is obtained with an output bias of 3.5 mA, but the efficiency at coincidence is reduced to about 50 percent.

The widths of the delay curves at half maximum are indicated in the figures and are close to what is expected for the clipping widths used. The maximum counting rates in figs. 16, 17 correspond to about 50 counts per second during the beam pulse, compared to 10^6 counts per second in one counter. The slope of the sides of the delay curves is, for the various curves, between 1 and 2 nsec per decade in counting rate, and is quite acceptable for a twofold coincidence rate of less than 10^{-4} of the singles rate in the first counter†.

4.3. STABILITY

The only two factors which are expected to introduce variability into the operating characteristics of the coincidence circuits are the

† The somewhat steeper slopes obtained by Wentzel[1]) were with 3-fold coincidences.

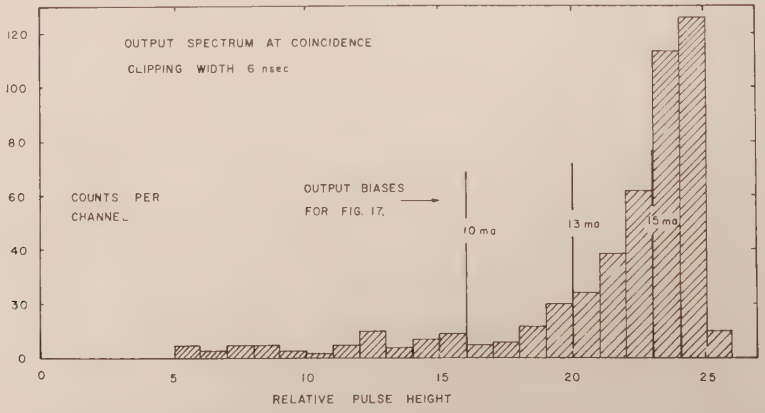

Fig. 15. Spectrum of output pulses, for 6 nsec clipping width, with the circuit operated by scintillation counters.

supply voltage and the temperature. The supply voltages are provided from supplies regulated to 2 percent and are monitored continually. The circuits have been designed to minimize the temperature dependent effects which appear primarily in the current-voltage

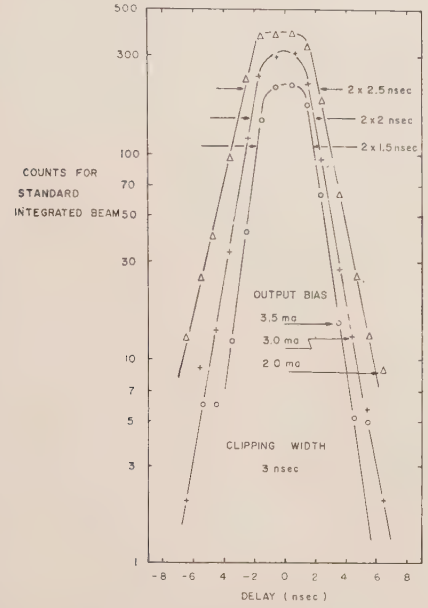

Fig. 16. Coincidence counting rate as a function of the relative cable delay at the inputs for 3 nsec clipping width.

characteristic of the base circuits of the transistors. The amplitude of the output signal at coincidence has been measured with the whole circuit at 20° C and at 40° C. At the two temperatures the output signals were the same within the 5 percent accuracy of the amplitude measurements.

4.4. MULTIPLEXING

The input resistance of the coincidence circuit described here is comparable with the impedance of the input cables. It is not possible to connect more than one coincidence circuit to one photomultiplier tube (P.M.T.) without significant loss in signal amplitude†. Yet in many experiments it is necessary to obtain several coincidence combinations from one counter. It is also often desirable to connect several counters to one coincidence input. Transistor "multiplexing" circuits have been made for connecting several P.M.T.'s to one coincidence input (mixing), and for connecting up to 5 circuits to one signal source (splitting).

The mixing circuit consists simply of several transistors as emitter input stages (grounded bases) with the collectors connected in parallel to an output cable. The response time of these circuits is determined primarily by the common collector capacitance. For more than two inputs, the collectors should be connected as stages of a lumped-element line. With this arrangement the output rise-times obtained are about 1 nsec.

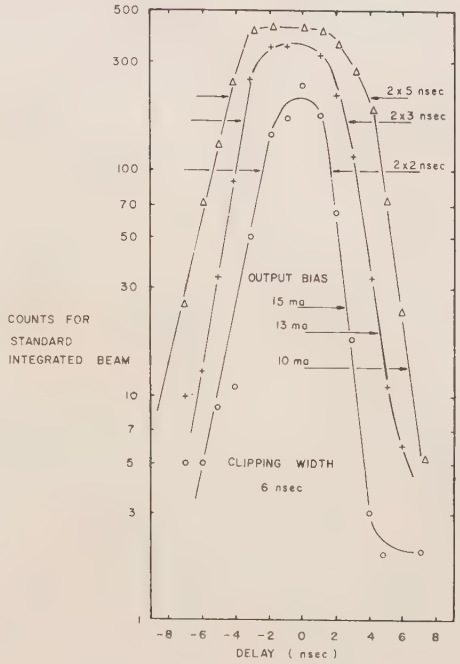

Fig. 17. Coincidence counting rate as a function of the relative cable delay at the inputs for 6 nsec clipping width.

The circuit used for coupling one P.M.T. to several coincidence circuits is shown in fig. 18. The large signal rise-time is about $2.5\ N\tau_\alpha$ where N is the number of output channels, and is, therefore, comparable to the rise-time of the signals from a P.M.T. for $N \leq 5$.

Several of the coincidence circuits have been constructed and operate uniformly as described here. Five circuits have been incorporated in an experiment on pion photoproduction now in progress. Several more are being constructed to form the basis of other experiments. It is felt

† Several input grids of vacuum tube coincidences circuits are often connected to one signal lead by connecting them as elements in a lumped component delay line.

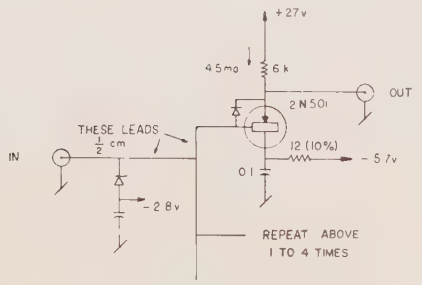

Fig. 18. Circuit for coupling one photomultiplier tube to 2 to 5 coincidence circuits.

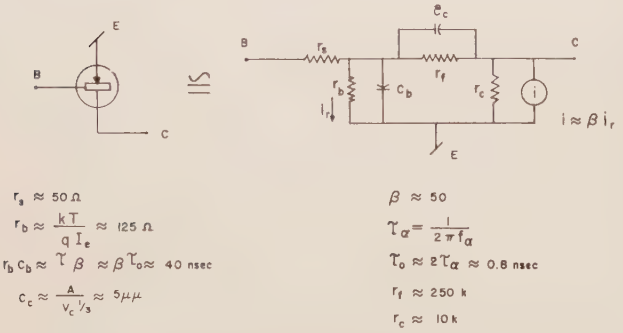

Fig. 19. Equivalent circuit of a base input stage, valid for transient time scales greater than τ_α.

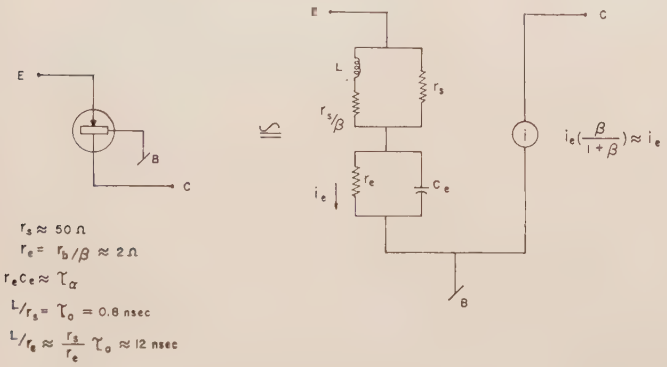

Fig. 20. Equivalent circuit for an emitter input stage for transient time scales greater than τ_α.

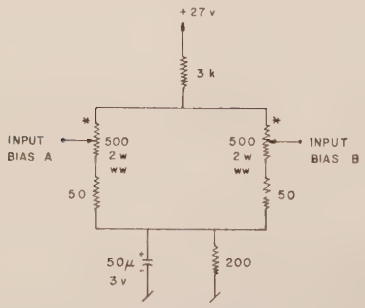

Fig. 21. Alternate input bias circuit. The voltage across the 50μ capacitor is used as + 1.5 V supply.

that the convenience, reliability, and stability of these circuits will make it feasible to perform experiments more complex than those which have been attempted before.

Appendix 1

An approximation to the small-signal equivalent circuit of the 2N501 transistor which is convenient for fast transients is shown in fig. 19. (The symbols r_b, etc. are often used in a different sense in the literature.) The large resistances r_f and r_c have a negligible effect on the response in low impedance circuits and can usually be ignored. The resistance r_s ("base spreading resistance") is ohmic, but the other parameters depend on the operating currents and voltages. Typical values and the nature of the principle dependencies are given in the figure. The typical values apply to an emitter current of about 10 mA and a collector voltage of a few volts. The representation shown becomes inadequate for time scales less than τ_0.

Neglecting C_c, r_f and r_c one can obtain the convenient equivalent circuit for a grounded base stage that is given in fig. 20. It should be noted that although the effective input resistance for slow signals is only about 4 ohms, the input impedance for fast signals approaches r_s. The input resistance can be taken as r_e only for transients whose time scale is longer than $L/r_e \approx 12$ nsec.

It has been found convenient to select the 2N501 transistors used in certain circuits. They are sorted into groups according to whether (1) $\beta < 50$, (2) $50 < \beta < 100$, (3) $100 < \beta$. Members of the second group are designated "2N501-2" and are used in critical circuits to ensure predictable performance.

Appendix 2

A more compact arrangement may be obtained by mounting the bias potentiometers on the coincidence boards. In this case the — 6.3 is supplied by an additional power supply†. The biases are derived on the individual boards with the coincidence bias circuits the same as in fig. 6. An input bias circuit is shown in fig. 21.

† Lambda Mod. LT-2095

NUCLEAR INSTRUMENTS AND METHODS 7 (1960) 135–144; NORTH-HOLLAND PUBLISHING CO.

AN EXTENSION OF THE TRANSFER MATRIX METHOD TO A BEAM TRANSPORT SYSTEM CONTAINING A SOLENOID

D. N. EDWARDS† and B. ROSE

A.E.R.E., *Harwell, Didcot, Berks., England*

Received 30 December 1959

The transfer matrix method of calculating beam transport problems is outlined, and extended to the case in which one of the elements is a solenoid, as is used in certain polarization experiments. The theoretical results are compared with measurements made with a proton beam and semi-quantitative agreement found.

1. Introduction

The study of polarization effects in nucleon scattering continues to be a very fruitful field of work as it gives direct information on non-central interactions between nucleons and nuclei. The phenomena is at present studied by observation of the differences in scattering to the right and to the left from an unpolarized target of a beam polarized in the vertical plane.

The conventional method of carrying out the investigation is to move a counter or counter telescope from one side of the beam to the other and compare counting rates in the two positions, care being taken to ensure that the efficiency of the counter is the same in the two positions, that the scattering angles are exactly equal and that numerous other small effects that may produce spurious asymmetries have been avoided or can be corrected for.

A significant advance of technique in the case of neutron scattering was made by Hillman, Stafford and Whitehead[1]), who used the longitudinal magnetic field of a large solenoid to rotate the direction of spin of the neutron about its direction of motion along the axis of the solenoid. In this way a tranversally and horizontally polarized beam was obtained, and the direction of the polarization could be reversed by reversing the magnetic field. Neutrons were scattered from the target into the vertical plane, and the experimental quantity of interest was the ratio of the counting rates in a particular counter for the two spin orientations.

Numerous advantages of this technique are fully outlined in the paper referred to. An additional advantage is that it allows one to use cumbersome counter arrays, which could be moved from one side of the beam to the other only with extreme difficulty. Furthermore, since systematic errors are largely eliminated, it makes possible accurate measurements of very small asymmetries.

As part of the study at Harwell of the nucleon-nucleon interactions, proton proton triple scattering experiments are being performed to determine certain of the Wolfenstein parameters[2]). These experiments involve the determination of the polarization of a beam of protons after scattering from hydrogen, the beam incident on the hydrogen being in a known state of polarization.

The final asymmetries in the experiment were expected to be small, from 0–5%, and the counting rates in a single counter telescope only a few counts per minute. Consequently in order to obtain significant data, it was necessary to reduce the spurious asymmetries in the

† Present address, University of Liverpool, Liverpool, England.

[1]) P. Hillman, G. H. Stafford and C. Whitehead, Nuovo Cimento **4** (1956) 67.

[2]) L. Wolfenstein, Phys. Rev. **96** (1954) 1654.

experiment to much less than 1% and to proliferate the detection system to increase the overall counting rate. These requirements therefore pointed to the use of a spin precessing solenoid which would eliminate a large number of systematic errors and allow the use of a large static counter array. In the event, an array of twenty five counters was used.

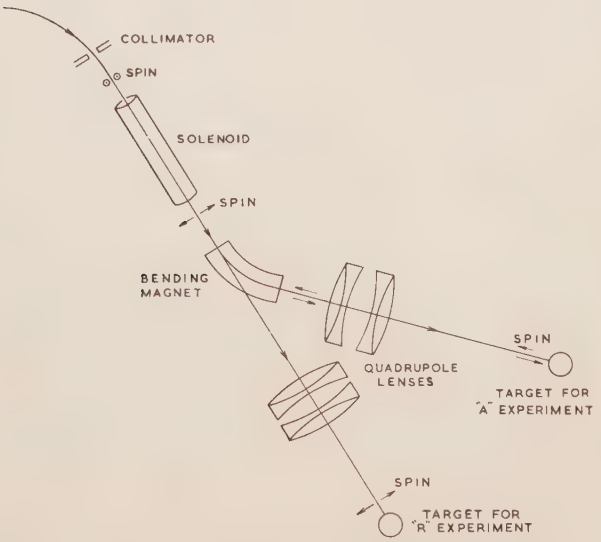

Fig. 1. Experimental arrangement of beams.

The difference between using a solenoid for neutron and proton experiments is that in the latter case there is a slight focussing action, and this will normally result in some difference in position of the beam spot for the two directions of solenoid current (and therefore of spin orientation). In particular, a movement up or down of the beam will result in a spurious asymmetry in the up and down scattering. In the experiment to measure R, it was necessary to keep the displacement of the centre of gravity of the beam spot to $\pm$ 0.02 cm in order to keep the correction for this effect to less than half of the statistical error of the measurement. It was necessary therefore carefully to study the optics of the proton beam to ensure that such an accuracy was obtainable.

The beam path for two typical experiments is illustrated in fig. 1. The straight through beam is suitable for a study of the Wolfenstein parameters R and D, and the deflected beam, in which the proton spin is precessed by the deflecting magnet so that it is parallel to the beam direction, is required for a study of the parameter A. The beam optics were studied by extending the transfer matrix method[3]), and finally the predictions of the theory were compared with experiment.

In this paper we describe briefly the transfer matrix method as applied to a beam transport system, and outline its extension to a system in which the displacements from the central orbit are not separable.

2. Transfer Matrix Method

This method is essentially a method of doing geometrical optics by simple matrix techniques. Consider a beam of protons moving with velocity v through a system of lenses, deflecting magnets etc. These optical elements will be assumed to be aligned so that the central ray emerging from one element enters the next one as the central ray. The central ray will be regarded as the z axis, though of course the axis is curved when the beam passes through a deflecting system. The velocity v of the protons will be constant in all we shall consider in this paper, and the angular divergence of the beam so small that the z component of velocity may be considered equal to v.

The position of any proton in the beam may be defined by its distance measured along the axis from an arbitrary position and its coordinates in an xy plane at right angles to the axis. The deviation and divergence of the proton from the axis may thus be represented by two vectors

$$\begin{pmatrix} x \\ \alpha \end{pmatrix} \quad \text{and} \quad \begin{pmatrix} y \\ \beta \end{pmatrix}.$$

2.1. STRAIGHT SECTION

Let us now consider a proton moving in a field free region or "straight section". If at the position $z = 0$, its position vector is

$$\begin{pmatrix} x \\ \alpha \end{pmatrix}$$

[3]) G. K. Green and E. D. Courant, Vol. 44, Handbuch der Physik p. 302;
H. Schneider, Nuclear Instruments 1 (1957) 269.

then it is obvious that at $z = l$, its position vector is

$$\begin{pmatrix} x + \alpha l \\ \alpha \end{pmatrix}$$

(see fig. 2). These vectors are related by the matrix equation

$$\begin{pmatrix} 1 & l \\ 0 & 1 \end{pmatrix} \begin{pmatrix} x \\ \alpha \end{pmatrix} = \begin{pmatrix} x + \alpha l \\ \alpha \end{pmatrix}$$

so that the effect of passing a proton through a

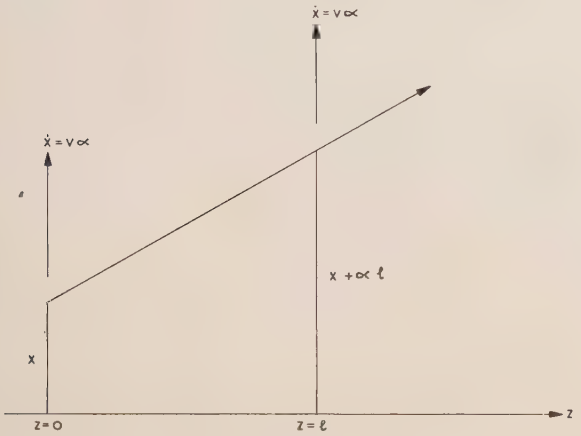

Fig. 2.
Change of vector on passing through a straight section.

straight section is to multiply its position vector by the above matrix, which we shall call L. An exactly similar relationship holds for the y-vectors.

2.2. THIN LENS

If a proton passes through a thin converging magnetic lens, its direction α is changed "instantaneously". A proton moving parallel to the axis is deflected so that it passes through the focus of the lens at a distance f along the axis, whilst a proton passing through the pole of the lens is undeflected. These two conditions may be written as

$$\begin{pmatrix} x \\ 0 \end{pmatrix} \rightarrow \begin{pmatrix} x \\ -x/f \end{pmatrix}$$

and

$$\begin{pmatrix} 0 \\ \alpha \end{pmatrix} \rightarrow \begin{pmatrix} 0 \\ \alpha \end{pmatrix}.$$

These conditions imply that passing through such a lens multiplies the position vector by the matrix

$$F = \begin{pmatrix} 1 & 0 \\ -1/f & 1 \end{pmatrix}$$

the transfer being made at the coincident principal planes.

A sequence of a straight section of length l_1, a converging lens of focal length f and another straight section of length l_2 is then represented by the matrix product

$$L_2 F L_1 = \begin{pmatrix} 1 - l_2/f & (l_1 + l_2 - l_1 l_2/f) \\ -1/f & 1 - l_1/f \end{pmatrix} = \begin{pmatrix} m_{11} & m_{12} \\ m_{21} & m_{22} \end{pmatrix}.$$

The ray whose position vector is

$$\begin{pmatrix} x \\ \alpha \end{pmatrix}$$

at the start of the straight section l_1 (which may be regarded here as the position of the "object") has at the end of l_2 a vector

$$\begin{pmatrix} m_{11}x + m_{12}\alpha \\ m_{21}x + m_{22}\alpha \end{pmatrix}.$$

There is a true optical image at this position if $m_{12} = 0$, for then the x coordinate is independent of the direction of the ray leaving the object, and the magnification of the system is m_{11}. These conditions are readily seen to be equivalent to the standard thin lens formulae

$$1/l_1 + 1/l_2 = 1/f$$

and magnification

$$= 1 - l_2/f = -l_2/l_1 .$$

2.3. QUADRUPOLE

In the simple approximation we are making, a quadrupole is equivalent to a converging lens of focal length f in one plane and a diverging lens of focal length $-f$ in the other. We may thus generalize our position vector to

$$\begin{pmatrix} x \\ \alpha \\ y \\ \beta \end{pmatrix}$$

and then the matrix for a single quadrupole becomes:

$$Q = \begin{pmatrix} 1 & l & 0 & 0 \\ -1/f & 1 & 0 & 0 \\ 0 & 0 & 1 & 0 \\ 0 & 0 & 1/f & 1 \end{pmatrix}.$$

A simple proof that the quadrupole field is equivalent to such a diverging–converging combination will now be given. Let the magnetic field configuration be

$$H_x = ky\,, \qquad H_y = kx\,, \qquad H_z = 0$$

where k is the field gradient, and the length of the magnetic field be b. Then the acceleration experienced by a particle of charge e and mass m moving through this field with velocity $\mathbf{v} = (\dot{x}, \dot{y}, v)$ is

$$\mathbf{a} = (e/mc)\,(-kvx\,,\ kvy\,,\ k(x\dot{x} - y\dot{y}))\,.$$

If we now make the approximation that the length b is so short that x and y do not change appreciably during the passage of the proton, the velocity acquired by the proton is

$$\int \mathbf{a}\,\mathrm{d}t = \mathbf{a}\,(b/v) = (bke/mc)\,(-x, y, 0)\,.$$

This means that a proton entering the quadrupole field at (x, y) in a direction parallel to the axis emerges so that in the x plane it intersects the axis after a distance mvc/bke, whilst in the y plane it appears to have left a point on the axis, a similar distance in front of the quadrupole. Q.E.D. This treatment of course takes no account of fringing field effects.

The matrix for a quadrupole pair, of focal lengths f_1 and f_2 respectively, and separated by a distance m may readily be shown to be

$$P = \begin{pmatrix} 1 - m/f_1 & m & 0 & 0 \\ -1/f_1 - 1/f_2 + m/f_1f_2 & 1 - m/f_2 & 0 & 0 \\ 0 & 0 & 1 + m/f_1 & m \\ 0 & 0 & 1/f_1 + 1/f_2 + m/f_1f_2 & 1 + m/f_2 \end{pmatrix}.$$

Positive values of f_1 or f_2 mean that the quadrupole concerned is focussing in the x direction.

2.4. WEDGE MAGNET

This is considered here to consist of a region of space (fig. 3a) with a magnetic field $\boldsymbol{H} = (0, H, 0)$ which is uniform apart from fringing fields. The beam enters at an angle ε_1 to the normal to the field boundary, and emerges at an angle ε_2. The angles ε_1 and ε_2 are to be considered as positive if the proton path within the magnetic field curves towards the normal to the field boundary. In fig. 3 both ε_1 and ε_2 are positive. The central orbit is deflected through an angle ϕ and has a uniform radius of curvature ρ.

The matrix for the x direction is determined from consideration of the orbits of two rays, one entering the magnetic field parallel to the axis but displaced from it, orbit a, and the other entering on the axis but inclined to it, orbit b. These rays are illustrated in fig. 3b.

The matrix for the y direction is determined from the fact that a fringe field is equivalent to a thin lens of focal length $\rho \cot \varepsilon_1$, the lens being converging when the axial ray is deflected towards the normal to the field boundary on entering the magnetic field, and vice versa. In passage through the magnet, the proton therefore sees two thin lenses separated by a distance $\rho\phi$.

The transfer matrix corresponding to the wedge magnet is found to be

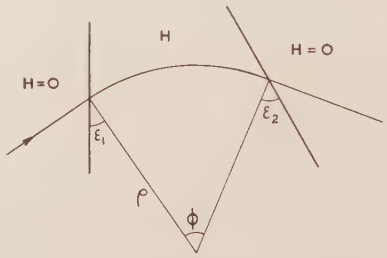

Fig. 3a

Fig. 3b

Fig. 3. Wedge magnet, and proton paths studied to determine matrix.

$$W = \begin{pmatrix} \cos(\phi - \varepsilon_1)\sec\varepsilon_1 & \rho\sin\phi & 0 & 0 \\ -\dfrac{\sin(\phi - \varepsilon_1 - \varepsilon_2)}{\rho\cos\varepsilon_1\cos\varepsilon_2} & \cos(\phi - \varepsilon_2)\sec\varepsilon_2 & 0 & 0 \\ 0 & 0 & 1 - \phi\tan\varepsilon_1 & \rho/\phi \\ 0 & 0 & -(\tan\varepsilon_1 + \tan\varepsilon_2 - \phi\tan\varepsilon_1\tan\varepsilon_2)/\rho & 1 - \phi\tan\varepsilon_2 \end{pmatrix}.$$

2.5. SOLENOID

Consider now a solenoid which we shall assume generates a uniform axial magnetic field $\boldsymbol{H} = (0, 0, H_z)$, apart from a limited region near either end. We shall consider first the effect of the uniform field and then of the fringing fields.

The orbit of a proton, projected upon the xy plane, is the segment of a circle (see fig. 4). The radius of the circle is independent of the position (x,y,z) and is equal to $(\dot{x}^2 + \dot{y}^2)^{\frac{1}{2}}\, mc/He$ when the velocity of the particle on entering the

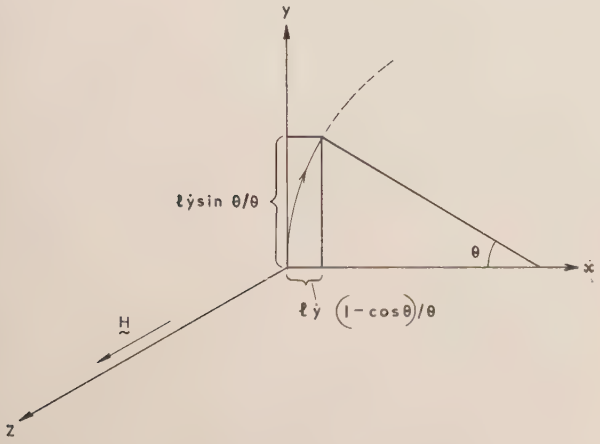

Fig. 4. Projection, on to plane perpendicular to axis, of proton path which is initially not parallel to the axis.

solenoid is $(\dot{x}, \dot{y}, v)$, whilst the angular velocity round the circle is He/mc. In the time l/v in which the proton passes through the length of the solenoid, the angular length of the circular segment is $\theta = Hel/mvc$.

Consequently it may be shown readily by making small constructions as in fig. 4 that on passing along the solenoid the vectors

$$\begin{pmatrix} x \\ 0 \\ y \\ 0 \end{pmatrix} \to \begin{pmatrix} x \\ 0 \\ y \\ 0 \end{pmatrix}, \quad \begin{pmatrix} 0 \\ \alpha \\ 0 \\ 0 \end{pmatrix} \to \begin{pmatrix} (l\alpha/\theta)\sin\theta \\ \alpha\cos\theta \\ -(l\alpha/\theta)(1-\cos\theta) \\ -\alpha\sin\theta \end{pmatrix} \text{ and } \begin{pmatrix} 0 \\ 0 \\ 0 \\ \beta \end{pmatrix} \to \begin{pmatrix} (l\beta/\theta)(1-\cos\theta) \\ \beta\sin\theta \\ (l\beta/\theta)\sin\theta \\ \beta\cos\theta \end{pmatrix}$$

and therefore the matrix representing the passage through the uniform field of the solenoid is represented by the matrix

$$M_{\text{unif}} = \begin{pmatrix} l & l\sin\theta/\theta & 0 & l(1-\cos\theta)/\theta \\ 0 & \cos\theta & 0 & \sin\theta \\ 0 & -l(1-\cos\theta)/\theta & 1 & l\sin\theta/\theta \\ 0 & -\sin\theta & 0 & \cos\theta \end{pmatrix}.$$

If the direction of the magnetic field is reversed, it is necessary to change the sign of θ.

We must now consider the effects produced at either end of the solenoid, where radial components of the magnetic field produce focussing effects.

Owing to the circular symmetry, the magnetic field near the ends may be written as $(H_r x/r, H_r y/r, H_z)$ where $r^2 = x^2 + y^2$.

Now, by applying Gauss's theorem to a cylindrically shaped surface with its axis on the axis of the solenoid, it may be shown that $H_r = -\frac{1}{2} r\,\partial H_z/\partial z = -\frac{1}{2} rH'$ for r small, so that we may write the magnetic field as $(-\frac{1}{2} x H', -\frac{1}{2} y H', H_z)$. The acceleration of a proton at

$$\begin{pmatrix} x \\ \alpha \\ y \\ \beta \end{pmatrix}$$

is given by

$$\boldsymbol{a} = (e/mc)(\dot{y}H_z + \tfrac{1}{2} vyH', -\dot{x}H_z - \tfrac{1}{2} vxH' \;\; 0)$$

where we have neglected a second order term in the z component.

The terms $\dot{y}H_z$ and $\dot{x}H_z$ are dependent upon the longitudinal field only and effects due to them should be included with the effects of the uniform central field. This is reasonable provided that the length of the solenoid is much greater

than its diameter, as it was for the solenoid used in the experiment, where the longitudinal field rose from 10 to 90% of its centre value over a distance of 0.075 l.

Since the fringing field is so short we may assume that x and y remain constant, and find the change in velocity of the proton is

$$\int \boldsymbol{a}\,\mathrm{d}t = \int \boldsymbol{a}\,\mathrm{d}z/v = \left((eH/2mc)\,y\,,\ -(eH/2mc)\,x,\ 0\right).$$

This means that on passing through the fringing field and entering the solenoid we have the following vector changes

$$\begin{pmatrix} x \\ 0 \\ y \\ 0 \end{pmatrix} \rightarrow \begin{pmatrix} x \\ +(eH/2mc)\,y \\ y \\ -(eH/2mc)\,x \end{pmatrix} \quad \text{and} \quad \begin{pmatrix} 0 \\ \alpha \\ 0 \\ \beta \end{pmatrix} \rightarrow \begin{pmatrix} 0 \\ \alpha \\ 0 \\ \beta \end{pmatrix}$$

so that the corresponding matrix is

$$M_{\mathrm{in}} = \begin{pmatrix} 1 & 0 & 0 & 0 \\ 0 & 1 & +\theta/2l & 0 \\ 0 & 0 & 1 & 0 \\ -\theta/2l & 0 & 0 & 1 \end{pmatrix}.$$

The matrix M_{out} for the end where the proton leaves the solenoid is obtained by reversing the sign of θ.

The complete effect of passing a proton through a solenoid is therefore represented by

$$S = M_{\mathrm{out}}M_{\mathrm{unif}}M_{\mathrm{in}} = \begin{pmatrix} \gamma & l\delta & \gamma t & l\delta t \\ -\varepsilon/l & \gamma & -\varepsilon t/l & \gamma t \\ -\gamma t & -l\delta t & \gamma & l\delta \\ \varepsilon t/l & -\gamma t & -\varepsilon/l & \gamma \end{pmatrix}$$

where

$\gamma = \frac{1}{2}\,(1 + \cos\theta)$

$\delta = \sin\theta/\theta$

$\varepsilon = \frac{1}{4}\,(\theta \sin\theta)$

$t = \tan\,(\frac{1}{2}\,\theta)$.

If the magnetic field is zero, $\theta = 0$ and the matrix reduces to that for a straight section of length l, as required.

The derivation of the effects of the solenoid fringing field depend upon the relationship $H_r/r = -\frac{1}{2}\,H'$ which was proved only for small values of r. An exact calculation of the fringing field was carried out for the solenoid actually used, which showed this relationship to be accurate to about 10% up to three quarters of the radius.

For the application in which the proton spin is turned through 90° on passage through the solenoid, the corresponding value of θ is $90°/\mu_{\mathrm{p}} = 32.3°$. The matrix corresponding to the conditions in which the solenoid field is reversed is obtained by changing the sign of θ.

3. Application to Experiment to Measure *R*

The beam arrangements for this experiment are illustrated in fig. 1, using the undeflected beam. The collimator is regarded as the object of the system. The matrix describing the system is therefore $M = L_3PL_2SL_1$, where L_1, L_2, L_3 represent the straight sections, of lengths l_1, l_2 and l_3 between the collimator and the solenoid, between the solenoid and the first quadrupole lens and between the second quadrupole lens and the target respectively.

We wish to obtain a true image of the collimator at the position of the target with the solenoid switched off, to study the effect on this image of switching on the solenoid, and the further effect of the divergence of the beam illuminating the object collimator. As a further condition it was desirable to specify the magnifications in the x and y direction, m_x and m_y, with the solenoid switched off.

The conditions for a focus are $m_{12} = m_{34} = 0$, as outlined in section 2.2, whilst the magnifications are m_{11} and m_{33}. We accordingly have four conditions, so that with a fixed position for object and image, we can specify the position and focal lengths of the two quadrupoles.
If we define

$$A = 1 + ml_3/f_1f_2 \qquad lC = (m + l_3 + l_2A)$$

$$B = m/f_1 + l_3/f_1 + l_3/f_2 \qquad lD = (ml_3/f_2 + l_2B)$$

then certain of the elements of the matrix M are

$$m_{11} = (A - B)\gamma - (C - D)\,\varepsilon$$

$$m_{12} = (A - B)\,(l_1\gamma + l\delta) + (C - D)\,(l\gamma - l_1\varepsilon)$$

$$m_{13} = (A - B)\,\gamma t - (C - D)\,\varepsilon t = m_{11}t$$

$$m_{14} = (A - B)\,(l_1\gamma + l\delta)\,t + (C - D)\,(l\gamma - l_1\varepsilon)\,t = m_{12}t$$

$$m_{31} = -(A + B)\gamma t + (C + D)\varepsilon t = -m_{33}t$$

$$m_{32} = -(A + B)(l_1\gamma + l\delta)t - (C + D)(l\gamma - l_1\varepsilon)t = -m_{34}t$$

$$m_{33} = (A + B)\gamma - (C + D)\varepsilon$$

$$m_{34} = (A + B)(l_1\gamma + l\delta) + (C + D)(l\gamma - l_1\varepsilon) .$$

When the solenoid is switched off the values become

$$m_{11} = (A - B) ;$$

$$m_{12} = (l_1 + l)(A - B) + l(C - D) ,$$

$$m_{13} = m_{14} = 0 ,$$

$$m_{31} = m_{32} = 0 ,$$

$$m_{33} = A + B ,$$

$$m_{34} = (l_1 + l)(A + B) + l(C + D) .$$

The four conditions we have imposed with the solenoid off lead to the solution

$$A = \tfrac{1}{2}(m_x + m_y) \qquad lC = -(l + l_1)A$$

$$B = \tfrac{1}{2}(-m_x + m_y) \qquad lD = -(l + l_1)B$$

and putting the overall length of the system $l_1 + l + l_2 + m + l_3 = L$, we find the explicit solutions for our four chosen variables

$$\frac{m}{L} = \frac{B^2}{(A - 1)(B^2 - A^2 + A)} , \quad \frac{f_1}{L} = \frac{B}{(A - 1)^2}$$

$$\frac{l_3}{L} = \frac{B^2 - A^2}{B^2 - A^2 + A} , \qquad \frac{f_2}{L} = \frac{B(B^2 - A^2)}{(B^2 - A^2 + A)^2} .$$

When the solenoid is switched on, it is apparent that the x component of a proton in the image plane now becomes a function of all of the components of its original position vector

$$\begin{pmatrix} x_0 \\ \alpha_0 \\ y_0 \\ \beta_0 \end{pmatrix}$$

and similarly for the y component. Let us first neglect the effect of the inclinations α_0 and β_0. The proton at $(x_0, 0)$ on the object plane becomes that at $(m_{11}x_0, m_{31}x_0)$ on the image plane, whilst that at $(0, y_0)$ emerges at $(m_{13}y_0, m_{33}y_0)$. Then it may readily be shown that if

$$\tan\xi = m_{31}/m_{11} \qquad \text{and} \qquad \tan\eta = -m_{13}/m_{33}$$

so that ξ and η are the angles through which the x and y axes respectively are rotated between the object and image planes, then

$$\tan\xi = (-m_y/m_x)\tan(\tfrac{1}{2}\theta)$$

and

$$\tan\eta = (-m_x/m_y)\tan(\tfrac{1}{2}\theta) .$$

The image is accordingly rotated and sheared with respect to the object. It should be noted that this is a general result which is quantitatively correct independent of the particular combination of quadrupoles, wedges and straight sections following the solenoid.

The effect on the image of beam divergence arises from the elements m_{12}, m_{14}, m_{32} and m_{34}. These elements each depend upon l_1, and cannot be made zero unless $\theta = 0$. Their minimum value is attained when $l_1 = -\frac{1}{2}l$, i.e. the solenoid is placed so that the object collimator is at its centre.

In the case of interest to us, two configurations were studied, namely, with the solenoid as close as possible to the object, and with it as close as possible to the first quadrupole. For the values $\theta = 32.3°$, $L = 13.5$, $l = 2.565$, $m_x = -0.74$ and $m_y = -0.22$, all lengths being in metres, the conditions for focus with the solenoid off lead to the values $m = 1.00$, $l_3 = 3.375$, $f_1 = 1.61$ and $f_2 = -1.38$. The effects of beam divergence on the image size were very small in the first case ($l_1 = 0$) and very large indeed in the second case ($l_1 = 6.56$). These effects are illustrated in fig. 5, where the assumption is made that the proton beam diverges in the horizontal plane from a point 2 ms before the object collimator, and that there is no vertical divergence of the beam. This assumption corresponds roughly to the conditions in the Harwell cyclotron.

It is clear therefore that the effect of beam divergence can be minimized by placing the solenoid as close to the object collimator as possible. Consideration of reversability implies that a position as close to the image as possible would also be satisfactory.

A more general requirement could be made, that we have a true focus when the solenoid is switched on. The conditions now lead to the solution:

$$A = \tfrac{1}{2}(m_x + m_y)/(\gamma - \varepsilon P)\,, \qquad C = AP\,,$$

$$B = \tfrac{1}{2}(-m_x + m_y)/(\gamma - \varepsilon P)\,, \qquad D = BP\,,$$

where $P = (l_1\gamma + l\delta)/(l_1\varepsilon - l\gamma)$, and we have explicit expressions for the four variables

$$\frac{m}{L - Pl - l - l_1} = \frac{B^2}{(A-1)(B^2 - A^2 + A)}\,,$$

$$\frac{l_3}{L - Pl - l - l_1} = \frac{B^2 - A^2}{B^2 - A^2 + A}\,,$$

$$\frac{f_1}{L - Pl - l - l_1} = \frac{B}{(A-1)^2}\,,$$

$$\frac{f_2}{L - Pl - l - l_1} = \frac{B(B^2 - A^2)}{(B^2 - A^2 + A)^2}\,.$$

Since $\gamma, \delta, \varepsilon$ and P are all even functions of θ, the solution holds for both directions of solenoid current.

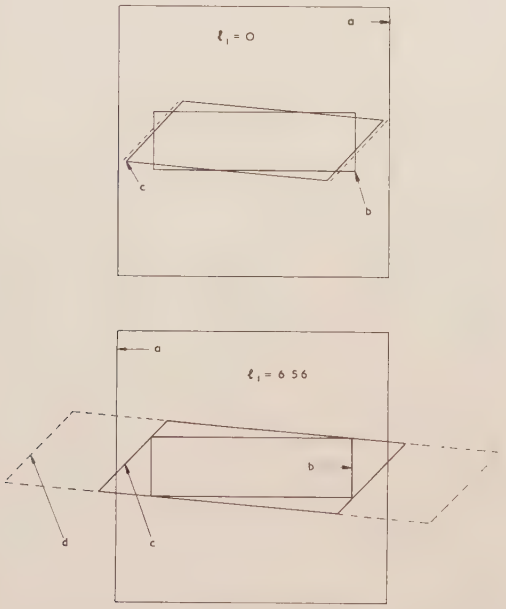

Fig. 5. Calculated effects on image size of switching on solenoid under various conditions of beam divergence, for $l_1 = 0$ and $l_1 = 6.56$ m. (a) Object; (b) Image with solenoid off; (c) Image with solenoid on, and no beam divergence, without refocussing; (d) Image with solenoid on, without refocussing, and beam diverging in horizontal plane only (see text).

With the above values for L, l_1, m and l_3, the values of the magnifications were virtually unchanged, so that the focussed image is virtually the same as (c) in fig. 5. The focal lengths were also almost unchanged for $l_1 = 0$, but for $l_1 = 6.56$ it was found that $f_1 = 1.72$ and $f_2 = -1.43$, a change of about 5%; a solution which would be perfectly acceptable in some cases. However this type of solution, in which the quadrupole currents for a true focus are a function of the solenoid current would be disadvantageous in cases where it is required to measure an asymmetry as a function of the solenoid current.

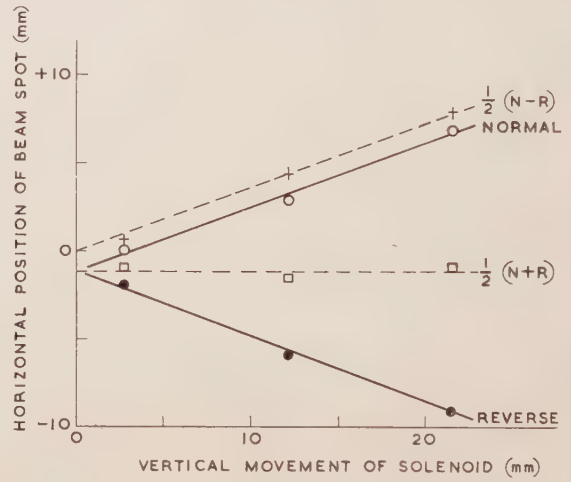

Fig. 6a

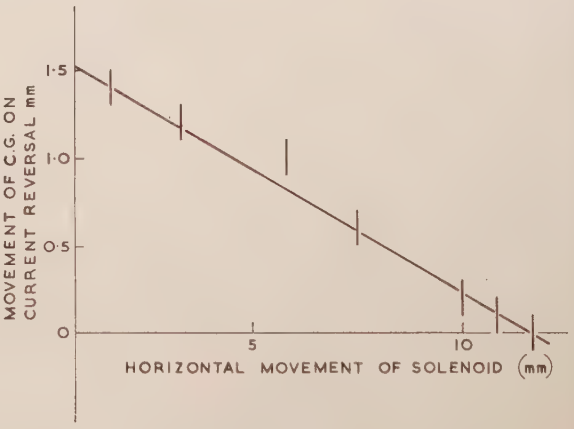

Fig. 6b

Fig. 6. Shift of beam spot on reversal of solenoid current, as a function of positions of the end of the solenoid nearest the object collimator. Points on 6(a) were measured by eye to the nearest mm; points on 6(b) were measured with a microdensitometer to $\pm$ 0.1 mm (see text).

On the basis of calculations of this sort, it was decided to place the solenoid close to the object collimator, and the experimental work

described later was based on this arrangement.

It will be apparent from fig. 5 that if the image is non-uniformly illuminated, the result of reversing the solenoid will be to produce a vertical movement of the centre of gravity of the beam spot. This centre of gravity was determined by exposing an Ilford B X-ray film to the proton beam for the two directions of solenoid current, and mapping the density of the image with a microdensitometer. The sensitivity of the blackening to exposure was measured and it was found that the position of the centre of gravity was not a critical function of assumptions made about the film sensitivity.

Let us suppose the centre of gravity of the incident beam is at the point $(x_0\, y_0)$ on the object plane. If we neglect the effects of beam divergence, then the centre of gravity will appear on the image plane at $(m_{11}\, x_0 + m_{13}\, y_0,\ m_{31}\, x_0 + m_{33}\, y_0)$. If the elements of the matrix for reversed solenoid current are denoted by primes, then it is easy to see from the equations of section 3 that

$$m_{11} = m'_{11}, \quad m_{13} = -m'_{13}, \quad m_{31} = -m'_{31}$$

and

$$m_{33} = m'_{33}\ .$$

Therefore the difference between the positions of the beam spots on reversing the solenoid current, is $(2m_{13}\, y_0,\ 2m_{31}\, x_0)$ whilst the mean position is $(m_{11}\, x_0,\ m_{33}\, y_0)$.

If therefore the position of the centre of gravity is given an x displacement only, which would be achieved in effect by moving the solenoid in the x direction, then the mean differences between the x coordinates of the two spots in unaffected, whilst the mean difference of the y coordinates is changed by m_{31} times the displacement.

Results of measurements made to observe these effects are shown in fig. 6. If the end of the solenoid near the collimator is displaced by 1 cm, the effective displacement of the object relative to the solenoid axis is $(l + l_1)/l$ cm, whereas if the other end is moved, the effective displacement of the object is l_1/l cm. Whilst the measurements were being carried out, the ratios $(l + l_1)l$ and l_1/l were respectively $\approx \frac{4}{3}$ and $\frac{1}{3}$. Consequently horizontal displacement by 1 cm of the end near the collimator should change the vertical difference between the spots by 0.21 cm compared with the observed value of 0.13 cm. Similarly, a vertical displacement of 1 cm should yield a difference of 0.59 cm compared with the experimental value of 0.72 cm. The mean horizontal position of the spots was not affected by a vertical displacement, within the accuracy of the measurements. It was also found that the position of the beams spots was much less sensitive to the displacement of the end of the solenoid remote from the collimator,

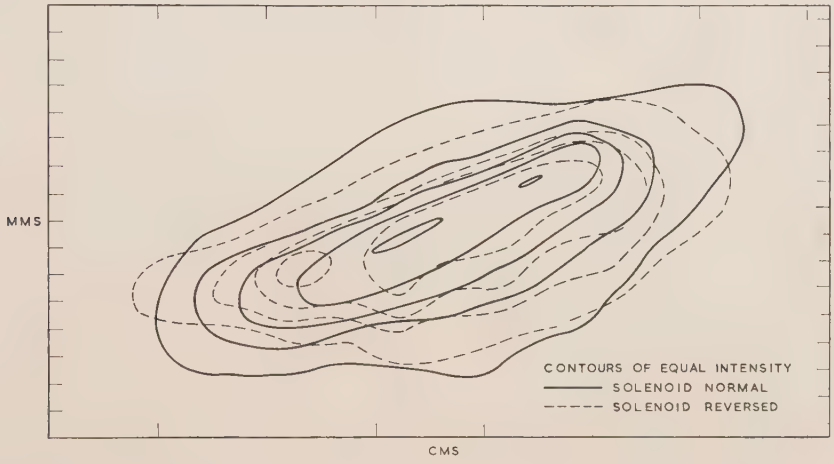

Fig. 7. Contour diagrams of beam spot intensity for opposite solenoid currents, illustrating rotation of the image even though its centre of gravity does not move.

though no quantitative estimate was made. This measure of agreement between theory and experiment was considered adequate in view of the approximations used.

Contour diagrams of the beam spot intensity for opposite solenoid currents are shown in fig. 7. The slight relative rotation of the images is apparent, though it is difficult to assess accurately because of small changes of shape of the spot on reversal of the solenoid current.

4. Conclusion

The extension of the transfer matrix technique to the use of 4×4 matrices containing elements which "mix" x and y coordinates makes it possible to calculate quickly the effect of introducing a solenoid into a beam transport system. The effect of the solenoid on the beam appears to conform with theoretical predictions within the rather limited tests carried out.

It was possible by careful measurements with a microphotodensitometer to estimate the position of the centre of gravity of the beam spot to $\pm$ 0.1 mm, and, by careful positioning of the solenoid, to keep its location fixed to this accuracy when the solenoid current was reversed.

It should be remarked that one does not expect these calculations based on a simple linear theory and the thin lens quadrupole approximation to give precise answers, but rather to enable one quickly to develope a feeling for the magnitudes involved, to determine roughly the range of possibilities open in a particular experiment and to provide starting points from which the optimum values of, say quadrupole currents or positions of magnetic devices may be determined by experiment.

It is a pleasure to thank Mr. A. E. Taylor and Mr. E. Wood for useful discussions and for much assistance during the experimental work. One of us (D. N. E.) wishes to acknowledge receipt of a Junior Harwell Fellowship.

NUCLEAR INSTRUMENTS AND METHODS 7 (1960) 145–152; NORTH-HOLLAND PUBLISHING CO.

A 4π-FISSION DETECTOR

A. DERUYTTER

Centre d'Etude de l'Energie Nucléaire, Mol, Belgium

Received 30 December 1959

A technique has been developed to prepare fission foils of uniform thickness on thin plastic films (VYNS-3) coated with Al, to be used as a cathode inside a 4π chamber. The optimum thickness of the Al-coating is 2.5 $\mu g/cm^2$ on both sides of the film. These films are brought in an ionisation chamber filled with a mixture of 98% A and 2% N_2. The influence of the thickness of the U^{235}-film on the discrimination between fission and alpha pulses has been studied.

The evaluated efficiency of the counter for a 1 mg/cm^2 $U^{235}O_2$-foil is $(92 \pm 1)\%$; for a 0.1 mg/cm^2 foil $(97.5 \pm 0.3)\%$.

1. Introduction

One of the basic problems generally encountered in the measurement of absolute fission cross sections is the determination of the efficiency of the counter. In view of experiments of that kind, we developed a fission counter based on a 4π geometry where the uranium oxyde film is seen by two anodes, which collect the ionisation produced by both fission fragments in order to increase the ratio of fission to alpha pulse height.

The techniques we developed could be used in other fission studies, like those involving the measurement of the mass distribution of the fission fragments, or cross section work where the quantity of fissile isotope has to be as large as possible and is normally limited by the spontaneous alpha pulse-rate.

The efficiency of a fission chamber (i.e. the ratio of detected to occuring fission events) is influenced by the alpha pile-up and the self-absorption of the fission foil.

The alpha pile-up decreases the discrimination between the alpha and the fission pulses. It depends upon the half life, the quantity of the isotope present, and the collection-time of the chamber. Assuming rectangular pulses with height P and duration time τ, the number of counts due to the superposition of n pulses is given by[1])

$$C(nP) = \left(\frac{n_0}{1 + n_0\tau}\right) \frac{(n_0\tau)^{n-1}}{(n-1)!} \exp(-n_0\tau) \qquad (1)$$

where n_0 is the number of desintegrations per unit of time and is fixed by the statistics of the experiment. The number of alpha pile-up pulses of the same order of magnitude as the fission pulses will decrease with τ, (so, electron collection must be used) and also by increasing the ratio of fission to alpha pulses.

To do this, a first method[1]) is to adjust the electrode distance and the gaspressure, so that the fission fragments lose only a fraction of their range in the counter gas. This method will increase the ratio, for unlike the alpha particle, the fission fragment has its largest specific energy loss at the beginning of its track. But even in a shallow parallel plate chamber, as the fragments are emitted isotropically, most of them move a larger distance in the counter gas than the electrode spacing. Collimators reduce the intensity too much.

Another method[2]) is to have two anodes looking at the same fission film. One uses then the sum of the 2 simultaneous fission fragment energies in the presence of a double alpha activity. Using formula (1) with the following values: for a 2π chamber:

$$\tau = 1\ \mu\text{sec}$$
$$n_0 = 10^6$$
$$n = 5$$

[1]) Rossi and Staub, Ionization Chambers and Counters (McGraw Hill Book Company, Inc. 1949) p. 204.

[2]) Y. B. Adamchuk *et al.*, Peaceful uses of Atomic Energy, Proceedings of the International Conference in Geneva, August 1955, Vol. 4, p. 216.

for a 4π chamber:

$$\tau = 1\ \mu\text{sec}$$

$$n_0 = 2 \times 10^6$$

$$n = 10\ .$$

One gets:

$$\frac{c\,(2\pi)}{c\,(4\pi)} = 22\ .$$

This indicates a much better discrimination for the 4π -chamber.

2. Fission Chamber and Electronic Equipment

The fission chamber (figs. 1 and 2) used is a parallel plate ionization chamber, with an electrode spacing of 0.9 cm. The anode voltage is 500 Volts. It is filled with 98% in volume of argon and 2% nitrogen up to a total pressure of 1 atmosphere. This gasfilling[3]) is not sensitive to a small oxygen contamination. A mass-spectrometric analysis of the gases used indicates: in A:

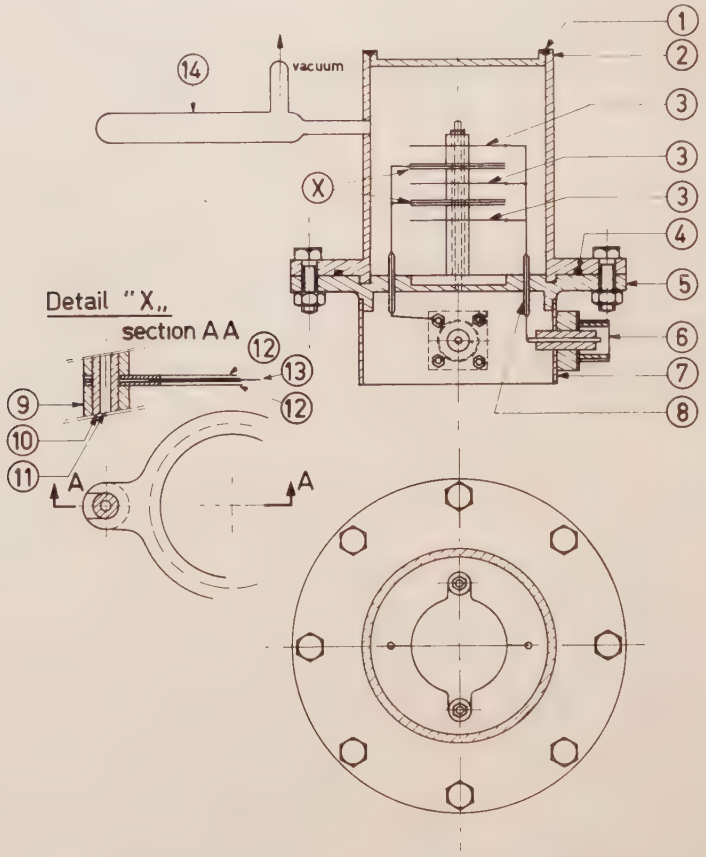

Fig. 1. Drawing of the fission chamber. Scale: 1/2. 1. argon welded; 2. aluminium cylinder; 3. aluminium foil 0.2 mm; 4. teflon gasket; 5. aluminium plate; 6. amphenol plug; 7. brass; 8. metal to glass seal Ediswan; 9. teflon ring shaped insulator; 10. plexiglass insulator; 11. brass; 12. brass; 13. transparent uranium foil; 14. cold trap.

The loss of fission pulses by selfabsorption in the foil is related to the foil thickness and homogeneity. So the main problem will be to prepare thin homogeneous uranium deposits on hardly absorbing conducting foils.

All the tests described below were made with uranium 235 (90% enriched).

[3]) Facchini and Malvicini, Nucleonics **13** (1955) 36.

0.012% O_2 and 0.058% N_2

in N_2:

0.01% O_2 .

With this filling the preliminary vacuum in the counter has not to be very high. Nevertheless we pump it out to 10^{-4} mm Hg. No variations were observed in pulse height and resolution for a measuring period of two months.

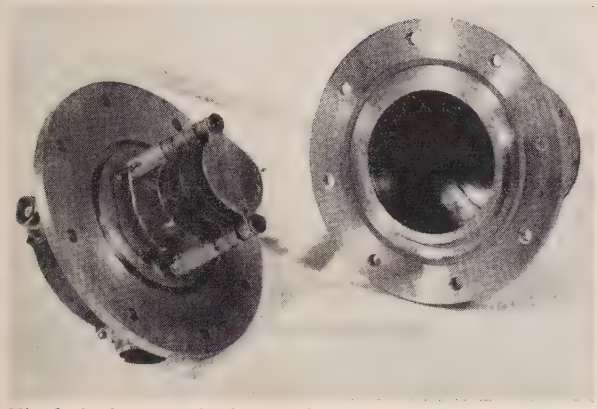

Fig. 2. A photograph of the fission chamber before assembly.

The aluminium chamber is constructed in view of measurements in neutron beams and has a cylindrical shape with two plane windows, the one argon welded, the other sealed with a teflon gasket. The foils (cathodes) and anodes are mounted on the base plate, the electrodes being separated by ring shaped teflon insulators. When comparing various fission films, the set of foils is measured simultaneously in the same chamber; after adjustment of the adjacent capacities, the results can then be accurately compared.

The window thickness is 5 mm Al, the thickness of the cylinder wall is 3 mm and of the base plate 10 mm, through which metal-to-glass seals are provided for the electrical contacts.

The electronic equipment (fig. 3) consists of a preamplifier, a linear amplifier, an automatic single channel selector, a scaler and a timer. The results are read and printed automatically in decimal form, on a paper tape by a commercial printing machine.

Most of the electronic equipment is of standard design, but the preamplifier was constructed to give a gain of 6 to 7 and a very low noise output. The neutron beam used is extracted from the BR1 reactor. To correct for pile fluctuations a monitor BF_3 counter (12B70 20th Century) is used.

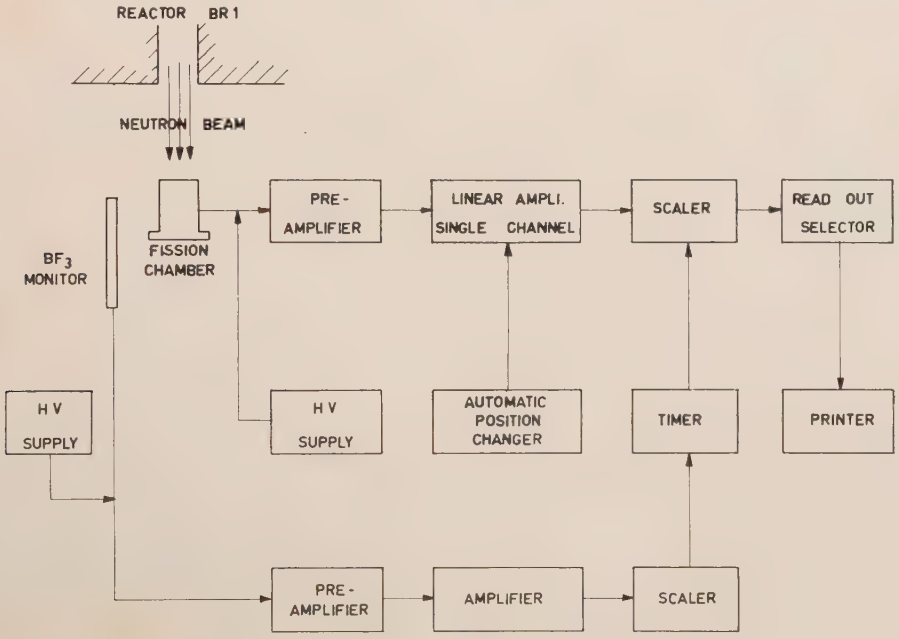

Fig. 3. Block scheme of the electronic circuitry.

3. Preparation of the Fission Foils

Three methods have been tested:

(I) painting[4]);

(II) sedimentation;

(III) electrolysis on aluminium[5]).

[4]) Glover and Borrell, Journal of Nuclear Energy **1** (1955) 214–217.

[5]) L. Koch, Dépôt de bioxyde d'U sur Al par électrolyse, Rapport CEA No. 550.

(I) Uranyl nitrate is dissolved in 12.5% alcohol, 50% cellulose nitrate (concentration 3%) and 37.5% acetone. This solution is painted on an aluminium foil and baked at 500° C for 15 minutes; uranylnitrate is converted into U_3O_8. The efficiency is about 90%.

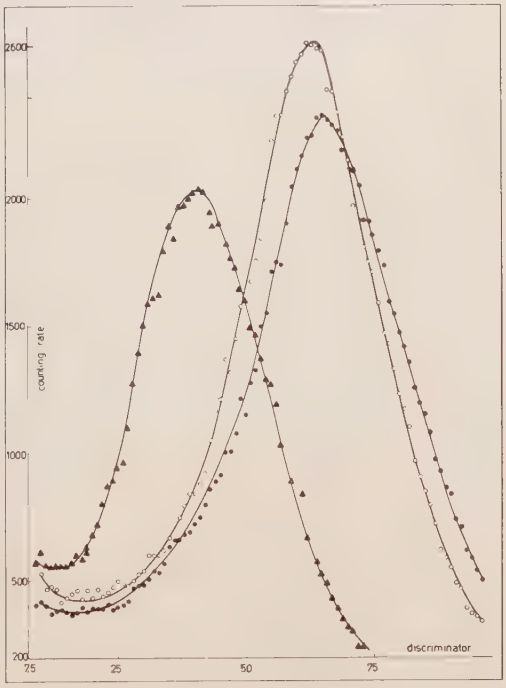

Fig. 4. Comparison of differential curves for Al ○, Ag ● and Au ▲ in a 5 $\mu g/cm^2$ film on both sides of 60 $\mu g/cm^2$ $U^{235}O_2$.

(II) Finely divided UO_2 or U_3O_8 suspended in water, as homogeneously as possible, is settled down on a nylon or VYNS-3† film.

(III) An Al foil of 0.12 mm thickness is roughed with carborandum and cleaned with trichlorethylene and a solution of 3% NaOH in water. The electrolyt is ammoniumoxalate 0.2 M, with pH 8 (not too basic). The electrolysis time is about one hour. The bath temperature is 80° C, the current 0.03 A/cm^2 (voltage $\simeq$ 5 V). The anode-cathode distance is 2 to 3 cm.

The check of the homogeneity of these foils was made with a ZnS scintillator and with nuclear plates. The results were satisfactory for the electrolytic method, but not for the painting method. Sedimentation gave much better results when the suspension was treated with ultra sounds (due probably to a fuller dispersion of the oxide particles) and for thick sources it may be satisfactory.

The electro plated foils were further treated as follows. The U film is covered with a film of VYNS-3/cyclohexanone (10 grams of VYNS-3 powder in 100 cc cyclohexanone). The aluminium support is dissolved in a solution of 10%

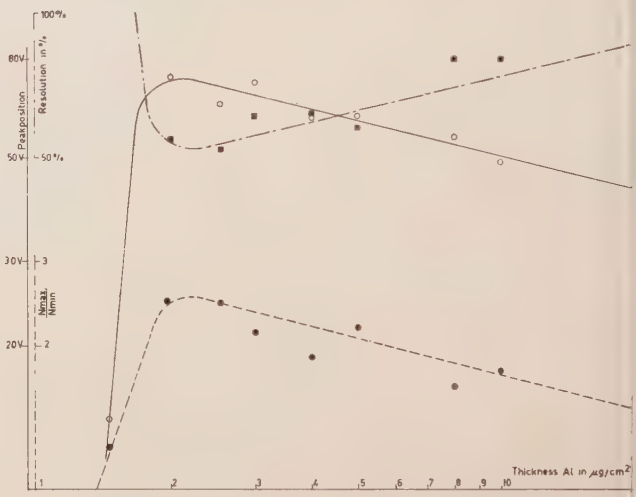

Fig. 5. Comparison of peak pulse height value ○, resolution of the fission peak ■ and the ratio of the peak to valley counting rates ●.

NaOH in water except for an outer ring which is left to hold the plastic film. The thickness of the plastic film was negligible; alpha counting rates from each side as measured with a 2π-scintillation counter were only slightly different.

To get electrically conducting foils, two methods have been applied:

1. Deposition of a metallic film on both sides by evaporation in vacuum.

2. Addition of 92.8 mg of graphite per cc to the VYNS-3 cyclohexanone solution.

The first method gives the best results. Ag, Au and Al layers of 5 $\mu g/cm^2$ have been compared (fig. 4). We kept Al because of its small resistivity and low atomic weigth.

Systematic measurements were carried out with several thicknesses of aluminium coatings,

† VYNS-3 or "vinilite" vinyl copolymer resin was supplied by Union Carbide Inter. Company, Plastics Dept., New-York.

to find out the best compromise between absorption and conductivity. Uranium oxide films of 1 mg/cm² were coated with aluminium films on both sides ranging from 20 to 1 μg/cm². The pulse height spectra of each of these foils are compared in table 1 and fig. 5. The criteria used were the peak pulse height value, the resolution of the fission peak, and the ratio of the peak to valley counting rates. Typical spectra are shown on fig. 6. From these results we conclude that the best aluminium coating is 2 to 2.5 μg/cm².

TABLE 1

Al coating thickness in μg/cm² on both sides	Peak pulse height in volts (total gain: 5×10^4)	Resolution of the peak	$\frac{N_{max}}{N_{min}}$
1	—	—	—
1.5	14	133 %	1.22
2	73.8	54 %	2.52
2.5	64.3	51.5%	2.50
3	72.2	62 %	2.14
4	60.5	61 %	1.89
5	60.0	57 %	2.20
8	56.3	81 %	1.65
10	49.0	80 %	1.77
20	40.9	77 %	1.55

4. Efficiency of the Fission Counter for Different Layer-Thicknesses

a. To calculate the efficiency of a 4π chamber, we notice that superimposed upon the "full" fission pulse spectrum, we detect a number of single fission pulses; i.e. it may happen that one fission fragment is absorbed in the foil, while the other one is detected. We estimate this number in the following way (fig. 7). Only pulses from a fragment leaving a surface layer of thickness:

$$\cos\theta\left(\frac{t}{\cos\theta} - R_0\right)$$

under an angle larger than θ_1 can be single pulses, θ being the angle between the fragment direction and the normal to the layer, t the film thickness, R_0 the mean range of a fission fragment (both in mg/cm²), and $\cos\theta_1 = t/R_0$.

The total fraction of single pulses is given by:

$$\frac{2}{t}\int_{\theta_1}^{\frac{1}{2}\pi} \sin\theta\, d\theta \left(\frac{t}{\cos\theta} - R_0\right)\cos\theta = \frac{t}{2R_0}.$$

We multiply by 2 as we have 2 surface layers.

Not all these single pulses are detected, for both fragments may be absorbed in the foil, when:

$$\frac{t}{\cos\theta} - R_0 \geqslant R_0 .$$

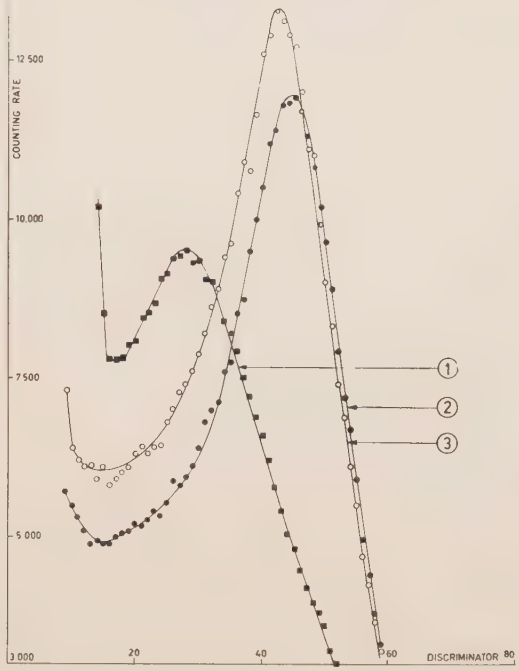

Fig. 6. Typical differential curves: 1. 1.5 μg/cm² Al on both sides (gain 200); 2. 2.5 μg/cm² (gain 70); 3. 5 μg/cm² (gain 70).

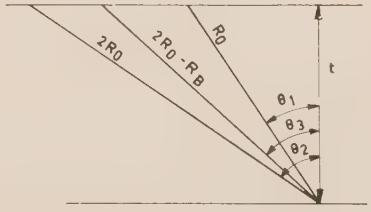

Fig. 7. Symbols are explained in the text.

This last fraction is:

$$\frac{1}{t}\int_{\theta_2}^{\frac{1}{2}\pi} \sin\theta\left(\frac{t}{\cos\theta} - 2R_0\right)\cos\theta\, d\theta = \frac{t}{4R_0}$$

with:

$$\cos\theta_2 = \frac{t}{2R_0}.$$

The fraction of single pulses in the spectrum is:

$$\frac{t}{2R_0} - \frac{t}{4R_0} = \frac{t}{4R_0}.$$

Taking for $R_0(UO_2)$ 8.28 mg/cm², based upon the value of (7.74 ± 0.25) mg/cm² [6]) for U_3O_8, this fraction for a 1 mg/cm² film is 3.0%, neglecting the absorption in the Al-coating and the VYNS film.

b. A certain bias B is necessary to discriminate for the alpha particles and the noise of the

The fraction of fission phenomena not detected at a bias B (R_B) is given by:

$$P = \int_{\theta_3}^{\frac{1}{2}\pi} \frac{1}{\pi t} \left[\frac{t}{\cos\theta} - 2\,(R_0 - R_B) \right] \cos\theta \sin\theta \, d\theta = \frac{tR_0}{[2R_0 - R_B]^2} . \quad (2)$$

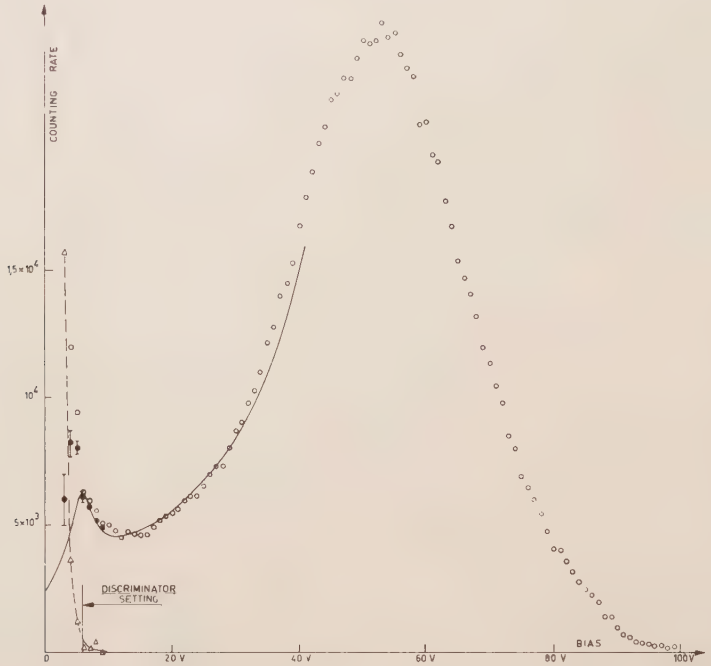

Fig. 8. Differential curve for 0.1 mg/cm² UO_2-film. O fission counting rate; ⊕ corrected fission counting rate; △ α-particle background. The solid line is the selfabsorption curve: $\frac{2tR_0}{[2R_0 - R_0]^3} \frac{\partial R_B}{\partial E_B} \Delta E_B$ used to extrapolate from 6 volts to zero bias.

electronic circuitry. We try to evaluate this loss and correct the counter efficiency accordingly. All fission events occuring under an angle smaller than θ_3 are detected, as single or double fission pulses. θ_3 is defined by:

$$\cos\theta_3 = \frac{t}{2R_0 - R_B}$$

where R_B is the fraction of the range to be lost in the chamber to form a detectable pulse. When $\theta > \theta_3$ it is impossible to detect a double fission pulse for then too much energy ($2R_0 - R_B$) has been lost in the film. For the calculation of R_B we need an energy calibration of the bias scale. This will be studied in 4(c).

The differential curve giving the fraction of pulses lost for a bias change ΔR_B (or ΔE_B in the energy scale) is given by:

$$\Delta P = \frac{2tR_0}{[2R_0 - R_B]^3} \frac{\partial R_B}{\partial E_B} \Delta E_B . \quad (3)$$

To evaluate (3), the density of energy loss by ionization along the path has to be known[7]).

c. Calibration of the bias scale. In an ionization chamber with electron collection the observed maximum counting rate-bias does not coïncide with the total energy loss of both fission fragments.

[6]) George J. Safford and E. Melkonian, Phys. Rev. **113** (1959) 1285–1293.

[7]) N. O. Lassen, Mat. Fys. Medd. Dan. Vid. Selsk. **25** (1949).

In such a chamber the pulse height is proportional to:

$$Q_0^- = N_0 e \left(1 - \frac{\bar{x}}{d} \cos\theta\right) \qquad (4)$$

and the pulse height distribution is a square distribution, where the maximum is obtained for $\theta = 90°$ and the minimum for $\theta = 0°$. Here Q_0^- is the induced charge during the transit time of the chamber, N_0 the total number of ion pairs formed, $\bar{x}$ is the centre of gravity of the ionization produced by a "mean" fission fragment, d is the electrode separation and θ has its usual meaning. This formula is right for an infinitely thin source and assuming that the observed maximum intensity coincides with the middle of the square distribution, a calibration can be made. Our films cannot be assumed to be infinitely thin, and experimentally we establish a considerable shift of the peak position with different uranium thicknesses (see figs. 8 and 9).

So we suppose that the pulse height is proportional to:

$$N_0 e \left(1 - \frac{t}{2R_0 \cos\theta}\right)\left(1 - \frac{\bar{x}\cos\theta}{d}\right) \qquad (5)$$

where we corrected (4) for the ionization loss in the foil of thickness t. (5) is a rough estimate; an accurate formula should take into account the shift of the center of gravity by absorption and the ionization density along the track. The expression (5) has its maximum for a θ value given by:

$$\cos^2\theta_{max} = \frac{td}{2R_0\bar{x}}$$

and its minimum for ($\theta = 0°$). We assume that the observed maximum intensity coïncides with the mean of the calculated maximum and minimum pulse height values. Considering $\bar{x}$ as the distance in the chamber gas where the fragments have lost half of their energy, and using the results of refs. [8]) and [9]) (i.e.: total NTP air range of an average 68 MeV fragment = 2.05 cm; NTP range of a 34 MeV fragment = 1.52 cm), we get:

$$\bar{x} = 0.53 \text{ cm (air)}$$

$$0.52 \text{ cm (98\% A; 2\% } N_2) .$$

Applying these corrections to the results of figs. 8 and 9 we obtain the following mean value:

$$1 \text{ volt} = (1.86 \pm 0.02) \text{ MeV} .$$

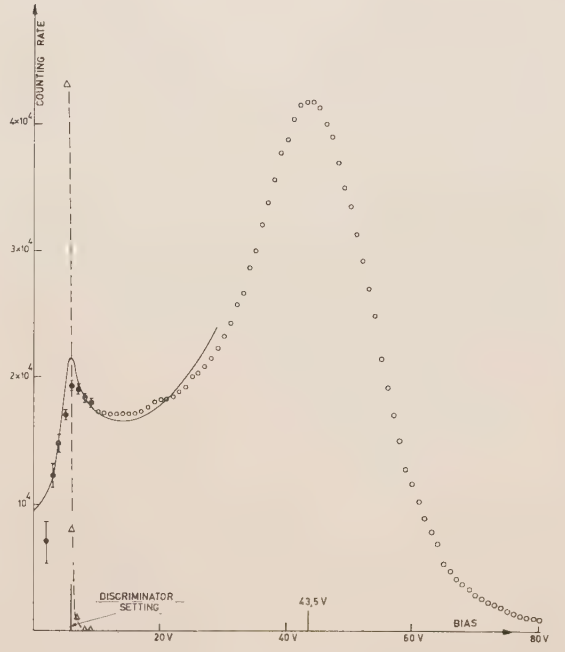

Fig. 9. Differential curve for a 1 mg/cm² UO_2-foil. The symbols are the same as in fig. 8.

d. Efficiency calculation based on experimental results and previous theoretical considerations.

The fit between the theoretical selfabsorption formula and the experimental results is reasonably good (see figs. 8 and 9). The theoretical pulse height distribution shows a maximum near 6 volts, caused by the rise of the specific ionization of the fission fragments near the end of the range[7]), analogous to that of alpha particles.

Two film thicknesses were studied (1 mg/cm² and 0.1 mg/cm²). The discriminator setting selected is the lowest point, where theoretical

[8]) Bohr, Boeggild, Brostroem and Lauritsen, Phys. Rev. 58 (1940) 839.

[9]) Boeggild, Brostroem and Lauritsen, Phys. Rev. 59 (1941) 275.

and experimental results are still in good agreement, and the α counting rate negligible. The loss by bias-setting is evaluated by measuring the areas under the differential curves; to this is added the fraction of fission events completely absorbed in the foil (corresponding to a negative bias).

This gives the following results:

for a 0.1 mg/cm² film- fission loss = (2.51 ± 0.25%;

for a 1.0 mg/cm² film: fission loss = (8 ± 0.8)%.

The errors correspond to an estimated 10% uncertainty on the evaluation of the correction.

The corresponding efficiencies are:

for 0.1 mg/cm²: 97.5 ± 0.3%

for 1.0 mg cm²: 92 ± 1 %.

The author wishes to thank Dr. M. Nève de Mévergnies for following the progress of this work with such encouraging interest, and for his many useful suggestions.

My thanks are further expressed to Mr. J. Marchal for the steady excellent technical assistance.

NUCLEAR INSTRUMENTS AND METHODS 7 (1960) 153–159; NORTH-HOLLAND PUBLISHING CO.

A METHOD OF LINEAR PULSE AMPLIFIER DESIGN

A. F. FISCHMANN-ARBEL and ISRAEL BAR-DAVID

Scientific Department, Ministry of Defence, Israel

Received 28 November 1959

The root locus method of feedback amplifier analysis is applied in order to obtain maximum possible gain from a simple circuit configuration consistent with additional requirements of fast rise time, stable gain, monotonic step response, linearity and fast recovery from overload. Coarse gain control may be realized by changing the feedback factor of such an amplifier; this eliminates distortions which may otherwise occur at low gain settings in the stage preceding the gain control and simultaneously increases the loop gain. Two practical design examples are given, with an overall gain of 50 000 and 2 000 respectively.

1. Introduction

The desirable properties of pulse amplifiers for use in proportional and scintillation counter spectroscopy have been adequately discussed in a paper[1]) describing the "DD2" amplifier. This satisfies most of the requirements, incorporating a number of novel and unconventional design ideas. Some weaknesses which are also found in many other existing high gain pulse amplifiers may however be enumerated.

(a) The comparatively low gain of the amplifying stages necessitates the use of a large number of valves.

(b) The amplifying stage preceding the coarse gain attenuator gives rise to distortions for input signals of large amplitude.

(c) In cases where the output stage is not included in the preceding feedback loop, its own distortions are added to those of the amplifier proper.

In order to overcome these drawbacks, the following steps are taken in the design of the amplifiers described below:

(a) The feedback loop shown in fig. 1 is analyzed by the root locus method[2]) in order to obtain maximum possible gain for given rise time, stability and loop gain.

(b) The coarse gain attenuator as normally used is abolished, the feedback factor being made adjustable in steps in its place. Thus the amplification of the first loop may be brought

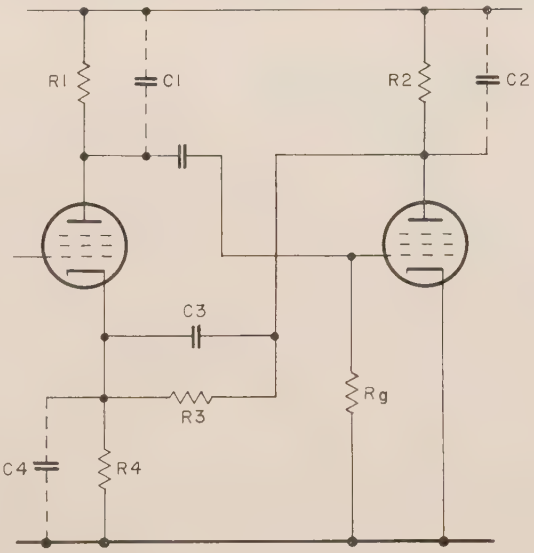

Fig. 1. Basic circuit and its open loop transfer function. $R_{1eq} = R_1//R_g$; $R_{2eq} = R_2//R_3$; $R_{4eq} = R_4//R_3$; $C_{2eq} = C_2 + C_3$; $C_{4eq} = C_4 + C_3$; $T_1 = R_{1eq}C_1$; $T_2 = R_{2eq}C_{2eq}$; $T_3 = R_3C_3$; $T_4 = R_{4eq}C_{4eq}$; $K_0 = g_{m1}g_{m2}R_{1eq}R_{2eq}$; $\beta_0 = R_{4eq}/R_3$; $K(p) = K_0/1/(1 + pT_1)\,(1 + pT_2)$; $\beta(p) = \beta_0/1 + pT_3/1 + pT_4$; $L(p) = K(p)\,\beta(p)$.

to the desired value, instead of being kept at maximum even for large input signals with the need for subsequent attenuation. This method prevents distortions for large input signals

[1]) E. Fairstein, Nonblocking Double-Line Linear Pulse Amplifier, Rev. Sci. Instr. **27**, No. 7 (1956).

[2]) J. G. Truxal, Automatic Feedback Control System Synthesis (McGraw Hill Book Co., N.Y. 1955) Ch. 4.

whilst simultaneously increasing the loop gain at lower gain settings. Furthermore for amplifiers having only one loop and with the gain control originally preceding the amplifier, adoption of the proposed system will also improve the signal to noise ratio.

(c) The output stage is fully or partially included in the preceding feedback loop, so that its own distortions are practically eliminated. In addition, its output impedance is reduced by at least one order of magnitude.

The "gain of 50 000" amplifier to be described is of the double delay line differentiating type. It uses 4 (amplifying) + 2 (output) valves in two feedback loops, as compared with the 10 + 2 valves in three amplifying loops + one output stage, in the "DD2" amplifier[1]), many other features of which are nevertheless incorporated in this amplifier. The "gain of 2 000" amplifier comprises a single loop of 2 + 1 valves.

2. Design of H.F. Response

An analysis of the basic circuit to be considered (fig. 1) shows that the approximate expression† for the loop transfer function $L(p)$ has three poles at $p_1 = 1/T_1$, $p_2 = 1/T_2$ and $p_4 = 1/T_4$ with one zero at $p_3 = 1/T_3$. The desing problem is to distribute these singularities in such a manner that the poles and zeros of the closed loop transfer function yield the following properties for the amplifier:

(a) Monotonic response for specified variations in the loop gain.

(b) Specified rise time substantially independent of loop gain variations.

(c) Specified minimum loop gain.

(d) Fast recovery from overload, as an additional requirement for large signal operation.

The closed loop transfer function $G(p)$ is obtained from $L(p)$ (fig. 1) as

$$G(p) = \frac{K(p)}{1 + L(p)} = \frac{K_0 (1 + pT_4)}{(1 + pT_1)(1 + pT_2)(1 + pT_4) + K_0\beta_0 (1 + pT_3)} \quad (1)$$

and may be brought into the form

$$G(p) = \frac{K_0}{1 + K_0\beta_0} \cdot \frac{(1 + pT_4)}{(1 + pT_a)(1 + pT_b)(1 + pT_c)} \quad (2)$$

The response of the circuit to a step input will depend on its zero $p_4 = 1/T_4$ and on its poles $p_a = 1/T_a$, $p_b = 1/T_b$ and $p_c = 1/T_c$, the loci of which may be drawn once a certain distribution of open loop singularities is decided upon. Fig. 2 shows the loci for three different distributions of open loop singularities. The exact location of the poles on the loci depends on the midband frequency loop gain $K_0\beta_0$. The rise time of this step function response may be shown (see Appendix) to be given by

$$T_R = [2\pi (T_a^2 + T_b^2 + T_c^2 - T_4^2)]^{\frac{1}{2}} \quad (3)$$

provided that the response is monotonic.

Requirements (a) and (b) as defined above will now be considered.

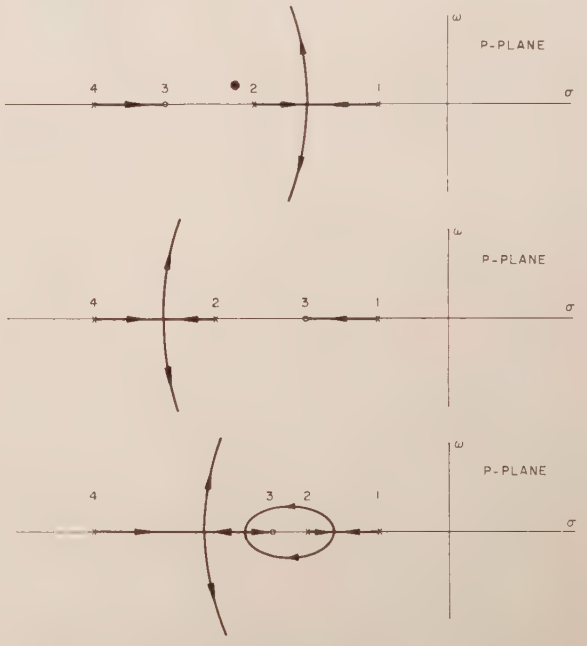

Fig. 2. Plausible distributions of singularities and respective loci of p_a, p_b and p_c.

First, for monotonic response p_a, p_b and p_c should remain real for all possible values of the loop gain. Thus, for maximum allowable loop gain the distance between two open loop poles which contribute converging loci, should be as large as possible.

† Assuming infinite internal resistance of the pentodes.

Second, in order to obtain a stable rise time, one of the time constants in expression (3) (except for T_4) should be large as compared with the others, and should depend only slightly on the loop gain.

Examination of eq. (1) and of the loci of fig. 2 shows that equating T_3 and T_1 satisfies these requirements. Thus, inserting $T_3 = T_1$ into (1), one obtains

$$G(p) = K_0 \frac{1 + pT_4}{1 + pT_3} \frac{1}{(1 + pT_2)(1 + pT_4) + K_0\beta_0} =$$

$$= \frac{K_0 (1 + pT_4)}{(1 + K_0\beta_0)(1 + pT_3)} \frac{1}{(1 + pT_a)(1 + pT_c)} . \quad (4)$$

The root locus presentation of (4), fig. 3,

Fig. 3
Favourable distribution of singularities and respectire loci.

shows that the cancellation of pole 1 by zero 3 results in a large separation between poles 2 and 4, which is in accordance with the first condition. Further, a computation of T_R from (3) shows that variations in loop gain will only slightly affect T_R provided the loop gain is large enough to move $1/T_a$ at least one octave beyond $1/T_3$. Consequently, variations in the loop gain should only be such that T_a is restrained between

$$\frac{1}{T_{crit}} \geqslant \frac{1}{T_a} \geqslant \frac{2}{T_3} . \quad (5)$$

The considerations for choosing $T_2 > T_1$ were the following: The loop gain is given by $1 + \beta_0 K_0 \approx \beta_0 K_0$. For given stray capacities K_0 is proportional to $T_1 T_2$. The value of one of these factors being fixed (by equating it to T_3), an increase in loop gain may only be effected by increasing the other.

The value of R_g (fig. 1) being limited by requirement (d) from above†, an increase in

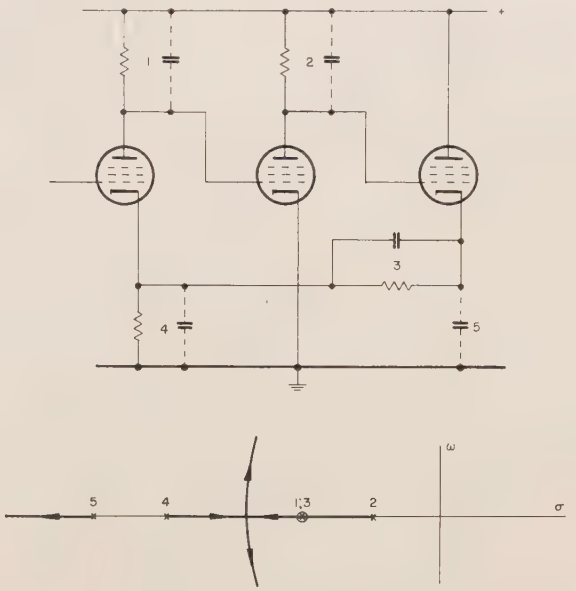

Fig. 4
(2 + 1) stage feed-back amplifier and root locus diagrams.

R_{1eq} is not feasable without impairing the speed of recovery from overload. However, the value of R_{2eq} may be raised to a very high value if advantage is taken of the "bootstrapping" of R_2, which is required in certain cases. Nevertheless, the increase in R_{2eq} does not appreciably influence the location of p_a, since the displacement of pole 2 to the right (fig. 3) is compensated by the resulting increase in loop gain.

It may be mentioned that the opposite (i.e. $T_1 > T_2$) is sometimes recommended for different considerations[4]).

In cases where the feedback loop is closed through a cathode follower, an additional pole is included in the open loop transfer function (see fig. 4). However, this pole causes no major change in the root loci, owing to its location to the extreme left of the pole zero diagram.

† It has been shown[3]) that a very favourable overload characteristic may be achieved by making the grid resistor in an *RC* coupled stage considerably smaller than the plate load of the preceding stage. This feature has also been incorporated in the "DD2" amplifier[1]).

[3]) G. E. Valley and H. Wallman, Vacuum Tube Amplifiers (Mc Graw Hill Book Co., N.Y. 1948) R.L.S. 18, pp. 115–117.

[4]) J. L. Stewart, Design of Amplifiers for Prescribed Closed Loop Characteristics, IRE Transactions, Vol. CT-3, No. 2 (June 1956).

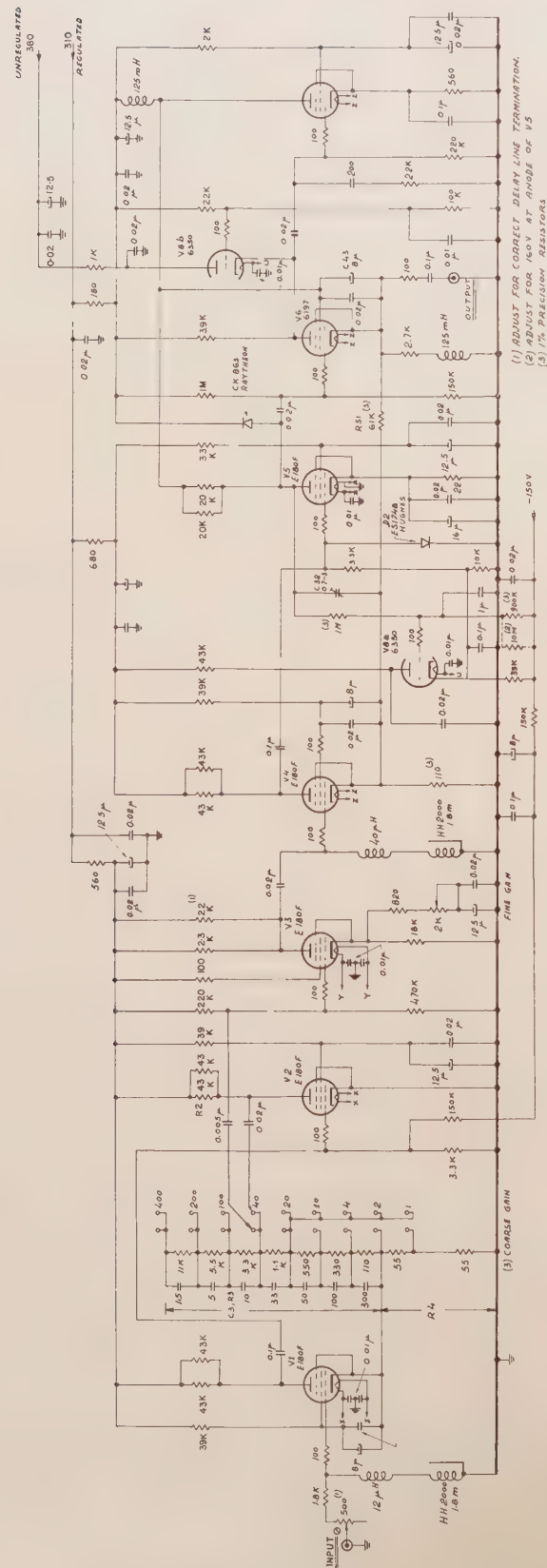

Control of the gain is accomplished by varying the feedback factor β_0, at the same time keeping T_3 constant to obtain fixed rise time. Since the loop gain $K_0\beta_0$ increases with β_0, this method of gain control inherently improves the performance at lower gain settings. However, steps must be taken to decrease K_0 whenever the increase in β_0 would cause the loop gain to rise beyond the limit prescribed by the requirement of monotonic response.

3. The "Gain of 50 000" Amplifier (fig. 5)

This amplifier consists of two loops which were designed according to the procedure just described.

Control of the gain is effected in the first loop by varying the resistance corresponding to R_3 from fig. 1. A reduction of R_3 will increase β_0, but decrease R_{2eq} simultaneously. However, the reduction of R_{2eq} is less than that of R_3, because of the shunting effect of R_2, so that a net increase in loop gain results. In addition, the reduction of R_{2eq} moves pole 2 to the left, thereby reducing the initial separation between poles 2 and 4 (see fig. 3).

Consequently, β_0 may not be increased beyond a certain limit without having to restore T_2 to its initial value. This could be achieved by adding capacitance to C_2, but in order to avoid this complication for the lower gain values, the output is taken from a voltage divider without increasing the loop gain any further.

T_3 is kept constant by adequately shunting the resistors of the β network with capacitors as shown in fig. 5.

In the second loop, R_{46} is bootstrapped from the "White Cathode Follower" via C_{43}. Closing the feedback loop directly through the output meets with certain difficulties, because inclusion of the White Cathode Follower into the feedback loop for all frequencies would create a root locus diagram similar to the one shown in fig. 4, but with pole 5 replaced by two poles close to each other and a very distant zero. Only a small loop gain is possible with such a pole zero configuration, for monotonic response.

Fig. 5. The "gain of 50 000" amplifier.

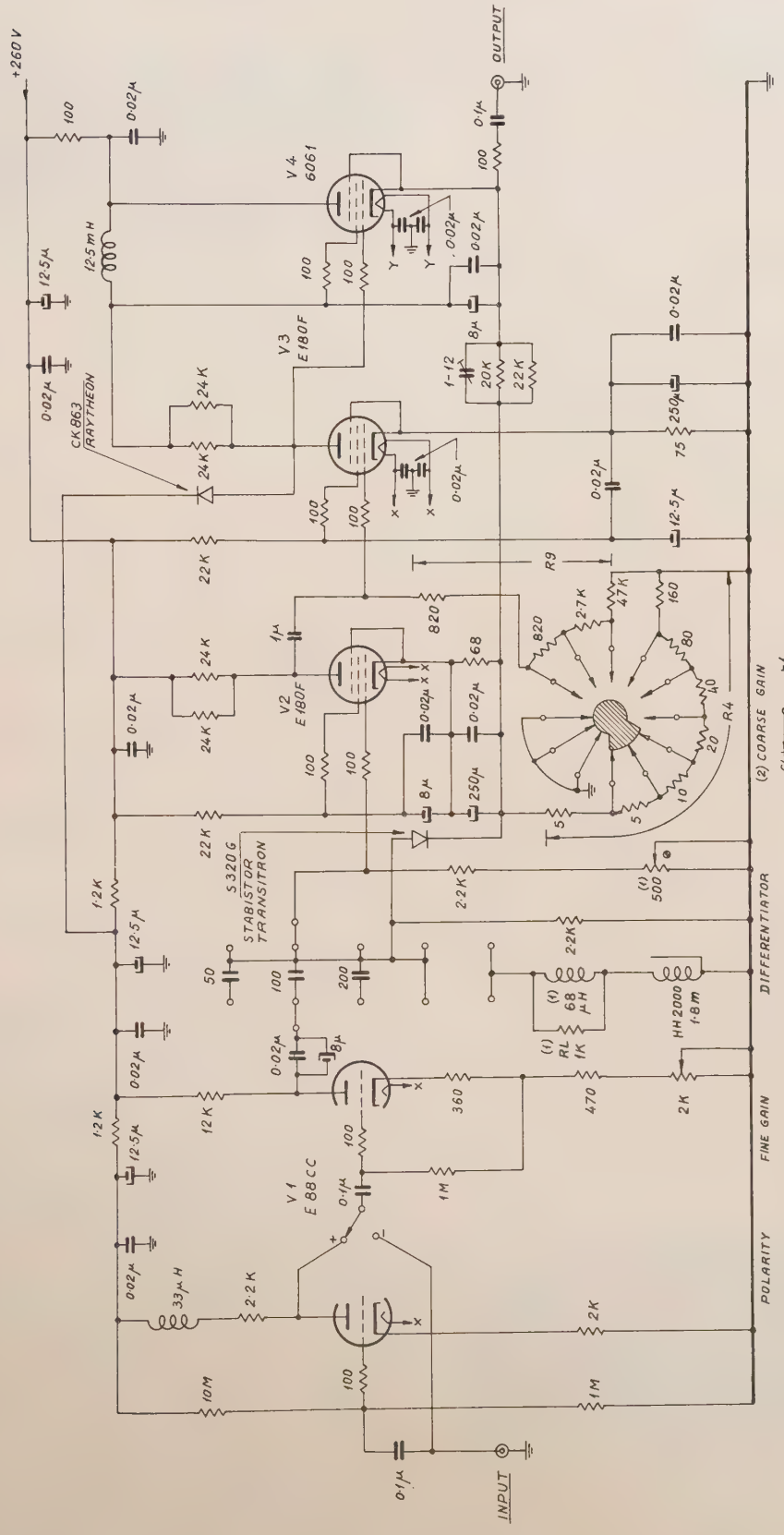

Fig. 6. The "gain of 2000" amplifier.

The feedback loop is therefore closed for high frequencies through C_{32} from the plate of V_5, and for the lower frequencies via R_{51} from the White Cathode Follower output to the cathode of V_4. This splitting up of the feedback loop ensures high gain stability by including the output stage in the feedback loop at midband frequencies, but preserves monotonic response by using a separate loop via C_{32}, at high frequencies.

Modern high gain valves are capable of diverting a considerable percentage of the plate current to the first grid, if the latter is driven positive. Hence, the signal at the plate will reverse its polarity, if the valve is considerably overdriven. Diode D_2 in the grid circuit of V_5 prevents grid current in V_5, which would render the feedback loop regenerative owing to the phase reversal at the plate of V_5. It is biased at -0.25 V in order not to shunt the plate load of V_4, at small signals.

4. The "Gain of 2000 Amplifier" (fig. 6)

This amplifier was designed to deliver positive output pulses only. The grid of V_4 receives positive pulses of high amplitude, but coupling it directly to the plate of V_3 ensures zero recovery time from overload. Further, as the grid of V_3 receives negative pulses only, there is not a single capacitor in the loop which could be charged at overload. Double pulse resolution of the amplifier is therefore excellent. Control of gain is effected by varying the resistance corresponding to R_4 in fig. 1. By this method g_{m1} and with it K_0 is reduced with increasing β_0, so that the loop gain is kept below the limit prescribed by monotonic response for the first 6 positions of the gain switch. The last three steps require K_0 to be further reduced this being accomplished by changing R_{1eq}.

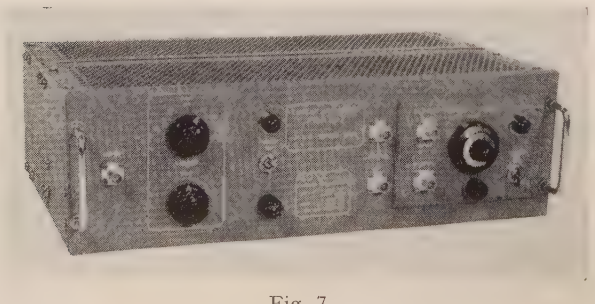

Fig. 7

Fig. 8

5. Layout Problems

Due to the very high gain bandwidth product of all the stages in both amplifiers, extreme care has to be taken in the design of the layout. Adequate screening must be provided between points of widely different potential levels.

PERFORMANCE

(a) The "Gain of 50 000" Amplifier. (The amplifier shown in fig. 7 incorporates a plug in discriminator unit.)

Output: $\pm$ 140V max. $\pm$ 100V linear
Risetime: 0.2 μsec
Load: 150 pF or 2 kΩ (max) for rated risetime
Gain stability: 0.3% for 10% change in line voltage
Linearity: better than 0.15%
Overload recovery: at 1000 times overload, 20 μsec.

(b) The "Gain of 2000" Amplifier (fig. 8)

Output: + 140 V max, + 100 V linear
Rise time: 0.25 μsec
Load: 150 pF or 2 kΩ (max), for rated risetime
Gain stability: 0.25% for 10% change in line voltage
Linearity: better than 0.1%
Overload recovery: at 100 times overload, immediate

Acknowledgement

This investigation was carried out under the auspices of the Scientific Department, Ministry of Defence, Israel.

Thanks are also due to Mr. Zwi Winter who carried out a preliminary investigation of the problem discussed in this article.

Appendix

Let

$$g(p) = G_0 \frac{1 + a_1 p + a_2 p^2 + \cdots}{1 + b_1 p + b_2 p^2 + \cdots}$$

be the transfer function of a network the step function response of which is monotonic. It has been shown by Elmore[5]) that the rise time T_R of the wave form at the output of such a network is given by

$$\frac{T_R^2}{2\pi} = b_1^2 - 2b_2 - (a_1 - 2a_2)$$

if it is energized by a step function.

If both the numerator and the denominator of $g(p)$ may be factorized, as in (2), it follows that

a_1 = sum of the time constants in the numerator.
a_2 = sum of the products of the time constants in the numerator taken two at a time.

Therefore
$(a_1^2 - 2a_2)$ = sum of the squares of the time constants in the numerator, and finally

$T_R^2/2\pi$ = (sum of the squares of the time constants of the denominator)

— (sum of the squares of the time constants of the numerator).

[5]) W. C. Elmore, The Transient Response of Damped Linear Networks, J. Appl. Phys. **19**, (January 1948).

NUCLEAR INSTRUMENTS AND METHODS 7 (1960) 160–166; NORTH-HOLLAND PUBLISHING CO.

THIN FILM THICKNESS DISTRIBUTION BY ALPHA ABSORPTION

M. DE CROËS, W. PARKER and K. SEVIER, Jr.

Institute of physics, Uppsala, Sweden

Received 4 Januari 1960

An instrument for the determination of thin film thickness distribution is described. Thickness distribution curves for films of organic compounds, metals, and aluminium oxide which are used primarily for counter windows and in connection with radio-active source preparation are presented. The principle employed, where the "gas-equivalent" of the film or foil of material is measured, provides results to a good degree of accuracy.

1. Introduction

When measuring low energy beta emission from isotopes and, in particular, where high resolution is required, it is desirable to know not only the thickness of the supporting backing material but also the uniformity of its thickness. Also when using thin films for Geiger counter windows, knowledge of the non-uniformity and thickness distribution is desired. Methods are available whereby the mean thickness of such materials may be determined but, with the possible exception of weighing, these involve expensive equipment. A technique which is becoming more and more frequently used is the absorption of alpha and beta particles through matter and the literature dealing with this kind of measurement is fairly extensive[1–7]). Of course, due to its comparatively high penetration ranges, beta radiation is more suitable for absorption measurements of films and foils on the order of 100 mg/cm^2. Since such thicknesses are seldom used in beta spectroscopy, where the foils or films are usually on the order of μg/cm^2 in thickness, alpha absorption is to be preferred.

The most common arrangement for alpha absorption is where the detector is placed in a fixed position and a suitable alpha emitting isotope, such as Po^{210}, is attached to a micrometer screw. The numbers of pulses obtained over a given time interval are plotted against the various micrometer settings at which these numbers of pulses are obtained. The measurement is carried out, using air as the gas medium. The introduction of a foil or film between the source and counter causes a decrease in the counting rate which may be compensated for by adjusting the micrometer screw. Thus the stopping power, or rather the "air-equivalent", can be read directly from the micrometer. It will be obvious that, using the above arrangement, only limited accuracy can be expected due to the fact that the solid angle subtended by the source with respect to the counter is constantly being changed.

2. Apparatus

In considering apparatus for the study of alpha particle stopping powers and their application to various other studies, two alternatives are to be considered:

1. The pressure of the gas medium is held constant while the source-film or the film-counter distance is changed.

2. The film, source, and counter are placed at a known distance apart while the gas pressure is changed.

The first of these is the easiest to utilize, but

[1]) K. Siegbahn, Thesis. Nobel Institute for Physics, Stockholm, Sweden, 1944.

[2]) W. C. Barber, Rev. Sci. Instr. **24** (1953) 469.

[3]) L. Mandel, Brit. J. Appl. Phys. **5** (1954) 287.

[4]) E. N. Shaw, Radioisotope Conference **2** (1954) 140.

[5]) O. Te-tchao, J. Phys. Rad. **17**, No. 12 (1956) 1019.

[6]) H. A. Enge *et al.*, Rev. Sci. Instr. **28**, No. 2 (1957) 145.

[7]) K. Ramavateram and D. J. Porat, Nuclear Instruments **4** (1956) 238.

the inverse-square effect of the intensity of the alpha beam and the uncertainty of the energy of the alpha particles entering or leaving the film add to the error of the calculations. The second has certain advantages which make it very attractive.

approximate measure of the uniformity of the film can be calculated from the difference in slopes of the two curves.

The apparatus constructed and used by the authors is based on that of Davison and can be seen in fig. 1. The vacuum chamber measures

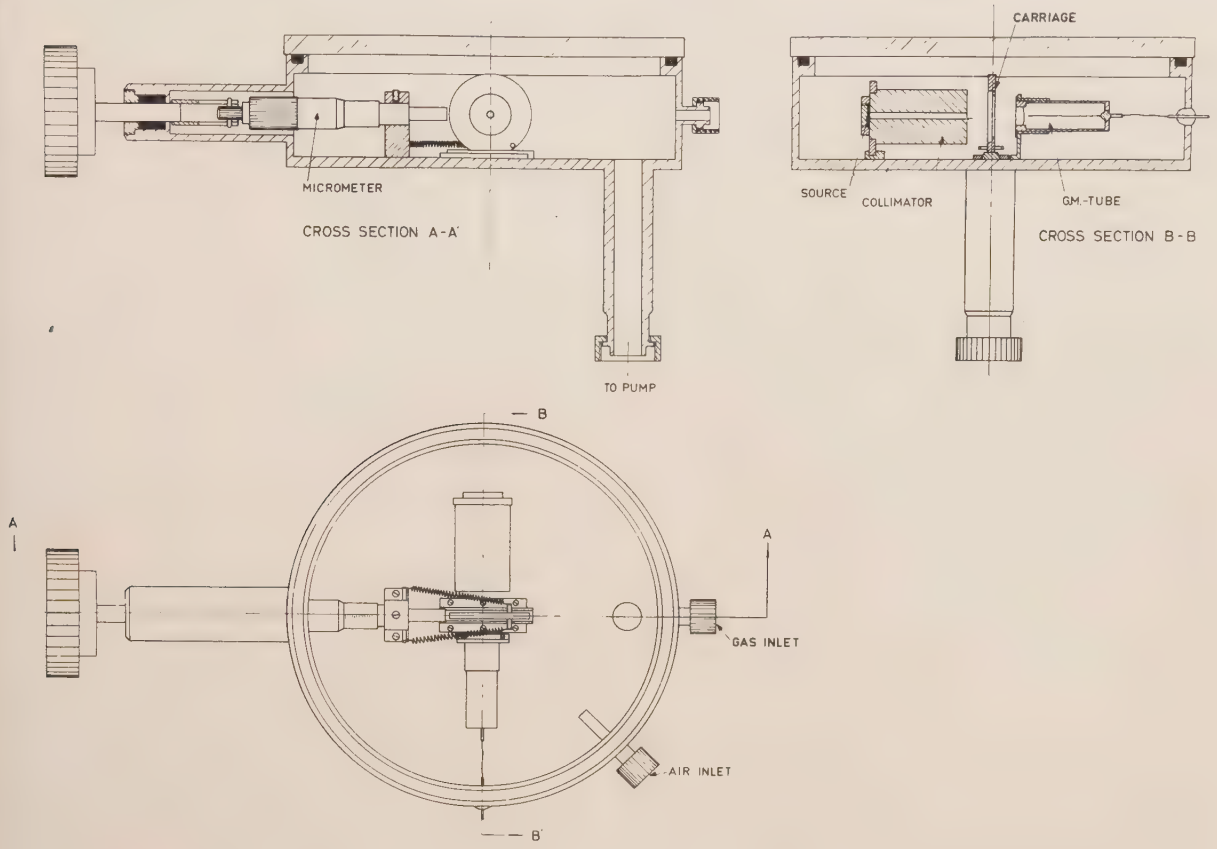

Fig. 1. Construction of the measuring apparatus.

Davison[8]) has described a method of interest where the source and counter, as well as the film to be measured, are held fixed and the counting rate is plotted as a function of pressure of dry air. Since this arrangement enables fixed geometry to be employed, the inverse-square effect is avoided resulting in a sharper cut-off at the end of the absorption curve. The pressure displacement of the curve obtained when a thin film is inserted into the path of the alpha beam is a measure of the thickness of the film and is called the "air-equivalent" of the film. An

200 mm diameter by 50 mm deep. There are three inlets, one connected to a vacuum pump, the other two for introduction of the gas measuring medium during and air after a measurement. A glass/metal seal is provided for the high voltage connection to the counter. Mounted on the chamber's base plate are the Po^{210} source, collimator, and counter. The foil or film to be measured is fitted in a traversable carriage intersecting the alpha particle path at right angles. The carriage may be moved across the alpha beam by turning a micrometer screw coupled to a rotating vacuum seal. The film to

[8]) W. H. V. Davison, J. Sci. Instr. 34 (1957) 418.

be measured is mounted on a ring which fits into the carriage. Hence, different points of the film can be brought into the alpha particle beam and measured for thickness. The chamber top is fitted with an "o"-ring and covered by a lucite plate. Collimation is obtained by use of two alternative collimators having diameters of 1 mm and 3 mm. Two 1 mc Po^{210} sources had been plated over an area of 3 mm diameter onto gold discs and covered with 0.6 mg/cm² mica†. The detector is a halogen filled Geiger counter. The gas medium used during measurements is nitrogen.

3. Calculations

When counting rate is plotted against the pressure of the gas in the chamber, there is a sharp drop-off signifying the limit of the range of the alpha-particles in the gas. When there is a uniform film or foil placed between the source and the counter and the counting rate is again plotted against the gas pressure, there will be found a sharp drop-off similar and parallel to the first but displaced to a lower pressure value by a certain amount, Δp. It is immediately obvious that the "gas-equivalent" of the film, signified by Δp, given in units of mass per unit area, will be expressed by:

$$x = \frac{D \cdot \Delta p}{760} \rho \cdot \frac{1}{A} \qquad (1)$$

where D is the source-counter distance; 760 mm Hg represents standard pressure; and A is the mass stopping power of the film material relative to that of the gas; and ρ is the density of the gas. Hence, the precision of the determination of the thickness of the film is dependent upon the accuracy of both the measurement of the gas pressure and the temperature dependent density of the gas. The mass stopping power of the film material can be determined by calculations using (1) and the value of A obtained from the "gasequivalent" of films of known thickness.

The mass stopping power of a material is dependent upon the energy of the alpha particles stopped by it. If E_1 is the energy of the alpha particle entering the film and E_2 is the energy of the particle leaving the film, then a good approximation of the best value of the energy at which the stopping power is measured is

$$\tfrac{1}{2}(E_1 + E_2)\,. \qquad (2)$$

Since the amount of gas between the source and the film and also the film and counter vary with pressure, the values of E_1 and E_2 will also change resulting in the difficulty of arriving at the best energy value for a given material's mass stopping power as calculated from absorption curve data. The value of (2) has been calculated for each of the measurements and the average of these was evaluated to be 3.4 MeV. Δp was measured for the same energy of alpha particle each time, i.e., Δp was measured always at $\frac{1}{2}$ of the maximum counting rate which is obtained at highest vacuum without a film interposed. Thus the difference in energy between the alpha particle leaving the source and that being detected is constant making (2) dependent upon the range of the particles as a function of particle energy[8]).

For future reference a very good improvement of accuracy of the energy value at which mass stopping powers or thicknesses are measured is made possible by constructing the measuring apparatus so that the source-film distance is equal to the film-counter distance. Here, then, the difference between the energy of the particle emitted by the source and E_1 is very nearly equal to the difference between E_2 and the energy of the particle being detected the correction of energy difference is a result of the non-linearity of the relationship of the range vs. energy of alpha particles. Thus, even though E_1 and E_2 change, (2) remains very nearly constant. The deviation from this constant is small since the difference between the energies of emitted and detected alpha particles was found to be about 2 MeV, dependent upon the thickness of the materials covering the source and used as counter window, and over this energy range the range of the particles increases nearly linearly with the energy[9]).

† Both Po^{210} sources were prepared by the Radio Chemical Centre, Amersham.

[9]) H. A. Bethe, Revs. Mod. Phys. **22**, No. 2 (1950) 213.

For thickness distribution determination, the pressure at which the absorption curve of the film intersects the count number where the Δp is read is reproduced in the chamber and a count is taken over a certain duration of time for various points of the film. This is made possible by the traversible carriage. The accuracy is primarily limited by the statistical error.

4. Results

Firstly, the approximate alpha mass stopping powers of various materials relative to that of nitrogen were calculated, A. The value of the thickness is mass per unit area was obtained by weighing a certain known small area of a film or foil of the material. In some cases, thin films of a metal were evaporated upon a thin foil, for

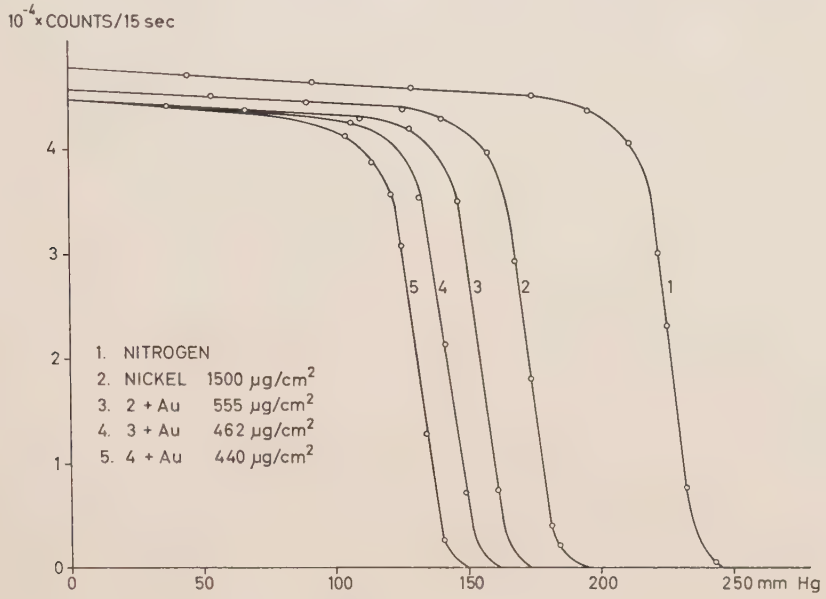

Fig. 2. Absorption curves for evaporated gold.

The number of counts corresponding to a unit change in thickness

$$\frac{\delta N_u}{\delta x}\Big|_{N_u},$$

at a certain count number, N_u, can be calculated to be, with the help of (1):

$$\frac{\delta N_u}{\delta x}\Big|_{N_u} = \frac{1}{N_a}\cdot\frac{\delta N_a}{\delta p}\Big|_{N_a}\frac{1}{x/\Delta p}N_u - \tag{3}$$

$$= \frac{N_u}{N_a}\frac{\delta N_a}{\delta p}\Big|_{N_a}\frac{760A}{D\rho}$$

where

$$\frac{\delta N_a}{\delta p}\Big|_{N_a}$$

is the slope of the absorption curve at the count number, N_a, at which Δp was measured.

which Δp is already known, over a certain known area. The uniformity of thickness of such evaporated metal films is very good[10]). The vapor source used was a V-shaped boat of tungsten with a dihedral angle of 90° and the distance of the foil from the boat was 9 cm. The area covered by the evaporated metal was of a diameter of 20 mm. The foils were weighed before and after the deposition and the thickness of the evaporated film accessed. The absorption curves for evaporated layers of gold are shown in fig. 2, while those of different thicknesses of nickel foil are shown in fig. 3. For thin films of aluminium oxide, zapon, mylar, and formvar, a certain known area of the absorption measured film was weighed and the thickness accessed. The absorption curves of various materials are shown in fig. 4. The value of the relative stopping

[10]) L. E. Preuss, J. Appl. Phys. **24**, No. 11 (1953) 1401.

powers were corrected for temperature and pressure to 20° C and 760 mm Hg. The average energy at which the absorption was measured was calculated to be, as stated before, 3.4 MeV by considering the pressure of nitrogen necessary to stop the alpha particles and the mass stopping power of nitrogen for alpha particles. The values of the relative mass stopping powers, with their standard errors, of various materials are listed in table 1.

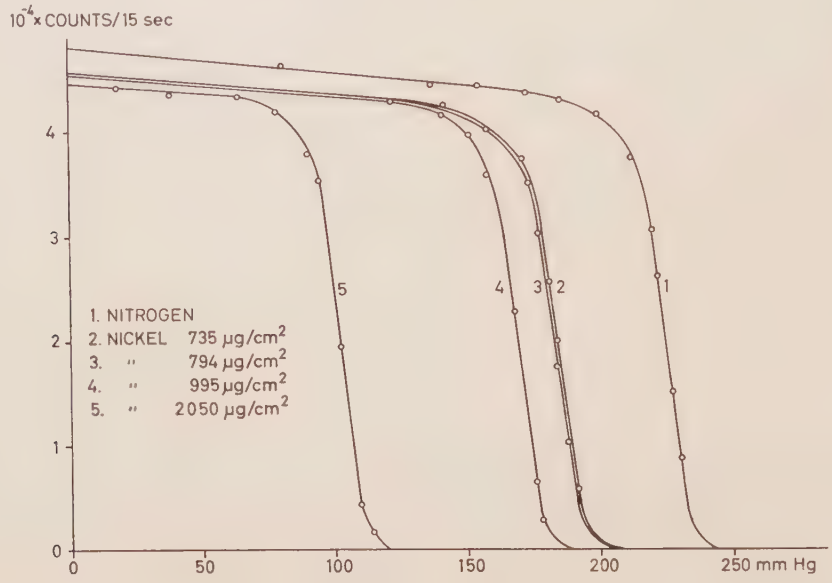

Fig. 3. Absorption curves for nickel foils.

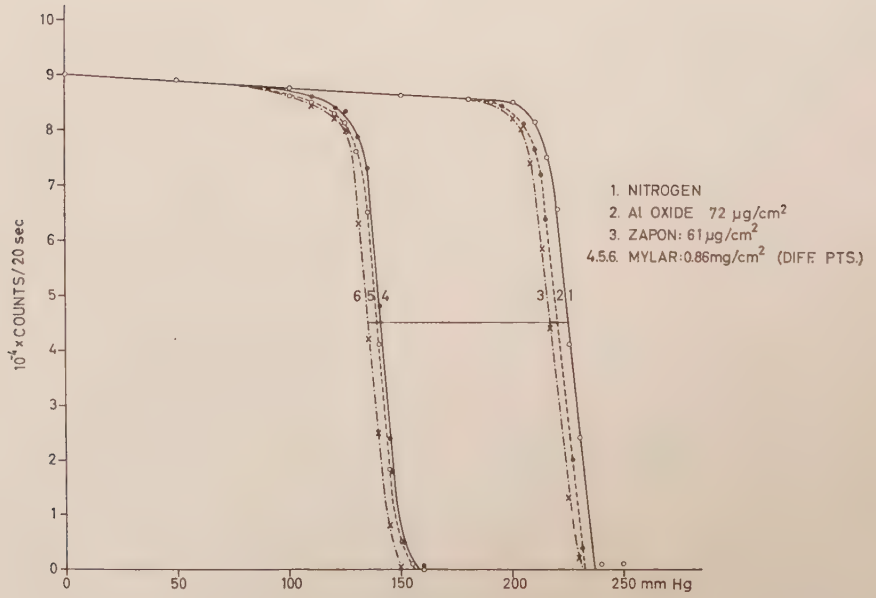

Fig. 4. Absorption curves for various materials. The curves for mylar are those measured at different points (diff. pts.) on the film.

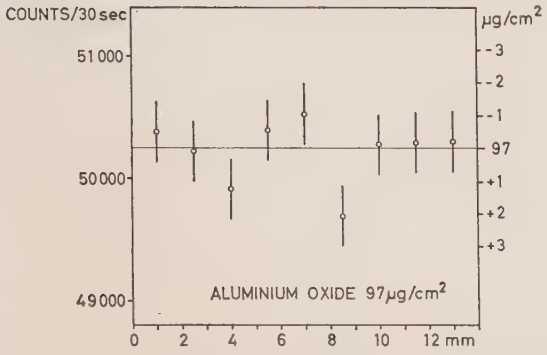

Fig. 5. Thickness distribution across an aluminium oxide film.

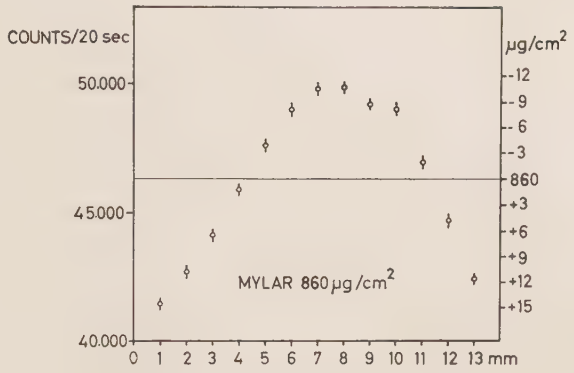

Fig. 8. Mylar film thickness distribution.

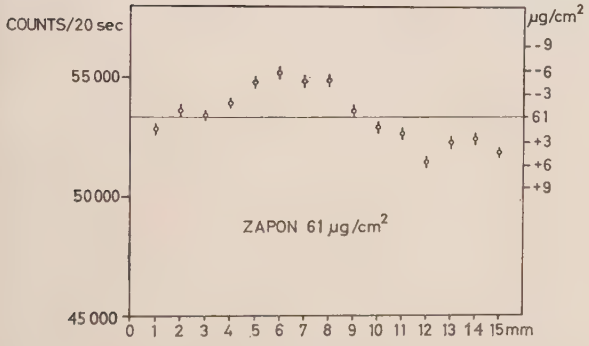

Fig. 6. Thin zapon film thickness distribution.

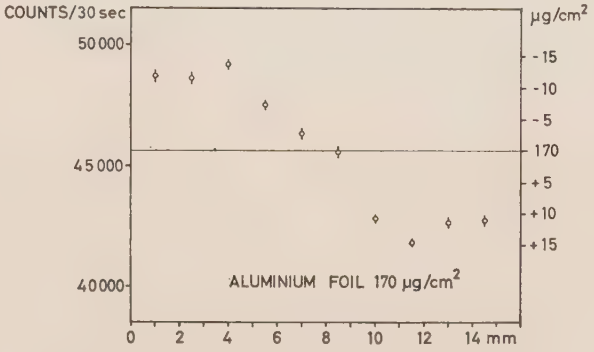

Fig. 9. Aluminium foil thickness distribution.

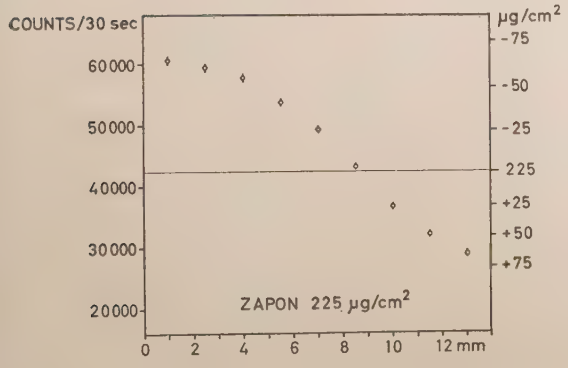

Fig. 7. Thick zapon film thickness distribution.

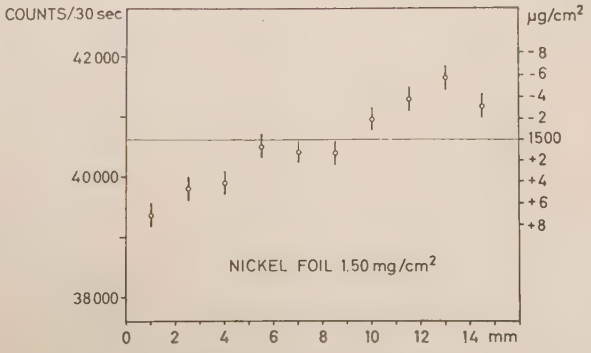

Fig. 10. Nickel foil thickness distribution.

TABLE 1

Material	Relative mass stopping power, A
Gold	0.275 ± 0.010
Silver	0.391 ± 0.010
Nickel	0.567 ± 0.011
Aluminium	0.776 ± 0.039
Aluminium Oxide	0.770 ± 0.038
Zapon	0.872 ± 0.076
Mylar	1.070 ± 0.099
Formvar	0.709 ± 0.045
Nitrogen	1.000 ± 0.000

Thickness distribution determination may be carried out according to the previously mentioned procedure. Using eq. (3) the resulting distribution calculations of thickness are very satisfactory; the standard error is not enough to seriously affect the thickness distribution calculations. Fig. 5 shows the extreme uniformity of the thickness of an aluminium oxide film. The scale in mm at the bottom of the figure is for the distance of the intersection of the alpha beam with the film as measured from the film's edge. Figs. 6 and 7 show the thickness distribution of two different zapon films. The thickness distribution of the two films are very different, but it should be noted that the thicker film was made by allowing several drops of zapon laquer to spread a 16 cm diameter distilled water surface while the thinner was made with only two drops. More uniform thick films of zapon are usually obtained by putting together several thin films. Figs. 9 and 10 show the thickness distribution of commercial aluminium and nickel foils respectively.

Acknowledgement

The authors wish to thank Prof. Kai Siegbahn for his suggesting the investigation and for his interest during the work.

NUCLEAR INSTRUMENTS AND METHODS 7 (1960) 167–173; NORTH-HOLLAND PUBLISHING CO.

A TRANSISTORIZED RING SCALER OF RESOLVING TIME 0.3 μs

G. W. HUTCHINSON, R. RUBINSTEIN and W. H. WELLS

Department of Physics, University of Birmingham

Received 11 December 1959

A transistor decade counter is described, employing a ring principle, and capable of accepting pulses at a minimum separation of less than 0.3 μsec. It includes a discriminator, pulse shaping circuit and a gating circuit. Printed wiring is used throughout.

1. Introduction

The counter consists of a ring of 5, needing 5 transistors and a switch transistor, preceded by a conventional scale of 2. The scale of 10 formed in this way can be directly coupled to another similar scale, and 4 of these, together with a mechanical register, comprise the complete unit.

A discriminator and pulse shaper, with gating facility, is incorporated in front of each unit.

2.

2.1. RING OF 5 (fig. 1)

In a ring counter, the circuit has only one pattern of on and off stages, and the position of this pattern round the ring is the indication of the number of counts recorded. One ring that has been used with valves[1]) has one "on" element holding all the others off by means of suitable feedback resistors, but the number of these feedback resistors needed is then large. Another ring, described by Carlson[2]), has a number of adjacent elements on holding the rest off, but, together with its gating circuit this is more complex than the one described here; also, time constants are introduced into the coupling elements. By using only resistive coupling, we have ensured that the times involved depend only on the transistors used, and faster operation was achieved by putting faster transistors into the same circuit with only minor modifications. One disadvantage is that in any circuit in which two transistor outputs are coupled to each transistor input, the maximum resolving time is a factor of two poorer than that expected from a conventional scale-of-two using the same type of transistor, since the gain bandwith is halved. In the present case, however, with a scale-of-two preceding, the overall resolution of the scale-of-ten is not less than that of the first scale-of-two.

The ring described here is essentially based on a valve version made by G. G. Scarrott in 1949; a similar transistor ring has been developed independently by Scarrott and Johnson (private communication).

Each transistor in the ring is connected through feedback resistors from its collector to the bases of its two neighbours: R_B to the right (say) and R_C (not equal to R_B) to the left. Due to the resistor chains R_B (or R_C) and R_D, when a transistor is on (its collector voltage almost equal to that of its emitter) the bases of the adjoining transistors should be biased positive with respect to their emitters, and therefore should be off. If this were so, there would be a pattern of on-off-on-off round the ring. This is impossible with an odd number of transistors; in our case, with a ring of 5 we have the two possiblilites of 3 on and 2 off, where 2 "on" must be adjacent, or 2 on and 3 off, where 2 "off" must be adjacent. Which of these two states occur depends on the current drawn

[1]) A. T. Starr, Radio and Radar Technique (Pitman Pub. Co., New York) p. 502.

[2]) A. W. Carlson, A.F.C.R.C.-TN-54-100; and Electronics 31 (1958) 89.

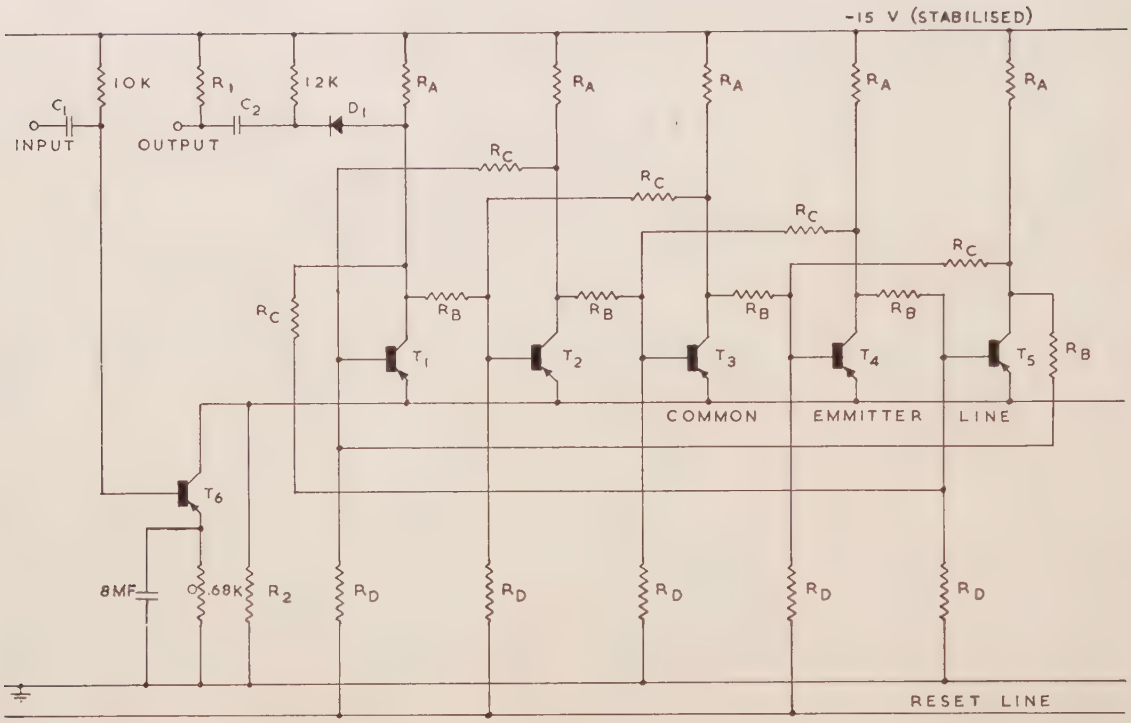

Fig. 1. Ring of 5. For component values, see table 1.

from the common emitter line by the switch transistor T_6 and the resistor R_2, down to earth: if this is large (i.e. the switch transistor hard on) there will be 3 on, but if small (switch transistor off, so that all current must pass through R_2) then only 2.

In the ring under consideration, the switch transistor is normally hard on, so that 3 transistors, say 1,2,4 if we number round the ring, are on together. Of the 2 adjacent ones, 1 and 2, base 1 is connected to collector 5 (off) by a small feedback resistor R_B, whilst base 2 is connected to collector 3 (off) by a large resistor R_C. Thus transistor 2 is not so firmly on as 1 (its base not quite so negative). If the switch transistor is now turned off, the total current from the 5 emitters is reduced so that only the state 2 on and 3 off can exist: it is transistor 2, being "least on" which goes off. We now, however, have 2 and 3 as adjacent off transistors where, as before, 3 is less firmly off due to the inequality of the feedback resistors. On turning the switch transistor hard on again, making conditions correct for 3 on and 2 off once more, transistor 3 comes on, and the sequence is (i) initially: 1,2,4 on (ii) switch transistor off: 1,4 on (iii) switch transistor on again: 1,4,3 on, where collector 1 and base 2 are connected by the smaller feedback resistor, etc.

In the ring considered here, with the switch transistor normally on, a positive pulse applied to its base (derived by differentiating the output of the preceding scale of 2) causes it to be turned off for a short time, and the pattern of the ring changes as described above; the net effect of a pulse into the switch transistor is therefore to change the state from 1,2,4 on to 1,3,4 on. Similarly a succession of pulses will take the ring through the cycle, 1,2,4; 1,3,4; 1,3,5; 3,5,2; 4,5,2; the 1,2,4 again etc. It is the inequality in feedback resistors which gives the sense of direction to the ring.

Although this ring has been made with 5 transistors, it is possible to use any odd number; 5 was chosen since, preceded by a scale of 2, it is the most convenient for practical use. An

even number, say 4, would have on-off-on-off as a stable configuration, with no 2 on transistors adjacent and could not therefore be switched by this method or show distinguishably different states.

the switch transistor was too great to permit operation at the speed required when this transistor was of the same type as those used in the ring. A faster transistor was therefore used in each case.

TABLE 1

Component values for the circuit shown in fig. 1

Component	1st Ring	2nd Ring	3rd Ring	4th Ring
T_1, T_2, T_3, T_4, T_5	SB 345	OC 45	OC 45	OC 71
T_6	SB 345	SB 345	SB 345	OC 45
C_1	220 pF	0.001 μF	0.001 μF	0.005 μF
C_2	Short circuit	Short circuit	0.001 μF	0.005 μF
R_1	Open circuit	Open circuit	1.5 kΩ 10%	3.3 kΩ 10%
R_2	3.3 kΩ 10%	3.3 kΩ 10%	3.3 kΩ 10%	10 kΩ 10%
R_A		All rings: 2.7 kΩ 5%		
R_B		All rings: 3.3 kΩ 5%		
R_C		All rings: 6.8 kΩ 5%		
R_D		All rings: 22 kΩ 5%		
All other resistors 10%.				

Resistor values in the ring were chosen to fit the following conditions:

(i) About 3 mA collector current in "on" transistors; with 680 Ω emitter load on the switch transistor, this required R_A to be 2.7 kΩ.

(ii) To give the sense of direction, the value of R_C was made twice that of R_B.

(iii) Transistors in the "off" state should have a base potential at least half a volt positive with respect to their emitter. With supply voltages as shown and under conditions (i) and (ii) this is satisfied by making the value of R_D seven times that of R_B.

(iv) Using (i), (ii) and (iii), the base current of the "least on" transistor is found to be

$$i = \frac{8.5 \times \frac{2}{3} R_B}{2.7 + \frac{2}{3} R_B} \cdot \frac{1}{2R_B} - \frac{6.5}{7R_B}$$

(i in mA, R_B in kΩ).

This is maximised with respect to R_B, and gives $R_B \approx 3.3$ kΩ.

As described in section V, four different rings are used in the complete unit; in the slower rings it was found that the input capacitance of

2.2. RESET (fig. 2)

Any one of the possible states of three transistors on can be chosen as the initial state, and from this, the succeeding stages are determined uniquely. To reset, the chosen three base biasing

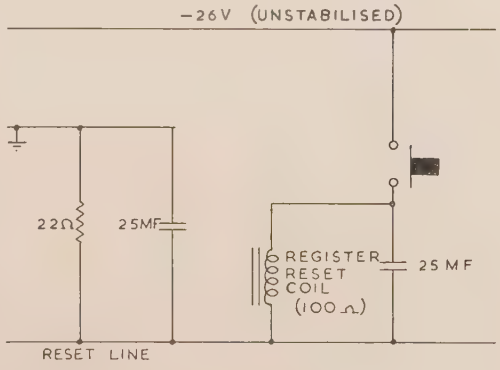

Fig. 2. Reset.

resistors R_D, normally connected to earth, are taken to the negative supply voltage; at the same time, the scale of 2 and mechanical register are also reset.

2.3. OUTPUT

The initial state having been chosen, and numbering the three on transistors 1,2,4 as before, the output is taken from 1. A collector

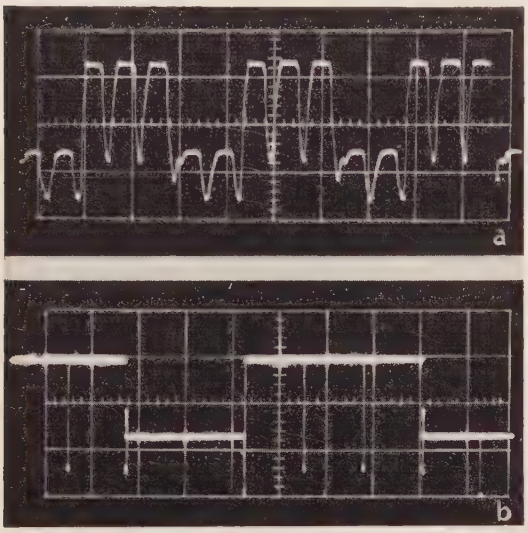

Fig. 3. (a) Collector waveform of 1st ring, when scaler input is 3 Mc/s. (b) Collector waveform of 4th ring, for the same input.

waveform is shown in fig. 3; this is differentiated and the positive pulse obtained from the front edge used to drive the next stage. The amount of differentiation required is not, of course, the same for each ring.

the scaler is minimised by using a sensitive meter (100 μA full scale deflection).

Four of the resistors are connected to the collectors of T_1, T_2, T_3 and T_4 so that they carry appreciable current only when the appropriate transistor is "off". Ideally, their values are required to be in the ratio $\frac{1}{4}:\frac{1}{3}:\frac{1}{2}:1$. The fifth resistor is connected to the output of the scale of

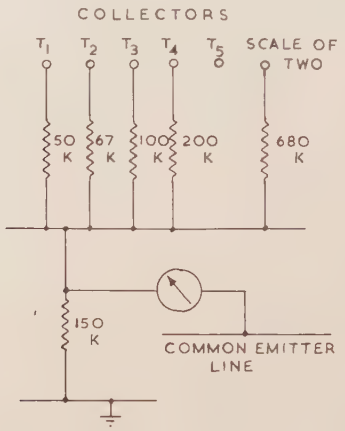

Fig. 4. Indication of Count.

two, and is adjusted so that the change of state of this circuit produces in it a current change of 11 μA. The sixth resistor is used to back off the meter so that its lowest reading is zero.

There is some freedom of choice in the values

TABLE 2

Component values for the circuit shown in fig. 5

Component	1st Scale	2nd Scale	3rd Scale	4th Scale
T_1, T_2	SB 345	OC 45	OC 45	OC 45
C_1, C_2	22 pF	100 pF	100 pF	100 pF
C_3, C_4	75 pF	100 pF	250 pF	250 pF
D_1, D_2	OA 5	OA 81	OA 81	OA 81
R_1	1.2 kΩ	1.0 kΩ	1.0 kΩ	560 Ω
R_2	1.0 kΩ	1.5 kΩ	1.5 kΩ	1.8 kΩ
All resistors 5%				

2.4. INDICATION OF COUNT (fig. 4)

The indication of count is by a meter scaled from 0 to 9. It is connected between the common emitter line and the junction of six resistors as shown in fig. 4. The effect of this network on

of this network. It was removed by arbitrarily making the influence of T_5 on the meter zero.

Resistor values necessary vary slightly between different scales of 10 due to variations in individual components. The values given in fig. 4,

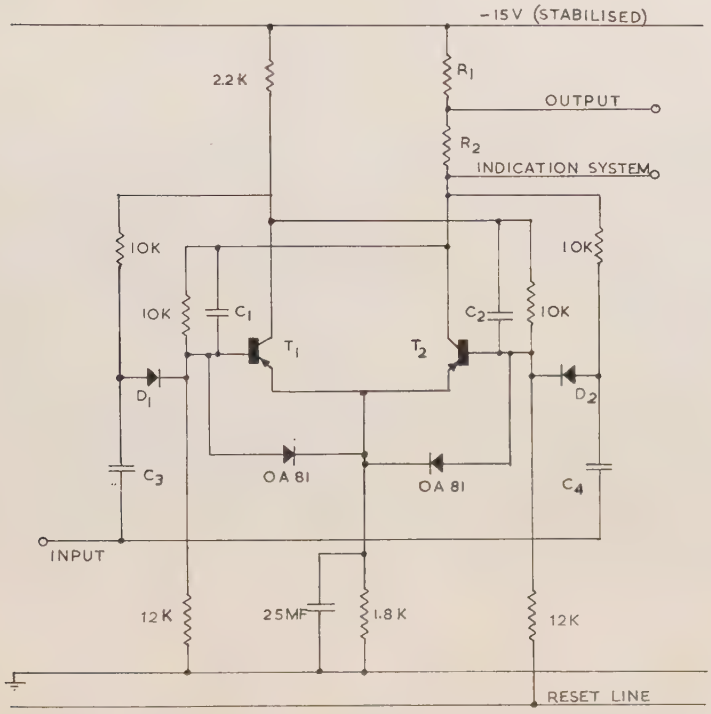

Fig. 5. Scale-of-two. For component values see table 2.

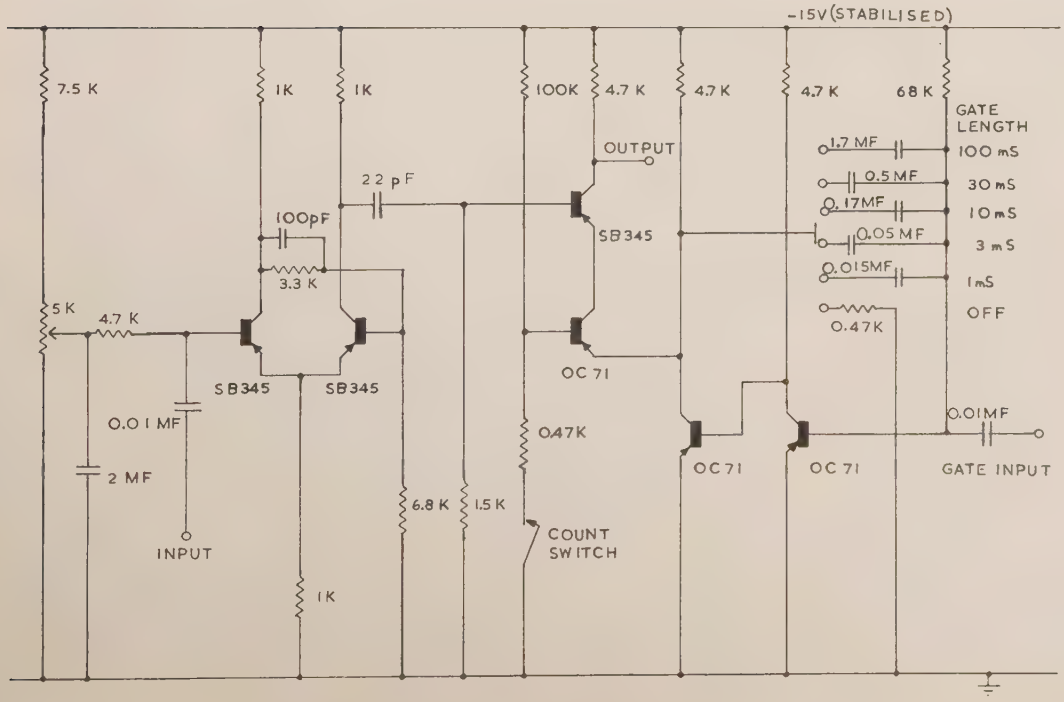

Fig. 6. Discriminator. All resistors 5%.

are only correct to within a few per cent. The procedure adopted, therefore, is to insert initially resistors of slightly higher values than calculated, and then to correct them by parallel resistors whose value is found by trial using variable resistors.

Fig. 7. Complete Unit. Front Panel.

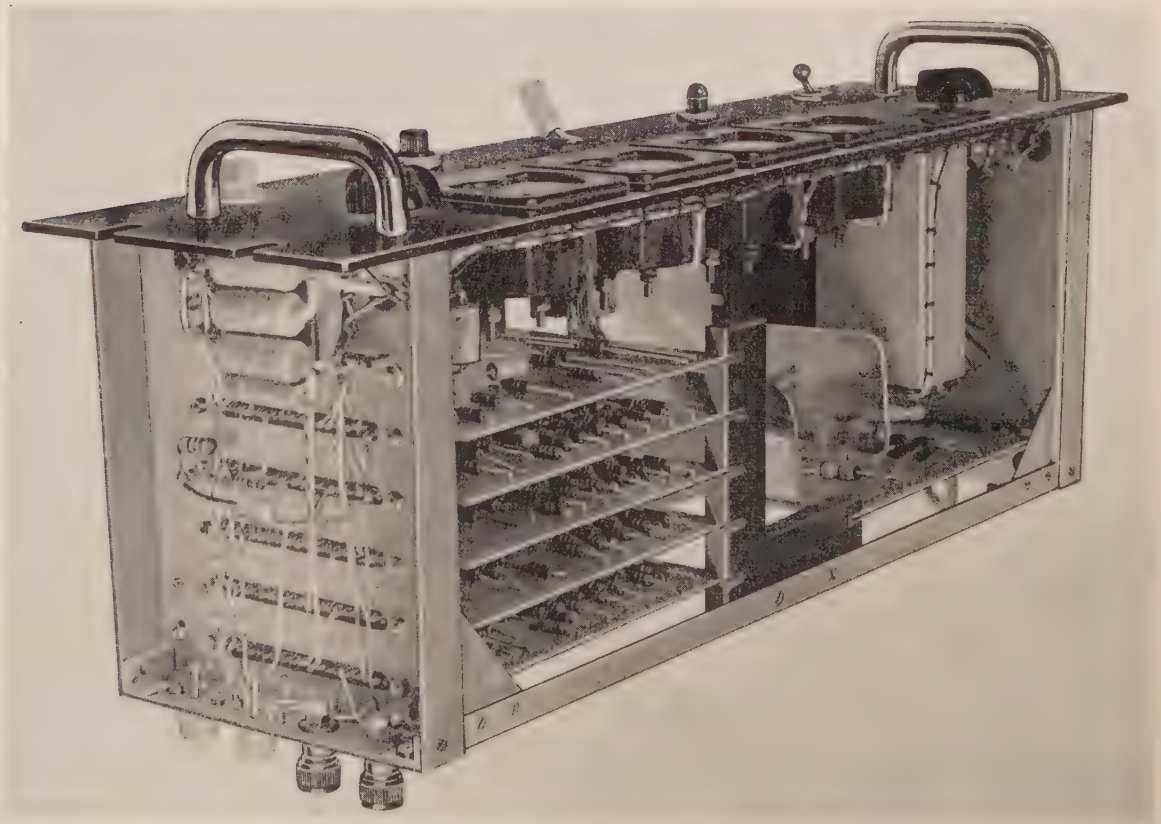

Fig. 8. Complete Unit. Top View, with cover removed.

3. Scale-of-Two (fig. 5)

Any scale-of-two with the appropriate resolving time can be used, the one adopted being based on a design by Bradshaw[3]). From one of the collectors, outputs are taken to the ring of 5 and to the indication system.

4. Discriminator (fig. 6)

Essentially, this is a Schmidt trigger followed by a single transistor pulse shaping circuit. A variable bias is applied to the first transistor, so that it will only accept pulses above a pre-set value in the range — 1 to — 8 volts, and up to a maximum of about — 25 volts. Although the scaler operates from positive pulses, it was convenient to make the discriminator operate from a negative input.

The Schmidt trigger gives a negative output of constant height but whose length depends on that of the input. This is inverted, and standardised in length by the third transistor, which though normally off, is turned hard on by the pulse. From this, an output is taken to the first scale-of-two.

The complete discriminator and standardiser, using S.B. 345 transistors, has a resolution of better than 3 Mc/s.

Also incorporated in this unit are the count switch, and a triggered gating system having 5 different live times, and opened by a positive pulse of about 4 volts. It is intended for use when the scaler is counting bursts of radiation from pulsed accelerators.

5. Complete Unit (figs. 7 and 8)

Each scale of 10 is made on a printed wiring card, which can be inserted into suitable connectors behind the counter panel. The complete unit comprises 4 scales of 10 with their meters, a common reset button, discriminator unit, mechanical register, driven from the 4th stage (fig. 9), and a power unit of transformer, diode rectifier and Zener diode voltage stabiliser. The discriminator and gate is on a single card, and the rectifiers, stabiliser and register drive on another.

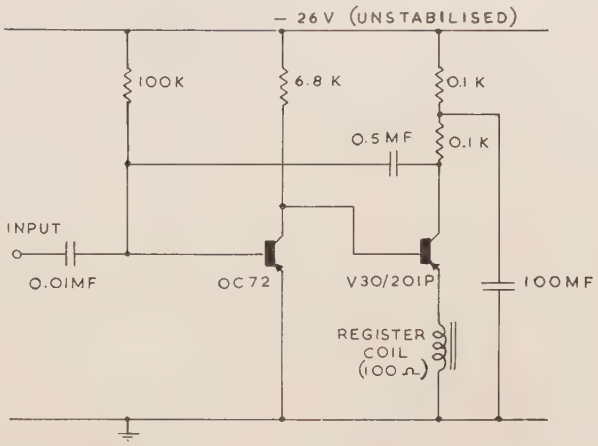

Fig. 9. Mechanical Register Drive. All resistors 10%.

Of the 4 scales of 10, the first is made with SB 345 transistors, the second and third with OC 45, but SB 345 as switch transistor, and the fourth with OC 45 for the scale-of-two and switch transistor, and OC 71 for the ring; each scale is capable of better resolution than the maximum imposed upon it by the previous one.

The count and reset lines are taken to terminals at the back of the scaler, so that a number of scalers may be operated simultaneously.

Acknowledgement

One of us (R. R.) is indebted to the Department of Scientific and Industrial Research for a Research Studentship.

[3]) Bradshaw, Electronic Engineering **31**, No. 372 (1959)96.

NUCLEAR INSTRUMENTS AND METHODS 7 (1960) 174–178; NORTH-HOLLAND PUBLISHING CO.

A "TIME EXPANDER" FOR PRECISION NEUTRON TIME-OF-FLIGHT EXPERIMENTATION

J. R. WATERS †

A.E.R.E., *Harwell, Didcot, Berks., England*

Received 19 December 1959

For accurate neutron time-of-flight experiments, narrow timing channels must be used. These are frequently generated by converting the time-of-flight of a neutron into a pulse of proportional amplitude and then performing a pulse height analysis. This converter, and also the one in the pulse height analyzer, are subject to drifting introducing inaccuracies into the measured data. The instrument described here replaces both of these converters with one entirely digital system which is inherently drift free. It uses a scaler to measure the number of fast "clock" pulses preceding the arrival of a neutron and then complements this number with slow pulses which are also fed into the memory and display unit of the original spectrometer. Thus it allows a spectrometer designed for 2 microsec timing channels to be used with $\frac{1}{4}$ microsec channels with no internal changes. Improved stability and reliability have been obtained by the use of transistors throughout.

1. Introduction

For the measurement of the interaction of low energy neutrons with matter, the time-of-flight method is of great importance. A pulsed source emits a short burst of neutrons which travel down an evacuated tube to strike a detector at a known distance from the source. By measuring the time-of-flight of the neutrons their energy can be determined. As the simpler experiments are performed there arises the need for improving the resolution that can be obtained with this type of apparatus. This can be done by reducing the length of the neutron burst, by going to longer flight paths and by using narrower timing channels. Already burst lengths of from $\frac{1}{4}$ down to 0.1 microsec in conjunction with flight paths of 100 meters or more make it imperative to reduce the width of the timing channels accordingly. Commercial time-of-flight analyzers have channel widths down to $\frac{1}{4}$ microsec although those manufactured a few years ago had 2 microsec channels. The piece of equipment described in this report makes it possible to use one of these earlier analyzers with $\frac{1}{4}$ or 0.1 microsec channel widths with no modification to it. Previously it had been possible to do this by the use of two "converters", as described in the next section, although at the expense of increasing the cost and complexity of the electronics.

2. Present Equipment

One of the usual ways to make narrow timing channels is to convert the time-of-flight of the neutron into a pulse of proportional amplitude in a "Time-to-Amplitude" converter[1]). This pulse is then fed into a multichannel pulse height analyzer. The system is shown in fig. 1 as a block diagram. Pulses from the detector are amplified and fed into the converter to stop a linearly rising voltage which was started by a pulse at a known time after the accelerator fired (called the "delayed start pulse"). The height of this voltage pulse is the signal required. After amplification and stretching it is fed into the pulse height analyzers. This in turn contains a converter which produces a train of pulses about 1 to 3 microsec apart whose number is proportional to the height of the input pulse. These pulses go to the memory and display unit

† Now at Rensselaer Polytechnic Institute, Troy, N.Y. U.S.A.

[1]) e.g. F. W. K. Firk, G. W. Reid and J. F. Gallagher, Nuclear Instruments **3** (1958) 309.

which contains either trochotrons or binaries which step around to generate the large number of channels (typically 100 or 256). It is not possible to feed a train of, say, $\frac{1}{4}$ microsec pulses directly into these units since they are unable to handle them. The disadvantage of this system of using two converters is that they are both analog in character and subject to gradual drifting so have pulse spacings of $\frac{1}{4}$ microsec and 2 microsecs and need not be exactly in phase with one another though locked together.

3. Time Expander

The principle of this sytem, which might be called a "Time expander" is clear from fig. 2 which is a simplified block diagram. Gate A is

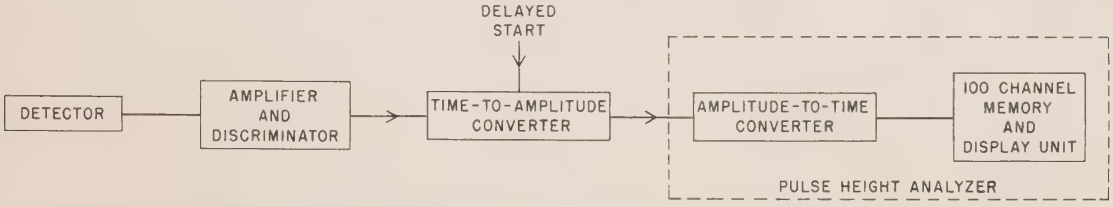

Fig. 1. Usual system for time-of-flight experiments using a multichannel pulse height analyzer.

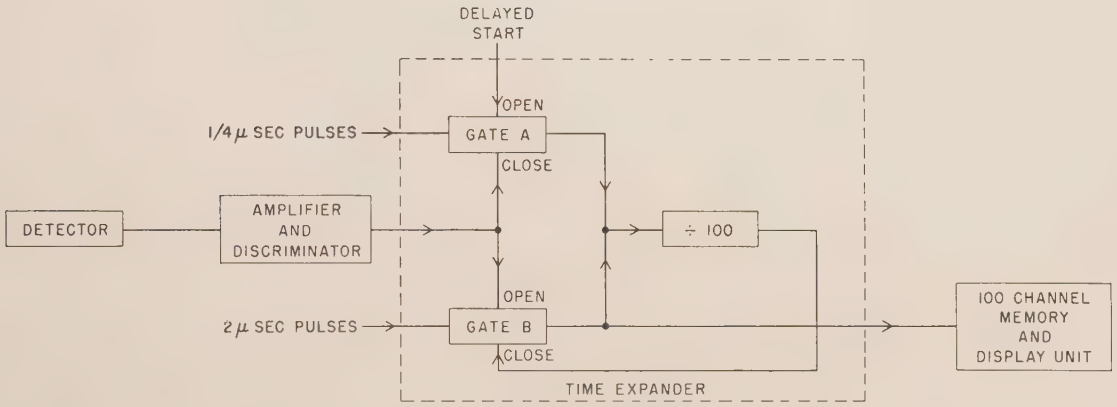

Fig. 2. Simplified block diagram of time expander.

altering the channel widths. Since typical experiments may take several days to complete, this necessitates frequent recalibrations of the channel widths and also of the absolute delay of any particular channel. The system to be described below replaces both of these converters with one unit which is essentially digital in character throughout and not subject to drifts.

For clarity, further discussion will relate to the problem of converting a 100 channel analyzer with 2 microsec channel widths to operate with $\frac{1}{4}$ microsec channels. It is assumed that there are available two trains of pulses locked in phase to the pulse which fires the accelerator, so producing the neutron burst. These trains opened by the delayed start pulse and allows the train of $\frac{1}{4}$ microsec pulses to pass through it into a fast scale of 100. When a neutron signal arrives, it closes gate A, and simultaneously opens gate B, to allow 2 microsec pulses through to the scaler. When the scaler reaches 100 its output pulse closes gate B. Suppose that there were n of the $\frac{1}{4}$ microsec pulses passed through gate A to the scaler and N of the 2 microsec pulses through gate B. Then:

$$n + N = 100$$

or

$$n = 100 - N .$$

Hence, by reading the spectrum stored in the memory and display unit of the pulse height

analyzer backwards (i.e., channel 100 as channel 0, 99 as 1, 98 as 2, etc.) the value of n is obtained. The neutron time-of-flight is just $n/4$ microsec plus the preset delay in the start pulse.

The circuit is inherently simple consisting essentially of two fast gates and a scaler capable of running at the required rate of 4 Mc/sec. There is no reason why this principle could not be extended to several hundred 0.1 microsec channels. Of course the time expander is only capable of accepting one neutron pulse per accelerator cycle in common with the equipment it replaces.

nearly coincident with a $\frac{1}{4}$ microsec pulse and so close the gate on top of this pulse. This would lead to a small pulse out to the scaler and errors in the timing. To overcome this the neutron pulse goes into a "staticizer" whose output is the next $\frac{1}{4}$ microsec pulse occurring after the neutron pulse. This pulse is suitably delayed and applied to gate A so that it closes midway between two $\frac{1}{4}$ microsec pulses thus ensuring a full amplitude output pulse.

The neutron discriminator also feeds AND gate B which passes a pulse only when timing gate A is open. This output is staticized against

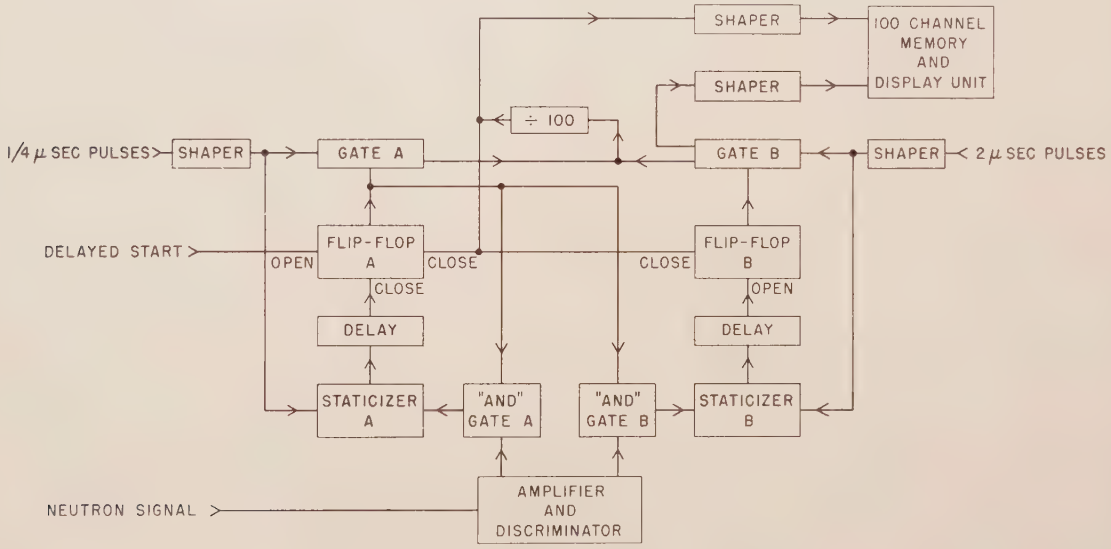

Fig. 3. Detailed block diagram of the time expander.

4. Circuit Details

The complete block diagram of the time expander is shown in fig. 3. The mode of operation is as follows.

The delayed start pulse enters flip-flop A turning it over and opening gate A. Shaped $\frac{1}{4}$ microsec pulses go through the gate and into the scaler. If a neutron pulse arrives it is amplified, standardized in the discriminator and fed into the AND gate A. The other input of this gate goes to flip-flop A so that there can only be an output from AND gate A when gate A is open. This output, essentially the neutron pulse, is then used to close gate A. However, since it occurs at random times it could be the 2 microsec pulse train and used to open gate B. This second staticizer is needed since the $\frac{1}{4}$ and 2 microsec trains need not be exactly in phase.

When the scaler reaches 100 its output pulse closes gates A and B. If no neutron pulse has occurred then gate A will still be open and B closed while a neutron pulse will leave A closed and B open.

The pulses from gate B are amplified and shaped so as to drive the 100 channel display unit which contains two trochotrons in series. The carry pulse from the scaler is delayed and fed into this unit as a "count" pulse to transfer the number from the trochotrons into the memory circuits.

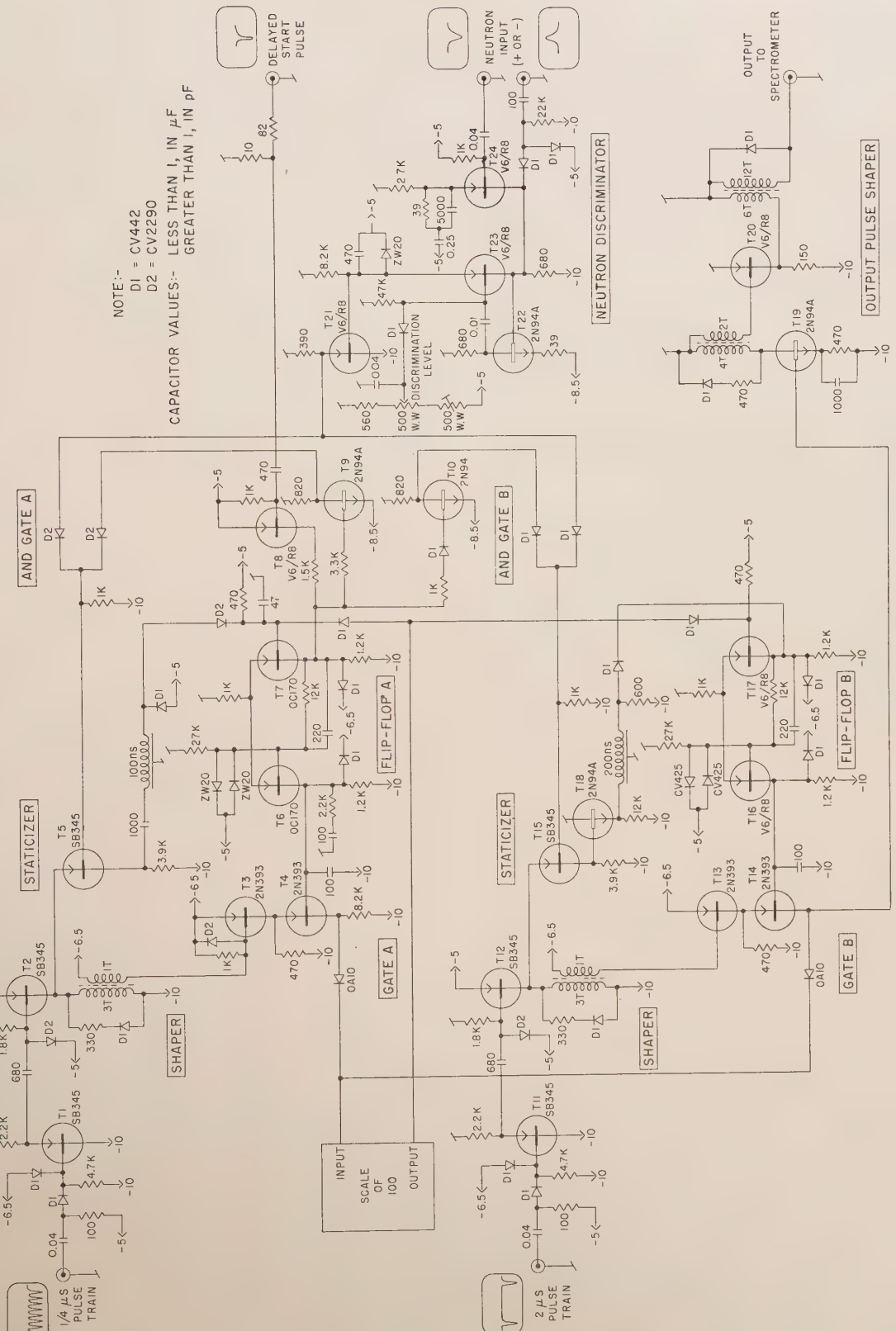

Fig. 4. Circuit diagram of the time expander.

The detailed circuit diagram of the time expander is shown in fig. 4 except for the scaler. This can be any available type provided that it can operate at the required rate, 4 Mc/sec in this case, and has a short carry time.

The shape and size of the pulses comprising the $\frac{1}{4}$ microsec and 2 microsec pulse trains are not critical since they are both standardized in shapers. The delayed start pulse should have a rise time of about 50 to 80 nanosec to ensure that gate A opens cleanly. The neutron pulse can be slower and of sufficient amplitude (5 V positive or 0.1 V negative) to trigger the discriminator.

The two parts of the circuit that handle the $\frac{1}{4}$ microsec and 2 microsec pulse trains are very similar except for the use of faster transistors for the narrower pulse spacing. Owing to the difficulty of obtaining 2N393 transistors at the time that the instrument was constructed these have been used very sparingly. It would be better to use this type for T1, T2, T5, T6 and T7 especially for timing channels narrower than $\frac{1}{4}$ microsec. The two transistors T9 and T10 drive the two AND gates. T9 is a 2N94A and passes a replica of the waveform in flip-flop A. This ensures that AND gate A passes a neutron pulse only when gate A is open, i.e. within 25 microsec after the delayed start pulse. T10 is a 2N94 and the circuit uses hole storage to delay the back edge of the flip-flop waveform by about 3 microsec. The neutron pulse from the discriminator is 3 microsec wide so that AND gate B is held open for at least 2 microsec. This ensures that at least one 2 microsec pulse will get through the staticizer T15. This problem does not arise with the other staticizer since the maximum waiting time is only $\frac{1}{4}$ microsec.

One of these time expanders has been constructed at AERE, Harwell, on eight 7″ × 7″ plug-in printed circuit panels, 4 of which were for the scaler. Tests have shown that it works as expected and is very stable against supply voltage changes. The first two $\frac{1}{4}$ microsec channels do not read correctly due to the timing ambiguities arising when the neutron pulse arrives within $\frac{1}{2}$ microsec of the delayed start pulse. This defect is not important though it could probably be reduced to one channel by taking sufficient trouble.

Acknowledgements

The author is greatly indebted to J. G. Page and F. H. Wells for the detailed design of the constructed instrument and for their generous assistance in making it work properly.

NUCLEAR INSTRUMENTS AND METHODS 7 (1960) 179–183; NORTH-HOLLAND PUBLISHING CO.

APPLICATION OF BIDIRECTIONAL DEKATRON TUBES IN LOW LEVEL BETA ACTIVITY MEASUREMENTS BY CANCELLATION TECHNIQUE

K. S. KUCHELA and L. H. PESHORI

Atomic Energy Establishment Trombay, India

Received 16 January 1960

A new approach employing cancellation technique for reducing background of G.M. counter (size: diameter = 2.5 cm, length = 5 cm) to less than 2 counts per minute has been developed for the measurement of low level beta activity of the order of 25 micromicrocuries. The method and electronics used for cancellation are described. This method is a simple alternative to the usual anticoincidence shielding and needs only two G.M. counters for determination of moderately low level beta activities. This technique has been successfully applied for the study of the activity of biological samples from sea.

1. Introduction

The measurement on samples of very low level beta activity becomes difficult on account of the background radiation, due to cosmic radiation, natural radioactivity of surroundings and radioactive contamination of counter. For a reasonable accuracy in any measurement, the counting rate produced by the sample has to be atleast a large multiple of that produced by the background radiation. Therefore there is a great necessity to reduce the background without loss of counting efficiency. The problem has been solved by the use of massive lead shield and anticoincidence technique[1]).

A new approach to the problem using cancellation technique and a comparison counter is described in the present paper, which dispenses with the complicated anticoincidence arrangement usually resorted to for reducing background. The system consists of a detecting channel responding to beta and gamma activities and a cancellation channel responding only to gamma radiation. The two channels are inserted into a cancellation circuit which reads the difference between them. Two selected end-window counters having nearly identical performance gave an effective background of 1.1 count per minute after cancellation (a reduction by approximately a factor of ten), the one having slightly more efficiency being used in the detecting channel.

2. Cancellation Principle

Referring to fig. 1, the pulses from the detecting channel pass through a gate before

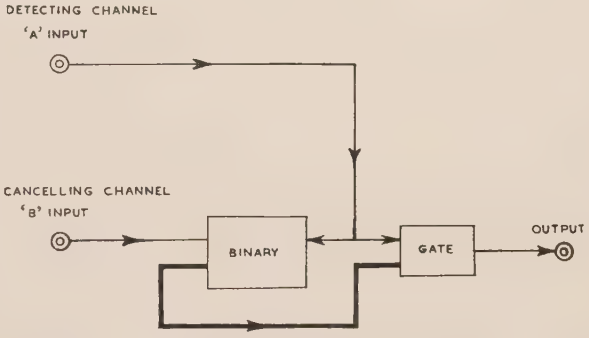

Fig. 1. Block diagram – Cancellation principle.

appearing at the output. Whenever there is a cancelling channel pulse at B, the binary is triggered and the gate is closed stopping the next detecting channel pulse from reaching the output, which however resets the gate. The binary referred to in fig. 1 is the familiar Eccles Jordan flip-flop circuit controlling the gate. The cancelling efficiency depends upon resetting

[1]) E. H. Cooke-Yarborough and J. Putman, Sci Instr. 26 (1949) 240, 198.

of the gate by detecting pulse. The system fails when more cancelling pulses arrive while the gate is closed. This difficulty is eliminated by storing the cancelling pulses in a bidirectional Dekatron tube[2]) and subsequently cancelling them by the detecting channel pulses.

3. Theory of the Method

The effective background counting rate depends primarily on the efficiency for gamma radiation detection and the plateau characteristics of the two detectors. The plateau characteristics should run close to each other and intersect at a suitable operating point. If N_1, N_2 and n are the counting rates in detecting, cancelling and output channels respectively and n' are the counts remaining in storage after the counting period t, then

$$(N_1 - N_2)\, t = nt - n' . \tag{1}$$

It has been stated earlier, that N_1 is greater than N_2. Under this circumstance, n' can be made very small compared to nt, and it can be neglected without introducing appreciable errors.

$$(N_1 - N_2)\, t = nt . \tag{2}$$

The standard deviation (s.d.) associated with these terms are

$$\sqrt{(N_1 + N_2)\, t} \tag{3a}$$

and

$$\sqrt{nt} = \sqrt{(N_1 - N_2)\, t} ,$$

if nt has Poisson distribution

$$\sqrt{(N_1 + N_2)\, t} ,$$

if nt behaves like the difference between two Poisson distributions.

Our experiments show that the s.d. of nt is neither

$$\sqrt{(N_1 - N_2)\, t}$$

nor

$$\sqrt{(N_1 + N_2)\, t} ,$$

but is approximately

$$\begin{aligned} &2\sqrt{nt} \quad \text{when} \quad N_1 t \approx N_2 t \\ &\sqrt{nt} \quad \text{when} \quad N_1 t > N_2 t . \end{aligned} \tag{3b}$$

[2]) Bacon and Pollard, "The Dekatron", Electronic Engg. 28 (1950) 173.

Expressions (3a) and (3b) are helpful to the extent that their comparison gives an indication of improvement in the s.d.

$$[2\sqrt{(N_1 - N_2)\, t} < \sqrt{(N_1 + N_2)\, t}]$$

and justifies the use of cancellation technique instead of a much simpler arrangement of two scalers.

Expressing N_2 in terms of N_1 (or N), the efficiencies of the detectors for gamma radiations α_1 and α_2 and the dead time T introduced by the quenching circuits, expression (4) is obtained for the effective background rate

$$n = \frac{(k-1)\,(1 - TN)}{\frac{k}{N} - T\,(k-1)} \tag{4}$$

where $k = \alpha_1/\alpha_2$. The resolution of the Dekatron has not been taken into account in eq. (4), as the drive circuit does not introduce any counting losses and the quenching period used with the detectors is more than twice the period required to handle a count in the dekatron.

When $k = 1$, eq. (4) reduces to zero. However, eq. (1) shows that $n = n'/t$. This can also be seen by the following probability considerations: If n' counts are in storage there is a certain probability of $(n' + r)$ counts arriving in the detecting channel before another count is added to the storage, in which case, r counts will be transmitted by the gate G. r is large when n' is small or zero and decreases as n' increases. Similar considerations show that n' is the total of all r in the counting period t. This is true whether k is equal to one or greater than one. In view of these arguments eq. (4) has to be modified to

$$n = \frac{(k-1)\,(1 - TN)}{\frac{k}{N} - T\,(k-1)} + \frac{n'}{t} .$$

If a small storage n'' is provided at the commencement of a measurement, eq. (1) will be modified to

$$(N_1 - N_2)\, t = nt - n' + n''$$

or

$$n = N_1 - N_2 + \frac{n' - n''}{t} .$$

This can be made to approach the true difference between N_1 and N_2 by a proper choice of n''—for instance, the counts left in storage in a previous background measurement.

4. Cancellation Circuit

The functional diagram of the cancellation circuit incorporating Dekatron storage is shown in fig. 2. At the commencement of a measurement the Dekatron is reset (glow on zero cathode) and the gate G which controls the transmission of detecting channel pulses is open. When a cancelling channel pulse arrives, the glow advances to the next cathode. The control binary which is d.c. coupled to the zero cathode of the Dekatron changes its state, closing the transmission gate G and at the same time opening the reset gate G'. Now, if a detecting channel pulse arrives, it passes through the reset gate G' and is inserted into the drive circuit so as to cause the glow to move from 1 to 0 at which position the transmission gate G reopens. If instead, more cancelling pulses arrive, the glow advances by the number of pulses received and the same number of detecting pulses are required to bring the glow back to zero.

A second Dekatron is used to increase the storage capacity of the system and to eliminate the loss of nine stored pulses due to a single cancelling channel pulse opening the gate G by moving the glow from 9 to 0. The Dekatrons are coupled by a reversible coupling circuit due to Churchill[3]).

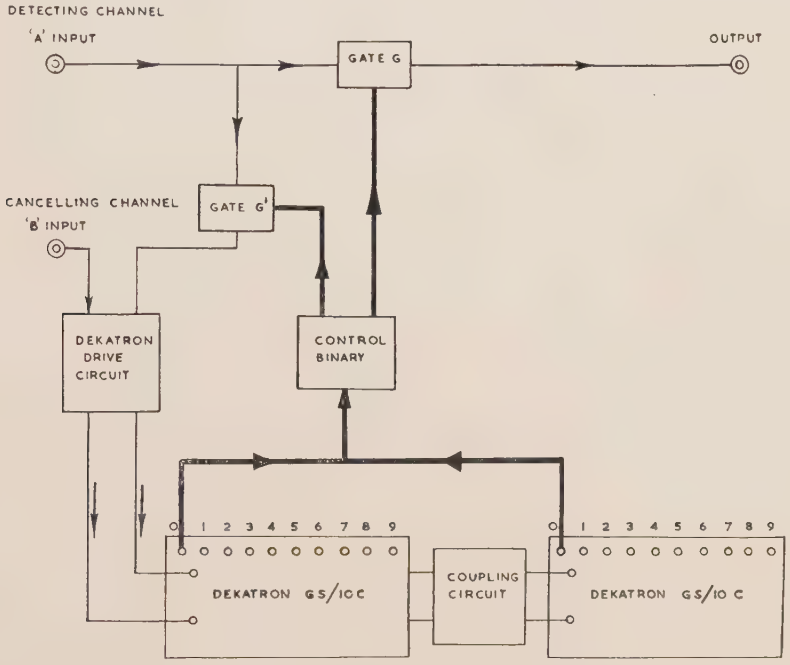

Fig. 2. Block diagram – Cancellation unit.

5. Reversible Drive Circuit

The drive circuit consists of four identical univibrators interconnected as shown in the block diagram of fig. 3. The univibrator can be triggered either by applying a positive pulse to the grid of the non-conducting section or by a negative pulse applied to the grid of the conducting section.

The rectangular waveform obtained at the univibrator T_1 is differentiated. The negative

[3]) J. L. W. Churchill, New Trigger circuits for use with cold cathode counting tubes", Jr. Britt. I.R.E. 12 (1952) 502.

edge of the differentiated output is applied to the grid of T_{4b} and the univibrator T_4 is triggered. The waveform obtained at this univibrator is applied to the B guides. The positive edge of used to couple negative edge of differentiated pulses to the grids of T_{4b} and T_{3b} as shown in fig. 3. If t is the duration of guide pulses and T is the duration of the pulses at T_1 and T_2, then

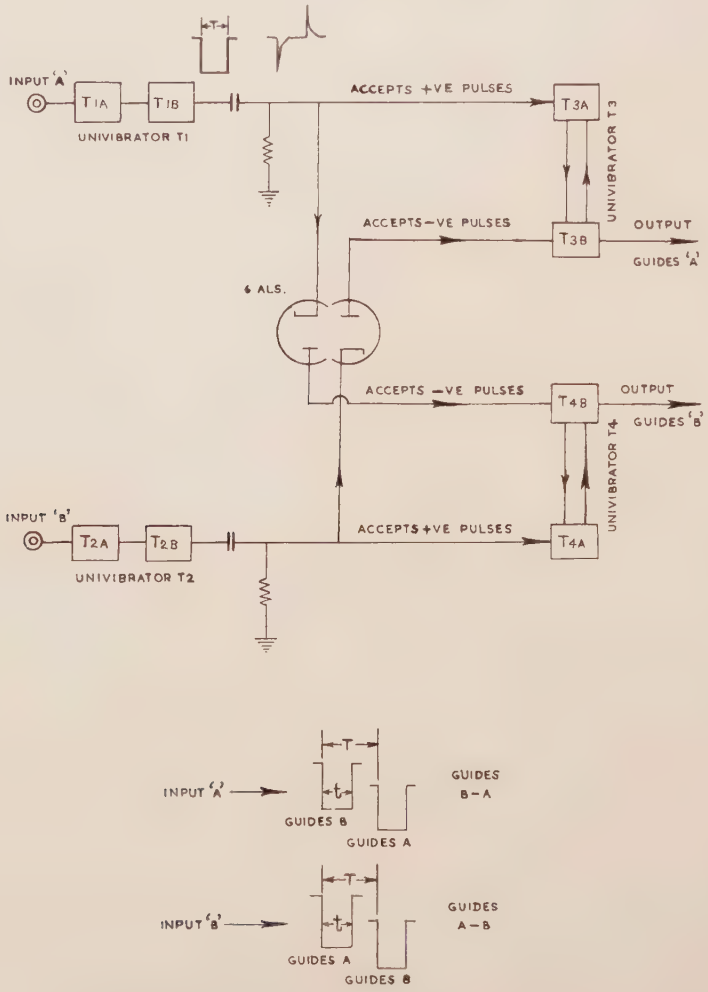

Fig. 3. Drive circuit – Bi-directional Dekatron tube.

the differentiated pulse, which occurs after time T, triggers univibrator T_3 and its output waveform is applied to the A guides. Thus when a detecting pulse triggers univibrator T_1, the guide pulses are applied in the sequence B–A, moving the glow in anticlockwise direction. Similarly, when a cancelling channel pulse triggers univibrator T_2, the sequence of guide pulses A–B, moving the glow in clockwise direction.

To avoid oscillations in the circuit diodes are the guide pulses will be separated by the time interval $(T - t)$. Since the univibrators are identical T is equal to t, so that the second pulse is applied to the guides on the tail of the first pulse. One of the advantages of this circuit, apart from its simplicity, is that, there is no loss of counts in the Dekatron, either when events arrive simultaneously in the two channels, or when one event arrives while the other is being processed in the drive circuit.

6. Results

The results obtained with two selected end window counters are summarized below:

Condition	Background of A	Background of B	Effective background
Without shield	26.3	23.5	3.2 C/min
$1\frac{1}{2}''$ lead shield	10.74	9.75	1.1 C/min

The method has been used in this laboratory for the determination of the activity of biological samples from sea, where the activities encountered are of the order of 25 micromicrocuries. Taking a counting time of one hour, assuming a counting efficiency of 16% (which we normally realize), with a background of 1.1 count per minute, one can estimate activities of the order of 25 micromicrocuries with a statistical accuracy of 95%.

Acknowledgments

The authors are indebted to Shri G. H. Vaze for his many interesting suggestions and to Shri A. S. Rao for his keen interest in this work.

NUCLEAR INSTRUMENTS AND METHODS 7 (1960) 184–188; NORTH-HOLLAND PUBLISHING CO.

THE PROPANE BUBBLE CHAMBER USED WITH THE BIRMINGHAM PROTON SYNCHROTRON

J. D. DOWELL, W. R. FRISKEN, G. MARTELLI† and B. MUSGRAVE

Physics Department, The University of Birmingham

Received 16 January 1960

The design of a piston operated propane bubble chamber which has been used in conjunction with the 1 GeV proton beam of the Birmingham synchrotron is described. The operating conditions and the method of analysis of photographs are discussed.

1. Introduction

The present paper contains a description of the general design features and operating conditions of a propane bubble chamber which has been used in the scattered out beam of the Birmingham proton synchrotron[1]). Satisfactory photographs were first obtained in February 1958, and the chamber has been used to study p–p elastic interactions at 1 GeV[2]) and the momentum distribution of protons in carbon[3]).

Propane bubble chambers operate at a temperature of about 60° C and at a pressure between 300 and 400 psig. These conditions govern the requirements for mechanical strength, but do not impose much restriction on the type of expansion, heating and photographic systems. The chamber described here has been designed so as to incorporate some of the best features of existing chambers. It has proved to be a compact device, efficient and reliable.

2. Chamber Body and Heating System

The design figures have been calculated so as to provide a safety factor of at least seven on all parts of the chamber.

The main body of the chamber (fig. 1) has been machined from a heat treated duraluminium bar 10″ in diameter. The visible volume is $9'' \times 2\frac{1}{8}'' \times 2\frac{1}{2}''$. The inside surfaces have been highly polished and anodized black to reduce reflections.

Two $1\frac{1}{2}''$ thick armour plate glass windows are clamped on "Gaco" P-60 "o-rings" by $1\frac{3}{8}''$ thick duraluminium plates, each one secured by sixteen $\frac{1}{2}''$ steel Whitworth studs. The o-ring grooves have been designed so that, when the o-rings are compressed, the clearance between glass and metal is several thousandths of an inch. Thus, even at working temperature, no contact can occur which could lead to breakage of the armour glass plates. In order to allow for any departure from flatness of the glass and metal surfaces, 0.010″ fibre gaskets are placed between the windows and the clamping plates.

The end wall of the chamber is provided with a duraluminium beam entry window $\frac{1}{8}''$ thick.

The chamber is heated by warm water circulating in channels machined in the body. These consist of $\frac{1}{2}''$ holes, drilled between the stud holes (fig. 1) and connected by U-shaped grooves machined on the top and bottom faces of the chamber. The grooves are covered by $\frac{1}{16}''$ hard rubber sheets sealed to the metal with araldite. The water circulates through the chamber in two parallel streams. It is pumped

† On leave of absence from the University of Pisa, Italy.

[1]) P. B. Moon, L. Riddiford and J. L. Symonds, Proc. Roy Soc. A. **230** (1955) 204.

[2]) J. D. Dowell, W. R. Frisken, G. Martelli and B. Musgrave, Proc. Phys. Soc. **74** (1959) 625.

[3]) J. D. Dowell, W. R. Frisken, G. Martelli and B. Musgrave, Proc. Phys. Soc. **75** (1960) 24.

through polythene tubes from a thermally insulated 10 gallon reservoir at a rate of 5 gallons/minute. A subsidiary heating coil surrounds the expansion mechanism. A 2 kW immersion heater, placed in the reservoir, is controlled by a commercial thermostat located in the ingoing stream, just before the chamber. The chamber is thermally insulated from the surrounding steel shield by $\frac{1}{4}''$ bakelite sheeting.

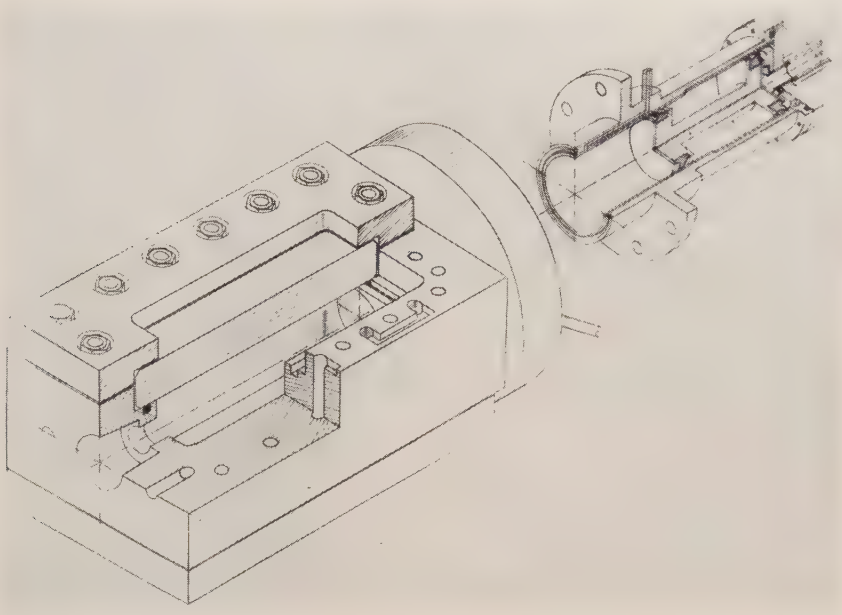

Fig. 1

It has been found that this sytem, which allows the water to be heated in a separate reservoir ensures an easy and accurate control of the temperature. After about three hours of heating from room temperature, equilibrium conditions are reached and a difference of less than $\frac{1}{4}°$ C is recorded between the temperatures of the ingoing and outgoing water.

3. Safety Shield

The chamber is completely surrounded by a steel safety shield (plate 1 and fig. 2). It consists of three detachable parts: the central box which contains the chamber, and the adjoining upper and lower cylinders, which were designed to safeguard against window rupture. The volume of these cylinders is such that, in the event of a window breaking at working temperature, the pressure within the shield would not exceed 3 atmospheres, which is well within the design limits. The two cylinders are connected together by a 2″ I.D. pipe, joined to an exhaust

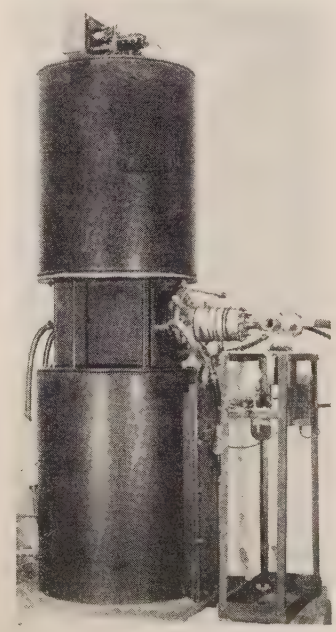

Plate 1

pipe. This exhaust line is normally closed by a rupture diaphragm, which would break at a pressure slightly above atmospheric, and thus allow the propane vapour to escape to the exterior of the building.

The assembled shield is made gas tight by means of a soft rubber gaskets and during operation is filled with nitrogen at a few cm Hg excess pressure.

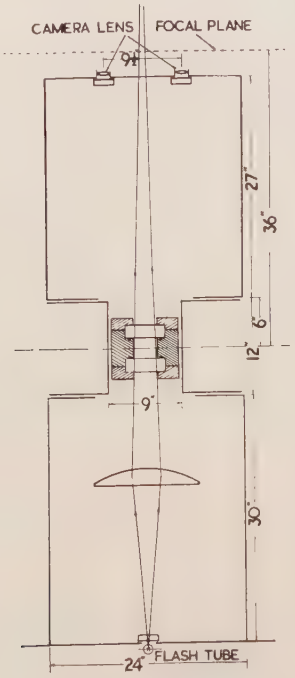

Fig. 2

4. Expansion System and Filling Apparatus

The chamber is expanded to a defined volume by a pneumatically operated piston in contact with the liquid propane. Thus the whole system is very easy to dismantle and the "dead volume" of propane is small.

The expansion cylinder is illustrated in fig. 1. It consists of a $\frac{1}{2}''$ wall brass tube with honed case-hardened steel cylinder liners of $2\frac{7}{8}''$ and $3''$ diameter, and communicates with the visible volume through a tapered section machined in the end of the chamber. It is secured to the chamber body by eight $\frac{1}{2}''$ Whitworth studs and sealed by an o-ring. The double-ended piston is of duraluminium and has a maximum stroke of $4''$. The step in the cylinder bore would prevent the piston from entering the chamber if a window should break. "Gaco" U distributor seals have been used as piston rings and have proved to be very satisfactory, enabling an expansion time of ≈ 3 milliseconds to be achieved. To avoid jamming in the cylinder, the piston is made long compared with its diameter.

Under operating conditions a pressure difference of 30 psi will recompress the liquid in about 1 second. To stop the piston at the end of the expansion stroke, an annulus of $\frac{1}{2}''$ rubber is fixed at the rear end of the cylinder, and has proved to be perfectly satisfactory, despite the large forces (≈ 2 tons) involved in decelerating the piston.

At a recycling rate of 1 every 10 seconds (pulsing rate of the synchrotron) the nitrogen gas, which serves as the pneumatic compression medium, is used up at 10 cu. ft/min (at N.T.P.).

A standard two position electro-pneumatic valve is used to control the expansion cycle. The electronics for this purpose are quite standard. When the valve solenoid is not energised, the high pressure acts directly on the back of the piston. When the current pulse is applied, the reservoir is shut off and the propane is allowed to expand towards atmospheric pressure. The fluctuations in the opening time of the valve after the application of this pulse are less than 1 millisecond.

The filling apparatus is connected to the chamber by a brass tube and a needle valve located in the expansion system.

Commercially pure propane is used to fill the chamber. Before filling, the chamber is first evacuated to 0.1 mm Hg pressure and then flushed several times with propane vapour. The propane is then distilled into the chamber by heating the propane cylinder to $\approx 20°$ C above room temperature. In this way the chamber is filled in about 4 hours.

5. Optical System

A twin-lens stereo-camera incorporating two 8 cm "Ental" f/5.6 objectives has been built, with the axes of the lenses perpendicular to the

film plane. The two objectives are $9\frac{1}{2}''$ apart and the distance of the focal planes from the chamber is 36″: this gives a stereo-angle of 16° and a demagnification of 10 ×.

Plate 2

Ilford 5G91 film has proved to be the most satisfactory from the point of view of both contrast and film speed. The film is advanced by an electromechanical device which incorporates a Geneva motion enabling an accurately reproducible displacement of the film to be obtained. This is very convenient when reprojecting the images using the same camera as a projector.

The camera is supported on the top plate of the shield which is accurately machined, and contains four $1\frac{3}{4}''$ windows for photographing and viewing. The line joining the centres of the lenses is perpendicular to the longest axis of the chamber. The camera is accurately and reproducibly located with respect to the chamber by two brass spigots which fit tightly into the lens openings in the camera base.

Dark field illumination is used. Light from a xenon filled flash bulb (spark 0.5 cm long) situated below the base of the shield passes through a glass window and is focussed by a 50 cm focal length, 33 cm diameter planoconvex lens through the chamber to a point about 150 cm above it (see fig. 2). Thus no direct light enters the camera lenses. Since the light scattered by the bubble is mainly in the forward direction, only 40 joules (28 μF, 1.7 kV) are required.

6. Operation of the Chamber

Accurately timed voltage pulses, which are used to control the synchrotron operation, are available also for synchronizing the timing of expansion and flash.

The proton beam is well collimated and its intensity adjusted so that between 10–20 particles per pulse enter the chamber.

The chamber has been operated in the temperature range 56° C to 63° C, with expansion ratios from 0.5% to 4%. At low expansion ratios and low temperatures, the bubble density is only a few bubbles per centimeter of track. Continuous tracks are obtained at 62° C with expansions of about 2%, although at this temperature spurious boiling is noticeable. A suitable working temperature is 60° C with expansions of about 2% to 3%. A flash delay of 2 to 3 milliseconds is used to obtain fine tracks, although if the delay is increased up to 10 milliseconds new tracks are still observed, and this indicates that the sensitive time is of this order. The thin beam entry window can be replaced by a pressure transducer. During some trial runs the pressure v time diagrams obtained from the pressure transducer confirm that the sensitive time is about 12 milliseconds. A photograph of 930 MeV proton tracks is shown in plate 2.

7. Analysis of Photographs

The accuracy of track measurements and also the possibility of using bubble counting methods

depend upon the size of bubble images obtained on the film. The minimum diameter of bubble images is limited by the overall resolution of the photographic system. This is affected by grain size of the film, depth of focus requirements and diffraction effects at small apertures.

Measurements were made on full size reprojections of photographs and the equipment was capable of measurements to 0.1 mm on the projected image. It was important therefore for the reprojected bubble size not to exceed 0.2 to 0.3 mm (0.02 to 0.03 mm on the film). Ilford 5G91 has a resolution of 110 lines/mm which contributed about 0.11 mm to the size of the reprojected image. Blurring of the image because of depth of focus considerations contributed less than 0.2 mm using a relative aperture of f/22. At this aperture diffraction effects accounted for an image diameter of about 0.1mm. The observed bubble image size was between 0.2 and 0.3 mm thus allowing the desired accuracy of measurement and permitting bubble counting for bubble densities not exceeding 30 to 40 per centimeter.

To facilitate analysis, events were traced with a very fine hard pencil on to high quality tracing paper. We are satisfied that measurements made on these drawings are at least as accurate as direct measurements on the images.

Two methods of measurement were used. The first consisted of measuring the coordinates of corresponding points on the two images with respect to a system of fiducial marks etched in the lower surface of the top window (see Bassi *et al.*[4])).

The second method involved measuring the coordinates of the vertex of an event and the angles made by the tracks with the fiducial axis. Computor programmes to obtain the spatial angles were prepared for both methods. To check for large errors in measurements the computor was also required to print out the angles of the tracks projected on to the horizontal plane. For consistency this angle should lie between the values of the corresponding angle measured on each of the two stereo images. Errors, calculated on the basis of an inaccuracy of $\pm$ 0.2 mm on a coordinate measurement, were also printed out.

Depth coordinates were determined to about $\pm$ 1.2 mm. In the great majority of cases scattering angles had an error of less than 1.5° and azimuthal angles less than 5°.

Acknowledgements

The continuous interest of Professor P. B. Moon in this project is gratefully acknowledged. The authors are also indebted to Mr. R. Joines and Mr. G. Young for valuable technical help and advice. J. D. D. and B. M. wish to thank the Department of Scientific and Industrial Research for maintenance grants and W. R. F. wishes to thank Queens University, Kingston, Canada, for the award of an R. S. McLaughlin travelling fellowship.

[4]) P. Bassi, A. Loria, J. A. Meyer, P. Mittner and I. Scotoni, Nuovo Cimento **5** (1959) 1729.

NUCLEAR INSTRUMENTS AND METHODS 7 (1960) 189–192; NORTH-HOLLAND PUBLISHING CO.

THE RESPONSE OF PLASTIC SCINTILLATORS TO HIGH-ENERGY PARTICLES

T. J. GOODING and H. G. PUGH

A.E.R.E., *Harwell, Didcot, Berks*

Received 8 January 1960

The response of the plastic scintillator NE 102 is calculated for protons, deuterons, tritons and alpha-particles up to 160 MeV and it is shown how a linear counter may be constructed. The results of the calculation are tested experimentally for protons and deuterons.

1. Introduction

It has been customary, where linearity is important, to use sodium iodide or caesium iodide crystals as total-energy detectors for heavy charged particles. With pulsed-beam accelerators it is common to have peak counting-rates of the order of 10^7 per second and because of their long decay times inorganic scintillators are unsuitable. These counting-rates can easily be handled with plastic scintillators in conjunction with 10 nsec linear gates which have been developed for this purpose[1]).

Plastic scintillators are, however, non-linear for heavily-ionizing particles and their response is not well-known. In this paper it is shown how the low energy proton data can be used to predict accurately the response for protons and deuterons up to 150 MeV and presumably for other particles. It is further shown how, by sacrificing the first few MeV of response, a counter may be constructed which is nearly linear for particles up to any specified energy.

2. Calculations

In organic scintillators the light output for a given energy loss is less when the density of ionization is high. There are various theoretical explanations for this non-linear response. Birks[2]) has obtained the following relationship between the light output and the energy loss in a small element of the track of an ionizing particle.

$$\frac{\mathrm{d}L}{\mathrm{d}x} \propto \frac{\mathrm{d}E/\mathrm{d}x}{1 + B\,\mathrm{d}E/\mathrm{d}x}$$

where L is the light output, $\mathrm{d}E/\mathrm{d}x$ is the rate of energy loss of the particle in the scintillator and B is a constant. Wright[3]), attributing the effect to a different mechanism obtains

$$\mathrm{d}L/\mathrm{d}x \propto \log\,(1 + a\,\mathrm{d}E/\mathrm{d}x)$$

where "a" is a constant. These two formulae fit the experimental data equally well[4]). We have chosen for computational convenience Wright's formula.

The range-energy curve for $CH_{1.105}$, which is the composition of the plastic scintillator NE 102, was determined by interpolating between C, CH and CH_2[5]). For energies from 1 to 150 MeV it can be represented approximately by a power law of the following form:

$$\mathrm{d}E/\mathrm{d}x = 16.94\,x^{-0.448} \text{ for protons}$$

$$\mathrm{d}E/\mathrm{d}x = 23.08\,x^{-0.448} \text{ for deuterons}$$

$$\mathrm{d}E/\mathrm{d}x = 27.71\,x^{-0.448} \text{ for tritons}$$

$$\mathrm{d}E/\mathrm{d}x = 67.76\,x^{-0.448} \text{ for alpha-particles}$$

where the energy is in MeV and the range x is in g/cm^2.

The light output for protons was then obtained by integrating the relation

$$L = \int_0^x \log\,(1 + a\,16.94\,x^{-0.448})\,\mathrm{d}x$$

[1]) G. B. B. Chaplin and A. J. Cole, Nuclear Instruments **7** (1960) 45.

[2]) J. B. Birks, Proc. Phys. Soc. A **64** (1951) 874.

[3]) G. T. Wright, Phys. Rev. **91** (1953) 1282.

[4]) F. D. Brooks, Progress in Nuclear Physics, Vol. **5** (Pergamon Press, 1956) 252.

[5]) Rich and Madey, Range-Energy Curves, UCRL 2301.

up to the range of the particle. The calculation was performed on the Harwell "Mercury" computer, to an accuracy of 0.1% of the light output for 160 MeV protons (arbitrarily normalized to unity), for several values of the parameter "a". The same normalization was used for the deuteron, triton and alpha-particle calculations. To determine the best value of the parameter "a" the calculations were compared with the known response of NE 102 to protons from 1 MeV to 14 MeV[6,7]). It was found to be 25 ± 2 mg/cm^2/MeV. Table 1 and fig. 1 show the results of the calculations for this value of the parameter.

Table 2 shows the response for 120 MeV deuterons, tritons and alpha-particles relative to that for protons of the same energy, with different values of the parameter "a". It will be seen that a measurement for example of the ratio L_d/L_p, where L_d and L_p are the responses for deuterons and protons, at a fixed energy will determine the value of the parameter "a".

To make the response more linear we introduce a thin absorber in front of the scintillator. The energy lost in the absorber by low-energy particles is greater than that lost by high-energy ones. This has the effect of straightening out the response curve but gives it an intercept on the energy axis. The thickness of absorber to give the best overall linearity depends both on the range of energies over which linearity is required and on the type of particle. For example, an absorber equal to the range of 13 MeV

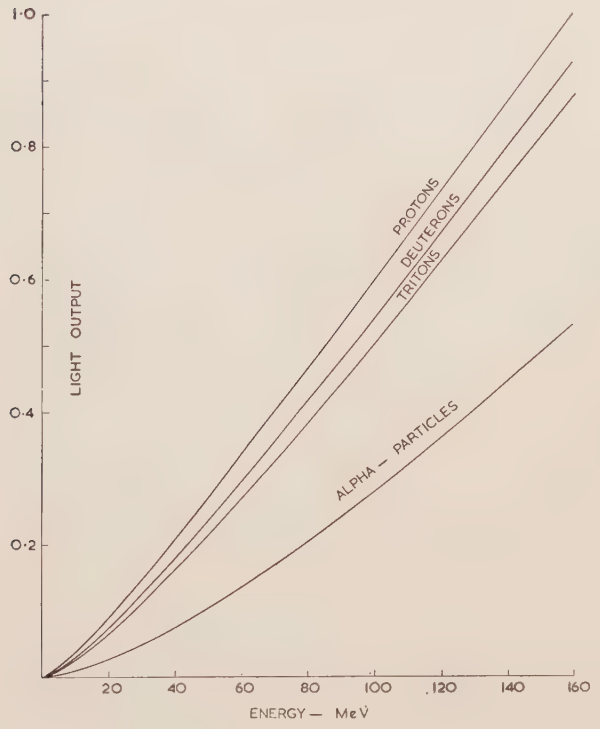

Fig. 1

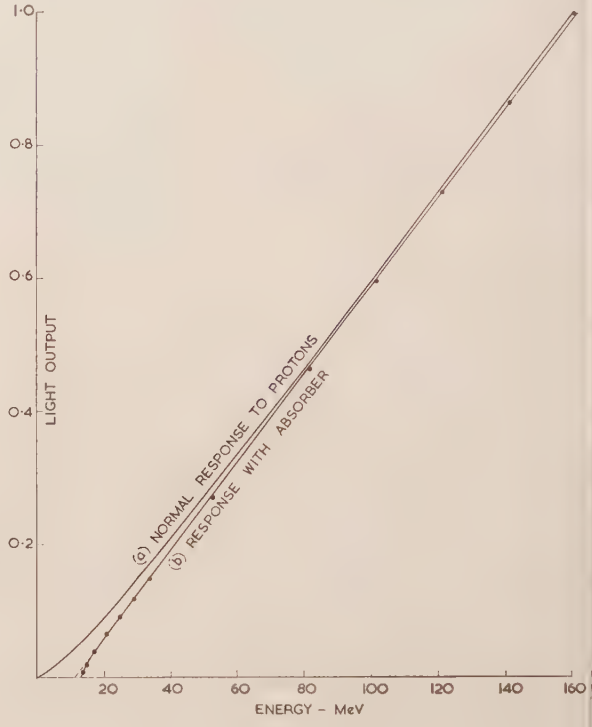

Fig. 2

Fig. 1. The calculated response of NE 102 to protons, deuterons, tritons and alpha particles. The response to a 160 MeV electron on this scale would be 1.16.

Fig. 2. (a) The response of NE 102 for protons, as in fig. 1. (b) The response when an absorber equal to the range of 13 MeV protons is placed in front of the scintillator, plotted as a function of the energy incident on the absorber. The points represent the calculated response while the straight line is the best overall fit for protons between 15 and 150 MeV.

[6]) H. C. Evans and E. H. Bellamy, Proc. Phys. Soc. **74** (1959) 483.

[7]) M. G. Rusbridge, Private Communication.

protons gives good overall linearity for protons from 15 MeV to 150 MeV as will be seen in fig. 2, whilst for protons between 10 MeV and 50 MeV an 8 MeV absorber is better.

TABLE 1

The calculated response of NE 102 to protons, deuterons, tritons and alpha particles. The parameter "a" is taken as 25 mg·cm^{-2}·MeV^{-1}. The light output for a 160 MeV electron on this scale would be 1.16. These results are plotted in fig. 1

Energy (MeV)	L_p	L_α	L_t	L_α
3	0.007	0.005	0.004	0.001
6	0.019	0.014	0.012	0.004
10	0.037	0.029	0.025	0.009
15	0.062	0.050	0.043	0.017
20	0.090	0.074	0.064	0.026
25	0.118	0.099	0.087	0.037
30	0.148	0.125	0.111	0.049
40	0.208	0.179	0.161	0.075
50	0.270	0.236	0.214	0.104
60	0.334	0.294	0.269	0.135
80	0.464	0.415	0.383	0.204
100	0.596	0.539	0.502	0.279
120	0.729	0.666	0.624	0.359
140	0.864	0.795	0.748	0.443
160	1.000	0.925	0.873	0.531

TABLE 2

The response of NE 102 to 120 MeV deuterons, tritons and alpha-particles given as a fraction of the response to protons of the same energy, for different values of the parameter "a"

mg·cm^{-2}·MeV^{-1}	L_α/L_p	L_t/L_p	L_α/L_p
10	0.953	0.919	0.647
15	0.936	0.893	0.577
20	0.925	0.872	0.529
25	0.914	0.856	0.492
30	0.904	0.839	0.462

3. Experimental Method

To verify these calculations the response of the plastic scintillator NE 102 has been measured for protons from 28 to 147.5 MeV and for deuterons from 46 to 120 MeV.

The scintillator was a cylindrical block of NE 102, 3 inches in diameter and 7 inches long. It was coupled to an E.M.I. 9531 B photomultiplier through a perspex light guide 3 inches in diameter and 1½ inches long. This light guide was found to be necessary to avoid non-uniform light collection from points near the photocathode. The protons entered the scintillator parallel to the axis through a 0.002 inch aluminium foil.

The absorber was a 0.050 inch thick NE 102 scintillator used as a dE/dx counter, and, including windows, the total thickness of material before the total-energy counter was sufficient to stop 13 MeV protons. A pulse from the dE/dx counter was used to open a fast linear gate; the output of the total-energy counter was passed through this gate and displayed on a multichannel pulse-height analyser.

For the proton measurements a low-intensity beam from the Harwell 110 inch synchrocyclotron was used. A range measurement gave the mean energy as 147.5 MeV and the energy spread as 3 MeV full-width at half-height. The pulse height spectrum from the counter was symmetrical with a width at half-height of 3%. As the proton energy spread was 2% the resolution of the counter for 147.5 MeV protons must therefore be about 2%. Other proton energies were obtained by placing aluminium absorbers in front of the dE/dx counter.

For the deuteron measurements a CD_2 target was bombarded with the normal 153 MeV proton beam. The energy spread of this beam was 7.0 MeV. Recoil deuterons were detected at angles of 20° and 35° to the incident beam, and to establish their identity coincidences were required between the dE/dx counter and a second dE/dx counter placed at the appropriate angle to detect the scattered protons. Two further measurements were made at 35° by slowing down the recoil deuterons with aluminium absorbers.

The linearity of the gate and associated amplifiers was tested with pulses from a mercury-switch pulse generator fed through a calibrated variable attenuator. The output measured on the multichannel pulse-height analyser was linear within ½% of the maximum signal. The pulses were taken from the anode of

the photomultiplier at a maximum level of 2 mA into 100 ohm load. To check that the photomultiplier was not saturating, its gain was reduced by a factor of ten. The linearity was not affected.

The results are shown in fig. 3 together with the calculated responses normalized to the 147.5 MeV proton measurement. The large errors on the deuteron measurements are principally due to uncertainties in the energy of the proton beam, the angular spread of the counters and the low counting rate.

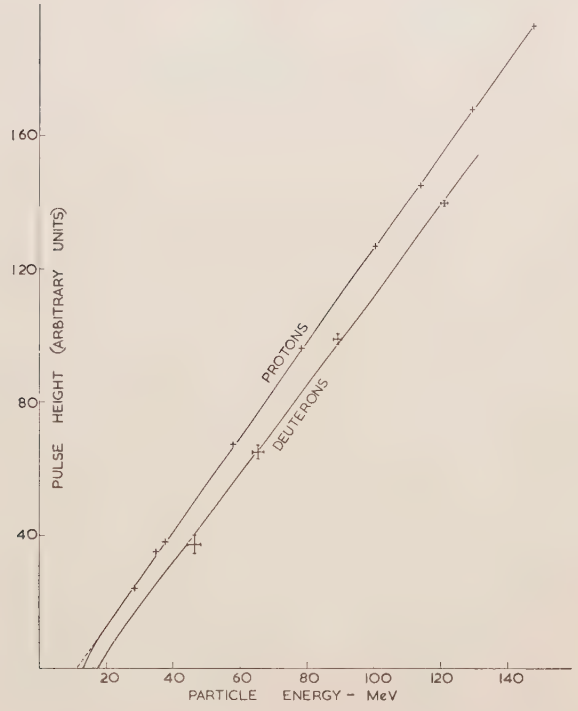

Fig. 3. Experimental results for protons and deuterons using the 13 MeV absorber. The lines represent the calculated response normalized to the 147.5 MeV proton measurement.

4. Conclusions

The proton measurements all fall within 1% of the calculated response showing that the low-energy proton calibration can be extended to higher energies by means of Wright's formula. The ratio of pulse-heights for protons and deuterons losing 120 MeV in the scintillator is 0.907 ± 0.01 giving an independent value of 28 ± 5 mg/cm^2/MeV for the parameter "a". This is in good agreement with the value $a = 25$ mg/cm^2/MeV used in the calculations and hence we may further predict that the response for tritons and alpha-particles will be close to the values given in table 1.

Acknowledgements

We wish to thank Mr. K. F. Riley and Mr. R. G. C. Artus for assistance with the measurements, Dr. R. W. Pringle of Nuclear Enterprises Ltd., for helpful discussions on light collection problems, and the cyclotron crew for their co-operation.

NUCLEAR INSTRUMENTS AND METHODS 7 (1960) 193–196; NORTH-HOLLAND PUBLISHING CO.

DERIVATION OF THERMAL NEUTRON SPECTRA FROM TRANSMISSION DATA

EDWARD A. BURKE and LESTER F. LOWE

Air Force Cambridge Research Center, Bedford, Mass.

Received 14 January 1960

A method formerly used for deriving X-ray spectra from transmission data has been employed to determine the spectrum of thermal neutrons. In this method a transmission curve of a neutron beam is obtained, a suitable Laplace transform fitted to the curve, and the spectrum derived from the inverse transform. An experimental test yielded results in reasonable agreement with theoretical expectations. The relative simplicity of the equipment and procedures employed should make this method a useful supplement to standard techniques.

1. Introduction

Many sources of nuclear radiations, such as reactors, produce nuclear particles or photons with a wide range of energies. Usually the energy distribution is a smooth continuous function. In many applications it is necessary to have some knowledge of this continuous energy spectrum. A method is described here that involves reconstruction of a neutron spectrum from transmission data.

The transmission technique was apparently first developed by Silberstein[1]) and used by others[2–4]) for determining continuous X-ray spectra. The simplicity of the equipment and experimental procedure employed in the transmission method have made it a useful supplement to the standard techniques of crystal diffraction and scintillation spectrometry.

A situation analogous to the X-ray case exists for thermal neutrons which generally have a smooth, continuous, "Maxwell-like" distribution of energies. The techniques currently used for determining the spectrum, namely, crystal diffraction and time of flight, require relatively elaborate apparatus as compared to that necessary for determining a transmission curve. Also, data obtained by these techniques cannot always be easily resolved. For example, high order reflections pose a difficult problem in the analysis of diffraction data. Consequently, it was thought that the transmission method could be extended to the neutron case as a useful alternative technique.

[1]) L. Silberstein, Phil. Mag. **15**, 7th Series (1933) 375.
[2]) J. R. Greening, Proc. Phys. Soc. A**63** (1950) 1227.
[3]) M. A. Greenfield, R. D. Specht, P. M. Kratz and K. Hand, J. Opt. Soc. Am. **42** (1952) 6.
[4]) P. K. S. Wang, R. J. Raridon and M. Tidwell, Brit. J. Radiol. **30** (1957) 70.

2. Method

The transmission curve of a collimated neutron beam is related to the velocity distribution of neutrons in that beam by the following equation:

$$N(x) = \int_0^\infty \exp\left[-\Sigma(v)x\right] f(v)\,\mathrm{d}v\,, \qquad (1)$$

where $\Sigma(v)$ is the total macroscopic cross section of the absorber at velocity v, x is the absorber thickness, $f(v)\,\mathrm{d}v$ represents the relative number of neutrons between v and $v + \mathrm{d}v$, and $N(x)$ is the ratio of the number of neutrons that pass through a thickness of absorber x to the number obtained without an absorber. In any real situation a neutron detector will usually have an efficiency that varies with neutron velocity. This means that the detector employed records a modified distribution $M(v)$ equal to $KE(v)f(v)$ where $E(v)$ is the efficiency of the detector as a function of neutron velocity and K is a normalization constant defined by

$$K = \int_0^\infty \frac{M(v)}{E(v)}\,\mathrm{d}v\,. \qquad (2)$$

The transmission curve for a real situation is then

$$T(x) = \int_0^\infty \exp\left[-\Sigma(v)x\right] M(v)\, dv \qquad (3)$$

where $T(x)$ is the ratio of the measured count rate after passing through a thickness x to the count rate without an absorber.

The problem is to determine the unknown function $M(v)$ in eq. (3). Since the unknown function occurs under the integral sign, eq. (3) is known as an integral equation. Specifically, it is a Fredholm integral equation of the first kind. Solution of this type of equation is usually attempted by series, polynomials, numerical quadrature, trial and error, or integral transforms. Several of these methods of solution were tested for hypothetical distributions. The best method of solution in terms of accuracy and minimum computation was found to be solution by integral transform. This is the method first proposed by Silberstein[1]) and applied by others[2–4]).

In the transform method, eq. (3) is converted into a Laplace transform by defining a new distribution function $\phi(\Sigma)\, d\Sigma = M(v)\, dv$. Then eq. (3) becomes

$$T(x) = \int_0^\infty \exp\left[-\Sigma x\right] \phi(\Sigma)\, d\Sigma\,, \qquad (4)$$

where it has been assumed that for the cases to be studied $\Sigma = 0$ when $v = \infty$ and $\Sigma = \infty$ when $v = 0$ to a sufficiently good approximation. To determine $\phi(\Sigma)$ in eq. (4) the measured values of $T(x)$ are fitted with a suitable Laplace transform selected from a table of such transforms. The inverse transform taken from the table is then $\phi(\Sigma)$. $M(v)$ is obtained from $\phi(\Sigma)$ by multiplying the latter by $d\Sigma/dv$ and $f(v)$ is obtained from $M(v)$ through eq. (2) and the relation $M(v) = KE(v)f(v)$. The quantity $d\Sigma/dv$ can be determined from the known relation between Σ and v.

As previously mentioned, the accuracy of the transmission technique was tested by applying it to several known distributions. These tests indicated that when the absorber thicknesses were spread over a range sufficient to drop the transmission to a few percent, the distribution was reproduced within about ten percent. In general, it was found that the greater the range over which values of the transmission were known, the greater the accuracy of the reproduction.

3. Experimental

In the experimental test of the transmission method the vertical port in the medical therapy room of the MIT reactor was used as a source of thermal energy neutrons. Neutrons emerging from this port after originating in the core, were thermalized in the heavy water coolant and filtered through a lead-bismuth shield to remove gamma radiations. The collimator employed was a stainless steel tube 40 inches long with a $\frac{7}{32}$-inch square slot running from end to end. Absorbers were inserted $13\frac{1}{2}$-inch from the lower end of the collimator by a remotely controlled turntable. Silver was used as the absorbing material because it did not exhibit any resonances for neutrons less than several electron volts, it was available in high purity sheets, and its cross section was of an order to give manageable thicknesses for the thinnest and thickest absorbers. A BF_3 proportional counter tube was employed as a detector.

Transmission data, corrected for coincidence losses and background appear in table 1. A sufficient number of counts were taken for each

Table 1

Comparison of experimental transmission data with a transform approximation

Absorber thickness (cm)	Corrected transmission curve†	Transform fit
0.0000	1.000	1.000
0.0230	0.908	0.907
0.0591	0.783	0.783
0.1322	0.586	0.588
0.1811	0.491	0.491
0.238	0.399	0.399
0.324	0.297	0.297
0.430	0.209	0.209
0.622	0.1152	0.1150
0.795	0.0691	0.0693
0.952	0.0446	0.0445
1.190	0.0230	0.0233
1.365	0.0148	0.0148

† Corrected for background and resolving time.

absorber thickness to reduce the standard error to less than $\pm$ 0.5%. The Laplace transform fit to the data is also shown in table 1 and as can be seen is generally within the standard error of the counting data. The transform that yielded this fit was

$$T_L(x) = \exp\left[bc^{\frac{1}{2}} - b\,(x + c)^{\frac{1}{2}} - ax\right] \qquad (5)$$

and its inverse transform

$$\phi(\Sigma) = \begin{cases} 0 & \text{when} \quad (\Sigma - a) < 0 \\ \frac{1}{2}\pi^{-\frac{1}{2}}\, b(\Sigma - a)^{-\frac{3}{2}} \exp\left[bc^{\frac{1}{2}} - c(\Sigma - a) - \frac{1}{4}b^2(\Sigma - a)^{-1}\right] & \\ \text{when} \quad (\Sigma - a) > 0 & \end{cases} \qquad (6)$$

where the values of a, b, and c, were found to be 1.30, 3.31, and 0.31, respectively. In order to obtain the neutron flux distribution as a function of velocity, $\phi(\Sigma)$ was multiplied by $d\Sigma/dv$ and divided by the normalization constant K and the efficiency of the detector, namely, $(1 - \exp(-\Sigma_d t))$, where Σ_d is the macroscopic cross section of the gas in the counter tube and t is the neutron path length through the tube. Calculation of $d\Sigma/dv$ was made from an empirical equation relating Σ and v. The equation used was

$$\Sigma = 8640/v + 0.381 \ln v - 3.04\,. \qquad (7)$$

This was found to agree within one percent with values of Σ in the thermal region[5]). Then

$$d\Sigma/dv = -8640/v^2 + 0.381/v\,, \qquad (8)$$

The flux distribution derived from the experimental data in the manner outlined is compared in fig. 1 with the theoretical Maxwell flux distribution calculated for a temperature of 293° K. As can be seen the experimentally determined spectrum closely resembles the Maxwell flux distribution. Results obtained with the hypothetical distributions previously discussed indicated that the experimentally determined distribution should not depart from the "true" distribution by more than $\pm$ 10%. Since the departure from the Maxwell flux distribution is slightly greater than this, there is some reason to suspect that the "true" distribution is actually shifted towards the low velocities. This can be attributed to the bismuth filter through which the neutron beam passes before emerging from the reactor. As mentioned by Hughes[6]), bismuth and other materials with a low capture cross section become relatively transparent for slow neutrons because the neutron wavelength is greater than the longest wavelength that can be reflected (hence scattered) from the crystallites of which the material is composed. This results in an intensity peak at low velocities when a thermal neutron beam is passed through a suitable filter. The transmission technique cannot be expected to reveal such fine structure since a smooth continuous velocity distribution is assumed. However, the filtering effect would manifest itself by causing the distribution to be shifted towards low velocities.

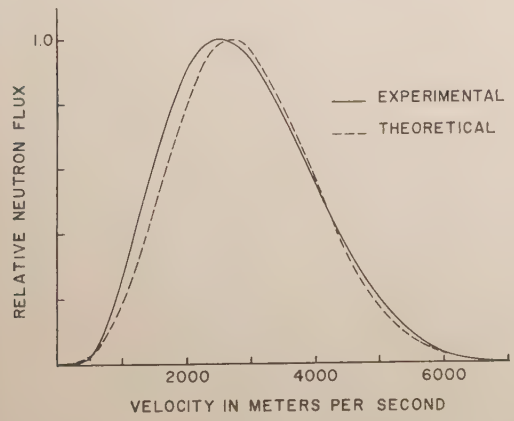

Fig. 1. Maxwell and experimentally determined spectra compared.

4. Conclusion

It has been shown that a neutron spectrum can be derived from transmission data by solving a Fredholm integral equation of the first kind. This type of equation can be solved by fitting transmission data with a Laplace transform and deriving the spectrum from the inverse transform. The relative simplicity of the equipment and procedures employed in the transmission method should make it a useful supplement to the standard techniques of crystal diffraction and scintillation spectrometry. The method has a limitation in that it is necessary to assume

[5]) D. J. Hughes, and R. B. Schwartz, BNL-325.

[6]) D. J. Hughes, Pile Neutron Physics (Addison-Wesley Publishing Company, Inc, 1953) pp. 239–242.

that the unknown spectrum is smooth and continuous. However, in many cases neutron spectra satisfy this condition. In such cases, it appears that the unknown spectrum can be reproduced within about 10%. This is comparable to the accuracy achievable with standard techniques.

Acknowledgments

The authors wish to thank Walter B. Jackson and Bartholomew J. Spada for the fabrication of the collimator and its associated equipment, and members of the MIT reactor staff for their co-operation and assistance in the experimental phase of the work.

NUCLEAR INSTRUMENTS AND METHODS 7 (1960) 197–200; NORTH-HOLLAND PUBLISHING CO.

A FAST LINEAR GATE CIRCUIT

F. P. G. VALCKX† and A. DYMANUS††

Fysisch Laboratorium der Rijksuniversiteit, Utrecht, The Netherlands

Received 4 January 1960

An electronic gate circuit is described, which is linear for pulses up to 10 V over an impedance of 200 Ω. The gate-pulse width is determined by an external clipping cable and can be varied from 500 ns down to 40 ns. The input can be of either polarity. The gate incorporates a fixed, well defined dead-time of about 50 μs, which assures stable operation also at high counting rates.

1. Introduction

A gate circuit transmits an input pulse, when a trigger pulse is also applied to the circuit. A linear gate should not modify the pulse-height spectrum of the input pulses. Both the transient of the trigger pulse when no input pulse is applied (pedestal), and the feed-through of the input pulses when the gate is closed, should be sufficiently small.

Within our knowledge all gates in the nanosecond region, thus far published, are basically pure crystal diode gates. Generally these are non linear for smaller pulses and also a pedestal cannot be avoided in most cases[1,2]).

For fast gates a major difficulty arises at high counting rates by the time jitter between the pulse which keeps the gate open (gate pulse) and the signal pulse. This jitter can introduce an important variation in output pulse height. Part of this jitter can be introduced by the circuitry preceding the gate, but also the gate-pulse generator can give a considerable contribution.

The present circuit is of a symmetrically balanced type, which is capable of giving a zero pedestal. It is linear over its whole region of operation, down to zero pulse height. The variation in output pulse height, caused by the jitter from the gate-pulse generator is suppressed by setting an upper limit to the counting rate the gate can feed through. For that purpose a fixed dead time is introduced in the circuit. When the output spectrum is recorded with a multichannel kicksorter, which has normally a rather long dead time, the overall counting rate is hardly decreased by the dead time in the gate circuit.

2. The Circuit

The basic element of the gate circuit consists of two 1 : 1 pulse transformers in series, separated by two fast crystal diodes††† (fig. 1). When the gate is not triggered the diodes are biased off by a positive voltage. A suitable negative gate

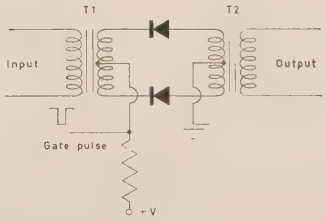

Fig. 1. Basic diagram.

pulse applied at the centre tap of the secondary windings of T1 drives both diodes into a highly conducting state, so opening the gate. When the circuit is well balanced, the pedestal arising from the gate pulse will be negligible, as the

† Present address: CERN, Geneva.

†† Present address: Harvard University, Cruft Laboratory, Cambridge, Massachussetts.

††† The idea of this transformer gate is originally from L. J. de Vries, I.K.O., Amsterdam.

[1]) A. V. Tollestrup and J. B. Lindsay, CERN Report 58-20 (1958).

[2]) E. L. Garwin, Rev. Sci. Instr. **30** (1959) 373.

currents in the loops give fluxes in T2 which are equal and of opposite sign. If the point of operation of the diodes in the conducting state is chosen well (with the right gate pulse height) then the variations in impedance of the two diodes can be made about equal and, of course, trigger pulse and the signal pulse can be adjusted. If necessary, the signal pulses can be given a constant delay with a suitable length of cable. The trigger pulse is applied to the first control grid of the 6BN6. In the quiescent state the tube is biased off by this grid. When the

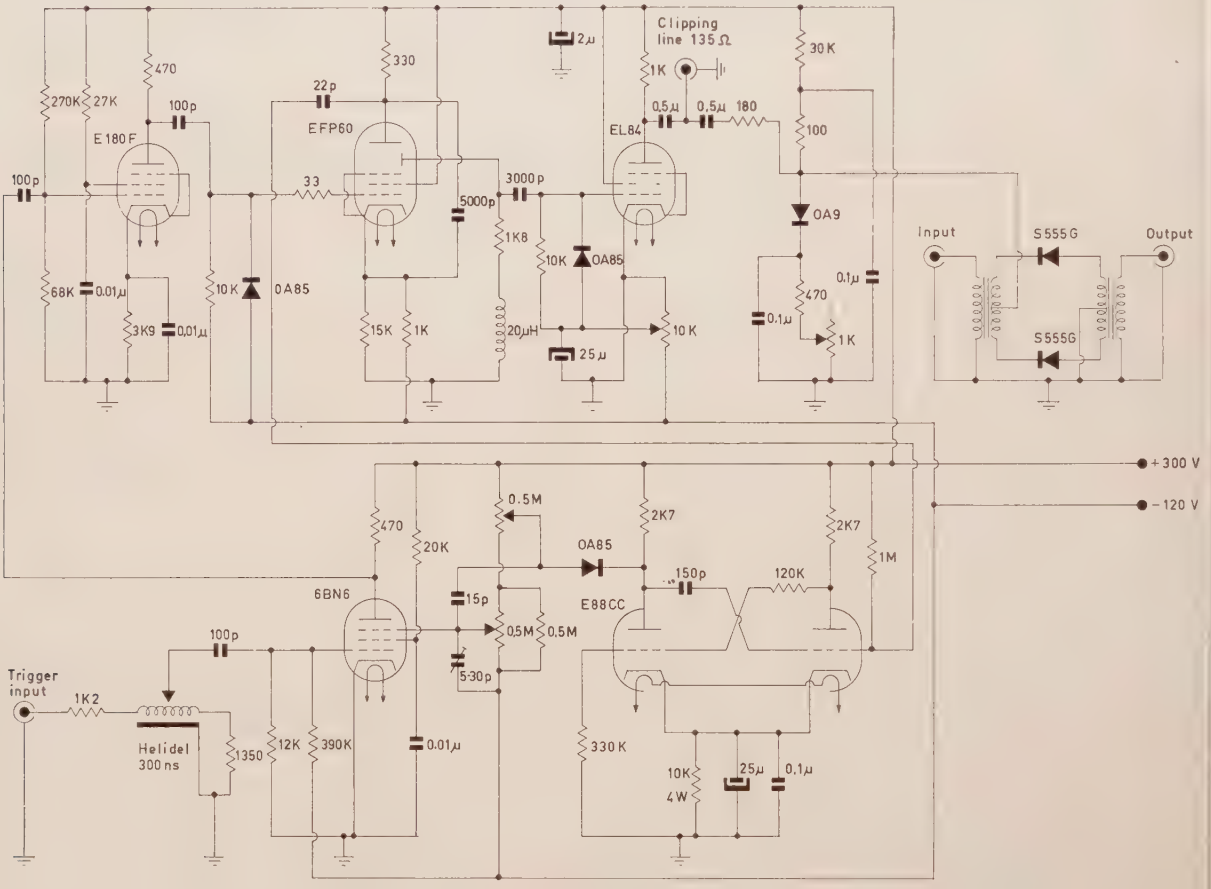

Fig. 2

they are of opposite sign. So the total impedance of the intermediate loop is practically constant for not too high pulses. Also it is not too serious when the compensation is not complete, as the diode resistance is only a fraction of the impedance of the windings. Therefore the gate can be linear over a wide range of input pulse heights.

The complete diagram is shown in fig. 2. The trigger pulse must be positive and at least 5 V high and of 60 ns half width. With the variable delay line the difference in time between the univibrator (E88CC) is not running, the trigger pulse is given through to and amplified in the E 180F, which in the quiescent state draws a current of 15 mA. The rise time of the pulse is also improved.

The gate-pulse generator consists of a EFP60 pulse generator, followed by a pulse shaper (EL84). The dynode pulse of the EFP60 (with the coupling to the EL84 removed) is about 500 ns long, 120 V high and has a rise time of 20 ns. This pulse drives the EL84, which is normally biased off, into a highly conducting

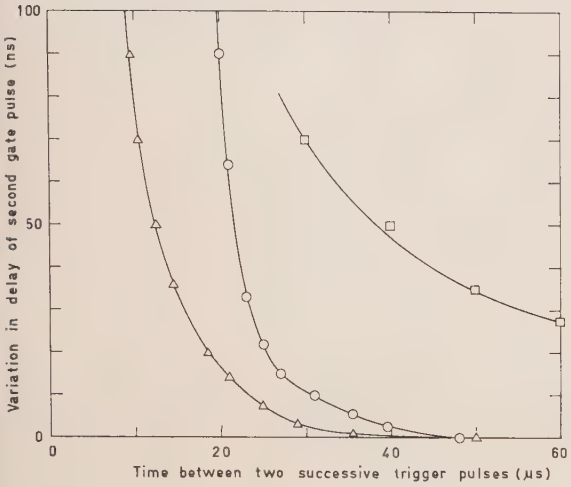

Fig. 3. Influence of counting rate on the jitter. The circles represent the circuit in normal operation, the triangles with the EFP60 triggered with a 13 V pulse and the squares are measured with the resistances in the cathode of the EFP60 increased by a factor 10.

state. The resulting anode pulse is flat topped and has a rise time of 8 ns. With a clipping cable the gate pulse can be given the desired length. With a resistor network the clipping cable is matched and the height of the pulse at the anode of the 0A9 diode, with the gate disconnected, is reduced to 30 V. The diode removes almost entirely the positive part of the clipped pulse.

For higher counting rates the time distance between the trigger pulse and the gate pulse is no more constant, but increases with increasing counting rate. This effect is shown in fig. 3 for two successive trigger pulses, as a function of the distance between these pulses. The repetition frequency of the double pulse generator was 500 Hz. The effect can be diminished by increasing the trigger-pulse height on the EFP60. The origin of this variation is the bias shift of the EFP60 cathode, as is shown by reducing the current through the cathode voltage divider down to 0.8 mA.

To overcome this difficulty the dead time is introduced in the circuit. With the differentiated anode pulse of the EFP60 a univibrator (E88CC) is triggered. The negative univibrator pulse of 50 μsec duration is d-c coupled to the second control grid of the 6BN6, which is then cut off completely, so no main trigger pulse can be given through. During the time the univibrator is flipping back the 6BN6 is in an intermediate position. To keep this time as short as possible, the coupling capacity in the univibrator is made small and the anode current is high (20 mA). Also, by the biased crystal diode only the lowest 10 V of the anode pulse is given through to the 6BN6. So the resulting rise time of the back edge of the pulse applied to the 6BN6 is reduced to 0.2 μsec.

The pulse transformers in the gating element are made with ferrite potcores (Philips Ferroxcube 3B). Each coil consists of 6 windings of H.F. Litze wire (12 × 0.08 mm). Between the coils a static shield is placed, to reduce capacitive feed-through. The transformers must be wound with great care in order to achieve the highest possible symmetry. As a slight assymetry is almost unavoidable, the remaining small pedestal can be removed by placing a small inductance in series with one of the two diodes.

A number of different types of diodes has been tested for the gating element. The best results gave the diodes Philips 0A9 and Transitron S555G.

One is free to select the impedance of the in- and output cables. In our experiment the signal pulses are first amplified with a Hewlett Packard distributed amplifier, so an impedance of 200 Ω has been chosen. The cables have to be matched properly at their far ends, as the gating element represents no constant impedance.

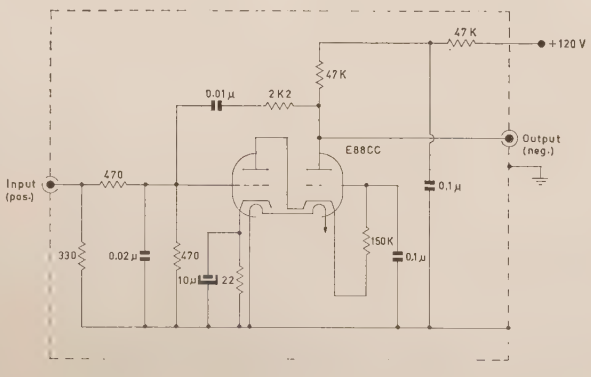

Fig. 4. Pulse lengthener and low noise preamplifier.

To be able to select the output pulses with a multichannel kicksorter, the pulses have to be stretched to about 2 μs. A crystal diode pulse lengthener is non linear for small pulses, therefore a passive R-C-stretcher is preferred, even with the inevitable loss of pulse height, (fig. 4). The pulses are then amplified with a low noise cascode preamplifier with a gain of 12 and an equivalent noise resistance of 250 Ω. After amplification with a standard 0.5 μs pulse amplifier the pulses can be recorded with the kicksorter.

3. Performance of the Circuit

The linearity of the gate has been tested with a mercury-switch pulse generator (fig. 5). The signal-pulse length was 12 ns, and the gate-pulse length 40 ns. The gate is linear up to 11 V input pulses. This is also about the bias voltage of the diodes. For pulses up to 11 V the feed-through of the signal pulse when the gate is not triggered is 0.3%. For higher pulses the feed-through increased rapidly. The remaining pedestal has the appearance of the strongly differentiated gate pulse and is 70 mV high.

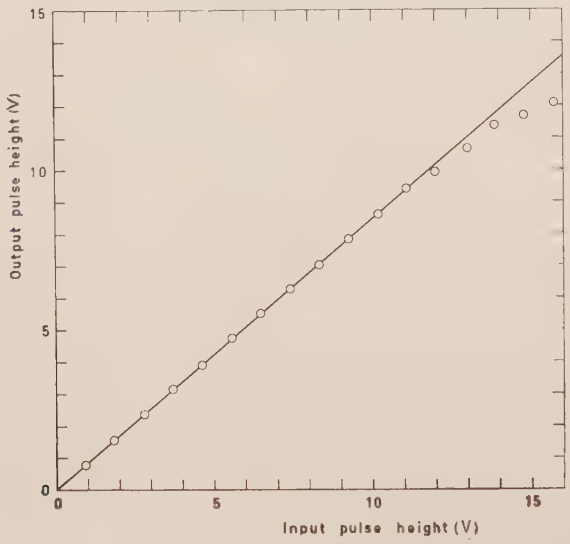

Fig. 5. Linearity of the gate.

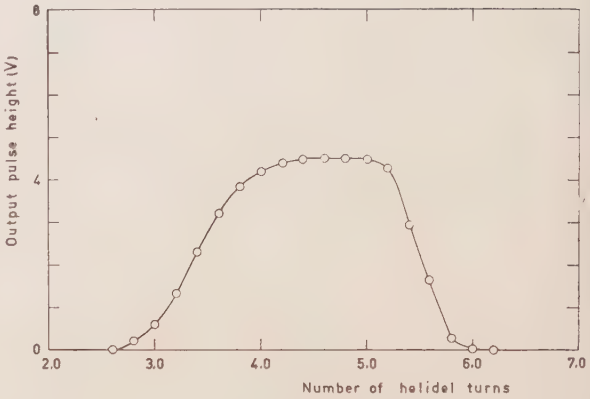

Fig. 6. Output pulse height versus helidel setting. One turn represents 20 ns.

In fig. 6 is shown the output pulse height as a function of the time delay between the trigger pulse and the signal pulse, for a gate-pulse width of 40 ns. The plateau of the curve is 15 ns, so a considerable jitter from the preceeding circuitry can still be tolerated.

It is evident that the polarity of the input and/or output pulses can easily be changed.

The circuit has been used quite satisfactorily in different experiments, performed with the Synchro Cyclotron of the CERN.

For some applications it can be useful to note that this gate can also be used in a reversed way. By inverting the polarity of the diodes and by driving a constant current through the diodes the gate is always open, except when the gate is triggered and the diodes are biased off by the gate pulse.

Acknowledgements

This work is part of the research programme of the "Stichting voor Fundamenteel Onderzoek der Materie", and was made possible by financial support from the "Nederlandse Organisatie voor Zuiver Wetenschappelijk Onderzoek". We want to thank B. A. Strasters for his active help.

NUCLEAR INSTRUMENTS AND METHODS 7 (1960) 201–203; NORTH-HOLLAND PUBLISHING CO.

NEUTRON-ABSORBING BRICKS MADE FROM CaB_6

J. W. BUTLER

Nucleonics Division, United States Naval Research Laboratory, Washington, D. C.

Received 19 January 1960

A technique is described for making relatively inexpensive neutron-absorbing bricks from commercially available CaB_6 powder. The bricks are 2-in. × 3-in. × 5-in., and are strong enough to withstand normal handling. They last indefinitely; the ones described are now 7 years old, used and stored under normal room temperatures and humidities. The procedure is to make a thick, dry mud with the powder and water, followed by compression in a mold at pressures of about 1 ton/in.^{2} or more. The bricks are then baked for 2 hours or longer at a temperature of about 750° C.

1. Introduction

The use of a high-efficiency neutron sink which will not radiate hard gamma rays is highly desirable in many applications involving the detection of neutrons from a particular source in the presence of an ambient neutron background. Two isotopes frequently used for such purposes are Li^6 and B^{10}. Li^6 has the advantage of emitting no gamma ray in connection with neutron absorption. B^{10}, upon neutron absorption, breaks up into an alpha particle and Li^7, which is left excited in its 0.478-MeV state roughly 6 percent of the time for thermal neutrons[1]). This state decays by emission of a gamma ray of the same energy. This gamma ray is relatively easily absorbed, so there is no serious disadvantage. B^{10}, on the other hand, has certain advantages over Li^6. (1) Its neutron-absorption cross section is higher than for Li^6; at 1 keV of neutron energy, B^{10} has approximately 4 times greater cross section[2]). (2) Its natural isotopic abundance ratio is higher than for Li^6—about 2.5 times higher. Thus, for the natural elements, boron has about a factor of ten higher neutron absorption cross section for 1-keV neutrons than has lithium.

Sheer and Tittman[3]) developed a method for preparing small B_4C bricks for use as neutron sinks. Kitzes and Hullings[4]) and McKinney and Rockwell[5]) developed an Al-B_4C system suitable for general use as a neutron sink. But for large-scale shielding, the high cost of B_4C makes its use prohibitive. For this reason, other materials were investigated by the present author for possible use in the making of neutron-sink bricks.

The cheapest source of boron (of at least 50 percent purity) found to be available commercially[6]) is CaB_6, which contains a minimum of 50 percent boron by weight. This source of boron is a factor of 20 cheaper for a given amount of the element boron than the compound B_4C. A technique was developed to make reasonably sized, fairly high-density, and long-lived bricks which could be used in building a neutron shield or sink in much the same way as Pb bricks are used for gamma-ray shielding.

2. Procedure

The CaB_6 powder composition is given in table 1. The first step is to mix the dry powder with water making a thick, fairly dry mud. The

[1]) S. Hanna, Phys. Rev. **80** (1950) 530; Petree, Johnson, and Miller, Phys. Rev. **83** (1951) 1148.

[2]) D. J. Hughes and R. B. Schwartz, BNL 325, Second Edition (1958).

[3]) C. Sheer and J. Tittman, Columbia University CUD-60 (1950); Rev. Sci. Inst. **22** (1951) 837.

[4]) A. S. Kitzes and W. G. Hullings, AECD-3476 (1951); ORNL-981 (1951).

[5]) V. L. McKinney and T. Rockwell, III, ORNL-242 (1953). See also AECD-3625 (1954).

[6]) The CaB_6 was purchased in 1951 from the Molybdenum Corporation of America. The current price is $ 1.80 per pound in quantities less than 300 pounds.

addition of the water apparently causes some slight chemical reaction because the emission of a peculiar odor accompanies the addition of the water. The mud is then placed in a compression mold which can be disassembled, such as the one shown in fig. 1. For this mold, approximately 0.003-in. clearance was allowed between the plunger and the other surfaces of the mold to allow seepage of the excess water. The mold was made from hardened steel, with the inner surfaces ground flat.

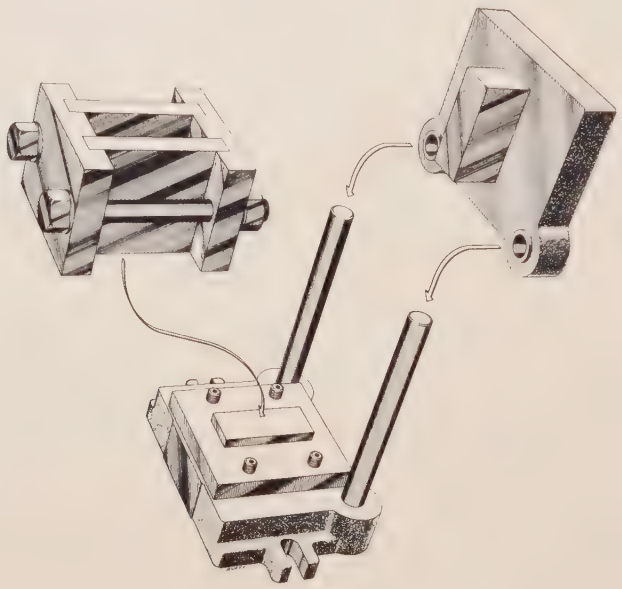

Fig. 1. Disassembled view of the mold. The mold was made from special hardened steel with the inside surfaces ground flat.

TABLE 1

Composition of commercial CaB_6 used in making the neutron-absorbing bricks.

Boron	52%
Calcium	31%
Carbon	8%
Iron	3%
Silicon	3%
Others	3%

The pressure required for making a satisfactory brick is at least about 1 ton/in.^{2}. The pressures most often used in the making of the bricks described here were the maximum available from the particular hydraulic press employed, 2 tons/in.^{2}. The extra pressure gives a denser brick, and one probably having slightly greater mechanical strength. Lower pressures than 1 ton/in.^{2} produces a brick with fairly low mechanical strength.

After compression, the mold is disassembled by removal of the nuts and bolts, and the "green" brick is transferred to a ceramic baking tray and placed into an oven. The bricks should be inserted into a cold oven and slowly brought up to temperature, in order to avoid too-rapid evaporation and expansion of the residual water left in the green bricks. Too-rapid heating causes fissures and perhaps complete breaking. Approximately two hours should be allowed for warm-up to the baking temperature of 750° C, and a minimum of about 2 more hours at that temperature is required for a stable, satisfactory brick. It is believed that a longer time yields a better brick, so the usual procedure used for the bricks described here was to keep the oven up to 750° C for about 6 hours, after which the power was removed and the bricks allowed to

cool overnight in the oven, at the slowest power-off cooling rate.

The temperature required in the oven was found to be fairly critical. The minimum acceptable temperature was in the vicinity of 600° C. Below this temperature, the baked bricks would crumble under small stresses. Above about 900° C, the bricks would deform in the furnace. The temperature used, therefore, was about 750° C.

3. Discussion

The process taking place during the manufacture of the bricks is not completely understood. Apparently, B_2O_3 is formed from a reaction between small amounts of decomposed CaB_6 and the water. (CaB_6 itself does not melt because its decomposition point is lower than the melting point.) B_2O_3 has a melting point of 577° C. Thus the critical minimum temperature in the vicinity of 600° C is probably due to the necessity of melting the small amount of B_2O_3 formed, and the B_2O_3 then serves as a binder, holding the brick together.

At temperatures about 900° C and higher, probably so much of the CaB_6 decomposes that the brick is deformed, but at lower temperatures only a relatively small amount decomposes.

The supposition that the binder in the bricks was B_2O_3 gave cause for some concern, because of the deliquescent nature of B_2O_3. However, as discussed below, the bricks do not appear to be influenced by usual laboratory humidities. When some bricks were deliberately dampened, however, they soon lost all cohesive strength.

4. Quality of the Bricks

The bricks weigh about 2 lb or 0.9 kg each, the average density of the bricks being 100 lb/ft^3 or 1.6 g/cm^3. The bricks are somewhat brittle and if dropped several feet onto a concrete floor will chip or break, but a drop of about one foot usually results in negligible damage. With normal handling, the bricks last indefinitely. The bricks described were made about 7 years ago, and are still in good condition, even though some of them have been stored continuously for the entire 7-year period in a space that was not air conditioned.

The bricks could be used as a structural material for interior rooms such as reactor rooms, accelerator rooms, experiment rooms, etc., provided a non-aqueous mortar or cement was used. The bricks which were stored for 7 years in non-airconditioned space were tested at 12 000 lb of force along the 2-in. dimension (approximately 1000 psi), and did not crumble or yield appreciably. This is equivalent in pressure to a wall 1000 ft high.

NUCLEAR INSTRUMENTS AND METHODS 7 (1960) 204–206; NORTH-HOLLAND PUBLISHING CO.

END-WINDOW PROPORTIONAL FLOW COUNTER TUBE

S. FORSÉN† and J. RYDBERG

Research Institute of National Defense, Dept 4 (FOA 4), Solna 8, Sweden

Received 3 February 1960

A simple and reliable end-window proportional flow counter is described. The influence of anode wire loop position and size, gas mixture and type of radiation source on the operation characteristics is given.

1. Introduction

The good properties of proportional counters (low coincidence loss at counting rates up to 10^6 cpm, low background, plateaus of several hundred volts with very small slopes, ability to discriminate between radiation of various energies, etc.)[1]) is by now well known to most scientists working with radioisotopes. In addition, end-window proportional flow counters of the Sugerman type[2]) offer further advantages such as practically infinite life-time and extremely high reproducibility.

The present paper will describe the design of a very simple and inexpensive counter of this type, and in addition some of the tests which have been made to obtain optimum operation conditions. During the last three years, about 20 of these counters have been built and used at our institute with excellent results.

2. Design

Fig. 1 shows the counting tube. All parts are made of stainless steel except the insulater and the mylar film. The internal dimensions are height, 60 mm, and diameter, 40 mm. The thickness of the stainless steel wall is 10 mm. The diameter is choosen larger than the end opening of the counter (25 mm in diameter) because the sensitivity of the counter decreases (somewhat depending on the gas mixture) close to the cathode wall[3]).

The advantage of using stainless steel is that the inside of the chamber can be thoroughly cleaned. Thus, when hydrochlorid acid is used for cleaning the chamber, the background is appreciably reduced and is lower than usually can be obtained with a brass chamber. Whether

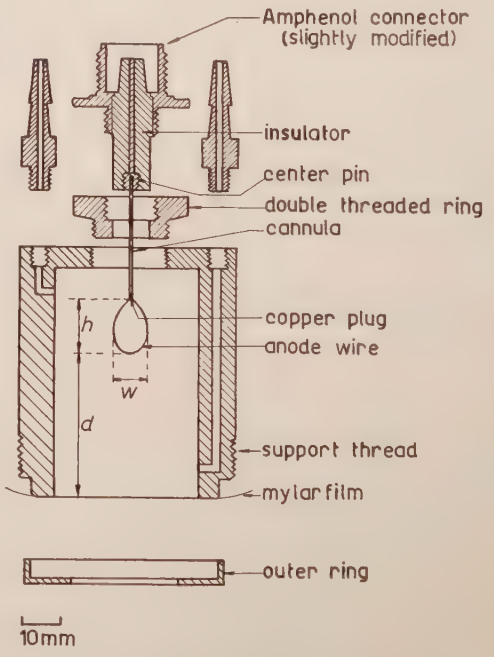

Fig. 1. Design of proportional counter tube.

† Present address: Atomic Energy Department, A.S.E.A., Västerås, Sweden.

[1]) E.g. W. J. Price "Nuclear Radiation Detection", McGraw-Hill Book Co., Inc., New York 1958.

[2]) N. Sugerman, Fermi Institute for Nuclear Studies, University of Chicago, private communication.

[3]) B. B. Rossi and H. H. Staub, Ionization chambers and counters (McGraw-Hill Book Co., Inc., New York 1949) Ch. IV.

this is due to a cleaning or an etching action on the cathode is not clear.

The window at the bottom end of the tube is mylar film aluminized on both sides—its thickness (≈ 0.9 mg/cm^2) permits α-particles with energies > 2 MeV to penetrate. The film is very easily attached to the chamber—since the inner diameter of the "outer ring" is only a few hundredths of a millimeter larger than the diameter of the corresponding part of the chamber, the film is simply placed on top of the ring and the chamber pressed down. This operation, at the same time, stretches the film and attaches it tightly to the chamber.

The anode is made of surgical stainless steel wire (diameter 0.04—0.05 mm). Its two ends are put into the hole of the hollow "anode pin" and held in place by a small conical copper plug.

The anode pin is part of a stainless steel cannula (1.0 mm in diameter), both ends of which have been cut off and filed flat. The upper end of the cannula (fig. 1) is pressed into a hole which has been drilled into the cut-off center pin of a slightly modified Amphenol coaxial connector, Type 82—805, (see fig. 1).

The design of the gas inlet and outlet and the "support thread", which is used for attaching the counter to its mechanical support, is obvious from the figure. The chamber can be used with internal sources if the mylar film and outer ring is replaced by some kind of sample changer. Such a device has been designed by S. Lindhe at AB Atomenergi. It is attached directly to the support thread.

The advantage of this simple design is that (a) by avoiding soldering, the chamber is more easily cleaned, (b) the chamber can easily be demounted (for replacing parts, cleaning, etc.), (c) the chamber is inexpensive to build (the main cost is the stainless steel tube).

3. Operating Properties

3.1. SELECTING OPTIMUM ANODE WIRE LOOP CONDITIONS

In order to find the optimum operating conditions, the influence of the anode wire loop on the plateau characteristics of the counter was investigated. For this purpose, two different wire diameters were choosen (0.04 and 0.05 mm) and the height and loop-to-window distances (h and d in fig. 1) were varied—h from 21 to 27 mm, and d from 23 to 2 mm. The loop width (w) was generally kept at $\frac{1}{2}$ of h. The length of the plateau is here defined as the maximum length of a line with 2% slope per 100 volts cutting the counting-rate versus voltage curve in at least two points. The first intercept is called the starting voltage of the plateau.

The gas mixture choosen in this test was 90% A—10% CH_4. The radiation was obtained from an external RaDEF point source covered by 0.05 mm aluminum which filters out all α and β radiation except the 1.17 MeV β coming from RaE. The amplifier (Tracerlab Ampliscaler) input sensitivity was set at 1 mV.

The results indicated that the plateau length increased with decreasing loop-to-window distance (d) in about the same way for both wire diameters; for $d = 23$ mm it was about 225 volts, for $d = 2$—5 mm about 400 volts. The starting potential of the plateau seemed to decrease slightly with d; it was found to be lower for the smaller wire diameter (around 1890 volts) than for the larger (around 1990). It was also found that the length of the plateau increased slightly with loop size (h and w).

Optimum operating conditions were found for $d = 2$—6 mm, $h = 27$ mm and wire diameter 0.04 mm. Fig. 2 gives the characteristics for these conditions.

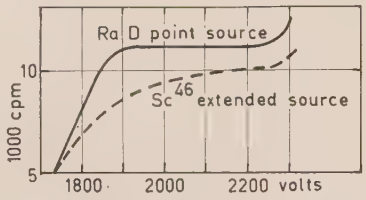

Fig. 2. Characteristics of counter for two β-sources—gas mixture 90% argon and 10% methane, wire diameter 0.04 mm, loop height 27 mm, window-to-loop distance 3 mm.

3.2. OPERATING CHARACTERISTICS FOR VARIOUS GAS MIXTURES

The characteristic of the counter is not so good for extended sources as for point sources;

it is also less good for low energy β's than for high energy β's. This is illustrated in figure 2 where the results with an extended Sc^{46} source (98% 0.36 and 2% 1.49 MeV β) is compared to that of the RaD point source. Because extended sources are easier to make than point sources (and thus more commonly used), further tests were made with extended sources: for β the Sc^{46} source, and for α a Pu^{239} (5.15 MeV α) source. No changes were made in loop size or position.

Table 1 gives the results for five different gas mixtures. All plateaus are practically flat ($\leq$ 0.5% slope per 100 volts) over most of the length indicated in the table. Figure 3 gives the results for pure methane, using the 2 mV input sensitivity of the amplifier.

All values in table 1 are for the same counter. With various counters, the same plateau length is usually obtained but the starting potential may vary by about $\pm$ 100 volts.

When the results with the different counting gases are compared, one finds that almost all gases can be used with success (exception: argon-nitrogen mixture for betas).

The choice of amplifier sensitivity depends on the gas mixture and type of radiation. A decrease in input sensitivity voltage to 1 mV decreases the starting potential of the characteristics by a few percent while an increase to 5 mV increases it by about 5%. An increase in input voltage decreases the β—γ background. With a 5 cm iron shield around the chamber, the background at 4000 volts (fig. 3) is 56 cpm for 1 mV sensitivity and 25 cpm for 2 mV sensitivity.

TABLE 1

Operation characteristics for various gas mixtures; 1 mV sensitivity for argon mixtures, 2 mV for other gases

Gas mixture	Type of radiation	Plateau	
		Starting potential, volts	Length, volts
90% argon, 10% methane	α	1300	> 400 †
	β	2000	300
3% nitrogen, 97% argon	α	1400	200
	β	($\approx$ 1800)	none
technical methane (96% pure)	α	2600	> 800 †
	β	3700	600
pure methane	α	2700	> 700 †
	β	3800	500
"gasol" (industrial gas, mainly propnae)	α	3600	> 1200 †
	β	> 4600	?

† After this length, the α-plateau goes into the β-sensitive area. In the absence of β's, the α-plateau is continious over the whole β-plateau.

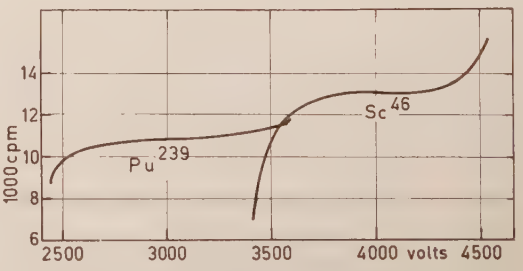

Fig. 3. Characteristics of counter for an α- and a β-source using pure methane.

Acknowledgement

The authors wish to thank Mr. S. Lindhe of the Atomic Energy Company (AB Atomenergi), Stockholm, for valuable discussions in connection with the design of the counter.

NUCLEAR INSTRUMENTS AND METHODS 7 (1960) 207–209; NORTH-HOLLAND PUBLISHING CO.

ANALYSE D'IMPULSIONS EN REGIME STATISTIQUE

F. SICARD

Département d'Electronique, C.E.N. *de Saclay*

Reçu le 10 février 1960

This paper deals with experiments done with pulses having a statistical time distribution. A commutation over several channels is studied. The counting loss and the efficiency of each channel are calculated in the case of a Poisson distribution.

1. Introduction

Dans deux précédents numéros de "Nuclear Instruments and methods"[1,2]), le calcul des pertes en comptage statistique a été abordé et des applications pratiques pour la constitution des échelles de numération utilisées en électronique nucléaire ont été données. Une généralisation de ces méthodes est proposée dans cet article.

2. Utilisation classique d'un sélecteur d'amplitude

L'utilisation normale d'un sélecteur d'amplitude consiste à l'attaquer par des impulsions ayant un spectre d'amplitude. Les intervalles de temps séparant deux impulsions successives ont une répartition statistique obéissant à la loi de Poisson (cas ou la fonction densité de probabilité des intervalles de temps est $f(t) = n \exp(-nt)$, n étant le taux de comptage moyen par seconde).

Si nous voulons analyser des impulsions se produisant avec un taux de comptage élevé, il est nécessaire de réduire le temps mort du sélecteur. Cette valeur ne doit pas toutefois être trop faible car le temps mort doit rester assez grand pour recouvrir le temps de restitution de l'ensemble détecteur-amplificateur.

En prenant certaines précautions (blocage du sélecteur jusqu'au retour à zéro de la tension d'entrée, temps mort cumulatif), il est possible d'obtenir une analyse qualitative convenable, même si le taux de perte sur le sélecteur est grand.

[1]) A. W. Pryor and A. G. Klein, Nuclear Instruments and Methods **4** (1959) 2.

[2]) J. Sandstad, Nuclear Instruments and Methods (Letter to the editor) **4** (1959) 243.

3. Utilisation pour analyse quantitative d'un sélecteur d'amplitude

Si l'on veut, de plus, procéder à une analyse quantitative du spectre des impulsions (par exemple calcul de la surface des pics en spectrométrie gamma) il faut corriger le plus exactement possible chaque canal de la perte qui lui correspond.

3.1. METHODES DE CORRECTION PAR CHRONOMETRE D'EFFICACITE

Une méthode classique pour effectuer cette correction, est celle utilisant un chronomètre d'efficacité. Celui-ci à partir du temps total de la mesure, permet de retrouver le taux de comptage réel pour l'ensemble des impulsions. On en déduit le taux de comptage effectif dans chaque canal.

3.2. METHODE PROPOSEE

Une autre méthode découle de la considération du schéma suivant. P1 et P2 représentent des portes électroniques commandées par la bascule B. A1 et A2 représentent deux sélecteurs d'amplitude. A chaque impulsion se présentant à l'entrée E, la bascule fonctionne et ferme alternativement les portes P1 et P2, de telle sorte que les impulsions paires sont aiguillées sur A2 et les impaires sur A1.

[3]) Halliday, Introduction à la Physique Nucléaire. Détection des particules chargées et des photons (190-1-2).

[4]) Labeyrie et Valladas, Cours d'Electronique Physique Les fluctuations dans les mesures de physique nucléaire (213–223).

[5]) E. Gatti and V. Svelto, Nuclear Instruments and Methods **4** (1959) 189).

Nous nous retrouvons, pour calculer les pertes sur A1 et A2 dans le cas de l'attaque d'une échelle lente par une bascule rapide. Par exemple, si l'ensemble bascule-porte a un temps

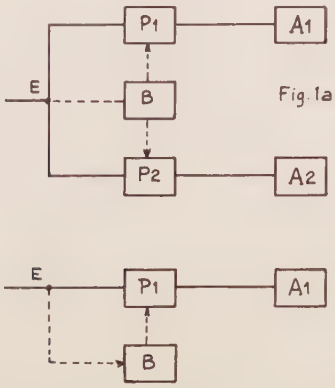

Fig. 1. Analyse par commutation sur deux voies: 1a. Deux voies effectives attaquées alternativement; 1b. Une seule voie attaquée une fois sur deux.

de commutation de 0.5 μsec, si le taux de comptage est de 10 000 chocs par seconde et le temps d'analyse de 10 μsec, un sélecteur ne perd que 0.5% des impulsions qui lui sont fournies. La perte sur l'ensemble du système est de 1%. Le schéma classique (attaque directe d'un sélecteur) aurait conduit à une perte de 10%.

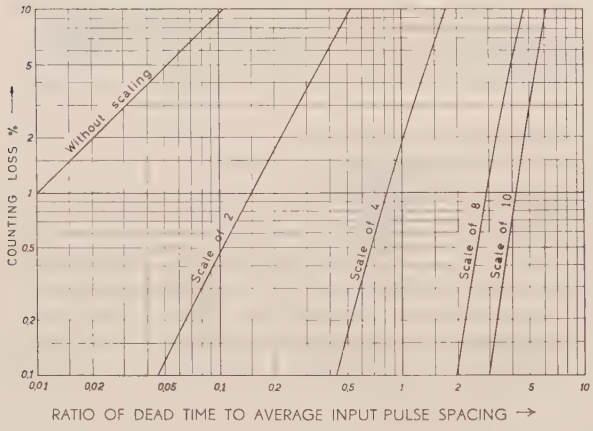

Fig. 2. Pertes après division.

En fait, il n'est pas nécessaire de mettre en service le deuxième circuit d'analyse. En effet, si le taux de comptage est suffisant, il suffit de doubler le temps de l'expérience ainsi que le nombre contenu dans un sélecteur pour obtenir le même résultat que précédemment. Ceci est applicable aussi bien aux sélecteurs à un canal que multicanaux. Dans ce dernier cas, les blocages étant prévus, l'opération est réalisable par l'adjonction d'un circuit extérieur.

4. Augmentation de la capacité de systèmes à bande magnétique

Le temps minimum qui doit séparer deux phénomènes inscrits sur une bande magnétique à plusieurs pistes utilisées dans les applications de calcul digital est de 50 μsec. Pour 1% de perte sur une seule piste, il ne faut pas dépasser 200 c/sec; avec commutation sur deux pistes, nous pouvons monter, toujours pour 1% de perte, à 3000 c/sec et, avec quatre pistes, à 14 000 c/sec. La quantité d'information que l'on peut emmagasiner sur une piste à qualité égale (1% de perte) varie comme les nombres:

$$1 — 7.5 — 17.5 .$$

5. Généralisation

Le tableau suivant donne, en fonction du taux de travail imposé à une voie d'analyse et du nombre de ces voies travaillant en parallèle, le pourcentage d'information originale perdue au total.

Nous supposons que la commutation apporte une perte négligeable par rapport à la perte sur la voie d'analyse et que, de plus, le temps nécessaire pour traiter une information est constant:

Taux de travail de chaque voie	Nombre de voies d'analyse en parallèle				
	1	2	4	8	10
0.002	0.2				
0.005	0.5				
0.01	1	0.25			
0.05	5	0.45			
0.1	10	1.6	0.08		
0.2	20	6	0.9	0.26	
0.3	30	12	3.2	0.3	0.075
0.4	40	21	8	1.2	0.65
0.5	50	30	15	5	2.7
0.6	60	45	26	13	8
0.7	70	57	40	26	18
0.8	80	70	57	45	36

6. Commutation avec mémoire tampon

Pour terminer ces applications, nous analyserons le cas suivant:

Les opérations d'analyse A1 et A2 sont supposées longues vis à vis du temps d'accès du canal C dans lequel on emmagasine les informations. On peut commuter ce canal sur

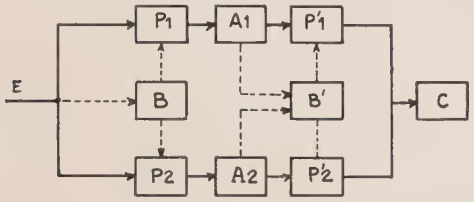

Fig. 3. Commutation avec mémoire-tampon.

l'une ou l'autre des voies d'analyse à condition de doter ces dernières d'une mémoire-temporaire, ou tampon. On peut alors utiliser une mémoire centrale C, dans laquelle se vide rapidement, en fin d'analyse, la voie A1, tandis que l'autre est prête à recevoir une deuxième information. Le rendement de la mémoire C est alors décuplé par rapport au schéma initial qui aurait consisté à mettre simplement bout à bout le circuit A1 et la mémoire centrale C.

7. Conclusion

En définitive, les remarques précédentes reposent sur une observation simple: le nombre d'évènements qui se produit en une seconde n'est pas le taux de comptage des impulsions électriques auxquelles ces évènements donnent naissance. Il faut en effet, pour déterminer le premier à partir du second, opérer un certain nombre de corrections (géométrie de l'ensemble de détection, rendements des détecteurs physiques, pertes de comptage).

De même, il semble possible de n'analyser volontairement qu'un certain nombre des impulsions qui se présentent, par exemple une sur deux. On procède donc à un échantillonnage: l'analyse porte sur un nombre d'impulsions moins grand que dans le procédé classique, mais on sait relier d'une manière plus précise l'ensemble des évènements effectivement analysés à celui des évènements disponibles avant échantillonnage. De plus, des méthodes moins rapides peuvent être employées pour un résultat équivalent et le rendement des voies d'analyse est augmenté dans de grandes proportions.

NUCLEAR INSTRUMENTS AND METHODS 7 (1960) 210–212; NORTH-HOLLAND PUBLISHING CO.

BLASENDICHTEMESSUNGEN IN EINER DIÄTHYLÄTHER-BLASENKAMMER

G. KESSELER und Ch. SCHLIER

Physikalisches Institut der Universität Bonn

Eingegangen am 1. März 1960

The bubble density of minimum ionizing electron tracks is measured in a diethylether bubble chamber over a wide range of temperature and pressure in the liquid. Some results can be compared with theory.

Messungen der Blasendichte b von Teilchenspuren in einer Blasenkammer sind schon von verschiedenen Autoren gemacht worden[1–6]). Sie sind in der Praxis wichtig, weil man aus b auf die Geschwindigkeit β der Teilchen schliessen kann (wenn dies auch selten ausgenutzt wird), und finden ferner Interesse im Zusammenhang mit den verschiedenen Theorien, die man über die Blasenentstehung gemacht hat[7]). Ausser von β hängt b von den Zustandsgrössen der überhitzten Flüssigkeit ab: Temperatur T und hydrostatischer Druck P.

Bei bisherigen Messungen ist b (T,P) immer nur für sehr begrenzte Bereiche der Parameter gemessen worden. Wir geben für Diäthyläther solche Messungen über ein erheblich grösseres P–T Gebiet an, das allerdings auch noch nicht den ganzen Bereich erfasst, in dem Messungen möglich sind.

Die Messungen entstanden im Anschluss an solche von Horlitz und Paul[5]), bei denen jedoch P nicht gemessen wurde, sondern als zweiter, die Flüssigkeit charakterisierender Parameter das Expansionsverhältnis δ bei einer festen Temperatur genommen wurde. Diesem ist für eine bestimmte Kammer zwar eine bestimmte Druckfunktion $P(t)$ (t = Zeit) bei der Expansion zugeordnet, doch kann man nicht erwarten, dass diese für verschiedene Kammern gleich ist.

Die Messungen geschahen in der in [5]) beschriebenen Kammer. Die Blasendichte wurde wieder als projizierte Blasendichte bestimmt, da nur eine Kamera benutzt wurde. Doch sorgte ein Auswahlverfahren (nur die ersten 3 mm von Spuren länger als 5 mm wurden berücksichtigt) dafür, dass die benutzten Spurenstücke der Compton-Elektronen im Minimum der Ionisation lagen. Eine Abschätzung ergibt, dass β für die berücksichtigten Teile der Spuren zwischen 0.78 und 0.95 liegt. Der Verkürzungsfaktor K, d.h. der Faktor um den die mittlere projizierte Blasendichte kleiner ist als die mittlere wahre Blasendichte, ergibt sich zu $K = 0.88\,^{+0,05}_{-0,10}$. Der genaue Wert ist ziemlich unwichtig, da man Absolutwerte von b selten braucht.

Die Druckmessung geschah mit einem piezoelektrischen Geber, dessen Spannungsverlauf auf einem Oszillographen photographiert wurde. Der Zündimpuls für die Blitzlampe wurde mit auf den Oszillographen geschrieben, und als Druck P wurde der Druck im Augenblick der Photographie genommen. Wegen des schnellen Blasenwachstums ist dieser Druck praktisch gleich demjenigen im Augenblick der Blasenentstehung.

Das Ergebnis der Messungen ist in Fig. 1 dargestellt. Die ausgezogenen Kurvenstücke

[1]) P. Bassi, A. Loria, J. A. Meyer, P. Mittner und I. Scotoni, Nuovo Cimento 4 (1956) 491.

[2]) D. A. Glaser, D. C. Rahm und C. Dodd, Phys. Rev. 102 (1956) 1653.

[3]) G. A. Blinov, I. S. Krestnikov und N. F. Lomanov, Sov. Phys. JETP 4 (1957) 661.

[4]) W. J. Willis, E. C. Fowler und D. C. Rahm, Phys. Rev. 108 (1957) 1046.

[5]) G. Horlitz und W. Paul, Nuclear Instruments 1 (1957) 340.

[6]) D. Hahn und A. W. Knudsen, International Conference CERN 1959, S. 506.

[7]) Eine gute Übersicht findet sich bei D. V. Bugg, Progr. in Nucl. Phys. 7 (1959) 2.

entstanden durch Interpolation von Kurvenscharen $b\ (T,\delta)$ und $P\ (T,\delta)$ und Elimination von δ: Der Fehler eines Punktes auf diesen Kurven ist in der Figur angegeben. Die gestrichelten Kurvenstücke beruhen teilweise auf Extrapolationen und sind nicht ganz sicher, stellen jedoch qualitativ wohl den richtigen

gross man auch das Expansionsverhältnis machte. In B waren die Messungen durch Annäherung an die Schaumgrenze gestört. In C wurden keine Druckmessungen gemacht, ausserdem hängt b hier so empfindlich von P ab, dass kleine, unvermeidliche Druckschwankungen den Fehler von b sehr gross machen.

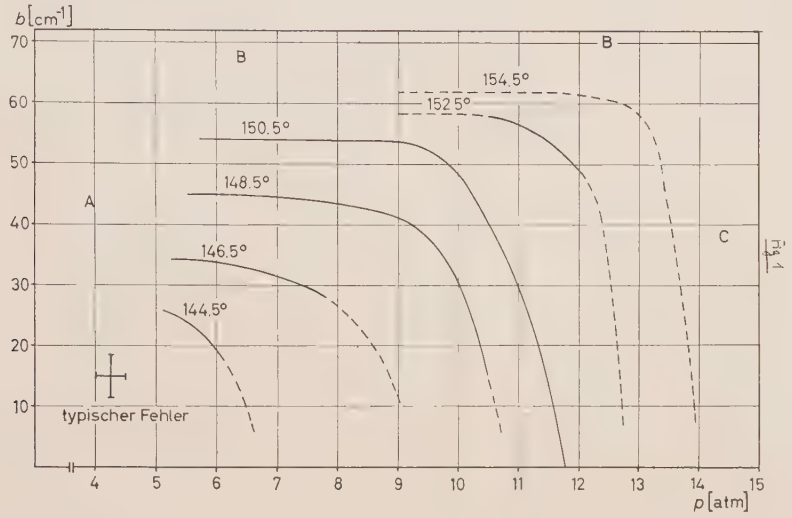

Fig. 1. Die mittlere projizierte Blasendichte als Funktion von P und T in einer Diäthyläther-Blasenkammer.

Verlauf dar. In den mit A, B, C bezeichneten Gebieten existieren keine Messungen: In A nicht, weil in der benutzten Kammer wegen der

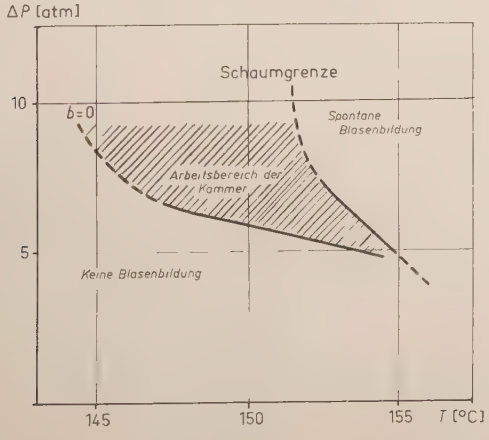

Fig. 2. Untere Grenze der Empfindlichkeit ($b = 0$) und Schaumgrenze in einer Diäthyläther-Blasenkammer. Es ist $\Delta P = P_\infty - P$ als Funktion von T an den betreffenden Grenzen angegeben.

spontanen Blasenbildung an den Wänden der Druck niemals tiefer sank als angegeben, wie

Ein Vergleich mit älteren Messungen ist nur qualitativ möglich, da diese sich auf andere Flüssigkeiten beziehen. In Übereinstimmung mit unserem Kurvenbild sind die Messungen von Glaser[2]) an Propan und Bassi[1]) an Pentan, nicht dagegen die bei Blinov[3]) angegebene Druckabhängigkeit für Propan und die Kurvenschar von Hahn[6]) für CF_3Br.

In Figur 2 sind noch die experimentellen Kurven für die Grenzen der Empfindlichkeit der Kammer nach unten ($b = 0$) und nach oben („Schaumgrenze") angegeben, und zwar ist die Druckdifferenz $\Delta P = P_\infty - P$ als Funktion der Temperatur T aufgetragen. Hierbei ist P_∞ der zur Temperatur T gehörige Sättigungsdampfdruck. Die Grenze $b = 0$ sollte nach der energetischen Theorie[8]) sich etwa wie $\sigma^{3/2}$ verhalten[9]) ($\sigma = \sigma(T) =$ Oberflächenspannung).

[8]) I. A. Pless und R. J. Plano, Rev. Sci. Inst. **27** (1956) 935; Die energetische Theorie ist z.B. in [7]) referiert.

[9]) D. A. Glaser, Handbuch der Physik **45** (1958) 314, Genauer heist es hier $\Delta p \sim \sigma^{3/2} f(T)$ [7]), doch ist im betrachteten Temperaturbereich $\partial f/\partial T \approx 0$.

Dies ist innerhalb der Messgenauigkeit erfüllt. Die Schaumgrenze wurde dadurch definiert, dass in der Kammer zum ersten Mal erhebliche Mengen spontaner Blasen neben den Spuren gebildet wurden. Sie sollte nach der Theorie von Fürth[10]), die von Bugg[7]) auf die Blasenkammer angewandt wurde, sich wie $\Delta P \sim \sigma^{3/2} T^{-1/2}$ verhalten (wobei der Faktor $T^{-1/2}$ sich gegenüber der Temperaturabhängigkeit von $\sigma^{3/2}$ praktisch nicht bemerkbar macht). Nach unseren Messungen ist das nicht der Fall. Wenn man den Ansatz $\Delta p \sim \sigma^n$ machen will, muss man $n \approx 5$ nehmen.

Wir danken Herrn Professor W. Paul für die stete Unterstützung dieser Arbeit, Herrn Dipl. Phys. S. Brandt für Hilfe bei der Auswertung der Filme, ganz besonders aber Herrn Dr. G. Horlitz, unter dessen Leitung der eine von uns (G. K.) diese Arbeit begann. Der Deutschen Forschungsgemeinschaft sei für die Unterstüzung durch Sachbeihilfen gedankt.

[10]) R. Fürth, Proc. Cambr. Phil. Soc. **37** (1941) 252; hier nach dem Referat in [7]).

NUCLEAR INSTRUMENTS AND METHODS 7 (1960) 213–214; NORTH-HOLLAND PUBLISHING CO.

AN ANTI-COINCIDENCE CIRCUIT FOR RANDOMLY DELAYED PULSES

S. ROZENSTEIN

Scientific Department, Ministry of Defence, Tel-Aviv, Israel

Received 15 December 1959

An anti-coincidence circuit is described consisting of a bistable multivibrator, a delay line and a primed univibrator. Operation is actuated by the leading edges of the incoming pulses. The over all dead time of the system is therefore not affected by this anti-coincidence circuit.

Anti-coincidence circuits are frequently used in pulse circuitry. The literature describes various anti-coincidence circuits for pulses which are generated simultaneously or with a constant delay time between their leading edges. For cases in which that time delay is randomly varied, the circuitry becomes comparatively more complicated and is associated with an increase of the resolving time. This article describes a simple anti-coincidence circuit for pulses randomly delayed up to a predetermined maximum. The circuit is actuated by the leading edges of the incoming pulses. The dead time depends only on the predetermined maximum delay which may be shorter than the width of the incoming pulses.

The block diagram of the anti-coincidence circuit is shown in fig. 1. The differentiated leading edge of the first pulse is fed to a terminated delay line as well as to the input of a Bistable multivibrator (Flip-Flop) which is thereby set to the "on" state. The reset trigger is supplied by an OR circuit to which the possible second pulse and the pulse output from the line are fed. If the second pulse is missing, the Flip-Flop is switched back by the line output. Its "on" period is then equal to the time delay τ_1 of the line. If τ denotes the time delay between the leading edges of the incoming pulses, then τ_1 must be chosen to be larger than τ_{max} where τ_{max} is the maximum delay expected. In case the second pulse exists, the Flip-Flop will be switched back earlier and its output duration will equal to τ. From a tap of the delay line, where $\tau_2 = \tau_{max}$, a triggering pulse is fed to a primed univibrator whose positive priming gate is supplied by the Flip-Flop during its "on" state. The univibrator may be triggered only while the priming gate exists. An output pulse may therefore only be developed if the second pulse has not appeared before $\tau = \tau_2$ otherwise the priming gate will be terminated before τ_2 and no output pulse will occur. The delay line section of time delay τ_3 is added in order to ensure reliable univibrator triggering when the Flip-Flop is switched back by the output of the line. For proper operation of the circuit it is required that the rise time of the incoming pulses be low compared to τ_{max}.

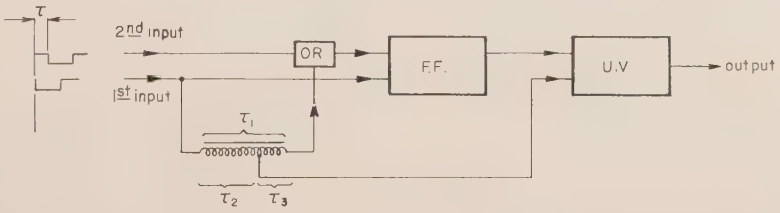

Fig. 1. Block diagram of the anti-coincidence circuit.

A practical circuit according to this block

diagram was designed using valves (fig. 2) but the same principle should be adaptable to transistor circuitry. The Flip-Flop valves are V_{1A}; V_{1B} where V_{1A} is the one normally on. P_1 controls the Flip-Flop sensitivity. The first negative input pulse is differentiated by C and R_0 (the characteristic resistance of the line) and univibrator valves are V_{2A}; V_{2B}. The priming gate is fed from the grid of V_{1B}. P_2 controls the sensitivity of the primed univibrator. The positive output pulse is fed from the anode of V_{2B}. Its amplitude and width are 10 V, 0.5 μsec respectively.

The circuitry of the Flip-Flop with associated delay line is very useful in applications where a

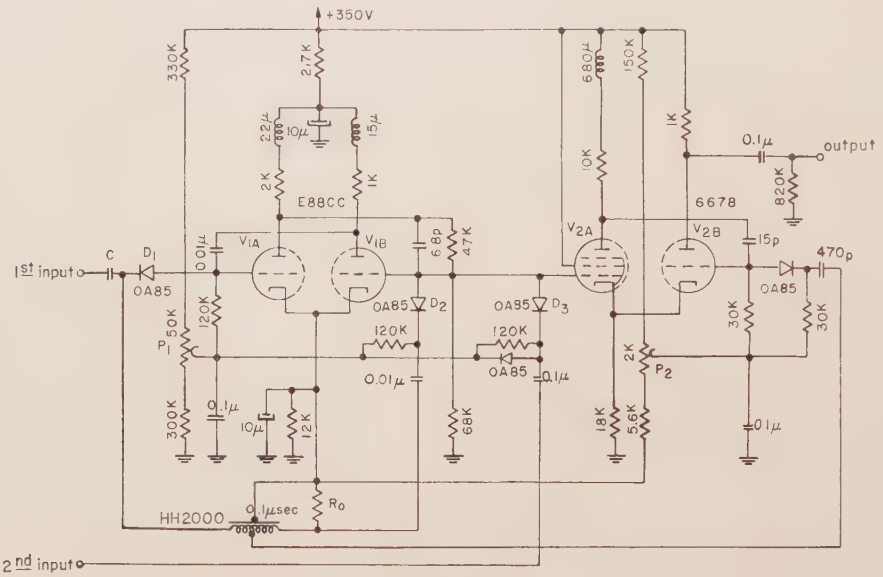

Fig. 2. Practical anti-coincidence circuit.

fed via diode D_1 to the grid of V_{1A}. The differentiator time constant must be short as possible while ensuring sufficient output for triggering the following Flip-Flop. The OR circuit is composed of diodes D_2; D_3. For reliable Flip-Flop operation the delay line shielding is connected to the cathode of V_1. That ensures through the back biasing of diode D_1 that the delayed transfer trigger will be sufficient to reset the Flip-Flop via the unbiased diode D_2. If τ is very small both grids of V_1 will be driven to cut-off but the Flip-Flop will return to its normal state because the shape of the negative second input pulse is preserved. The cathode coupled primed short pulse of accurate width is required. In such cases the usual univibrators are inferior due to the dependence of the output width on valve characteristics and power supply stability. The use of a delay line as the timing element is preferable to the use of RC time constant.

Acknowledgement

This work was carried out under the auspices of the Scientific Department, Ministry of Defence, Israel. The auther wishes to thank Mr. A. F. Fishmann-Arbel for fruitful discussions. Thanks are also due to Mr. E. Gross for the editing of the paper.

NUCLEAR INSTRUMENTS AND METHODS 7 (1960) 215–216; NORTH-HOLLAND PUBLISHING CO.

A CONVENIENT METHOD OF CONSTRUCTING ACCELERATOR SECTIONS

K. R. CHAPMAN and S. GOWARIKER

Physics Department, Birmingham University

Received 8 January 1960

A method for the construction of focussing and accelerator sections for use with ion sources is described. The advantages of this method are stated and details given of the performance. A possible extension of the application of this technique is described.

1. Introduction

When working with electron or ion beams it is frequently necessary to construct short focussing and accelerator sections for use between the source and the main accelerating tube.

A method has been developed, in this laboratory, for constructing such sections which is particularly useful when dealing with aperture lenses and constant gradient accelerator sections; but is not only confined to these particular types. The chief advantage is extreme simplicity whilst ensuring mechanical alignement and rigidity. Further the sections are entirely interchangeable, completely vacuum tight and uneffected by dusty or humid conditions.

2. Method of Construction

There is no one unit that will meet all requirements but in order to explain the construction, two units we have used will be described.

The first unit is shown in fig. 1 and consists of the aperture lens and accelerator section used on a proton ion source. It is necessary with this unit to apply approximately 8 kV across the aperture lens and 40 kV across the whole unit, this being the required injection energy into the main accelerator tube. Many orthodox methods of construction were used, such as assembling all the electrodes on a structure of rods and spacers but considerable trouble was encountered owing to the short overall length required, the number of lead-outs and the difficulty of mainting a vacuum tight structure. All these difficulties were eliminated by the construction detailed below. The structure was assembled using Araldite spacer rings and then the whole encapsulated in Araldite. Units have been made with separate connections to each electrode and more recently with the necessary grading resistances included in the encapsulation. These units have now been in continuous use for many months on the Synchrotron in this laboratory and have given no trouble whatsoever. They withstand the applied voltage and the convenience of requiring only one E.H.T. lead is considerable.

It should be mentioned that with a short simple structure of this type it is possible to avoid machining the Araldite rings by suitably mounting the assembly on a spacing core which may be removed after encapsulation.

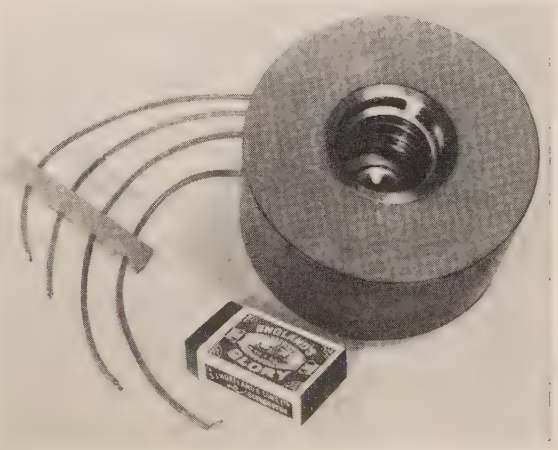

Fig. 1

Fig. 2

The second unit shown in fig. 2 performs exactly the same function as the first. It was constructed early on in the development as an alternative and proved equally satisfactory. It was, however, discontinued in favour of the first type as in this particular application this was easier to construct. However with short tubular electrodes the alternative method might be found more suitable. This assembly was made by casting a hollow Araldite cylinder closed at the base. Two disc electrodes were bonded to either side of the machined base to form the aperture lens. The ring electrodes, which formed the accelerator section, were accurately located in holes drilled in the walls of the cast cylinder and these holes, through which the lead-outs emerged were then filled with Araldite. This gave a good vacuum-tight structure.

3. Performance

The Araldite proved to be a reliable low vapour pressure material capable of withstanding the ion and secondary electron bombardment to which the inside surface was subjected without changing its electrical properties.

A unit that had been in use for 14 hours a day for some 10 months was recently removed for examination and whilst the inside of the Araldite had a dark brown colour there was no sign of tracking on the surface and the insulation had not deteriorated. The inside surface is required to withstand 8 kV across a length of $\frac{1}{4}''$ but no electrical breakdown has occured, the performance from a vacuum point of view was also satisfactory. Since the unit is completely encapsulated it is virtually unaffected by external conditions such as dust and humidity.

4. Extension of the Method

At present a complete experimental accelerator tube for 250 kV operation is being made. Conventional "Dished" electrodes will be used and as this renders any use of a core almost impossible, the assembly will be made on spacer rings and then encapsulated with its grading resistors. The earlier tubes will use porcelain spacers to ensure against electrical breakdowns but it is hoped later to determine the suitability of Araldite spacers at this voltage.

5. Conclusions

This method of construction is capable of considerable flexibility and enables reliable and robust experimental focussing and accelerator sections to be easily constructed in the laboratory. It should be possible to extend the method to produce inexpensive and reliable acceleration tubes of the constant gradient type.

Acknowledgements

The earlier assemblies were constructed by the authors in this laboratory with the exception of that shown in fig. 2 which was constructed for us in the department by Mr. Mac-Cassidy. More recently all the encapsulation has been completed to our design by "Miles Hivolt Ltd" and it is a pleasure to record our appreciation for the very helpful way our rather unorthodox requests have been met.

NUCLEAR INSTRUMENTS AND METHODS 7 (1960) 217–218; NORTH-HOLLAND PUBLISHING CO.

LETTERS TO THE EDITOR

LENTILLES QUADRUPOLAIRES SANS FER A GRADIENT CONSTANT

ALBERT SEPTIER

Laboratoire d'Electronique et Radioélectricité de la Faculté des Sciences de Paris, B.P. No. 9 – Fontenay-aux-Roses

Reçu le 8 janvier 1960

Dans le but de réaliser des lentilles magnétiques sans fer à convergence forte, nous avons étudié la possibilité d'obtenir des répartitions d'induction magnétiques à gradient radial parfaitement constant dans tout l'espace utile. Nous avons envisagé successivement les systèmes suivants:

nappes de courant minces de largeur $2b$ disposées sur un carré de côté $2b$;

nappes minces de largeur $2l$ inférieure au coté du carré $2b$;

bobines épaisses de section $2b \times 2a$ disposées en carré de côté $2b$;

bobines épaisses de section $2l \times 2a$, avec $l < b$.

Les conducteurs sont supposés infiniment longs, et disposés parallèlement à Oz; la densité de courant j est constante dans toute la section des bobines.

1. Nappes minces en carré de largeur 2*b* (fig. 1a)

Les nappes AB et CD transportent des courants $(-I)$ et les nappes BC et DA des courants $(+I)$. On a $I = 2bej$ (e, est l'épaisseur de la nappe, telle que $e \ll b$, et $2b$ le côté du carré).

Les expressions des composantes de B sur OX et OX sont les suivantes[1]), en posant $u = X/b$.

Le gradient radial est donné par

$$K(X) = K(0)\,(1 + \tfrac{1}{4}u^4)^{-1} \text{ sur } OX \qquad (1)$$

et

$$K(x) = K(0)\,(1 - \tfrac{1}{4}v^4)^{-1} \text{ sur } Ox \qquad (2)$$

avec

$$v = x/b \quad \text{et} \quad K(0) = -\mu_0 I/\pi b^2\,. \qquad (3)$$

C'est une fonction décroissante de u sur OX et croissante de v sur Ox. En des points $X = b$ sur OX et $x = Ox$, le gradient sera respectivement de 0.8 $K(0)$ et de 1.33 $K(0)$. Mais en $X = \frac{1}{2}b$ et $x = \frac{1}{2}b$, l'écart entre K et $K(0)$ ne serait que de 1.5% environ. Les écarts relatifs entre la valeur idéale de l'induction

$$B_i = K(0)r \quad (\text{avec } r = X \text{ ou } x)$$

et l'induction réelle, sont environ 5 fois plus faibles que ceux de K.

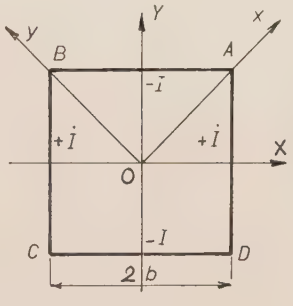

Fig. 1a

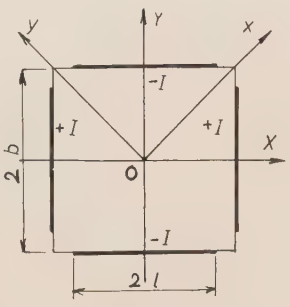

Fig. 1b

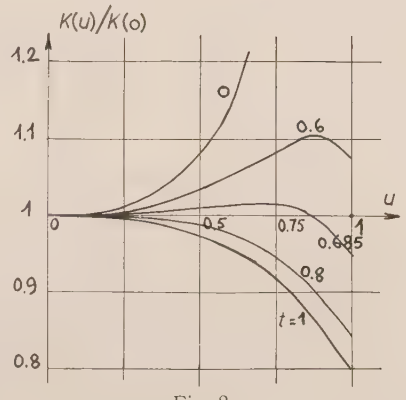

Fig. 2

2. Nappes minces de largeur 2*l*, inférieure à 2*b* (fig. 1b)

Nous avons ensuite étudié la variation du gradient sur OX lorsque le rapport $t = l/b$ est différent de 1.

[1]) A. Septier et G. Chartier, C. R. Ac. Sc. Paris **249** (1959) p. 64–66.

La figure 2 donne les variations du rapport $K(X)/K(0)$ pour différentes valeurs de t. Pour $t = 0.685$ on obtient un gradient constant à mieux de 2% près jusqu'en $u = 0.95$; les faibles valeurs de t conduisent à une sur-compensation. Pour $t = 0$ on a le cas de quatre fils disposés sur les axes OX et OY.

3. Bobines épaisses à section rectangulaire $2a \times 2b$ (fig. 3)

Les bobines ont une section $S = 2a \times 2b$ et transportent un courant $\pm I = \pm 4\,abj$. Si on

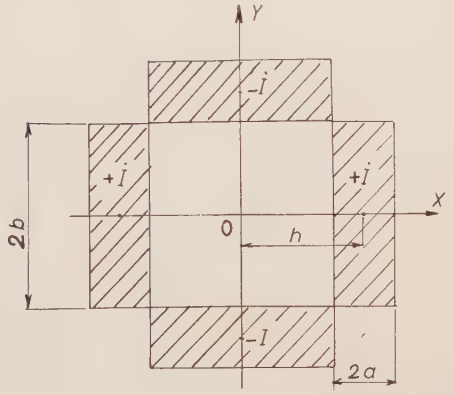

Fig. 3

pose $\lambda = \mu_0 I/8\pi ab$, $\alpha = a/b$, $b + a = h$, $(h + a)/b = \nu = 1 + 2\alpha$ et $u = X/b$, le gradient suivant OX est donné par

$$K(u) = 2\lambda \left[\operatorname{Arc\,tg} \frac{1 + u^2 - \nu^2}{2\nu} + \operatorname{Arc\,tg} \frac{1 - u^2 - \nu^2}{2\nu} \right]. \tag{4}$$

En $X = 0$ on aurait

$$K(0) = -\frac{\mu_0 \dot{I}}{2\pi ab} \operatorname{Arc\,tg} \frac{2ah}{h^2 - a^2}. \tag{5}$$

Pour $\alpha = 0.5$ $(b = 2a)$; le gradient réduit ne varie plus que de 3% entre $X = 0$ et $X = b$.

[2]) P. Grivet et A. Septier, CERN 58-25 (octobre 1958); Nuclear Instruments **6** (1960) 126; 243.

4. Bobines épaisses de largeur $l < b$

En posant $l/b = t$, on obtient sur OX, pour des bobines de section $2a \times 2l$

$$K(u) = 2\lambda \left[\left(\operatorname{Arc\,tg} \frac{1 - t^2 + u^2}{2t} + \operatorname{Arc\,tg} \frac{1 - t^2 - u^2}{2t} \right) - \right. \tag{6}$$

$$\left. - \left(\operatorname{Arc\,tg} \frac{\nu^2 - t^2 + u^2}{2\nu t} + \operatorname{Arc\,tg} \frac{\nu^2 - t^2 - u^2}{2\nu t} \right) \right]$$

et

$$K(0) = \frac{\mu_0 \dot{I}}{2\pi al} \left(\operatorname{Arc\,tg} \frac{1 - t^2}{2t} - \operatorname{Arc\,tg} \frac{\nu^2 - t^2}{2\nu t} \right). \tag{7}$$

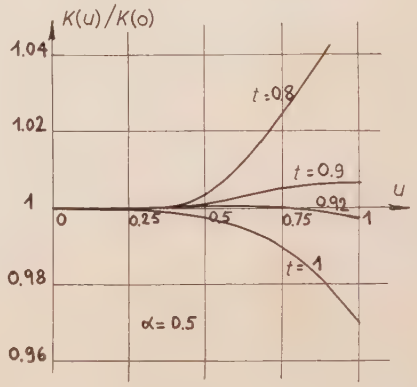

Fig. 4

Pour $\alpha = 0.5$ les courbes de la figure 4 montrent que si $l/b \neq 0.92$ on peut obtenir un gradient $K(u)$ constant à 2×10^{-3} près. Ce résultat est nettement supérieur à celui qu'on obtient dans la pratique avec les lentilles classiques à pôles ou $K(u)$ peut varier de 5 à 20% selon les cas[2]).

Des lentilles de ce type, bien que le gradient y soit inférieur à celui des lentilles à fer pourraient être intéressantes, soit vers les très basses énergies, pour éviter les effets néfastes des champs rémanents, soit vers les très hautes énergies, en régime pulsé, ce qui permettrait d'obtenir des gradient plus élevés que dans les lentilles à fer où on se heurte aux phénomènes de saturation.

NUCLEAR INSTRUMENTS AND METHODS 7 (1960) 219–220; NORTH-HOLLAND PUBLISHING CO.

LOSS OF ACTIVITY FROM BETATRON IRRADIATED SAMPLES BY DIFFUSION

H. FUCHS and K. H. LINDENBERGER

Physikalisches Institut der Universität Heidelberg, Germany

Received 10 February 1960

Experiments have been performed in our laboratory to establish relative integrated cross sections for photonuclear reactions leading to positron emitters[1,2]). The ratios of the residual activities were measured by counting the number of annihilation quanta with a NaJ spectrometer.

Since the neutron emission in the C^{12} (γ,n) reaction results in a recoil energy of the C^{11} nucleus of around 100 keV, the following hypothesis was tried to explain the abnormal behavior of the polyethylene samples: After slowing down only part of the C^{11} nuclei are attached to the lattice again, whereas the rest catches protons from the polyethylene and forms a hydrocarbon compound, which escapes from the sample by diffusion. The dependence of activity loss and of the halflife deviation on the sample thickness could be explained by the fact that the mean square of the displacement by diffusion is proportional to the time. In the 0.2 mm polyethylene samples the diffusion process seems to be completed, before counting was begun, whereas in the 1.5 mm samples diffusion time and C^{11} halflife may be of the same order

TABLE 1

Sample material	Thickness (mm)	Activity relative to graphite	$\frac{T_{1/2}^{exp} - T_{1/2}^{g}}{T_{1/2}^{g}}$
Graphite	2	100	0
Polystyrene	1	100 ± 0.5	$(0 \pm 0.2) \times 10^{-3}$
	4	100 ± 0.5	$(0 \pm 0.2) \times 10^{-3}$
Polyethylene	0.2	87 ± 2	$(0 \pm 5) \times 10^{-3}$
	1.5	97 ± 1	$(25 \pm 5) \times 10^{-3}$
	8	100 ± 1	$(4 \pm 0.2) \times 10^{-3}$

Relative activities and halflives for different samples containing carbon irradiated with 34 MeV bremsstrahlung. The measurement was begun 30 minutes after the end of irradiation and the decay curves were followed for several halflives. Each measured activity has been divided by the number of C^{12} atoms per cm^2 in the sample and by the activity as found for the monitor sample. Corrections for selfabsorption, counting geometry and counter dead time have been applied. For easier comparision the activity as measured with 2 mm thick graphite has been set equal 100 and all other activities are given relative to this. $T_{1/2}^{exp}$ is the halflife, which gives the best fit to the decay curve, $T_{1/2}^{g}$ is the halflife for graphite. Listed errors are standard deviations.

As a check of the reproducibility of this technique samples containing carbon from different materials and of different thickness were irradiated with 34 MeV bremsstrahlung always together with a 2 mm thick graphite sample, which was used as a monitor. The C^{11} activities resulting from the process C^{12} (γ,n) were compared, also the halflife was established in each case. The results are summarized in table 1.

[1]) P. Brix, H. Fuchs, K. H. Lindenberger and C. Salander.

[2]) K. H. Lindenberger and J. A. Scheer. Both papers to be published in Zeitschr. f. Physik.

of magnitude. In the 8 mm samples finally the diffusion time appears to be large compared to the halflife. The observed dependence of the losses on the sample material could be understood if one makes the assumption that the tendency of the C^{11} nucleus to form a hydrocarbon compound will be influenced by the chemical structure of the probe.

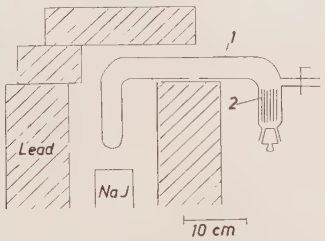

Fig. 1
Counting arrangement for the detection of diffusing activity. 1 = Glass tube. 2 = Irradiated sample.

As a first check on this hypothesis 0.2 mm thick sheets of polyethylene were enclosed in a vacuum tight aluminium container for irradiation and counting. No loss of activity could be observed. For further studies an apparatus as shown in fig. 1 was used. The sample material was placed in one leg of the U-shaped airfilled tube and was irradiated in the collimated beam of the betatron. During counting the other leg was positioned in front of the NaJ-crystal, whereas the crystal was shielded from the leg with the sample material by 10 cm of lead. Fig. 2 shows the observed counting rate as function of time if the sample consists of 0.2 mm thick polyethylene sheets. A transport of activity from the irradiated material to the detector region is observed during the first part of the measurement. The slope of the rising part of the activity curve was found to be proportional to $1/p$, p being the air pressure in the tube. This confirms the assumption that activity escapes from the sample material in gaseous form and reaches the detector region by diffusion.

With the apparatus of fig. 1 some other

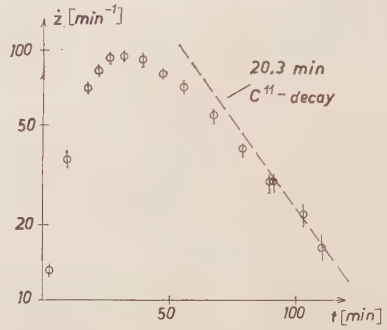

Fig. 2. Counting rate z in a logarithmic scale as obtained in the arrangement shown in fig. 1. t gives the time after the end of the irradiation.

materials were tested for loss of activity. Losses of order of magnitude of ten percent were observed for: (1) 0.5 mm thick sheets of paraffine (C^{11})† (2) ethylalcohol as liquid (C^{11}), (3) pressed discs of hydroboric acid (O^{15}).

Because yields and cross sections for nuclear reactions are frequently deduced from residual activities, careful checks on possible losses of activities by diffusion should be made, if the recoil given to the daughter nucleus by the nuclear reaction is sufficient to break the chemical bound.

We are greatly indebted to Dr. H. v. Buttlar, who first suggested to us the possibility of escape of activity in gaseous form. We appreciate the support of the Deutsche Forschungsgemeinschaft and the Bundesministerium für Atomkernenergie und Wasserwirtschaft.

† In parentheses the observed activity is given.

NUCLEAR INSTRUMENTS AND METHODS 7 (1960) 221–222; NORTH-HOLLAND PUBLISHING CO.

FURTHER COMMENTS ON ERRORS IN POLARIZATION MEASUREMENTS

EDWARD J. BURGE

Wheatstone Laboratory, King's College, London

Received 5 February 1960

In a recent letter[1]) it was pointed out that the fractional error in measurements of the polarization of a beam of particles could be significantly reduced, for the same total incident flux, by using counters over a range of azimuthal angles of the order $\phi = \pm 20°$. The expression given for the root mean square fractional error was

$$f = \frac{1}{T^{1/2}} \left(\frac{\pi}{2\phi}\right)^{1/2} \left\{\frac{1 + (P')^2}{(P')^2}\right\}^{1/2}$$

where T is the total number scattered at a given angle θ, i.e. for $\phi = 0 \to 2\pi$, and

$$P' = \frac{P \sin\phi}{\phi} = \frac{L - R}{L + R}$$

with L and R the number scattered to left and right respectively into a range of azimuthal angles from $-\phi$ to $+\phi$.

The derivation of this formula involved the combination of the errors $\delta(L - R)$ and $\delta(L + R)$ and the root mean square value was used. This method is not strictly correct, as the errors are not independent, and a derivation which aims at avoiding this difficulty has been made. The expression obtained is not significantly different for values of P less than about 0.5, but yields interesting values for f as P approaches unity.

We have

$$\frac{1 + P'}{1 - P'} = \frac{L}{R}$$

therefore

$$\frac{2}{(1 - P')^2} \delta P' = \frac{\bar{R}\delta L - \bar{L}\delta R}{\bar{R}^2}$$

and since L and R can be taken as independent, and $\bar{R}$ and $\bar{L}$ as mean values,

$$\frac{2}{(1 - P')^2} \{\overline{(\delta P')^2}\}^{1/2} = \frac{(\bar{R}^2\bar{L} - \bar{L}^2\bar{R})^{1/2}}{\bar{R}^2}.$$

It follows that,

$$f = \frac{1}{T^{1/2}} \left(\frac{\pi}{2\phi}\right)^{1/2} \left\{\frac{1 - (P')^2}{(P')^2}\right\}^{1/2}$$

which differs from the previous expression by having a minus sign inside the brackets.

[1]) E. J. Burge, Nucl. Instr. and Meth. 6 (1960) 101–102.

1	$P = 0.1$	$P = 0.2$	$P = 0.5$	$P = 0.7$	$P = 0.9$	$P = 0.99$
0.5°	133.3	65.6	23.2	13.7	6.5	1.92
1°	94.2	46.5	16.4	9.7	4.6	1.35
2°	66.7	32.9	11.6	6.8	3.3	0.97
4°	47.2	23.3	8.2	4.8	2.3	0.70
7°	35.8	17.6	6.3	3.7	1.8	0.58
10°	30.0	14.8	5.2	3.1	1.5	0.52
15°	24.7	12.2	4.3	2.6	1.3	0.52
20°	21.5	10.6	3.8	2.3	1.13	0.52
30°	18.0	8.9	3.2	1.9	1.03	0.60
40°	16.2	8.0	2.9	1.7	1.01	0.68
50°	15.2	7.5	2.8	1.7	1.04	0.77
60°	14.7	7.3	2.7	1.7	1.10	0.86
70°	14.7	7.3	2.7	1.8	1.19	0.97
80°	15.0	7.4	2.8	1.9	1.29	1.08
90°	15.7	7.8	3.0	2.0	1.43	1.23

Values of $fT^{1/2}$ have been calculated for a range of P and ϕ and are given in the table. For $T = 10\,000$ particles, $fT^{1/2}$ gives the percentage error directly. It is clear that the largest value of P is unity and as $P \to 1$ the error in P cannot be symmetrical. The formula is derived on the further assumption that the errors are small enough for the square and higher powers of the fractional error to be neglected with respect to the fractional error. Provided the error in P is less than 10% this is a fair assumption, and for small values of P this may be achieved by making T larger than 10 000.

The conclusions drawn in the earlier communication are still valid and are more significant when P is small and the statistical errors tend to be large. For $P > 0.5$ the range of ϕ could conveniently be taken rather less than $\pm 20°$.

The author wishes to thank Dr. A. R. Stokes for confirming the revision of this formula.

BOOK REVIEWS

J. SHARPE: *Nuclear Radiation Measurement* (Nuclear Engineering Monographs; No. VIII; Editor W. K. MANSFIELD) (Temple Press Limited, London, 1960. 71 pages, 12 s. 6 d.)

This monograph is intended for university and technical college students, research assistants and qualified technicians. The attention is concentrated on the basic physical operation of different detectors. The booklet is rich in tables and diagrams, which make the text easy to read. Little attention has been paid to technical aspects. The booklet gives an excellent survey of the problems connected with nuclear radiation measurements and is a good introduction for students who begin to study and use detectors.

The first chapter contains a short introduction. In the second chapter the interaction of radiation with matter is discussed thoroughly. General considerations concerning detectors are given in chapter three. A few remarks concerning the electronic apparatus and low level counting are given in chapter four. (An error on p. 52 gives rise to the false idea that one can date old organic samples very easily with the C^{14}-method. If a counter gives 30 counts per minute for modern carbon, corresponding to a little more than 2 g in the sensitive part of a counter, 2 counts per minute correspond to about 21 500 years not to 45 000 years, for which age one can expect roughly 0.1 counts per minute, if one uses the value 5570 years for the half-life.) In chapter five some applications of detectors for alpha and beta particles, fission products, neutrons as well as gamma- and X-rays are reviewed.

INGRID OLSSON

Who's Who in Atoms. 1960. *An international Reference Book*. Valancey Press, London. Two volumes, 983 p. Price £ 10.10.

This is the second edition of an annual reference book containing a list of individuals all over the world who are in one or the other way connected with atomic and nuclear research and development. Each entry gives biographical data, containing, for example, vocational position, age, education, publications, and societies, and also a note about nuclear interests and the present address of residence.

A brief scanning of this book reveals that the list of names is not entirely representative. Thus, a few well known names were found to be missing and some biographical notes directly misleading. Furthermore, it is surprising that it was possible to find entries not translated to English. It must be kept in mind, however, that the editor has been forced to make a compromise between rendering this enormous quantity of material free of errors and having it published while it is still up to date. Moreover, most inaccuracies probably originated in the collection of the data.

Nevertheless, this book, listing more than 12 500 names and the use of which is also facilitated by its clear typographical setting-up, will be of great value as a reference work for offices the world over having correspondence concerning atomic and nuclear matter.

OLOV BERGMAN

ERRATA

J. A. Dattilo and J. van Bladel: Fields in gap-excited circular ducts (Nuclear Instruments, Vol. **6**, No. 3 (1960) p. 283.

By some oversight the labeling of the figures has been omitted. The abscissa is z/a in figs. 2, 3 and 4, f/f_c in figs. 5 and 6. The fields components are in units of V/a in figs. 2 and 3, and $Y_0 V/a$ in fig. 4, the kicks in units of $9V \cos \varphi_0$ (fig. 5) and

$$\frac{9V \sin \varphi_0}{c} \quad \text{(fig. 6)}.$$

Finally, the curves are labeled according to the value of f/f_c in figs. 2 to 4, r/a in figs. 5 and 6.
The top curve in figs. 2, 3, 4 and 6a corresponds to the value 0.9.

Correction to: K. A. Dolmatova and V. M. Kelman, A longitudinal β-spectrometer with compensated spherical aberration, Nuclear Instruments **5** (1959) 269-279.

The numbers of the last three figures in the article have been confused, viz. fig. 15 has been erroneously placed under No. 16, fig. 16 under No. 17 and fig. 17 under No. 15.
Since this has led to a confusion between the corresponding legends, explanation presented in the text should be taken as a guide.

Spotlight on Industry

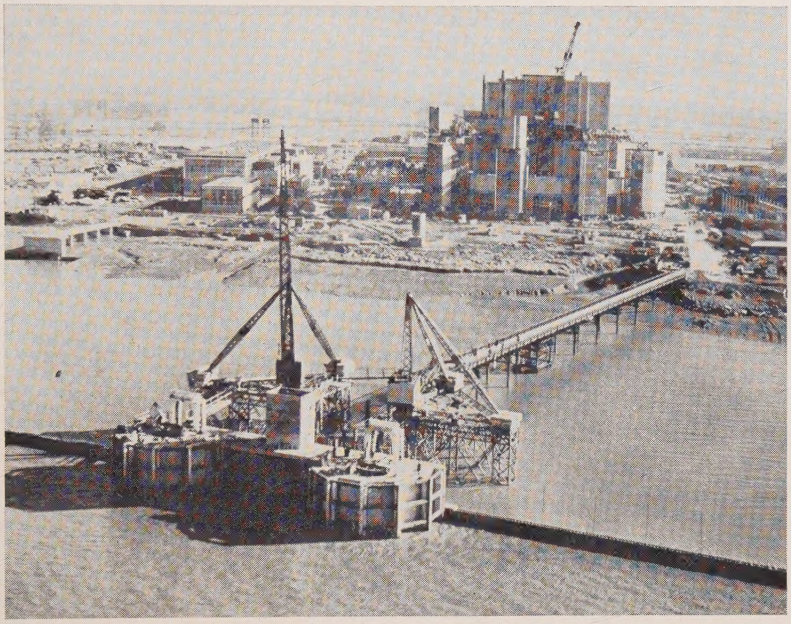

General view of Bradwell Nuclear Power Station.
Left: The Turbine House. Right: Nos. 1 and 2 reactors and the Goliath crane.

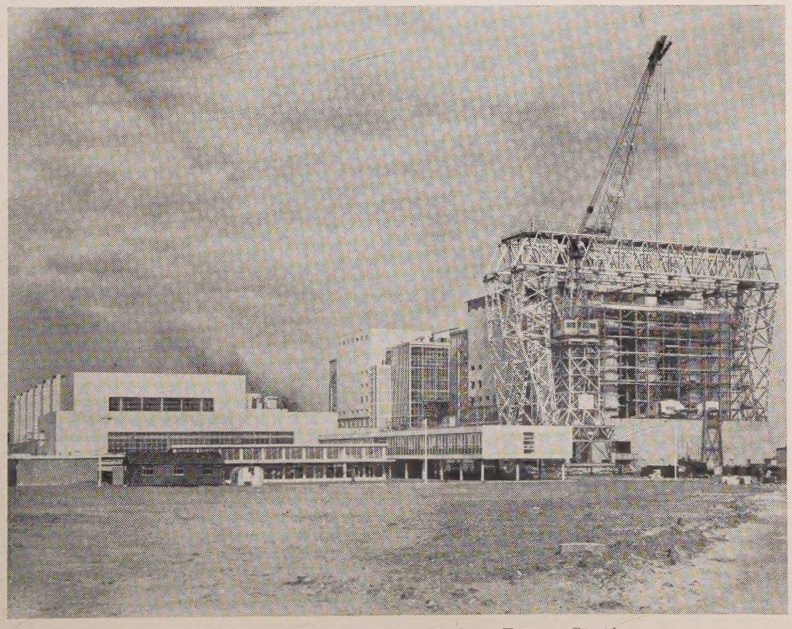

General View of Berkeley Nuclear Power Station.
Foreground: The intake system for the cooling water supply—River Severn.
Background: Right: No. 1 Reactor. Left: The Turbine House.

BRADWELL
NUCLEAR POWER STATION

BRADWELL, ESSEX, ENGLAND
(300 MW)

The Nuclear Power Group, Radbroke Hall, Knutsford, Cheshire, England

The station, when completed, will have a guaranteed net output of 300 000 kilowatts, the plant consisting of two natural uranium carbon dioxide gas-cooled graphite moderated reactors, supplying heat to twelve boiler units. Six boilers will be associated with each reactor, and will be placed in two groups of three on opposite sides of the reactor to form one complete unit. There will be six turbo-alternators each of 52 000 kilowatts capacity.

Each reactor core will comprise a vertical cylinder approximately 45 feet in diameter by 31 feet high, built up from graphite blocks and containing about 2600 fuel channels. The core will be contained in a spherical steel reactor pressure vessel which, in turn, is surrounded by a concrete biological shield about 8 feet thick.

The uranium fuel elements will be uranium rods, approximately one inch in diameter and sheathed in magnesium alloy. Carbon-dioxide gas at a pressure of 130 lb per square inch will transfer the heat produced in each reactor to its six associated boiler units, via five feet diameter ducts. Six blowers, each connected to the outlet of a boiler, will circulate the gas back into the bottom of the reactor vessel.

Three 20 000 kilowatt turbo-alternators (a total of 90 000 horse-power) are to be used for supplying power to these blowers.

The reactors will be re-fuelled on load, the fuel channels being replenished progressively—a few at a time.

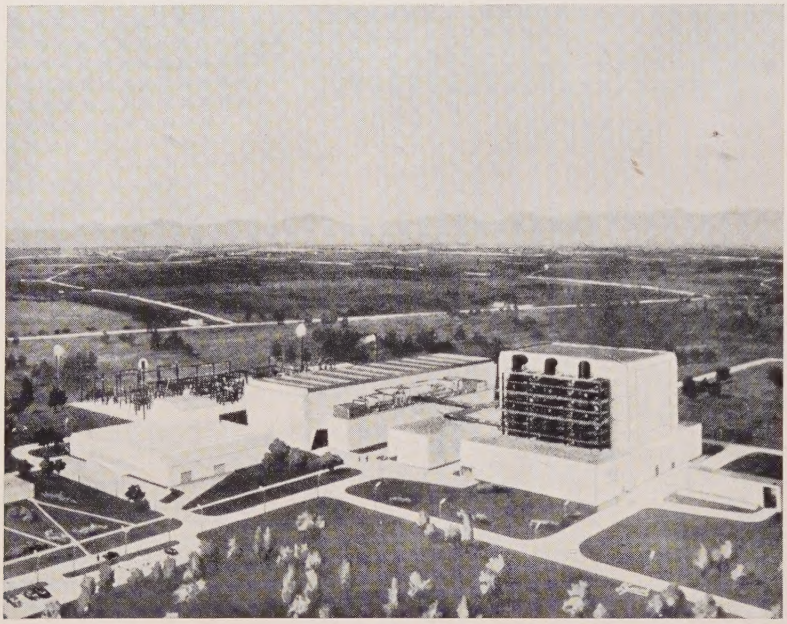

Artist's Impression of Latina Nuclear Power Station.

BERKELEY NUCLEAR POWER STATION

BERKELEY, GLOUCESTERSHIRE, ENGLAND, (275 MW)

The Nuclear Power Group, Radbroke Hall, Knutsford, Cheshire, England

The station, when completed, will have an output of 275 000 kilowatts, or over 360 000 horse-power. The plant will consist of two natural uranium carbon dioxide gas-cooled graphite moderated reactors, supplying heat to sixteen boiler units. Eight boilers will be associated with each reactor and will be grouped round it to form one complete unit. There will be four dual-pressure turbo-generators, each of 83 000 kilowatts capacity.

Each reactor core will comprise a vertical cylinder approximately 48 feet in diameter by 30 feet high, built up from graphite blocks and containing 3250 vertical fuel channels. The core will be contained in a cylindrical steel pressure vessel three inches thick, which, in turn, is surrounded by a concrete biological shield having a thickness of 8 feet 6 inches.

The fuel elements will be uranium rods, approximately one inch in diameter and sheathed in magnesium alloy. Carbon dioxide gas at a pressure of 125 lbs. per square inch will transfer the heat produced in each reactor to its eight associated boiler units through five feet diameter ducts. Eight blowers, each connected to the outlet of a boiler, will circulate the gas back into the reactor vessel.

The reactors will be re-fuelled on load, the fuel channels being replenished progressively—a few at a time.

LATINA NUCLEAR POWER STATION

LATINA, ITALY (300 MW)

The Nuclear Power Group, Radbroke Hall, Knutsford, Cheshire, England

The nuclear power station now being built at Latina, some forty miles south of Rome, is a joint enterprise between Italian and British industrial concerns, AGIP Nucleare of San Donato Milanese, near Milan, and The Nuclear Power Plant Company Limited of Booths Hall, Knutsford, Cheshire.

The customer for the power station is the Societa Italiana Meridionale per l'Energia Atomica (S.I.M.E.A.) of Latina, an organisation owned jointly by AGIP Nucleare and the Istituto per la Ricostruzione Industriale (I.R.I.).

Work started at Latina in November 1958, and the station will be completed in 1962.

Reactor type: Natural uranium, graphite moderated, carbon dioxide cooled.

Number of reactors: One.

Rated output: 705 MW heat, 229 MW electrical gross, 200 MW electrical net.

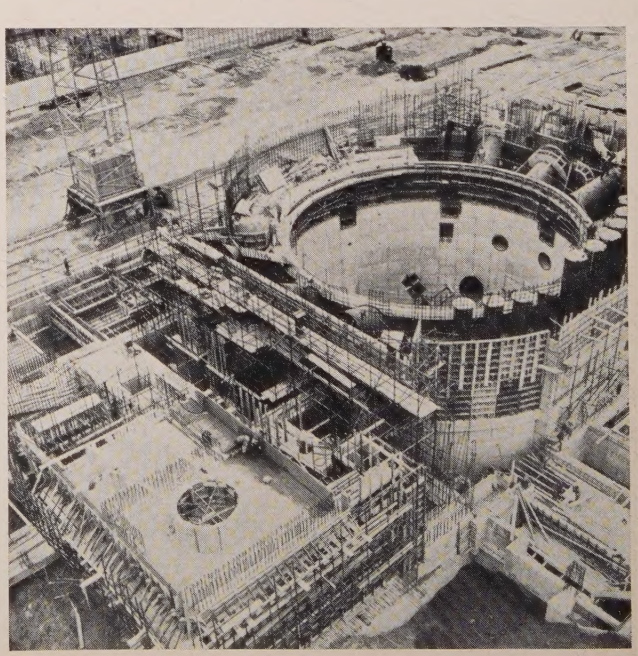

(Latina Nuclear Power Station)
The reactor building showing the vault and main biological shield, CO_2 inlet ducts, and boiler support structure.